

Regulation of cell migration and division by Rab GTPases

Katharina Vestre

Thesis for the degree of Philosophiae Doctor



Department of Biosciences
Faculty of Mathematics and Natural Sciences

UNIVERSITY OF OSLO

2022

© Katharina Vestre, 2022

*Series of dissertations submitted to the
Faculty of Mathematics and Natural Sciences, University of Oslo
No. 2544*

ISSN 1501-7710

All rights reserved. No part of this publication may be
reproduced or transmitted, in any form or by any means, without permission.

Cover: Hanne Baadsgaard Utigard.
Print production: Graphics Center, University of Oslo.

Table of Contents

Acknowledgements	V
List of publications	VII
Abbreviations	IX
Introduction	1
1. Intracellular membrane traffic	1
2. The Rab GTPase family	3
2.1 Rab proteins as molecular switches	3
2.2 Rab GTPases as regulators of intracellular traffic	6
2.3 Rab6	8
2.4 Rab7b	11
2.5 Roles of Rab proteins beyond intracellular transport	14
3. Small GTPases and the cytoskeleton	15
4. Cell migration	16
5. Primary cilia and the cell cycle	19
5.1 Intraflagellar transport	21
5.2 IFT27	23
Aim of the thesis	25
Summary of included papers	27
Paper 1	27
Paper 2	28
Paper 3	29
Methodological considerations	31
Cell lines and <i>in vitro</i> generation of DCs	31
Methods to deplete proteins	33
Microscopy	34
Cell migration studies	37
Discussion and future perspectives	41
1. Rab proteins in cytoskeletal remodeling	41
1.1 Rab6 in cell migration	41

Table of Contents

1.2	Rab6 in cancer metastasis	43
1.3	Rab7b in DC maturation	43
1.4	Rab7b as a physical link between lysosomes and myosin II	44
1.5	Relevance of Rab7b in immune cells.....	45
2.	IFT27 in cell division	46
2.1	Regulation of Rab-like proteins	46
2.2	IFT27 as a regulator of cell division	47
2.3	IFT27 in diseases	49
3.	Concluding remarks	50
	References	51

Acknowledgements

The work presented in this study was carried out from October 2017 to June 2022 in the laboratory of Professor Cinzia Progida at the Department of Biosciences, Faculty of Mathematics and Natural Sciences, University of Oslo.

First, I would like to thank Professor Cinzia Progida for giving me the opportunity to continue as a PhD student in her lab. Thank you for your dedication and support – I could not ask for a better supervisor. Your enthusiasm when I shared new results or showed something exciting at the microscope was always inspiring. I also want to thank my co-supervisor, Professor Oddmund Bakke. Thank you for sharing your knowledge and giving valuable feedback on my work.

It has been a pleasure to work with all past and present members of both the Bakke and Progida groups. Thanks to you, I know that apples are false fruits and that Spaniards eat grapes on New Years Eve. Thank you for all the help and support, the nerdy discussions and for making eleven a special number in my heart. A big thanks also goes to the Imaging platform, for helping me explore the microscopic world.

For me, one of the best parts of being a scientist has been to meet and work with people from all over the world. The work presented in this thesis would never have been possible without collaboration and support from colleagues. Thanks to all my co-authors for contributing with their expertise and knowledge. A special thanks to Noemi, who I had the joy of sharing an office with. You always found time for me, even on your busiest days. I also want to thank Marita for everything she taught me in the lab, and Irene for her invaluable support and cheerful mood. With you, even a failed experiment can be fun. And thank you, Kelly, for the support, motivational frog notes and banana breads.

I am deeply grateful to all my family and friends who have cheered on me and reminded me why I love biology. Thanks for all the fun facts we have shared. Last, but not least, I want to thank my dearest Johannes. You have always encouraged me to be ambitious and supported me at every step of this journey.

Oslo, June 2022

Katharina Vestre



List of publications

Paper 1

Rab6 regulates cell migration and invasion by recruiting Cdc42 and modulating its activity

Katharina Vestre, Ingrid Kjos, Noemi Antonella Guadagno, Marita Borg Distefano, Felix Kohler, Federico Fenaroli, Oddmund Bakke and Cinzia Progida

Cellular and Molecular Life Sciences 2019, 76: 2593–2614

Paper 2

Rab7b regulates dendritic cell migration by linking lysosomes to the actomyosin cytoskeleton

Katharina Vestre, Irene Persiconi, Marita Borg Distefano, Nadia Mensali, Noemi Antonella Guadagno, Marine Bretou, Sébastien Wälchli, Catharina Arnold-Schrauf, Oddmund Bakke, Marc Dalod, Ana-Maria Lennon-Dumenil and Cinzia Progida

J Cell Sci. 2021, 134 (18): jcs259221

Paper 3

IFT27 regulates cytokinesis by interacting with CENPJ and Aurora B

Katharina Vestre, Anne Kristin McLaren Berge, Ingrid Kjos and Cinzia Progida

Manuscript

Part of the introduction is based on the following review:

Rab and Arf proteins at the crossroad between membrane transport and cytoskeleton dynamics

Ingrid Kjos, Katharina Vestre, Noemi Antonella Guadagno, Marita Borg Distefano and Cinzia Progida

Biochimica et Biophysica Acta (BBA) - Molecular Cell Research 2018, 1865: 1397-1409

Abbreviations

BMDCs	Bone marrow-derived DCs
DCs	Dendritic cells
ER	Endoplasmic reticulum
FRET	fluorescence resonance energy transfer
GAP	GTPase activating protein
GDF	GDI displacement factor
GDI	GDP dissociation inhibitor
GEF	Guanine-nucleotide exchange factor
GFP	Green fluorescent protein
GGTase	Geranylgeranyl transferase
GTP	Guanosine triphosphate
GTPase	Guanosine triphosphatases
IFT	Intraflagellar transport
kDa	Kilodalton
LPS	Lipopolysaccharide
MDDCs	Monocyte-derived dendritic cells
MPR	Mannose-6-phosphate receptor
REP	Rab escort protein
RNAi	RNA interference
ROCK	Rho-associated protein kinase
siRNA	Small interfering RNA
SNARE	soluble N-ethylmaleimide-sensitive factor attachment protein receptor

STxB	Receptor-binding, nontoxic B-subunit of Shiga toxin
TGN	<i>Trans</i> -Golgi network
TIRF	total internal reflection fluorescence
TLR	Toll-like receptor

Introduction

1. Intracellular membrane traffic

Eukaryotic cells are organized in many different membrane-bound compartments that have distinct functions. The coordination and communication between these compartments is crucial for the cell to function properly. Complex vesicular trafficking pathways allow the cell to exchange molecules between compartments, and to communicate with the extracellular environment.

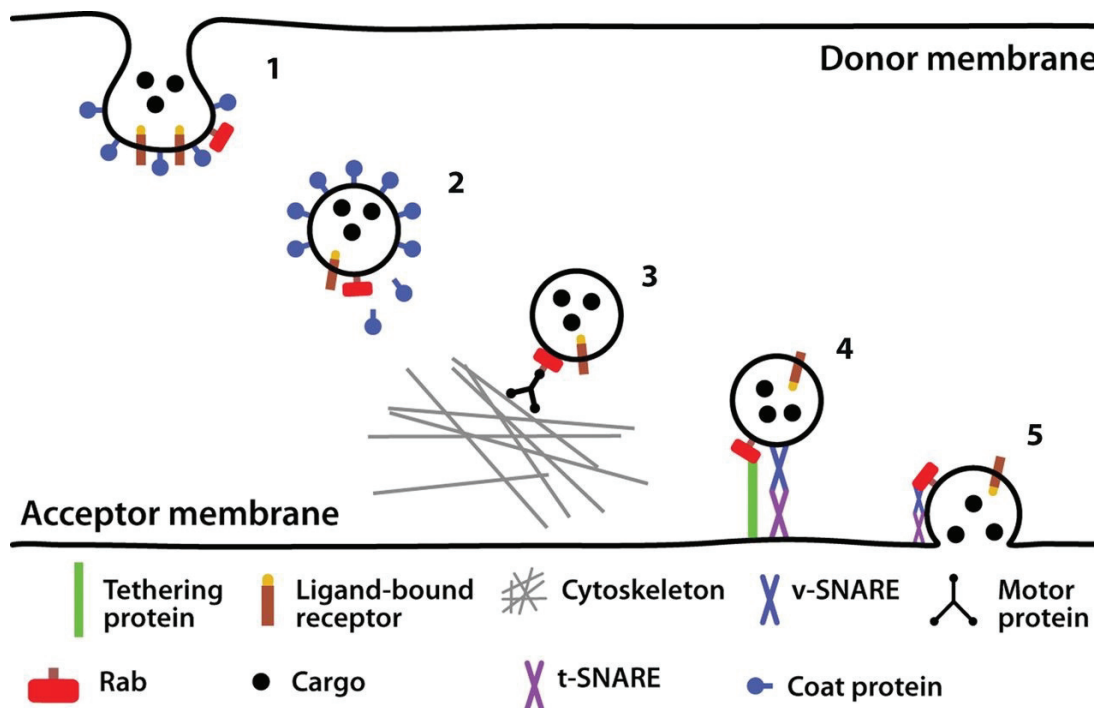


Figure 1: The main steps of intracellular vesicular traffic. First, coat proteins are recruited to the donor membrane and form a coated vesicle containing selected cargo that buds off the membrane (1 and 2). The vesicle moves along cytoskeletal tracks with the aid from motor proteins that can be recruited by Rab proteins (3) and interacts with tethering proteins that bring it in close proximity to its target membrane (4). Finally, SNARE proteins mediate vesicle fusion and the cargo is delivered to its target destination (5). Figure from (Watson, 2015).

The vesicular transport can be divided into several steps (Figure 1), beginning with the sorting of cargo and formation of a carrier vesicle. Usually, cytosolic coat proteins such as clathrin, COPI or COPII, are recruited to the donor membrane to form a coated vesicle. The inner layer of coat proteins associates with cargo or cargo receptors to concentrate them in a membrane patch, while the outer layer induces membrane curvature to form a bud (Dacks and Robinson, 2017). After this, scission occurs and the vesicle pinches off the donor membrane. Scission can be driven by dynamin and related proteins that form a ring around the neck of the bud, or by the actin cytoskeleton (Chappie and Dyda, 2013; Römer et al., 2010).

After its formation, the transport vesicle moves toward its target compartment along cytoskeletal tracks of actin or tubulin. The movement is mediated by different motor proteins that connect the vesicle to the cytoskeleton. Myosin motor proteins mediate the movement along actin filaments, while dynein or kinesin mediate the movement along microtubules. As the vesicle approaches its target destination, it can interact with tethering proteins that bring it in close proximity to the acceptor compartment. There are three classes of tethering factors: long coiled-coil proteins, Complexes Associated with Tethering Containing Helical Rods (CATCHR) tethers, and Class C multisubunit tethering complexes (Gillingham and Munro, 2019; Ungermann and Kümmel, 2019). Finally, SNARE (soluble N-ethylmaleimide-sensitive factor attachment protein receptor) proteins mediate the fusion of the transport vesicle with its acceptor membrane. When the SNARE proteins on the vesicle interact with matching SNAREs on the target membrane, they form a complex that brings the membranes close together and catalyzes membrane fusion (Zhang and Hughson, 2021).

To ensure that all cargos are delivered to their correct destination, each of the different trafficking steps described is tightly controlled. Several diseases, including immunodeficiencies, neurodegenerative disorders and cancer, are associated with defects in membrane trafficking (Yarwood et al., 2020). This illustrates how important the intracellular membrane traffic system is for the cell to function properly.

2. The Rab GTPase family

Rab proteins are small guanosine triphosphatases (GTPases) that play a crucial role in regulating intracellular transport. More than 60 different Rab proteins have been identified in humans, making the Rab family the largest branch of the Ras superfamily of small GTPases (Diekmann et al., 2011; Homma et al., 2021). The other main members of the superfamily are the Ras, Rho, Arf and Ran GTPases (Goitre et al., 2014). All members of the Ras superfamily contain a highly conserved guanosine triphosphate (GTP) binding domain called the G motif. They also contain so-called “Switch regions” that change conformation upon nucleotide binding, allowing the GTPase to function as a molecular switch (Pylypenko et al., 2018). Five regions are specific to the Rab family, and called Rab family (RabF) motifs (Pereira-Leal and Seabra, 2000). Furthermore, the Rabs can be divided into subfamilies that are defined by subfamily sequence motifs (RabSF) (Pereira-Leal and Seabra, 2000).

In addition to the typical Rabs, different Rab-related proteins are considered part of the family (Homma et al., 2021). This includes the ‘large Rab GTPases’ (Rab44, Rab45 and Rab46) and six ‘Rab-like’ proteins (Rab12A, Rab12B, Rab13, Rab14/Ift27, Rab15/Ift22, and Rab16). In contrast to the typical Rabs, which are between 20-30 kilodaltons (kDa) in size, the large Rab GTPases have molecular weights between 70 and 150 kDa and contain long N-terminal regions in addition to the C-terminal Rab-like GTPase domains. The knowledge on these atypical Rabs is currently limited, but they have been implicated in membrane trafficking and cell differentiation (Tsukuba et al., 2021). The Rab-like proteins contain a Rab-like GTPase domain, but lack the C-terminal prenylation motif required for membrane insertion of classical Rabs. Several of the Rab-like proteins regulate intraflagellar transport (Blacque et al., 2018; Huet et al., 2014; Schafer et al., 2006).

2.1 Rab proteins as molecular switches

Rab GTPases function as molecular switches by cycling between two conformational states: an active, GTP-bound form and an inactive, GDP-bound form. The conformational changes involve two regions of the Rab protein called switch I and switch II. When GTP is bound, the switch regions change from an unfolded state to well-defined conformations (Müller and Goody, 2018; Vetter and Wittinghofer, 2001). Since these regions contribute to effector binding, most Rab proteins specifically interact with effector proteins in their GTP-bound active state

(Pylypenko et al., 2018). By alternating between GDP and GTP-bound forms, the Rab proteins change their ability to bind to membranes and effectors, and are able to regulate a variety of processes.

The nucleotide cycle of Rab proteins is controlled by two types of regulatory proteins called guanine-nucleotide-exchange factors (GEFs) and GTPase activating proteins (GAPs) (Borchers et al., 2021). GEFs activate Rab proteins by facilitating the release of GDP. Since there is a large excess of GTP over GDP in the cytosol, the release of GDP leads to the binding of GTP and activation of the Rab protein. The GTPase activating proteins (GAPs), on the other hand, inactivate Rab proteins by stimulating their intrinsic ability to hydrolyze GTP into GDP. Rab GEFs and GAPs can be specific for a single GTPase, or specific for a Rab subfamily (Lamber et al., 2019).

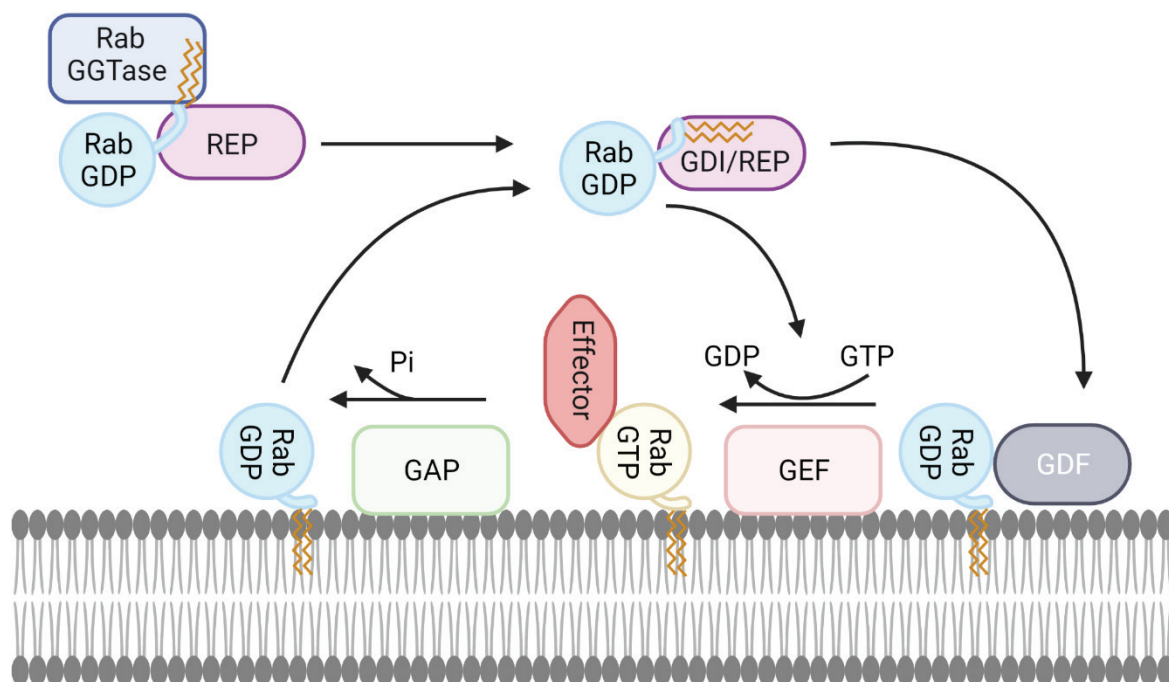


Figure 2: The Rab cycle. After its synthesis, the Rab protein associates with Rab escort protein (REP) and is presented to Rab geranylgeranyl transferase (Rab GGTase). This enzyme catalyzes the addition of a hydrophobic tail to the C-terminal end of the Rab protein, allowing it to associate with membranes. The GDP-bound prenylated Rab is kept soluble in complex with REP or GDP dissociation inhibitor (GDI) until it is recruited to its target membrane. Here, the Rab protein specifically associates with its target membrane either via a nucleotide exchange factor (GEF) that exchanges GDP with GTP, or via a GDI displacement factor (GDF) which dissociates the Rab from GDI/REP before activation by its GEF. At the membrane, the activated Rab interacts with effector proteins to perform its function. After this, a GTPase activating protein (GAP) catalyzes GTP hydrolysis and inactivates the Rab. Finally, GDI extracts the GDP-bound Rab from the membrane, so that it can enter a new cycle. Figure created with BioRender.com, based on a figure by (Pylypenko et al., 2018).

Depending on their nucleotide state, Rab proteins localize to the surface of membranes or to the cytosol. Different proteins assist Rab proteins in this cycling, as shown in Figure 2. After their synthesis, the GDP-bound Rab proteins first bind to Rab escort protein (REP) in the cytosol. This complex presents the Rab to a Rab geranylgeranyl transferase (Rab GGTase) which catalyzes a prenylation reaction where two geranylgeranyl groups are added to one or two Cys-residues at the C-terminal end of the Rab protein (Homma et al., 2021; Seabra et al., 1992). The hydrophobic geranylgeranyl groups function as a lipid anchor, and enable the Rab protein to associate with membranes. After prenylation, REP keeps the Rab soluble until it reaches its target membrane where it dissociates from REP and is activated by a specific GEF. The GTP-bound Rab protein can then recruit its effector proteins to a specific membrane (Pylypenko et al., 2018).

When the Rab protein has performed its function, and is no longer needed in its active state, it hydrolyzes GTP and converts back to its GDP-bound form. Rabs have low intrinsic GTP hydrolysis activity, and depend on GAPs to catalyze this process. Once inactivated, Rab GDP dissociation factor (GDI) binds the GDP-bound Rab and solubilizes it from the membrane (Ullrich et al., 1993). REP and GDI work in similar ways, and mask the lipid anchor of the Rab protein so that it is kept soluble until it reaches its target membrane. While REP binds both prenylated and unprenylated Rabs, GDI preferentially binds to prenylated Rabs. As a result, REP is important for presenting the newly synthesized Rabs for prenylation, while GDI plays a role in recycling prenylated Rabs from membranes back to the cytosol (Leung et al., 2006; Zhen and Stenmark, 2015).

A long debated question is how each Rab protein is targeted to its specific membrane within the cell. Before the Rab can interact with its target membrane, it must be displaced from the complex with REP or GDI. A protein called GDI displacement factor (GDF) can interact with the Rab-REP/GDI complex and catalyze its dissociation (Dirac-Svejstrup et al., 1997; Sivars et al., 2003). It has been suggested that membrane localized GDFs are crucial for specific membrane insertion (Müller and Goody, 2018; Pfeffer, 2017). However, it is not clear whether this mechanism is applicable to all Rabs (Homma et al., 2021). Others have argued that GEFs are the most important determinants of specific Rab localization on membranes, since GDIs preferentially bind to GDP-loaded, inactive Rabs. Rab activation by a GEF would thus promote GDI dissociation and membrane insertion. Studies supporting this model have shown that membrane-specific GEFs are sufficient for targeting a Rab GTPase to its specific

membrane, and that retargeting of GEFs to different membranes affects the localization of their corresponding Rab GTPases (Blümer et al., 2013; Cabrera and Ungermann, 2013; Schoebel et al., 2009). In addition, GAPs, effector molecules, and other factors may also contribute to the precise targeting of Rab GTPases to various cellular membranes (Müller and Goody, 2018). Recently, it has also been shown that phosphorylation of Rab proteins affect their interaction with GEFs and GDI, adding yet another layer of complexity to Rab regulation (Xu et al., 2021).

2.2 Rab GTPases as regulators of intracellular traffic

The first members of the Rab family were identified in yeast, and found to share similarities with the Ras proteins (Gallwitz et al., 1983; Schmitt et al., 1986). Soon after, it was discovered that these proteins are involved in regulating vesicle transport (Goud et al., 1988; Salminen and Novick, 1987; Segev et al., 1988). Mammalian homologues were also identified and found to localize to distinct membranes within the cell (Chavrier et al., 1990). Today, Rab proteins are well established as master regulators of intracellular traffic. Numerous studies have demonstrated how Rab proteins can regulate many different steps of membrane trafficking, including sorting, transport, tethering and fusion of vesicles (Homma et al., 2021; Pfeffer, 2017; Zhen and Stenmark, 2015). Rab proteins carry out this function by recruiting specific effector molecules to the- appropriate membranes. The effector proteins preferentially bind the active (GTP-bound) Rabs, and perform the downstream functions of the GTPase. Many different Rab interactors have been identified, and they vary considerably in both their structure and function (Pylypenko et al., 2018). For example, Rab proteins can interact with molecular motors to regulate vesicle transport (Huang et al., 2001; Kjos et al., 2018; Lindsay et al., 2013; Ueno et al., 2011), or recruit tethering molecules to bring the vesicle closer to its target membrane (Angers and Merz, 2011; Lürick et al., 2016). Other examples of Rab effectors include sorting adaptors, kinases and phosphatases (Zhen and Stenmark, 2015). Each Rab can have multiple effector proteins, and regulate many different processes. A single effector molecule can also bind different Rab proteins simultaneously (Lürick et al., 2016). For example, Rabenosyn-5, a regulator of membrane tethering and fusion of early endosomes, interacts with both Rab5 and Rab4 (De Renzis et al., 2002).

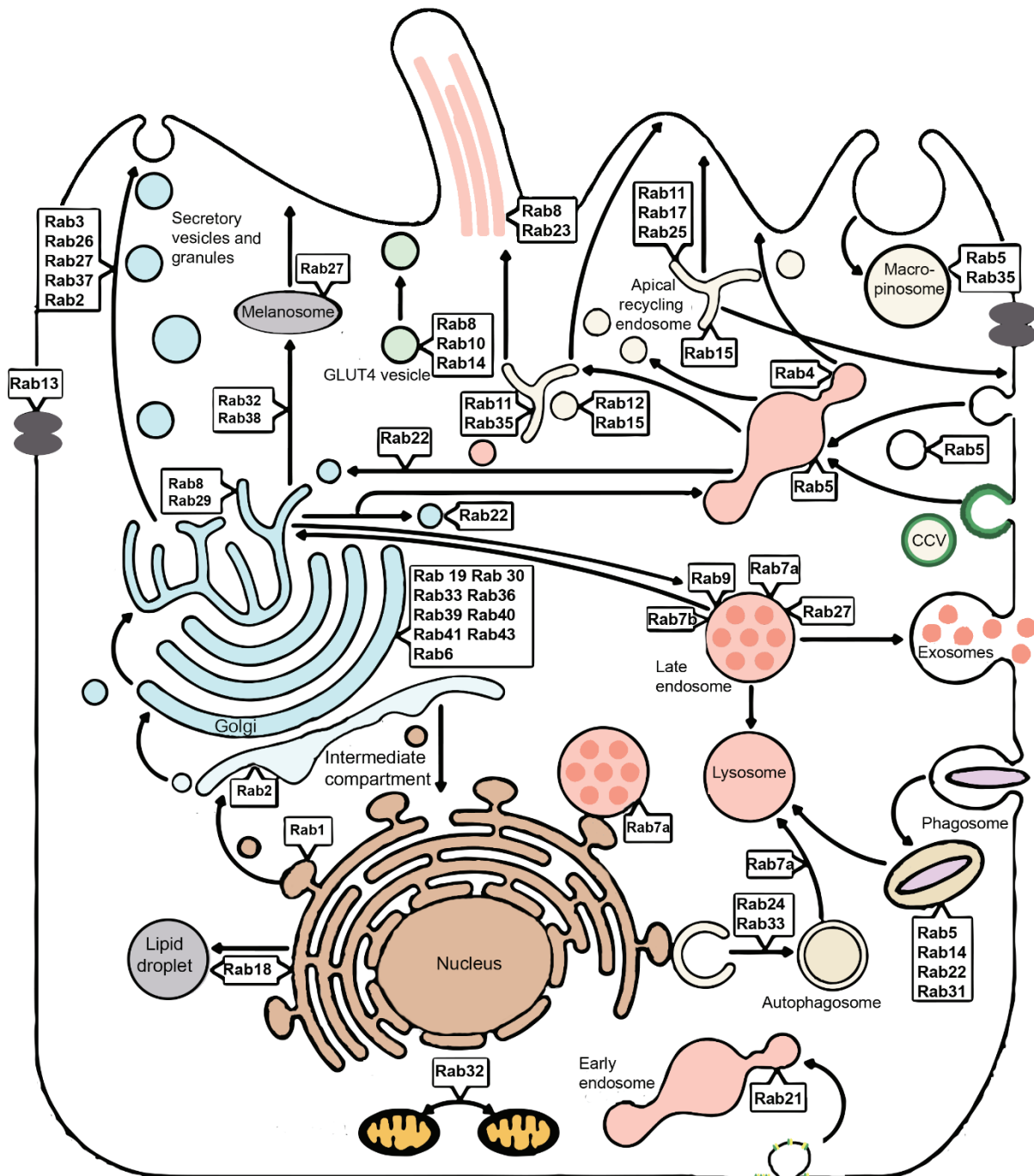


Figure 3: Intracellular localization of Rab GTPases. The figure shows the localization and pathways regulated by selected Rab proteins in an epithelial cell. Figure modified from (Zhen and Stenmark, 2015) with updates from (Kucera et al., 2015) (reversed arrow for Rab9 pathway) and (Progida et al., 2010) (addition of Rab7b).

As illustrated in Figure 3, different Rab proteins regulate specific trafficking routes, and have distinct intracellular localizations. In this way, Rab GTPases contribute to membrane identity and ensure that cargos are delivered to their correct destinations within the cell (Pfeffer, 2013; Zhen and Stenmark, 2015). Due to their specific localizations, Rab proteins are used as molecular markers of different organelles. For example, Rab5 localizes to early endosomes

(Bucci et al., 1992), while Rab7a is present on late endosomes and lysosomes (Bucci et al., 2000). Two different Rab proteins can also localize to the same compartment, but occupy different microdomains and control separate pathways. For instance, there are distinct domains enriched in Rab5 and Rab4 on early endosomes (Sönnichsen et al., 2000). Rab5 regulates the early endocytic pathways, and controls the fusion of early endosomes (Bucci et al., 1992; Gorvel et al., 1991). Rab4, on the other hand, regulates a recycling route from the early endosome to the plasma membrane (van der Sluijs et al., 1992). Also on maturing endosomes, there are Rab5-positive domains together with Rab7a. A recent study showed that these Rab5-positive domains converge and give rise to a new Rab5-positive endosome, while the remaining endosome turns Rab7a-positive (Skjeldal et al., 2021). Rab proteins can also function in so-called “Rab cascades”, where the activation of one Rab causes the activation of another by recruiting a GEF specific for the other Rab (Borchers et al., 2021). For example, Rab5 can recruit a GEF for Rab7a onto endosomal membranes (Langemeyer et al., 2020). In this way, Rab proteins can control the order of events, determine the identity of membranes and link different transport pathways together.

2.3 Rab6

Rab6 was identified as a Golgi-associated small GTPase by Goud and colleagues in 1990 (Goud et al., 1990). As more isoforms were discovered later, the first described Rab6 was renamed Rab6A. Four proteins with similar sequences and electrostatic potentials are now grouped together in the Rab VI subfamily: Rab6A, Rab6A', Rab6B, Rab6C (Pereira-Leal and Seabra, 2001; Stein et al., 2012). Rab41, a slightly less similar protein, is sometimes considered a fifth member of the family, and called Rab6D (Goud et al., 2018; Liu et al., 2013). The ubiquitously expressed Rab6A and Rab6A' are produced by alternative splicing of the *RAB6A* gene, and differ by only three amino acids (Echard et al., 2000). Rab6B is encoded by a separate gene and is predominantly expressed in the brain (Opdam et al., 2000). Rab6C is also expressed in a limited number of human tissues, such as brain, testis and breast. It is produced by a retrogene derived from the *RAB6A'* transcript (Young et al., 2010).

Rab6A and Rab6A' localize to the same intracellular compartments, are expressed at similar levels and exhibit the same GTP-binding properties (Echard et al., 2000). Most effectors bind both isoforms, with one exception being the kinesin-like motor protein Rabkinesin-6 which preferentially binds Rab6A (Echard et al., 2000). Although some studies have pointed to

functional differences between the Rab6A and Rab6A' (Del Nery et al., 2006; Echard et al., 2000), others have shown that the two isoforms have overlapping roles in both endosome-to-Golgi transport (Utskarpen et al., 2006) and Golgi-to-ER transport (Young et al., 2005). As the two isoforms are both biochemically similar and largely redundant in function, they are often collectively referred to as “Rab6” (Goud et al., 2018; Patwardhan et al., 2017; Progidia, 2019; Shomron et al., 2021) a convention that will also be followed in this thesis.

Rab6 is the most abundant Golgi-associated Rab protein, and localizes to late Golgi/*trans*-Golgi network (TGN) membranes and post-Golgi vesicles (Bardin and Goud, 2021; Goud et al., 2018). Several studies have established Rab6 as a central regulator of many different transport pathways connected to the Golgi complex, as illustrated in Figure 4. In addition, Rab6 is involved in maintaining Golgi integrity and homeostasis (Starr et al., 2010). To perform its multiple roles, Rab6 recruits a wide range of different effector proteins. At least 15 different interactors of Rab6 have been described (Goud et al., 2018), including actin motors (Miserey-Lenkei et al., 2010), microtubule motors (Hill et al., 2000; Short et al., 2002) and Golgi-localized tethering molecules (Rosing et al., 2007). In addition, Rab6 is involved in crosstalk with other Rab proteins, including Rab11 (Miserey-Lenkei et al., 2007) and Rab8 (Grigoriev et al., 2011).

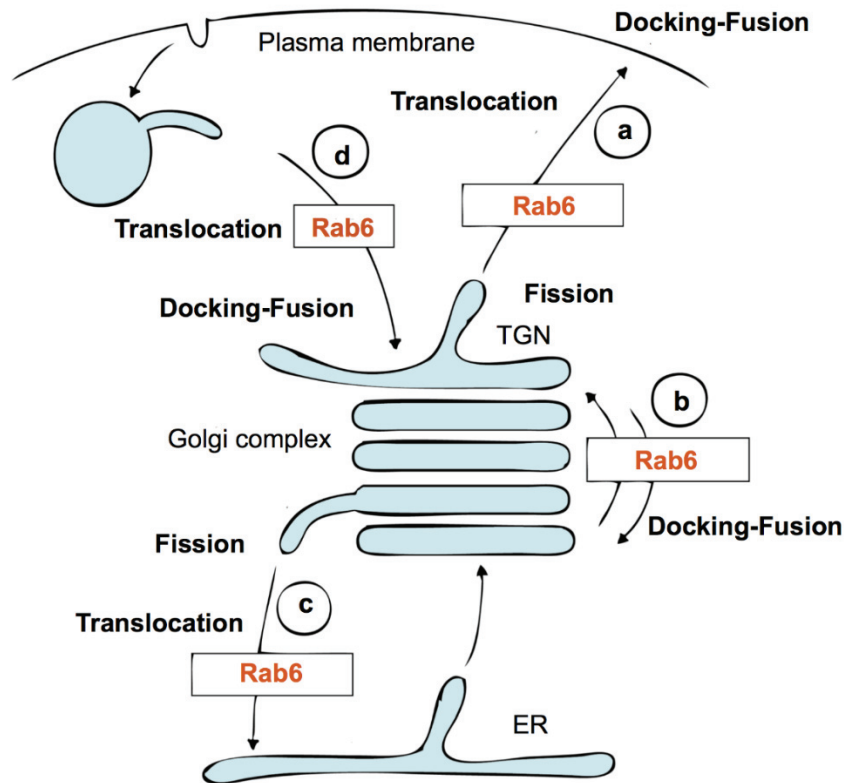


Figure 4: Rab6 regulates multiple transport pathways connected to the Golgi complex. By recruiting different effector proteins, Rab6 controls fission, translocation and docking-fusion of vesicles in different trafficking routes including a) Golgi to plasma membrane, b) intra-Golgi transport, c) Golgi to the endoplasmic reticulum (ER) and d) endosomes to Golgi. Figure modified from (Valente et al., 2010).

In anterograde transport, Rab6 regulates a route between Golgi and the plasma membrane, which is important for exocytosis. White et al. found that in cells overexpressing green fluorescent protein (GFP)-tagged Rab6, the majority of GFP-Rab6-positive vesicles moved from the Golgi toward the cell periphery (White et al., 1999). Later, it was demonstrated that Rab6 regulates the movement of exocytic vesicles by interacting with the kinesin motor KIF5B (Grigoriev et al., 2007). To target the exocytic vesicles to their correct destination on the plasma membrane, Rab6 interacts with the cortical protein ELKS (Grigoriev et al., 2007). Serra-Marques et al. further showed that an additional kinesin motor protein, KIF13B, contributes to the transport of Rab6 secretory vesicles to newly polymerized microtubule ends to which KIF5B binds poorly (Serra-Marques et al., 2020). A third kinesin, KIF1C, also binds Rab6 to regulate the movement of vesicles and control Golgi organization (Lee et al., 2015). In the pathway between Golgi and the plasma membrane, Rab6 plays an additional role in the fission of transport vesicles from the Golgi by interacting with both the kinesin KIF20A and the actin

motor myosin II (Miserey-Lenkei et al., 2017; Miserey-Lenkei et al., 2010). The central role of Rab6 in the secretory pathway is further supported by a study showing that inactivation of Rab6 causes a broad reduction of protein secretion (Fourriere et al., 2019). Recently, it was also demonstrated that Rab6 is involved controlling the positioning of ER exit sites, which act as starting points of the protein secretory pathway (Shomron et al., 2021). Here, Rab6 forms a complex with the dynein–dynactin-binding protein Bicaudal-D2 (BicD2) to maintain Golgi-associated ER exit sites at the cell center.

In retrograde transport, Rab6 is involved in regulating pathways between endosomes, Golgi and the endoplasmic reticulum (ER). Depletion of Rab6, or expression of its dominant negative mutant, inhibits transport of the receptor-binding, nontoxic B-subunit of Shiga toxin (STxB) from early/recycling endosomes to the TGN (Del Nery et al., 2006; Mallard et al., 2002). In addition, Rab6 regulates retrograde transport of ricin between these compartments (Utskarpen et al., 2006). From the Golgi to the ER, Rab6 regulates a COPI-independent pathway. Martinez and colleagues found that overexpression of a constitutively active mutant of Rab6 resulted in redistribution of Golgi proteins to the ER, suggesting a role for Rab6 in Golgi-to-ER trafficking (Martinez et al., 1997). In line with this, expression of the dominant negative mutant of Rab6 blocks the delivery of STxB and recycling of the Golgi glycosylation enzyme GalNAc-T2 to the ER (Girod et al., 1999). Indeed, Rab6 is required for the recycling of Golgi enzymes to the ER, which is essential for maintaining Golgi homeostasis (Sengupta et al., 2015). Rab6 may regulate this transport pathway through the interaction with dynactin. The dynactin complex binds the motor protein dynein-1 that moves toward the minus end of microtubules (Matanis et al., 2002; Young et al., 2005).

2.4 Rab7b

In 2004, Yang and colleagues identified a small GTPase that shared approximately 68 % similarity with Rab7a and named it Rab7b (Yang et al., 2004). They further found that Rab7b, similar to Rab7a, localizes to late endosomes and lysosomes. However, it was later demonstrated that Rab7b also localizes to the TGN and Golgi (Progida et al., 2010). In fact, these two GTPases regulate different transport pathways. Rab7a mediates the transport to late endosomes and lysosomes, and is important for the degradation of several molecules such as epidermal growth factor (EGF) and its receptor EGFR (Bucci et al., 2000; Ceresa and Bahr, 2006). Rab7b, on the other hand, does not influence this degradative pathway, but instead

regulates a retrograde transport pathway from endosomes to the TGN (Progida et al., 2010). Silencing of Rab7b causes mislocalization of TGN markers such as TGN46 to endosomes, and affects the trafficking of the late endosomal markers CI-MPR and cathepsin. Furthermore, the retrograde transport of the B-subunit of cholera toxin is delayed in Rab7b-depleted cells (Progida et al., 2010).

The pathway from endosomes to the TGN is important for the recycling of sorting receptors. Newly synthesized lysosomal enzymes are transported to lysosomes by binding the mannose-6-phosphate receptor (MPR) in the TGN. The acidic pH of endosomes triggers their release from the receptor, which is then transported back to the TGN to repeat the cycle. Rab7b plays a role in this pathway, as depletion of this GTPase impairs the recycling of MPR (Progida et al., 2010). In addition, Rab7b regulates an MPR-independent pathway involving the transmembrane sorting receptor sortilin. Silencing of Rab7b resulted in delayed retrieval of sortilin, and it was found that Rab7b specifically interacts with the cytoplasmic tail of sortilin to control its recycling (Progida et al., 2012).

To understand more of how Rab7b regulates these trafficking pathways, Borg and colleagues searched for interacting partners of this small GTPase (Borg et al., 2014). They identified myosin II as a direct interactor of Rab7b, and found that Rab7b-mediated transport was dependent on this motor protein. When myosin II was depleted or chemically inhibited, the Rab7b-positive vesicles moved slower, were increased in size and clustered in the perinuclear region. Furthermore, Borg et al. demonstrated that not only the intracellular transport, but also other myosin II-dependent processes, were affected by Rab7b (Borg et al., 2014). Since myosin II contracts and crosslinks actin filaments, it is involved in processes that require cytoskeletal remodeling. Rab7b was found to affect such actomyosin-dependent processes, including stress fiber formation, cell spreading and migration. Borg et al. proposed a model (Figure 5) in which Rab7b regulates actin cytoskeleton dynamics through phosphorylation of the myosin II light chain (MLC). They found that Rab7b modulates RhoA activity, and suggested that Rab7b affects myosin phosphorylation through the RhoA-Rho kinase (ROCK) pathway. When Rab7b activates RhoA, this leads to activation of the downstream effector ROCK kinase, which then phosphorylates myosin II and in this way affects actin remodeling (Borg et al., 2014).

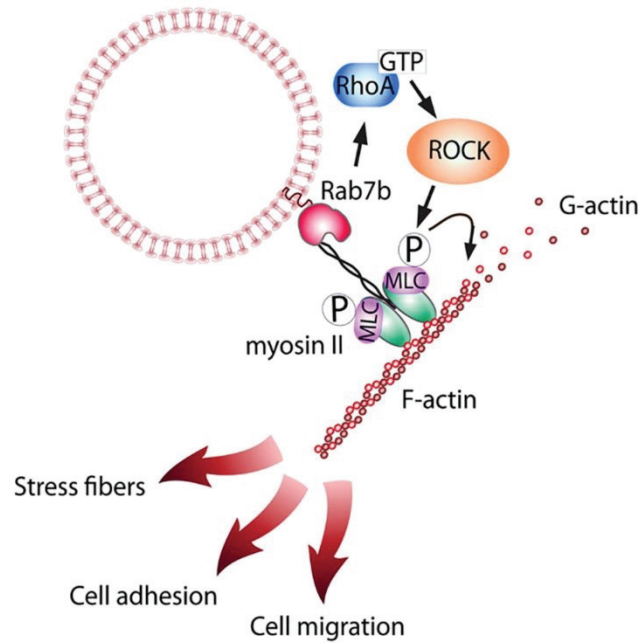


Figure 5: Model of Rab7b regulation of actin dynamics. Rab7b interacts directly with myosin II, and modulates the activity of RhoA. This leads to the activation of RhoA-Rho kinase (ROCK), which through phosphorylation of the myosin II light chain (MLC) affects actin remodeling. As a result, actomyosin-dependent processes such as stress fiber formation, cell adhesion and cell migration are affected. Figure from (Borg et al., 2014).

Rab7b is highly expressed in skeletal muscle, lung, placenta, heart and peripheral blood leukocytes (Yang et al., 2004). In immune cells, Rab7b plays a role in the regulation of Toll-like receptor (TLR) signaling. Toll-like receptors specifically recognize conserved molecular patterns of bacteria and viruses, and activate signaling pathways to initiate immune responses. One example of a well-studied TLR is TLR4, which recognizes the bacterial component lipopolysaccharide (LPS) to detect infections (Poltorak et al., 1998). At the plasma membrane, TLR4 binds LPS and is taken up by endocytosis. Wang and colleagues found that TLR4 localizes to Rab7b-positive compartments in LPS-treated macrophages and that Rab7b negatively regulates TLR4 expression (Wang et al., 2007). After Rab7b knockdown, the amount of TLR4 on the plasma membrane increased, and the receptor remained for a longer time in early and late endosomes. As a result, TLR4-dependent signaling and production of proinflammatory mediators by the macrophages increased. Conversely, increased expression of Rab7b downregulates TLR4 signaling by affecting the recycling of the receptor to the cell surface (Klaver et al., 2015; Wang et al., 2007). Later, Yao et al. found that Rab7b also negatively regulates the signaling by TLR9 (Yao et al., 2009). After activation, TLR9 relocates from the ER to late endosomes and lysosomes, where it colocalizes with Rab7b. Similar to TLR4, silencing of Rab7b resulted in increased signaling by TLR9, underlining a role for this small GTPase in the regulation of TLR trafficking (Yao et al., 2009).

Rab7b is highly expressed in dendritic cells (DCs) (Yang et al., 2004), professional antigen-presenting cells take up foreign material in peripheral tissues, and present it to T cells in the lymph node to initiate adaptive immune responses (Cabeza-Cabrerizo et al., 2021). Sensing of pathogenic stimuli causes DCs to enter a complex developmental program called maturation. The maturation of DCs causes considerable changes in their properties and involves both membrane trafficking and cytoskeleton remodeling (Banchereau et al., 2000; Reis e Sousa, 2006). These changes include decreased antigen uptake, increased antigen presenting capabilities and increased migration (Chabaud et al., 2015b; Dalod et al., 2014). When DCs are stimulated by the bacterial component lipopolysaccharide (LPS), Rab7b mRNA levels dramatically increase, suggesting a specific role for this Rab in DC maturation (Berg-Larsen et al., 2013). However, whether Rab7b has a specific function in regulating any of these processes in DCs is not known.

2.5 Roles of Rab proteins beyond intracellular transport

Although Rab proteins are mostly known for their role in membrane trafficking, increasing evidence demonstrates that these small GTPases are important for several other cellular processes as well. Due to their ability to recruit a plethora of different effector proteins, Rab proteins can function as coordinators in events that require tight temporal and spatial control. For example, as described in the previous section, Rab7b can modulate actin cytoskeleton organization and affect processes such as cell migration (Borg Distefano et al., 2015; Borg et al., 2014). Rab proteins can also influence cell migration by regulating the transport of adhesion molecules (Allaire et al., 2013; Pellinen et al., 2006). Moreover, several Rab proteins are involved in the different steps of cell division (Gibieža and Prekeris, 2018; Miserey-Lenkei and Colombo, 2016), including Rab5 which regulates the alignment of chromosomes on the metaphase plate (Lanzetti, 2012), Rab11 which contributes to mitotic spindle organization (Hehnly and Doxsey, 2014), and Rab35 which controls cytokinesis (Kouranti et al., 2006). In addition, different Rabs play critical roles in signaling events, and are thus crucial for embryonic development and neurite outgrowth (Nassari et al., 2020; Numrich and Ungermann, 2014; Villarroel-Campos et al., 2016).

3. Small GTPases and the cytoskeleton

The cytoskeleton is a system of protein filaments that provides the cell shape and motility, physical robustness and internal structure. It allows the cell to rearrange its inner components as it grows, divides, moves and responds to changes. The three types of filaments that constitute the cytoskeleton are microtubules, intermediate filaments and actin filaments. In intracellular transport, the cytoskeleton plays a key role as it provides tracks for the transport vesicles to move along. Microtubules have a more rigid structure than actin filaments, and are involved in long-distance transport and the positioning of organelles (Barlan and Gelfand, 2017). Actin filaments are flexible, and in addition to providing cell shape, they function as tracks for short-range transport. Intermediate filaments are most known for their role in providing mechanical strength, but there is also evidence that supports their involvement in membrane traffic (Margiotta and Bucci, 2016; Styers et al., 2005).

The cytoskeleton is highly dynamic, and interacts with hundreds of accessory proteins that regulate and connect the different filaments. This includes different motor proteins and adaptors that connect cytoskeletal tracks to vesicles and organelles (Cross and Dodding, 2019), actin-binding proteins that regulate actin polymerization (Pollard, 2016), and microtubule-binding proteins that regulate microtubule assembly (Goodson and Jonasson, 2018). Members of the Ras superfamily of small GTPases are also important regulators of the cytoskeleton. Most known for this role is the Rho family, which has 20 members in humans. The most studied Rho GTPases, Rho, Rac and Cdc42, have well established roles in regulating the actin cytoskeleton and thereby control processes such as cell migration, cytokinesis and macropinocytosis (Croisé et al., 2014; Crosas-Molist et al., 2021; Mosaddeghzadeh and Ahmadian, 2021; Ridley, 2015a). More than 70 effector proteins for these GTPases have been identified, including kinases that activate downstream phosphorylation cascades, and scaffolding proteins that organize signaling cascades (Mosaddeghzadeh and Ahmadian, 2021). In this way, the Rho GTPases activate signaling networks that contribute to actin polymerization, cell adhesion, cell polarity and microtubule stabilization (Crosas-Molist et al., 2021; Mosaddeghzadeh and Ahmadian, 2021).

More recently, the Rab GTPases have also been linked to the regulation of the cytoskeleton. Many of these small GTPases can interact directly with cytoskeletal components. One example is the previously mentioned interaction between Rab7b and myosin II, which plays a role in both trafficking and cytoskeletal dynamics. Another example is Rab1, which directly interacts

with WASP homologue associated with actin, membranes, and microtubules (WHAMM). This protein contributes to Arp2/3-mediated actin assembly, and is important for membrane tubule elongation. Rab1 negatively regulates the activity of WHAMM, and thus slows down actin assembly when it recruits WHAMM to membranes (Russo et al., 2016). Furthermore, Rab proteins can interact with the Molecules Interacting with CasL (MICAL)-family proteins. MICALs oxidize actin molecules, and cause actin depolymerization (Frémont et al., 2017). Both Rab13 and Rab35 interact with members of this family to coordinate vesicular trafficking and actin reorganization (Rahajeng et al., 2012; Terai et al., 2006).

In addition to interacting with cytoskeletal components, Rab GTPases can regulate the cytoskeleton through crosstalk with the Rho GTPases. For example, Rab7a interacts directly with the Rho GTPase Rac1, and modulates its activity. This interaction is important for late endosomal transport in osteoclasts, but also for cell migration (Margiotta et al., 2017; Sun et al., 2005b). Also Rab5 can control Rac1 activity, and the interaction between these two GTPases is important for cell migration (Palamidessi et al., 2008). Furthermore, there are several examples of Rab GTPases that control the activity of the Rho GTPase Cdc42. Rab8 modulates the activity of Cdc42 in epithelial cells to control polarization and lumen formation (Bryant et al., 2010), while Rab14 interacts with Cdc42 to establish cell polarity (Lu and Wilson, 2016). Similarly, also Arf GTPases are involved in crosstalk with Rho GTPases. For example, Arf6 interacts with Rac1 at the plasma membrane and in this way regulates membrane ruffling and cell migration (Cotton et al., 2007; Radhakrishna et al., 1999; Santy and Casanova, 2001; Zhang et al., 1999). Another example is the crosstalk between Arf1, RhoA and RhoC. By modulating the activity of RhoA and RhoC, Arf1 affects the phosphorylation of the myosin light chain and in this way influences cancer cell invasiveness (Schlienger et al., 2014). All these examples highlight how intracellular membrane transport and the cytoskeleton are interconnected, and how different GTPases can cooperate to coordinate complex cellular processes.

4. Cell migration

Cell migration is a fundamental cellular process that strongly depends on the cytoskeleton. It is essential for embryonic development, immune surveillance and tissue repair. At the same time, cell migration plays a role in diseases such as cancer and immune disorders (Crosas-Molist et

al., 2021; Worbs et al., 2017). It is therefore important that the process of cell migration is tightly regulated.

Cells can adopt different motility modes, which can be both cell-type dependent and regulated by the extracellular environment. The best characterized type of cell migration is the mesenchymal mode, typical of fibroblasts or cancer cells moving on a flat, two-dimensional (2D) substrate and characterized by strong cell-substrate adhesion (Figure 6, top). This classical mode of migration is often described as a multistep cycle, beginning with polymerization of actin at the cell front. The actin filaments drive the plasma membrane forward to form protrusions, which can be lamellipodia (thin, sheet-like protrusions) and/or filopodia (small, finger-like protrusions) (Lehtimäki et al., 2017). Lamellipodia formation involves activation of the Rho GTPase Rac1, while filopodia formation involves Cdc42 (Ridley, 2015a). The protrusions are stabilized by the formation of adhesions that link the cytoskeleton to the underlying substrate. The cell can bind to extracellular matrix proteins via transmembrane receptors termed integrins and form different types of adhesion complexes (Doyle et al., 2022). Finally, the adhesions at the cell rear detach and the back of the cell retracts using actomyosin contractility, which is promoted by RhoA. After this, the cycle repeats and a new protrusion is formed at the front of the cell (Ridley et al., 2003; Yamada and Sixt, 2019).

In recent years, it has become clear that cells can adopt a number of migration modes that differ from the classical 2D cycle (Bodor et al., 2020). During wound healing or in the developing embryo, cells often move as groups or sheets rather than individually. In this type of migration, known as collective cell migration, the cells are physically connected and retain cell-cell junctions during movement. This allows the cells to communicate and coordinate their cytoskeletal dynamics (Mishra et al., 2019).

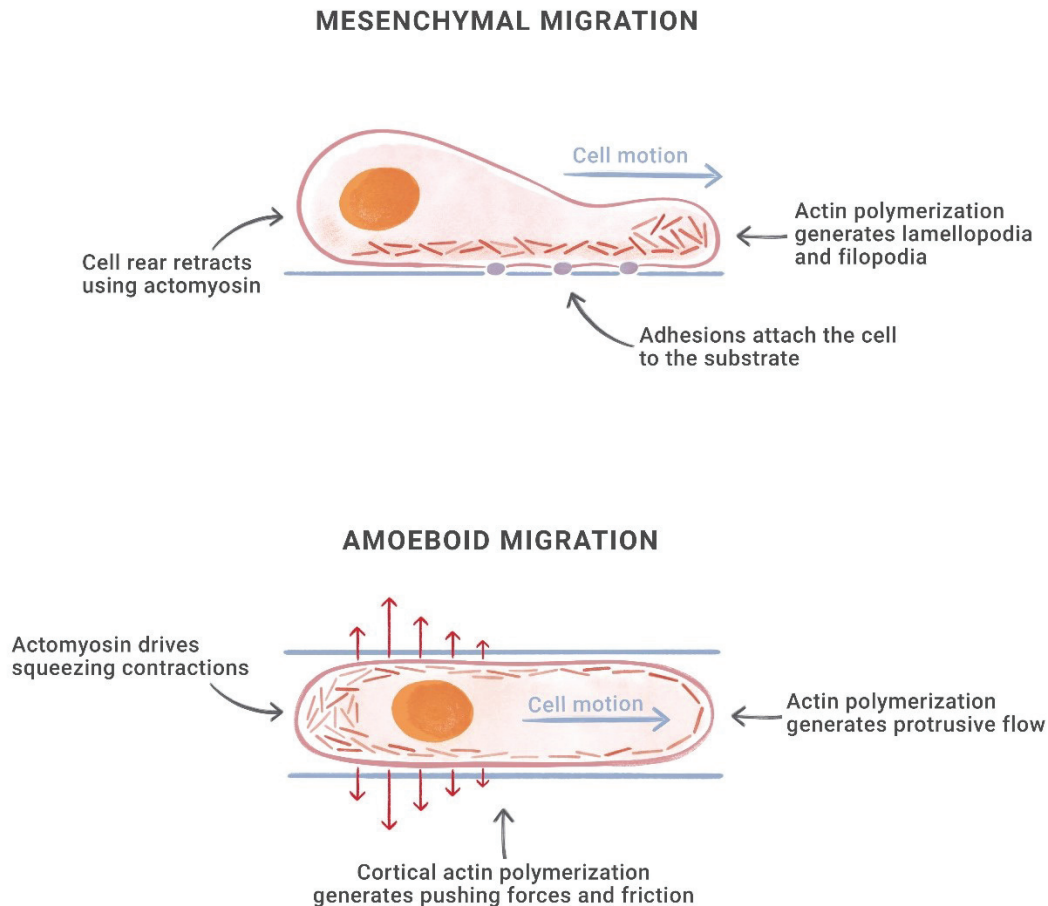


Figure 6: Comparison of mesenchymal migration on a flat surface, and amoeboid migration in a microchannel. Top: Example of mesenchymal migration on flat surfaces. The cell forms protrusions such as lamellipodia and filopodia at its front. The protrusions are stabilized by adhesions to the underlying substrate. After this, the adhesions at the back detach and the cell rear retracts using actomyosin. Bottom: Example of amoeboid migration in a confined environment. This type of migration is characterized by actin polymerization at the front to generate protrusive flow, together with squeezing contractions driven by actomyosin at the cell rear. Cortical actin polymerization generates pushing forces and friction, enabling the cell to move independently of adhesion molecules. Figure made by Katharina and Linnea Vestre, based on figures by (Callan-Jones and Voituriez, 2016; Heuze et al., 2013).

Another type of motility is the amoeboid migration used for example by immune cells (Figure 6, bottom). In this type of migration, the cells adopt round or irregular shapes and undergo cycles of expansion and contraction to squeeze through gaps in the extracellular matrix (Liu et al., 2015). In contrast to the classical 2D migration, amoeboid migration is characterized by weak or absent adhesion. For instance, DCs migrate independently of integrin-mediated adhesion in confined environments such as micro-fabricated channels. Instead, their movement depends on forces generated by actin polymerization, and myosin-driven contractions (Heuze et al., 2013; Lämmermann et al., 2008; Renkawitz et al., 2009). The DC generates pressure against the walls of the channel by polymerizing its cortical actin network. By building up a pressure gradient, the cell is able to create friction and move through the channel independently

of adhesion molecules. At the cell front, actin polymerization promotes protrusive flowing, and at the cell rear, myosin II drives squeezing contractions and propels the rigid nucleus through narrow spaces (Barbier et al., 2019; Chabaud et al., 2015b; Heuze et al., 2013). The DC also uses its actin cytoskeleton to deform the nucleus when passing through constrictions (Thiam et al., 2016). This motility mode is highly efficient, and allows the immune cells to pass through complex and narrow environments without damaging them by proteolysis.

The complex 3D environment that surrounds cells *in vivo* largely affects how they migrate. Under these conditions, the cells need to navigate through narrow structures and interact with their neighbors. To overcome different challenges, cells can flexibly change between different migration modes (Liu et al., 2015; Vargas et al., 2017; Yamada and Sixt, 2019). For example, under conditions of low adhesion and high confinement, slow mesenchymal cells can spontaneously switch to a fast amoeboid migration mode (Liu et al., 2015).

5. Primary cilia and the cell cycle

Similar to cell migration, cell division is a fundamental cellular process that requires tight control and cytoskeletal remodeling. Before a cell divides, it passes through an orderly series of events that is altogether known as the cell cycle. A plethora of different proteins are involved in regulating this cycle and ensuring that problems are solved before the cell progresses to divide. For example, if the cell detects DNA damage, it can halt the cell cycle and attempt to repair the damage (Smith et al., 2020). The cell can also activate a checkpoint at the very end of division if the chromosomes are not properly segregated between the two daughter cells (Steigemann et al., 2009).

As illustrated in Figure 7 the cell cycle is divided in four phases: G_1 , S, G_2 and M phase. A cell that has exited the cell cycle enters a resting state known as G_0 . In the G_1 and G_2 phases, the cell grows and monitors its internal and external environment to ensure that it is ready to divide. In the S phase, the cell synthesizes DNA to make a duplicate of each chromosome. In M phase, the cell divides. The main events of M phase are the nuclear division (mitosis) and the cytoplasmic division (cytokinesis). During this phase, the microtubule cytoskeleton rearranges to form the mitotic spindle, which aligns at the cell equator and segregates the duplicated chromosomes. The actin filaments form a contractile ring around the middle of the dividing cell

that pinches the cell in two after the daughter nuclei have formed. This results in the formation of two separate cells that can continue the cycle, or exit it and enter the G_0 resting state.

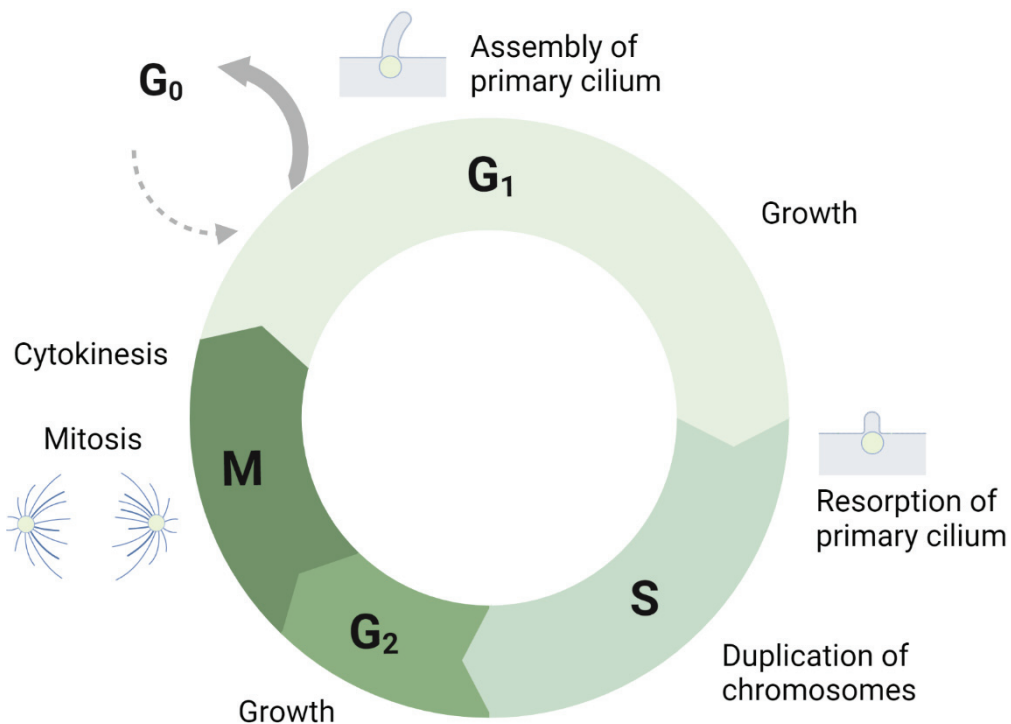


Figure 7: The cell cycle. In G_1 , the cell grows and prepares for the next steps of the cycle. As the cell progresses towards S phase, the primary cilium is disassembled. In the S phase, the cell replicates its DNA to have two copies of each chromosome. In G_2 , the cell grows again and prepares for cell division, which happens in the M phase. In M phase, the chromosomes are distributed into a pair of daughter nuclei (mitosis) and the cytoplasm is divided in two (cytokinesis). As the cell exits the cycle, it will again assemble a primary cilium, either in G_0 or G_1 phase. Figure created in BioRender.com.

As the cell prepares to divide, it loses a specialized organelle called the primary cilium (Figure 7). Almost all cell types exhibit this sensory organelle that protrudes from the cell surface. The primary cilium functions as an antenna, and is involved in many crucial signaling pathways for development and tissue homeostasis (Gigante and Caspary, 2020). Defects in cilia are associated with a group of diseases called ciliopathies that affect many different tissues and organs. Prevalent symptoms of these diseases include cystic kidneys, obesity, retinal degeneration, skeletal malformations and brain anomalies (Reiter and Leroux, 2017).

The primary cilium consists of a microtubule scaffold, the axoneme, which extends from a structure called the basal body. The axoneme of the primary cilium is composed of a ring of nine microtubule pairs, but unlike the motile cilia (or flagella) it has no central microtubule pair to initiate movement. The basal body derives from the mother centriole of the centrosome

(Kumar and Reiter, 2021). During mitosis, the centriole duplicates and functions as an organizer of the mitotic spindle. Afterwards, it migrates to the cell surface to form the basal body. Because of this dual role of the centriole, the cilium must be disassembled prior to mitosis (Breslow and Holland, 2019; Malicki and Johnson, 2017). Thus, the regulation of cilium assembly and disassembly is closely linked to the cell cycle. Indeed, key regulators of mitosis can also function in primary cilia regulation, and ciliary proteins have roles in cell division (Doornbos and Roepman, 2021; Vitre et al., 2020). For example, the ciliary protein IFT88 plays a role in spindle orientation in mitosis (Delaval et al., 2011), while the cell cycle regulator anaphase-promoting complex controls the length and disassembly of primary cilia (Wang et al., 2014).

5.1 Intraflagellar transport

The membrane that surrounds the cilium is continuous with the plasma membrane. Nevertheless, the composition of the ciliary membrane and cytoplasm are distinct from their surroundings. A region at the base of the cilium called the transition zone functions as a diffusion barrier, and prevents molecules from passively entering the cilium. Since there are no ribosomes in the cilium, all the required proteins need to be imported (Lechtreck et al., 2017). A specialized transport system termed intraflagellar transport (IFT) mediates the transport into and out of both motile and primary cilia (Kozminski et al., 1993) (Figure 8).

IFT involves large protein arrays called IFT trains that move along axonemal microtubules. The trains are assembled from two complexes, IFT-A and IFT-B, at the ciliary base. These complexes interact with microtubule motors and cargos to mediate the transport of molecules into and out of the cilium. Anterograde movement toward the ciliary tip is mediated by kinesin-2 (Cole et al., 1998). At the ciliary tip, the IFT trains remodel into retrograde trains that interact with dynein-2 in order to move back to the base of the cilium (Pazour et al., 1998). IFT-A and IFT-B move together within the cilium, but have different functions. IFT-B is composed of 16 subunits and contributes to anterograde transport. IFT-A, on the other hand, is involved in retrograde transport, and is composed of six subunits and the adaptor TULP3 (Nakayama and Katoh, 2020). Another protein complex called the BBSome connects to the IFT complexes and acts as a cargo adaptor for ciliary membrane proteins. For this reason, the BBSome is essential for the trafficking of signaling receptors (Nakayama and Katoh, 2020).

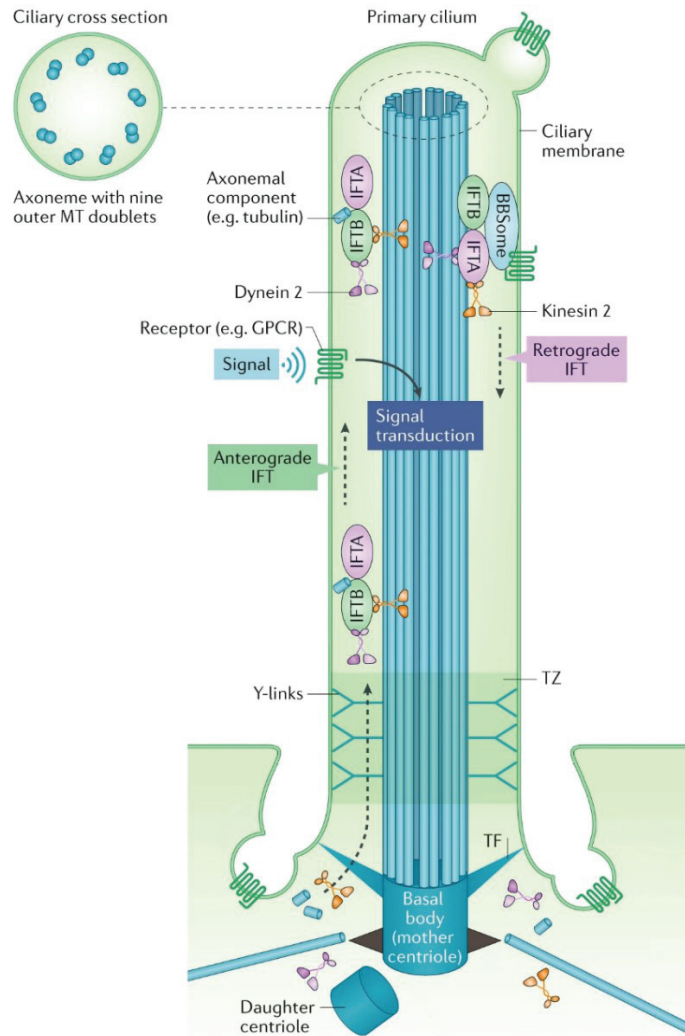


Figure 8: Intraflagellar transport (IFT) in the primary cilium. The non-motile primary cilium extends from the basal body, which derives from the mother centriole. The microtubule scaffold, called the axoneme, consists of a ring of nine microtubule pairs. The transition zone (TZ) functions as a diffusion barrier, and contains specialized structures called Y-links and basal body transition fibers (TFs). IFT trains mediate transport toward the ciliary tip (anterograde IFT) and back to the base of the cilium (retrograde IFT). In anterograde IFT, the IFT-B complex interacts with kinesin-2 to mediate movement along the axonemal microtubules. In this way, cargo such as tubulin is transported into the cilium. At the ciliary tip, the IFT trains remodel and IFT-A interacts with dynein-2 to move back to the base of the cilium. The BBSome connects to the IFT complexes and works as a cargo adaptor for ciliary membrane proteins such as signaling receptors. This allows the primary cilium to function as a cell antenna and transduce signals from the extracellular environment. Figure modified from (Anvarian et al., 2019).

The IFT proteins typically have protein-protein interaction domains such as tetratricopeptide repeats (TPR), WD40 repeats and coiled-coils. These domains both promote interactions between the different IFT proteins, and enable them to function as adaptors (Jordan and Pigino, 2021). However, two IFT proteins, namely IFT22 and IFT27, do not contain these types of domains. In fact, these proteins share sequence similarities with the Rab GTPases, and are also known as Rab-like proteins (Qin et al., 2007; Schafer et al., 2006; Silva et al., 2012). The Rab-like proteins are most likely unable to bind membranes, since they lack the C-terminal

prenylation motif that is found in classical Rabs. However, both IFT22 and IFT27 have GTP binding domains and detectable GTPase activity. While IFT22 lacks the G4 motif and has a highly diverse G5 motif, IFT27 contains all five Rab motifs for GDP/GTP binding (Bhogaraju et al., 2011; Wachter et al., 2019).

5.2 IFT27

IFT27 was first characterized in the single-celled green algae *Chlamydomonas reinhardtii*, where it was found to localize to the flagellum and basal body (Qin et al., 2007). Qin and colleagues demonstrated that GFP-IFT27 co-localized with other IFT proteins and moved bidirectionally in the *Chlamydomonas* flagellum. In addition, they found that IFT27 affected cytokinesis and suggested a role for this protein in cell cycle regulation (Qin et al., 2007). IFT27 is part of the IFT-B complex, where it interacts directly with IFT25 to form an IFT25/27 subcomplex (Luckner et al., 2005). IFT25/27 becomes part of the IFT-B core by interacting with the IFT81/74 subcomplex. While the interaction between IFT27 and IFT25 is nucleotide-independent, the association of IFT27 with the rest of IFT-B requires it to bind GTP (Bhogaraju et al., 2011; Huet et al., 2014; Liew et al., 2014). IFT25 and IFT27 associate with the rest of the IFT-B complex before entry into the flagellum, suggesting that they are involved in regulating the initiation of anterograde IFT (Wang et al., 2009). In the unicellular parasite *Trypanosoma brucei*, IFT27 controls both anterograde and retrograde ciliary transport and is involved in flagellum formation (Huet et al., 2014). Huet and colleagues found that IFT27 is involved in the import of the IFT-A complex and dynein motors into cilia, as well as in the assembly of the IFT-B complex (Huet et al., 2014).

In mice, IFT27 controls sperm flagella formation and is required for spermatogenesis and male fertility (Zhang et al., 2017). Other studies in mouse cells have shown that IFT27 plays an important role as a link between the IFT complex and the BBSome. In IFT27 knockout mice, the BBSome and its regulators Arl6 and Lztfl1 accumulate in primary cilia (Eguether et al., 2014). IFT27 interacts directly with and stabilizes the nucleotide-free form of Arl6, promoting its activation (Liew et al., 2014). Activated Arl6 in turn triggers BBSome coat formation and the sorting of membrane proteins into the cilium. Lztfl1 functions downstream of IFT27 to regulate the transport of signaling receptors out of the cilium (Eguether et al., 2014). These interactions have important consequences for the hedgehog signaling pathway. Indeed, Eguether et al found that IFT27 knockout mice have defects in almost all steps of the signal

transduction cascade (Eguether et al., 2018; Eguether et al., 2014). The mice lacking IFT27 have multiple developmental defects typical of defective hedgehog signaling, including abnormal kidneys, polydactyly and cleft palate, and die before birth (Eguether et al., 2018; Eguether et al., 2014). Similarly, zebrafish injected with morpholino oligos to prevent expression of IFT27 also display typical ciliopathy phenotypes (Aldahmesh et al., 2014). In humans, different mutations in IFT27 are associated with Bardet-Biedl syndrome (BBS), a ciliopathy characterized by multiple symptoms, including kidney dysfunction, polydactyly, retinal degeneration, intellectual disabilities and obesity (Aldahmesh et al., 2014; Schaefer et al., 2019). These symptoms have been linked to the role of IFT27 in BBSome transport, but the precise mechanisms underlying the disease are unknown.

IFT27 is an evolutionary conserved protein present in the majority of ciliated organisms, but it is absent in the fruit fly *Drosophila melanogaster* and the nematode *Caenorhabditis elegans*. There are also differences in IFT27 functions between species and cell types. For example, knockdown in *Trypanosoma brucei* causes shortening of the flagella. However, in mouse embryonic fibroblasts lacking IFT27, the cilia length and numbers are normal. Furthermore, a possible role of IFT27 in cell division has been reported in *Chlamydomonas* (Qin et al., 2007). Whether this function also applies for other organisms remains to be investigated. Only one study partially addressed the role of IFT27 in mammalian cell division in (Taulet et al., 2017). Taulet et al. found that IFT27 interacts with the mitotic regulator Aurora B kinase, and that depletion of IFT27 prevents Aurora B localization at the central spindle in anaphase (Taulet et al., 2017). As the majority of studies on IFT27 have focused on its role in cilia, the knowledge on IFT27 in cell division is currently limited.

Aim of the thesis

The overall aim of this thesis was to investigate and characterize novel roles of members of the Rab family of small GTPases in cell migration and cell division.

The more specific aims of the included papers were as follows:

Paper 1:

The small GTPase Rab6 regulates multiple transport pathways connected to the Golgi apparatus. To mediate these different trafficking routes, Rab6 interacts with several effector proteins, and one of them is the actin motor protein myosin II. Our lab found that another small GTPase, Rab7b, by interacting with myosin II, regulates actomyosin dynamics and plays a dual role in both intracellular transport and cell migration. Therefore, the aim of paper 1 was to investigate whether Rab6 has a similar role in the regulation of actomyosin dynamics and cell migration, with particular focus on the crosstalk with Rho GTPases.

Paper 2:

Dendritic cells (DCs) are cells of the immune system. Upon encountering a pathogenic stimulus, DCs start a maturation process that involves considerable changes in their phenotype and functions. Interestingly, Rab7b is highly expressed in DCs and its mRNA levels dramatically increase 4 hours after pathogenic stimuli. However, the specific function of Rab7b in these specialized immune cells is not known. The aim of paper 2 was to characterize the role of Rab7b in DCs, focusing on the specialized functions that characterize DC maturation.

Paper 3:

IFT27 is a Rab-like GTPase known for its role in intraflagellar transport, the bidirectional trafficking required for the function and maintenance of cilia. Mutations in IFT27 cause Bardet Biedl-syndrome (BBS), a ciliopathy characterized by a broad range of symptoms. However, how these mutations interfere with IFT27 function has not been investigated before. Previous work in single-celled organisms suggested that IFT27 is also involved in cell division, but not much is known about this function of IFT27 in mammalian cells. The aim of Paper 3 was to investigate the role of IFT27 in mammalian cell division, and characterize disease variants of IFT27 to improve our understanding of the mechanisms behind BBS.

Summary of included papers

Paper 1

Rab6 regulates cell migration and invasion by recruiting Cdc42 and modulating its activity

Rab6 is a small GTPase that regulates several transport pathways connected to the Golgi complex. By interacting with many different effector molecules, Rab6 controls both retrograde trafficking between endosomes, Golgi and the ER and anterograde trafficking between Golgi and plasma membrane. One of the effectors of Rab6 is the actin motor protein myosin II. Through this interaction, Rab6 controls the fission of transport vesicles from the Golgi. Another Rab protein, namely Rab7b, also interacts with myosin II, and in this way regulates not only trafficking, but also actin cytoskeleton dynamics and cell migration. We therefore investigated whether Rab6, similar to Rab7b, affects cell migration through its interaction with myosin II. To do this, we performed wound healing assays and found that knockdown of Rab6 increases cell speed. We further found that depletion of Rab6 affected actin dynamics, causing an increase in the formation of actin protrusions, and myosin II phosphorylation. Moreover, we showed that Rab6 modulates the activity of the Rho GTPase Cdc42 at the cell periphery. We finally provided a molecular mechanism behind this regulation by showing that Rab6 interacts with both Cdc42 and its GEF Trio. In this way, we demonstrated that a Rab protein can control the local activation of Rho GTPases to regulate the cytoskeletal rearrangements required for cell migration.

Paper 2

Rab7b regulates dendritic cell migration by linking lysosomes to the actomyosin cytoskeleton

Rab7b is a small GTPase that localizes to late endosomes, lysosomes and the *trans*-Golgi Network (TGN) and regulates the retrograde trafficking of different sorting receptors. By interacting directly with the actin motor protein myosin II, Rab7b not only mediates the movement of transport vesicles, but also modulates cytoskeletal remodeling. Rab7b is highly expressed in dendritic cells (DCs), which are specialized immune cells that patrol the body in order to find and take up foreign material. When DCs encounter antigens, they begin a maturational process and migrate to the nearest lymph node to initiate an adaptive immune response. Previous studies had demonstrated that there is a dramatic increase in Rab7b levels shortly after pathogenic stimuli, but the function of this small GTPase in DCs was unknown. Therefore, we investigated whether Rab7b could be involved in the changes that occur during DC maturation. Our results demonstrated that silencing of Rab7b did not prevent the maturation of DCs or their ability to present antigens. However, we found that Rab7b interfered with the polarization of the actomyosin cytoskeleton required for efficient cell migration. In the absence of Rab7b, LPS-treated DCs moved slower and less persistently and retained the macropinocytic activity that is typical of immature DCs. Furthermore, Rab7b knockout DCs had a reduction in myosin II phosphorylation and impaired lysosomal signaling. Finally, we demonstrated that Rab7b interacts with the lysosomal Ca²⁺ channel TRPML1 to mediate the local activation of myosin II at the cell rear required for cell migration, thus functioning as a physical link between lysosomes and the actomyosin cytoskeleton.

Paper 3

IFT27 regulates cytokinesis by interacting with CENPJ and Aurora B

IFT27 (also known as RABL4) is a Rab-like GTPase known to regulate intraflagellar transport (IFT), the transport system that is required for the function and maintenance of cilia. Genetic studies have linked different mutations in IFT27 to Bardet Biedl syndrome (BBS), a disease characterized by a broad range of symptoms, including retinal degeneration, kidney dysfunction, polydactyly and obesity. These symptoms have mainly been explained by defects in primary cilia function, but increasing evidence suggests that the IFT proteins also have additional roles in regulation of the cell cycle and proliferation. We therefore investigated whether IFT27 plays a role in cell division, in addition to its canonical role in ciliary transport. Our results showed that knockdown of IFT27 increased cell proliferation, and that the localization and expression of IFT27 is cell cycle dependent. After telophase, we observed a strong increase in IFT27 expression, and found that the protein localizes to the midbody. We also demonstrated that overexpression of GFP-IFT27 caused a delay in abscission. To further investigate how IFT27 regulates this process, we searched for novel interactors and identified the microtubule regulator CENPJ as interacting partner of IFT27. Finally, we showed that disease variants of IFT27 cause defects in cytokinesis, and were unable to bind both CENPJ and the mitotic regulator Aurora B. Taken together, our findings reveal a novel role for IFT27 in cytokinesis, and suggest that defects in cell division could contribute to the symptoms of BBS.

Methodological considerations

Cell lines and *in vitro* generation of DCs

In the papers included in this thesis, we have used various types of mammalian cells to answer different biological questions. In paper 1 and 3, we used different immortalized cell lines. These cells are cost effective, easy to use and provide consistent samples of pure populations (Kaur and Dufour, 2012). Immortalized cell lines are able to divide indefinitely and can be kept in culture for long periods. However, cell lines that are kept in culture for too long change due to selective pressures and genetic drift. This can make them less reliable models and affect reproducibility (Hughes et al., 2007). Therefore, the passage number should be monitored, and the cells should be exchanged regularly from frozen stocks. Furthermore, cell lines should be monitored for contamination by mycoplasma regularly. In addition, a cell line can become contaminated by another cell line. STR profiling, isoenzyme analysis, and contamination tests should be routinely used to authenticate cell lines (Capes-Davis et al., 2019; Hughes et al., 2007).

The cervical cancer cell line HeLa, used in both paper 1 and 3, was the first successful attempt to culture a continuous human derived cell line (Gey et al., 1952). Today, HeLa is still one of the most commonly used cell lines. These cells are well characterized and easy to transfect with siRNAs or DNA constructs. Furthermore, their flat, epithelial morphology make them well suited for imaging studies. The human osteosarcoma U2OS cell line (Pontén and Saksela, 1967) used in paper 1 and 3 offers similar advantages. In paper 1, we also used the human retinal pigment epithelium RPE-1 cell line. These cells have been immortalized through transfection with human telomerase reverse transcriptase (hTERT), and offer an alternative to cancer cell lines (Bodnar et al., 1998; Jiang et al., 1999). We also used the human non-small cell lung carcinoma cell line H1299 for the xenotransplantation into zebrafish experiments in paper 1. The H1299 cells were chosen because they have known invasion/metastasis potential and have been successfully used for similar experiments in previous studies (Moshal et al., 2011; Paul et al., 2015; Vaughan et al., 2015). In both paper 1 and 3, several of the experiments were repeated with different cell lines to verify that the results were not particular for only a specific cell type. For example, the results from the migration assays initially performed on U2OS cells in Paper

1 were confirmed using RPE-1 cells. In paper 3, we confirmed the localization of IFT27 to the midbody and its effect on cell proliferation in both HeLa and U2OS cells.

In paper 2, we used primary cells, namely monocyte-derived DCs (MDDCs) and bone marrow-derived DCs (BMDCs) for our experiments. These cells provide a more physiologically relevant model, as they are obtained from fresh, healthy tissues and are not immortalized. However, for this reason the amount of cells available for each experiment is limited. Furthermore, primary cells are more challenging to transfect than standard cell lines.

To obtain MDDCs, we used monocyte precursors from buffy coats from human blood donors. For the BMDCs, we used the bone marrow of C57BL/6 mice. The cells were grown in culture medium supplemented with specific cytokines to generate DCs. In the body, there are many different subtypes of DCs that can be classified based on their location, properties and transcriptional profiles. Monocytes can give rise to functionally different DCs depending on the cytokine mix added. Therefore, the cytokines should be chosen so that the type of DCs generated best fits the purpose of the experiment (Cechim and Chies, 2019). The most commonly used cytokines for generating MDDCs is a mix of interleukin 4 (IL-4) and granulocyte-macrophage colony-stimulating factor (GM-CSF), which was used in our experiments in paper 2. These cytokines inhibit the monocytes from differentiating into macrophages (Cechim and Chies, 2019). For the BMDCs, it is common to use GM-CSF only to generate DCs, and we followed a protocol used in previous studies where BMDC migration was investigated (Chabaud et al., 2015a; Faure-André et al., 2008; Vargas et al., 2016b). To generate mature DCs, different agents can be used, including inflammatory signals such as tumor necrosis factor (TNF) and bacterial derivatives (Brunner et al., 2000; Han et al., 2009; Jonuleit et al., 1997; Zobywalski et al., 2007). In our experiments, we used the bacterial derivative LPS, which is one of the most widely used agents to stimulate DC maturation (Alloatti et al., 2016; Bretou et al., 2017; Granucci et al., 1999; Vargas et al., 2016b). LPS is a molecule present on the outer surface of almost all Gram-negative bacteria, and induces DC maturation by stimulating TLR4 signaling (Michelsen et al., 2001; Park and Lee, 2013).

Methods to deplete proteins

A typical way to study the function of a particular protein is to deplete the protein of interest from cells and investigate the consequences of this depletion. RNA interference (RNAi) is a fast and effective method for this purpose (Dana et al., 2017). This method takes advantage of a biological process in which double-stranded RNA is involved in specific suppression of gene expression. By introducing specific small interfering RNA (siRNA) molecules into cells, it is possible to prevent the translation of a protein of interest. The siRNA molecules can be delivered through lipid transfection reagents, electroporation or via the use of viruses. The latter method can be effective for cells that are difficult to transfect, but requires strict laboratory safety procedures. Lipid-based transfection is fast and easy to perform, and was used for all our experiments with cell lines. However, these reagents are not suitable for the primary immune cells used in paper 2. For these cells, we instead used electroporation to transfect cells. Even though this method works on primary cells, the silencing efficiency is much lower compared to what was achieved in cell lines.

A major concern that needs to be addressed in all experiments using RNAi, is the risk of off-target effects (Cullen, 2006; Neumeier and Meister, 2021; Seok et al., 2018). Off-target effects can occur when the siRNA used also targets other genes than the one it was designed to target, thus affecting their expression. The best way to control the specificity of an effect caused by RNAi silencing, is through rescue experiments (Cullen, 2006). In these experiments, cells are first depleted of the protein of interest with siRNAs, before the protein is re-introduced through transfection with a DNA construct. If the re-introduction of the gene abolishes the effect caused by silencing, this is a strong indication that the effect is specific. This control was included for several of the experiments in paper 1. However, rescue experiments can be difficult to include if the transfection efficiency is low, as was the case in paper 2 where we used primary cells. In paper 3, rescue experiments were also challenging due to the cell-cycle dependent expression of the protein. An alternative to rescue experiments is to verify the effects caused by silencing using different siRNA molecules that target non-overlapping regions of the gene of interest. In many of the experiments included in this thesis, we compared the effects in two groups of silenced cells, where we used two different siRNA sequences to target the protein of interest. When using RNAi, there could also be non-specific effects related to the siRNA delivery method. Therefore, we included a negative control using an siRNA that does not target a specific gene in all RNAi experiments in this thesis.

The effect of RNAi is only temporary, and the protein of interest is not completely depleted. Therefore, it is often referred to as a gene knockdown. A gene knockout, on the other hand, involves modifications to the DNA of the organism that causes the gene of interest to be completely removed. Due to the challenges associated with transfecting primary cells in paper 2, we also used knockout cells from genetically modified mice. The mice used were so-called conditional knockout mice, as the *Rab7b* gene was not removed from all cells in the organism. Instead, the gene was depleted specifically from cells positive for CD11c, which includes BMDCs. The advantage of using a conditional knockout is that it only affects the cells of interest. This allows the cells to develop within a normal physiological environment. In terms of animal welfare, there is also a lower risk that the knockout will affect the health and wellbeing of the animal, compared to when a complete knockout is introduced.

Microscopy

The microscope is one of the most important tools in cell biology. In the papers included in this thesis, we used various techniques of advanced light microscopy, including laser scanning confocal microscopy, spinning disk confocal systems, super-resolution microscopy, fluorescence resonance energy transfer (FRET) microscopy, total internal reflection fluorescence (TIRF) microscopy and optical tweezers.

In confocal microscopy, laser light is used to excite fluorescent molecules. The emitted light passes through a pinhole that cuts off signals that are out of focus, so that only a thin plane at a specific depth of the sample is imaged. This offers a major advantage compared to conventional wide field fluorescence microscopy, where light collected from below and above the focal plane generates blur and a higher background.

In laser scanning confocal microscopy, the sample is scanned point-by-point using a focused laser beam. The laser scanning instruments allow very thin optical sectioning and high resolution. However, it can be time consuming to produce images. For high-speed imaging of fast moving objects, a spinning disk system may provide a better alternative. In this system, a rotating disk with a pattern of hundreds of pinholes is used. The pinholes are arranged so that every part of the image is scanned while the disk is spinning. This improves the speed of image acquisition and reduces photo damage. However, the spinning disk systems cannot deliver as

thin optical sections as the laser scanning systems. There are thus advantages and disadvantages with both these types of confocal microscopes. We used both laser scanning and spinning disk confocal microscopes in all three papers included in this thesis. Spinning disk microscopes were used to image fast intracellular events such as the movement of vesicles (Paper 1) and macropinosome dynamics (Paper 2). In addition, we used a spinning disk microscope for time-lapse imaging over several hours to study cell division, since this microscope allowed us to use lower laser power and thus reduces photo toxicity (Paper 3).

The resolution of optical microscopes is limited by the diffraction of light. Consequently, the smallest resolvable distance between two points cannot be less than half the wavelength of the imaging light. This means that the resolution is limited to around 200 nanometers in conventional confocal microscopes (Sigal Yaron et al., 2018). However, it is possible to overcome this limit through different techniques known as super-resolution microscopy. In paper 2, we took advantage of the Airyscan detector from Zeiss to achieve super-resolution. Instead of a physical pinhole, this system uses a 32-element detector array where each detector element behaves as a pinhole of very small diameter. The system combines this with linear deconvolution to achieve an almost two-fold increase in resolution in all three spatial dimensions. By using this system in Paper 2, we could study the intracellular localization of Rab7b and TRMPL1 in DCs in more detail, and distinguish small vesicles. In Paper 3, we used the super-resolution mode to image GFP-IFT27 in U2OS in order to make an accurate 3D reconstruction of its localization to the midbody ring.

Confocal microscopy makes it possible to determine if two proteins share the same intracellular location. However, protein interactions happen at a few nanometers range. Advances in super-resolution technologies has made it possible to reach resolutions of tens of nanometers, but to detect interactions that occur at length scales below 10 nanometers, FRET microscopy can be used (Grecco and Verveer, 2011). FRET microscopy is suitable for studying intermolecular associations, detect conformational changes of proteins and investigate other biological phenomena that produce changes in molecular proximity (Grecco and Verveer, 2011) (Figure 9).

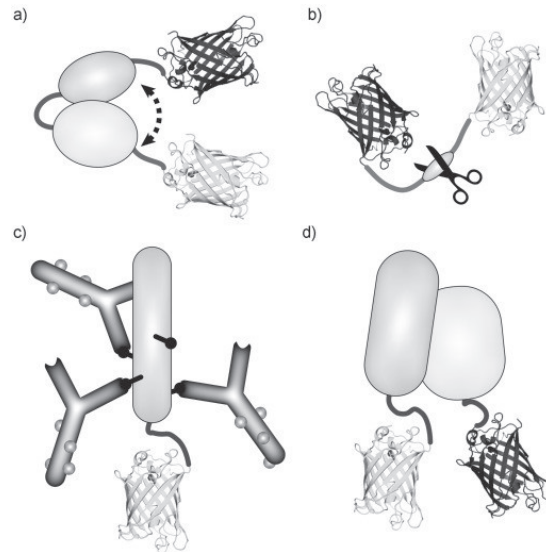


Figure 9: Examples of FRET sensors. A) FRET sensor to detect a conformational change. A conformational change in the linking proteins causes a change in the distance and orientation between the donor and acceptor fluorophores, producing a FRET signal. B) A FRET sensor to detect cleavage. When the linker between the donor and acceptor fluorophores is cleaved by a protease, there is a loss of FRET signal. C) FRET between a donor fluorophore and multiple acceptors occurs on binding of the probe molecule. D) FRET to detect interactions between two different proteins labelled with donor or acceptor fluorophores. Figure from (Grecco and Verveer, 2011).

The technique is based on a physical process by which energy is transferred from an excited donor fluorophore to an acceptor fluorophore. When the donor fluorophore is excited by a laser, it may transfer its excitation energy non-radiatively to a nearby acceptor through long-range dipole-dipole interactions (Deal et al., 2020; Grecco and Verveer, 2011). This process, called FRET, will cause the donor channel signal to be quenched and while the acceptor channel signal increases. The occurrence of FRET is often measured by exciting the donor fluorophore, determining the emission of the donor and the acceptor, and plotting the ratio of the two in each pixel of the image.

In paper 1, we used a biosensor based on FRET to detect Cdc42 activity. The conformational change associated with GTP binding brings the two fluorescent proteins of the biosensor in close proximity and produces a FRET signal. It is thus possible to detect the regions in which Cdc42 is active (GTP-bound) within the cell.

Another specialized microscopy technique we used in paper 1 is total internal reflection fluorescence (TIRF) microscopy, also known as “evanescent wave microscopy”. This technique was developed in the early 1980s and provides a way to selectively excite fluorophores in close proximity to a solid surface, without exciting fluorescence in regions

farther from the surface (Axelrod, 1981). TIRF microscopy takes advantage of the refractive index differences between the glass and the cell interior, which regulates how light is refracted or reflected at the interface. The excitation light travels through a solid medium (i.e. a glass coverslip) at an angle large enough for the beam to totally internally reflect (TIR) rather than refract through the surface. This generates a thin electromagnetic field capable of exciting fluorophores near the surface (Axelrod, 2001). It is thus possible to image fluorophores near the cover glass interface with a high signal-to-noise ratio, making TIRF microscopy ideal for studying events that occur at the plasma membrane of cells. Examples of phenomena that are well suited to study using TIRF microscopy include endocytosis, exocytosis, and focal adhesion dynamics (Poulter et al., 2015). In paper 1, we used TIRF microscopy to study the movement of Rab6-positive vesicles toward the cell surface and filopodia.

Finally, in paper 1 we used optical tweezers to investigate filopodia dynamics. Optical tweezers is a tool that takes advantage of the ability of light to exert force on matter, and uses focused laser beams to precisely manipulate small objects (Ashkin et al., 1986; Choudhary et al., 2019). Advances in optical tweezers has made it possible to measure down to piconewton forces, and movements on the angstrom scale (Choudhary et al., 2019). We used optical tweezers in paper 1 to measure forces exerted by filopodia on optically trapped beads and the retraction velocity of these dynamic actin-based protrusions.

Cell migration studies

In paper 1 and 2, we used different methods to study cell migration. One of the most commonly used methods is the wound healing assay, which we used in paper 1. To perform the assay, a confluent layer of cells is scratched to remove cells from a defined area of the dish. The scratch area is then monitored over time as the remaining cells start to migrate in order to close the artificial wound. To generate wounds of equal sizes, we used the IncuCyte Wound Maker tool. After time-lapse imaging, we performed two types of analysis. Firstly, the cell confluency in the wound area was estimated by automated analysis using the IncuCyte software. Secondly, we manually tracked single cells to determine the cell speed and directionality. In this way, we could exclude effects of cell proliferation and variations in wound size.

The wound healing assay is easy to perform, can be used for many different cells and is reproducible (Kauanova et al., 2021). However, since the cells move on a flat glass or plastic surface, it does not reflect well how cells migrate in the complex three-dimensional environment of body tissues. Indeed, this method is not suitable to study the adhesion-independent amoeboid motility mode used by DCs (Heuze et al., 2013; Lämmermann et al., 2008). Therefore, we used different migration assays to study immune cell migration in paper 2.

One of the tools used in paper 2 to study migration of DCs in confined environments was microfabricated channels (Vargas et al., 2016a; Vargas et al., 2014). In this system, microfabricated chambers are made using the gas-permeable polymer polydimethylsiloxane (PDMS) and attached to a glass coverslip to create 3D channels with specified dimensions (e.g. 5 x 5 or 5 x 8 μm). Before use, the channels are coated with extracellular matrix proteins such as fibronectin. As cells are loaded into central chambers, they will spontaneously enter the channels and can be imaged while they migrate in this confined environment (Figure 2).

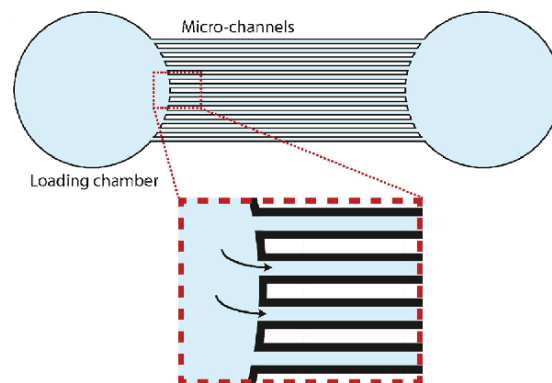


Figure 10: Microchannels to study migration in a confined environment. Cells are loaded into the loading chamber before they spontaneously enter the microfabricated channels. Figure modified from (Vargas et al., 2016a).

Using this system, we could measure cell speed as well as changes in direction in paper 2. Another advantage of using microchannels is that the cells are forced to adopt similar shapes, making it possible to generate average protein distribution maps and more easily compare cells under different conditions. However, the cells can only move along one line in the microchannels, and it is thus not the optimal system for measuring effects on cell directionality. For this reason, we also used a different cell migration assay in paper 2, namely the collagen migration assay. In this assay, we seeded cells in 3D collagen gels to mimic the environment between cells in tissues, and the cells could freely move in all directions. By adding the

chemoattractant chemokine (C-C motif) ligand 21 (CCL21) to the cell medium surrounding the gels, we stimulated the DCs to move in a specific direction, and could measure their persistency toward the target by single cell tracking. One problem using this assay is the possibility of variability in the collagen matrix structure, since the polymerization is sensitive to both pH, temperature and time (Sung et al., 2009). It is thus important to keep the procedure for collagen gel preparation as similar as possible for each experiment.

In paper 1, we also performed *in vivo* cancer cell invasion experiments. For these xenotransplantation experiments, we used zebrafish embryos and injected H1299 cancer cells into the otic vesicle. The cancer cells were stained so that we could identify them as they migrated into the surrounding tissues. In this way, we could confirm that the effect on cell migration by *in vitro* experiments was also relevant for migration *in vivo*. Even if this type of xenotransplantation experiment involves human cancer cells injected into a fish, and thus does not reflect a normal physiological setting, this is a widely used method (Hason and Bartůněk, 2019; Zampedri et al., 2021; Zhang et al., 2015). While traditional assays using immunosuppressed mice can be time-consuming and expensive, the zebrafish model provides a fast and cost-effective alternative (Teng et al., 2013). Since zebrafish embryos lack adaptive immunity, this allows the transplanted human cells to survive and spread (Astell and Sieger, 2020). Furthermore, transparency of the zebrafish embryos make them well suited for imaging, and the movement of fluorescently labeled cells can easily be tracked (Hason and Bartůněk, 2019).



Discussion and future perspectives

Members of the Rab family of GTPases are most known as key regulators of intracellular trafficking, controlling all steps from vesicle formation to movement, docking and fusion. Their ability to regulate and coordinate these processes relies on interactions with a broad range of effector proteins, such as adaptors, tethers, motor proteins and kinases (Zhen and Stenmark, 2015). Increasing evidence demonstrates that the interactions between Rab proteins and their effectors is important not only for vesicular transport, but also for many other cellular processes. In this thesis, we have studied Rab6 and Rab7b, as well as the Rab-like GTPase IFT27. Our work has given new insight into how these small GTPases are involved in the processes of cell migration and proliferation.

1. Rab proteins in cytoskeletal remodeling

1.1 Rab6 in cell migration

In paper 1, we found a novel role for Rab6 in the regulation of cell migration and invasion. Several Rabs have been shown to affect cell migration and invasion by controlling the transport of adhesion molecules such as integrins (Allaire et al., 2013; Jeong et al., 2018; Kessler et al., 2012; Pellinen et al., 2006). It is likely that also Rab6, as an important regulator of several transport pathways connected to the Golgi, could influence migration indirectly through this role. Indeed, knockdown of Rab6 has been shown to affect the function and distribution of $\beta 1$ integrin (Shafaq-Zadah et al., 2016). Recently, Rab33b, another Golgi-associated Rab, was shown to regulate cell migration (Bjørnstad et al., 2022). Similar to Rab6, depletion of Rab33b promotes cell migration and delays protein secretion. Bjørnstad et al. found that Rab33b regulates focal adhesion dynamics by controlling the delivery of cargo such as integrins to the adhesion sites. It is possible that Rab6, similar to Rab33b, also affects cell migration through its role in the secretory pathway. In support of this hypothesis, Rab6 was shown to regulate the transport of various cargos toward focal adhesion sites (Fourriere et al., 2019). However, our study shows that Rab6 can also affect cell migration by interfering with actomyosin dynamics.

We identified Cdc42 as an interactor of Rab6 and demonstrated that Rab6 modulates the activity of this Rho GTPase at the cell periphery. This provides a new example of crosstalk between a Rab and a Rho GTPase. The role of Rho GTPases in regulation of actin dynamics is well established, while the contribution of Rab GTPases to this process is less characterized. An increasing number of studies report that Rab proteins can regulate the activity of Rho GTPases and in this way influence actin-dependent processes (Borg et al., 2014; Bryant et al., 2010; Palamidessi et al., 2008; Sun et al., 2005a; Wang et al., 2016). The molecular mechanisms underlying this crosstalk are currently not well understood. Our finding that Rab6 also interacts with Trio demonstrates how Rabs could modulate Rho GTPase activity through recruitment of their GEFs. This is consistent with what was described for Rab 5 and Rac (Palamidessi et al., 2008), where Rab5 recruits the GEF for Rac to ensure a precise spatial and temporal activation of the Rho GTPase. Rab proteins can also recruit GAPs for Rho GTPases to modulate their activity. For example, Rab27a recruits Slp1, which in turn interacts with the RhoA GAP Gem-interacting protein (GMIP) (Johnson et al., 2012). In this way, Rab27a can downregulate RhoA, which in turn promotes local actin depolymerization. Other ways of regulation may also exist, and the relationship between Rho and Rab GTPases should be further investigated to fully understand the processes that they are involved in.

In addition to modulating Cdc42 activity, we found that Rab6 influences myosin II phosphorylation. Rab6 interacts directly with myosin II, and through this interaction mediates the fission of transport vesicles from the Golgi (Miserey-Lenkei et al., 2010). However, since myosin II is important for cytoskeletal dynamics, this interaction could also be linked to the role of Rab6 in cell migration. Indeed, another Rab that interacts directly with myosin II, Rab7b, plays a dual role in both intracellular trafficking and cell migration (Borg et al., 2014). How depletion of Rab6 causes a decrease in myosin II phosphorylation needs to be further investigated, but it is possible that it occurs via the interaction with Cdc42. Indeed, Cdc42 is known to regulate kinases and phosphatases that can control myosin II phosphorylation (Edwards et al., 1999; Manser et al., 1994; Vicente-Manzanares et al., 2009).

Cell migration is a process that requires tight temporal and spatial regulation. By ensuring that Cdc42 is activated at the correct localization at the right time, Rab6 could influence myosin II phosphorylation and in this way ensure that the actomyosin dynamics are properly controlled. Using a FRET-based biosensor for Cdc42, we found an increase in Cdc42 activity at the cell periphery when Rab6 is silenced. Activation of Cdc42 in this region promotes the formation of

filopodia (Ridley, 2015b), and in line with this we found an increase in the number of filopodia and the amount of F-actin in Rab6-depleted cells. We also showed that Cdc42 is present on Rab6-positive vesicles that move toward the cell periphery, and that knockdown of Rab6 increased the percentage of Cdc42-positive vesicles in the front of migrating cells. It is therefore possible that Rab6 is involved in regulating the localization of Cdc42, ensuring that the correct amount of active Cdc42 is present at the leading edge of migrating cells.

1.2 Rab6 in cancer metastasis

Dysregulation of cell migration can cause several diseases and drive tumor metastasis. The *in vivo* experiments we performed in Paper 1 demonstrate the relevance of Rab6-mediated control of cell migration in cancer. Indeed, knockdown of Rab6 resulted in increased invasion of cancer cells xenotransplanted in zebrafish embryos. This could be linked to Rab6 role in modulating Cdc42 activity, since deregulation of Rho family members in cancer cells is associated with increased motility and invasiveness (Crosas-Molist et al., 2021; Porter et al., 2016). In particular, Cdc42 is upregulated in several types of human cancers, and inappropriate activation of Cdc42 contributes to oncogenesis (Stengel and Zheng, 2011). Also, Cdc42 is involved in the formation and regulation of protrusions associated with invasion and metastasis (Stengel and Zheng, 2011). Increased filopodia formation has also been shown to drive cancer cell invasion (Jacquemet et al., 2015). Therefore, it is likely that in the absence of Rab6, over activation of Cdc42 increases cell migration and invasion by promoting protrusion formation. Several Cdc42 GEFs are also altered in cancers, including Trio (Murphy et al., 2021). In fact, targeting Trio and other GEFs that activate Cdc42 has been proposed as a strategy for cancer therapy (Maldonado et al., 2020). Stimulation of Rab6 activity could provide an alternative target. Indeed, in line with our results from paper 1, reduced expression of Rab6 promotes cancer, as a microRNA that decreases Rab6 expression is highly expressed in various lung cancer tissues (Huang et al., 2015).

1.3 The role of Rab7b in DC maturation

In paper 2, we explored the role of Rab7b in DCs. From previous studies, we knew that Rab7b is highly expressed in these immune cells, and that a burst of expression occurs during LPS-induced maturation (Berg-Larsen et al., 2013; Yang et al., 2004). Why DCs upregulate the expression of Rab7b during maturation was unknown. Therefore, we investigated whether

Rab7b is involved in regulating the functions that are important during DC maturation, such as antigen uptake, antigen presentation and cell migration. While we did not observe differences in antigen presentation ability in DCs silenced for Rab7b, cell migration was inhibited. Furthermore, DCs lacking Rab7b sustained their macropinocytic activity after LPS-induced maturation. Since Rab7b interacts directly with myosin II, and in this way influences both intracellular transport and actin remodeling (Borg et al., 2014), we investigated whether this interaction could be important for these two functions of DCs.

Myosin II plays a crucial role in antigen uptake through macropinocytosis and cell migration. DCs use an amoeboid-like migration strategy, which depends on contractile forces driven by myosin II (Chabaud et al., 2015b; Lämmermann et al., 2008). Upon maturation, in order to migrate fast and persistently, DCs increase the amount of actin and myosin at the cell rear (Vargas et al., 2016b). During macropinocytosis, which mainly occurs in immature cells, the DCs concentrate actin and myosin at the cell front. Myosin II at the cell front is crucial for the formation of macropinosomes, and allows the transport of engulfed antigens towards lysosomes (Chabaud et al., 2015b). Thus, by reorganizing their actin cytoskeleton, the DCs can alternate between efficient migration and antigen capture. As the DCs mature, they switch to a faster and more persistent migration mode and reduce their macropinocytic activity (Chabaud et al., 2015b; Vargas et al., 2016b). Our experiments in paper 2 demonstrated that cells lacking Rab7b moved slower and less persistently, and had increased macropinocytic activity. The Rab7b knockout cells also had more actin and myosin in the front compared to wild type cells. Furthermore, depletion of Rab7b caused defects in polarization. This suggests that Rab7b is involved in regulating the distribution of actin and myosin in DCs. The strong increase in Rab7b expression upon DC maturation could thus be necessary for the actomyosin rearrangements required for the switch from antigen capture to fast cell motility.

1.4 Rab7b as a physical link between lysosomes and myosin II

From previous studies in cell lines, it is known that Rab7b localizes to and regulates the transport to the late endocytic/lysosomal compartments (Progida et al., 2010). In addition, Rab7b directly binds myosin II only in its active, GTP-bound form (Borg et al., 2014), and as a consequence it specifically recruits the motor protein when bound to membranes. Therefore, it is likely that Rab7b is involved in the recruitment of myosin II from macropinosomes to lysosomes in DCs, and thus also in the transport of internalized antigens toward late endocytic

compartments. This could provide an explanation for why macropinocytosis is retained when Rab7b is absent, since the myosin II is not properly redistributed to the rear of Rab7b KO-cells where the lysosomes are concentrated. We also found that lack of Rab7b reduces myosin II phosphorylation at the cell rear, confirming that Rab7b controls actomyosin dynamics by regulating local myosin phosphorylation.

Our findings in Paper 2 show that the link between Rab7b, myosin and lysosomes is important for the signaling events associated with DC maturation. A previous study demonstrated that when DC maturation is triggered, the lysosomes release calcium via the channel TRMPL1, which in turn activates myosin II at the cell rear to promote fast migration (Bretou et al., 2017). However, how lysosomes are associated with myosin II was unknown. We found that Rab7b interacts with TRMPL1, and therefore propose that Rab7b functions as a physical link between the lysosomal calcium channel TRMPL1 and myosin II. According to our model, Rab7b brings myosin II in close proximity to TRPML1, so that it can be activated by the local calcium release from this channel at the cell rear.

1.5 Relevance of Rab7b in immune cells

DCs are used for cell vaccines in cancer immunotherapy (Filin et al., 2021; Yu et al., 2022). However, the clinical efficacy of this type of therapy needs to be improved. A major challenge with DC vaccines is that only a limited number of injected DCs migrate to the lymph node, where they can present their antigens to T cells and initiate an immune response (Perez and De Palma, 2019; Verdijk et al., 2009). It is therefore of particular interest to improve our knowledge on the molecular mechanisms that underlie DC motility. This knowledge can then be applied to engineer DCs that migrate more efficiently to lymph nodes (Perez and De Palma, 2019). Our work provides important pieces of information to this field, showing that Rab7b is required for fast and efficient migration of DCs *in vitro*. However, in order to fully understand the physiological role of Rab7b, *in vivo* experiments such as footpad injections of labelled DCs (Vargas et al., 2016b) and ear paintings with imiquimod (Baptista et al., 2016; Oliveira et al., 2022) should be performed to determine if the migration of DCs through complex tissues is similarly affected.

Further studies could also elucidate additional pathways regulated by Rab7b. For example, Rab7b has been shown to regulate TLR4 and TLR9 signaling in immune cells (Wang et al., 2007; Yao et al., 2009), but the molecular mechanisms behind this regulation are not fully

characterized. Wang et al. found that the amount of TLR4 on the plasma membrane increases after Rab7b knockdown, and the receptor remains for a longer time in early and late endosomes (Wang et al., 2007). They suggested that Rab7b promotes the translocation of TLR4 into lysosomes, but how Rab7b mediates this transport is not known. Similarly, Yao et al. showed that Rab7b regulates TLR9 signaling, possibly by transporting the receptor into lysosomes for degradation (Yao et al., 2009). Since TLRs are important for activating immune cell responses, it would be interesting to further explore how Rab7b regulates TLRs in DCs and other immune cells. This could provide important answers to why these cell types in particular express Rab7b, and deepen our understanding of the functions of this small GTPase.

2. IFT27 in cell division

2.1 Regulation of Rab-like proteins

In paper 3, we studied the role of IFT27 in mammalian cell division. This small GTPase is considered an extended member of the Rab family, and is also known as Rab-like protein 4 (RABL4). The Rab-like proteins contain a GTPase domain, but lack the C-terminal prenylation motif required for membrane insertion (Yan and Shen, 2021). This suggests that the Rab-like proteins work in a different manner than the classical Rabs, which cycle between membranes and the cytosol. Little is known about how the Rab-like proteins perform their function, as they have received less attention than the typical members of the family. It is still possible that Rab-like proteins can associate with membranes via interactions with membrane-bound proteins. IFT proteins could also associate with non-membrane-bound organelles. For example, we found that IFT27 localizes to centrosomes. We also discovered that IFT27 interacts with the centrosomal protein CENPJ in a nucleotide-independent manner. Previously identified effectors of IFT27, including IFT25 and Arl6, also bind IFT27 independently of GTP (Liew et al., 2014). This further indicates that Rab-like GTPases may be regulated in a different way than by the classical GTP/GDP, membrane/cytosol cycle. One possibility is that their functions are regulated by post-translational modifications such as phosphorylation. Indeed, phosphorylation is emerging as an essential regulatory mechanism of Rab function (Homma et al., 2021; Xu et al., 2021). Several Rab proteins are phosphorylated in their switch II regions by the leucine-rich repeat kinase 2 (LRRK2) (Steger et al., 2016), and this phosphorylation can affect their binding to effector proteins. For example, the primary ciliogenesis regulator

RILPL1 specifically interacts with the LRRK2-phosphorylated forms of Rab8A and Rab10 (Steger et al., 2016). It is therefore possible that phosphorylation of IFT27 could similarly control when and where it interacts with its specific effectors.

2.2 IFT27 as a regulator of cell division

IFT27 is a poorly characterized protein, and its functions have mostly been studied in unicellular organisms. The majority of literature on IFT27 has looked at its role in ciliary transport and function, although a few early studies suggested an additional role in cell cycle regulation (Qin et al., 2007; Wood et al., 2012). Recently, it is becoming increasingly clear that many of the IFT proteins have dual roles in ciliary transport and cell cycle regulation (Doornbos and Roepman, 2021; Izawa et al., 2015; Vertii et al., 2015). Indeed, the cell reuses many of the components of the primary cilium as it prepares to divide. The centriole, for example, functions both as the basal body of the cilium, and as an organizer of the mitotic spindle in dividing cells. Our finding that IFT27 regulates cell division adds further support to this emerging view.

Our experiments in paper 3 show that IFT27 localizes to the midbody, and that its depletion causes increased cell proliferation. Furthermore, we show that IFT27 levels increase during cell division, with a burst of expression occurring during cytokinesis. Intriguingly, we found that cytokinesis is delayed in cells overexpressing GFP-IFT27. While the cells overexpressing IFT27 progressed normally through telophase and were able to form midbodies, they remained connected for an extended period before abscission. This suggests that IFT27 is involved in regulating the timing of abscission. How IFT27 controls this process needs to be further investigated, but our identification of CENPJ as a novel interactor of IFT27 could provide important answers. Similar to IFT27, CENPJ localizes to the midbody during cytokinesis. Previous evidence indicates that CENPJ may play a role in cytokinesis, but its role in this process remains to be characterized (Chou et al., 2016). One possibility is that CENPJ regulates the stability of the microtubules in the intercellular bridge, as it binds tubulin and regulates microtubule nucleation and stabilization (Hung et al., 2004). In this way, IFT27 could control the stability of the intercellular bridge via interactions with CENPJ. The tubulin binding properties of CENPJ are affected by its phosphorylation status, and it would thus be interesting to investigate whether IFT27 recruits a kinase to this interactor.

From previous work, it is known that IFT27 binds the Aurora B kinase (Taulet et al., 2017). Whether Aurora B is involved in CENPJ phosphorylation is unknown. However, the

structurally similar kinase Aurora A has been shown to phosphorylate CENPJ at Ser 467 during mitosis (Chou et al., 2016). Both Aurora A and Aurora B localize to the midbody during cytokinesis (Afonso et al., 2017), and *in vitro* studies have shown that they have common substrates (Magnaghi-Jaulin et al., 2019). It is thus possible that IFT27 recruits either Aurora A or Aurora B to phosphorylate CENPJ in the midbody. The activity of the Aurora kinases themselves is also controlled by phosphorylation (Carmena et al., 2009), and IFT27 could interact with further kinases to control the activities of both CENPJ and Aurora B in time and space. If IFT27 indeed is involved in regulating the activation of Aurora B, this could provide an explanation for the delay in abscission we observed upon overexpression of the GTPase. Aurora B kinase is involved in many steps of cell division, including a checkpoint occurring just before abscission (Lens and Medema, 2019; Petsalaki and Zachos, 2021; Steigemann et al., 2009). Normally, Aurora B is inactivated by dephosphorylation at the end of cytokinesis, but in cases where the chromosomes are not properly segregated, the kinase remains active and delays abscission. It is possible that overexpression of IFT27 leads to over activation of Aurora B and in this way delays completion of cytokinesis in a similar manner as when the abscission checkpoint is triggered.

There are differences in the cell division machinery of complex multicellular organisms and that of a single celled organism such as the algae *Chlamydomonas reinhardtii*. Nevertheless, we found several similarities between our studies of IFT27 in HeLa cells, and previous reports of *Chlamydomonas* cell division. Similar to reports by Wood et al. on *Chlamydomonas* (Wood et al., 2012), we observed that IFT27 accumulates in the cleavage furrow and is strongly upregulated in dividing cells. This suggests that some of the functions of IFT27 in cell division are evolutionary conserved. However, the midbody has only been described in animal cells, while other eukaryotic cells form different types of structures at the end of division (Eme et al., 2009). These structures include the chitin-rich septum formed at the division site of fungi, and the phragmoplast in plants, which serves as a scaffold for the formation of a new cell wall (Eme et al., 2009). Little is known about the mechanisms behind abscission in *Chlamydomonas*, but it is possible that IFT27 plays similar roles in the algae and in mammalian cells. Even though IFT27 is present in most ciliated organisms, there are species that lack this GTPase, including *Drosophila melanogaster* and *Caenorhabditis elegans* (Yan and Shen, 2021). It would be interesting to compare the cell division machineries of different organisms with and without IFT27, to understand why some of them lost this GTPase as they evolved. Since abscission remains the least understood step of cytokinesis in all organisms (Frémont and Echard, 2018),

further investigation of the role of IFT27 in this process could provide valuable new insights into this process.

2.3 IFT27 in diseases

Ever since it became clear that primary cilia are connected to a group of severe diseases known as ciliopathies, this previously overlooked organelle has received increasing attention. Many of the symptoms associated with ciliopathies have been explained by defects in signaling pathways connected to primary cilia, such as the Hedgehog pathway. However, the fact that ciliary proteins have additional roles in the cell adds another layer of complexity to our understanding of these diseases. For example, Bardet Biedl syndrome, which can be caused by the mutations in IFT27 we studied in Paper 3, is often associated with cognitive impairment and developmental delays (Chandra et al., 2021). It is known that cell proliferation needs to be tightly controlled as the brain forms, and regulation of abscission timing has been suggested to control brain growth and structure (Homem et al., 2015; McNeely and Dwyer, 2020). Our study revealed that BBS-associated variants of IFT27 cause defects in cytokinesis. It is therefore tempting to speculate that these defects could affect brain development. Furthermore, mutations in the IFT27 interactor CENPJ have been linked to the neurodevelopmental disorder microcephaly, which is characterized by reduced brain size (Bond et al., 2005; Faheem et al., 2015). This further suggests that alterations in the IFT27-CENPJ regulation of cell division can also contribute to developmental defects.

That IFT27 regulates cell division could have implications for cancer. Indeed, several BBS genes have been linked to renal cancer (Beales et al., 2000). Since silencing of IFT27 increases proliferation, this suggests that IFT27 may function as a brake in cell division and prevent uncontrolled growth. Furthermore, cytokinesis defects similar to the ones we observed for the disease variants of IFT27 are connected to tumorigenesis. The generation of tetraploid cells after failed cytokinesis can function as a starting point for generating cells with abnormal chromosome content, which is thought to contribute to cancer development (Lens and Medema, 2019). IFT27 could also influence cancer development through its interaction with CENPJ, since overexpression of CENPJ has been shown to increase tumor growth, angiogenesis and metastasis (Chen et al., 2020). Furthermore, the link between IFT27 and Aurora B is also interesting for cancer research. Overexpression of Aurora B has been observed in many tumors, and the kinase is considered an attractive drug target for cancer therapy (Ahmed et al., 2021;

Borah and Reddy, 2021; Yeung et al., 2008). Various inhibitors of Aurora B, such as barasertib, have been tested in clinical trials (Borah and Reddy, 2021). Interestingly, Aurora B inhibitors can cause impairments in cytokinesis and induction of polyploidy (Oke et al., 2009; Shamsipour et al., 2014). Understanding more about the interaction between Aurora B and IFT27 in cytokinesis will provide important knowledge that may be used in drug development.

3. Concluding remarks

The work of this thesis sheds new light on the many and diverse roles of Rab proteins. In paper 1, we found a novel role of Rab6 in cell migration, and provided a new example of how crosstalk between Rho and Rab GTPases can influence this process. Furthermore, we demonstrated that Rab6 regulates cancer cell invasion. In paper 2, we characterized the specific role of Rab7b in DCs, and proposed a model in which Rab7b functions as a physical link between lysosomes and the actomyosin cytoskeleton. By controlling lysosomal signaling and local activation of myosin II, Rab7b regulates the migration of these specialized immune cells. In paper 3, we discovered a novel role of IFT27 in cytokinesis and for the first time described the localization of this protein to the midbody. We also demonstrated that disease variants of IFT27 cause defects in cytokinesis, which sheds new light on our understanding of Bardet Biedl-syndrome.

Common to all these studies is the fact that the cell uses the same proteins in different pathways and processes. Therefore, to completely understand different cellular processes, we should not only study them as separate systems, but look at how they are interconnected. How the cell manages to coordinate all its complex processes so elegantly remains one of the most fascinating mysteries of biology, and many questions remain unanswered. By characterizing the diverse functions of Rab proteins, we gain a deeper understanding of how the cell can coordinate different processes in time and space. Ultimately, this new knowledge can be used to improve how we treat diseases such as immune disorders, ciliopathies and cancer.

References

- Afonso, O., A.C. Figueiredo, and H. Maiato. 2017. Late mitotic functions of Aurora kinases. *Chromosoma*. 126:93-103.
- Ahmed, A., A. Shamsi, T. Mohammad, G.M. Hasan, A. Islam, and M.I. Hassan. 2021. Aurora B kinase: a potential drug target for cancer therapy. *Journal of Cancer Research and Clinical Oncology*. 147:2187-2198.
- Aldahmesh, M.A., Y. Li, A. Alhashem, S. Anazi, H. Alkuraya, M. Hashem, A.A. Awaji, S. Sogaty, A. Alkharashi, S. Alzahrani, S.A. Al Hazzaa, Y. Xiong, S. Kong, Z. Sun, and F.S. Alkuraya. 2014. IFT27, encoding a small GTPase component of IFT particles, is mutated in a consanguineous family with Bardet-Biedl syndrome. *Hum Mol Genet*. 23:3307-3315.
- Allaire, P.D., M. Seyed Sadr, M. Chaineau, E. Seyed Sadr, S. Konefal, M. Fotouhi, D. Maret, B. Ritter, R.F. Del Maestro, and P.S. McPherson. 2013. Interplay between Rab35 and Arf6 controls cargo recycling to coordinate cell adhesion and migration. *Journal of cell science*. 126:722-731.
- Alloatti, A., F. Kotsias, J.G. Magalhaes, and S. Amigorena. 2016. Dendritic cell maturation and cross-presentation: timing matters! *Immunological reviews*. 272:97-108.
- Angers, C.G., and A.J. Merz. 2011. New links between vesicle coats and Rab-mediated vesicle targeting. *Seminars in Cell & Developmental Biology*. 22:18-26.
- Anvarian, Z., K. Mykytyn, S. Mukhopadhyay, L.B. Pedersen, and S.T. Christensen. 2019. Cellular signalling by primary cilia in development, organ function and disease. *Nature Reviews Nephrology*. 15:199-219.
- Ashkin, A., J.M. Dziedzic, J.E. Bjorkholm, and S. Chu. 1986. Observation of a single-beam gradient force optical trap for dielectric particles. *Opt. Lett.* 11:288-290.
- Astell, K.R., and D. Sieger. 2020. Zebrafish In Vivo Models of Cancer and Metastasis. *Cold Spring Harb Perspect Med*. 10.
- Axelrod, D. 1981. Cell-substrate contacts illuminated by total internal reflection fluorescence. *The Journal of cell biology*. 89:141-145.
- Axelrod, D. 2001. Total Internal Reflection Fluorescence Microscopy in Cell Biology. *Traffic (Copenhagen, Denmark)*. 2:764-774.
- Banchereau, J., F. Briere, C. Caux, J. Davoust, S. Lebecque, Y.J. Liu, B. Pulendran, and K. Palucka. 2000. Immunobiology of dendritic cells. *Annu Rev Immunol*. 18:767-811.
- Baptista, M.A.P., M. Keszei, M. Oliveira, K.K.S. Sunahara, J. Andersson, C.I.M. Dahlberg, A.J. Worth, A. Liedén, I.C. Kuo, R.P.A. Wallin, S.B. Snapper, L. Eidsmo, A. Scheynius, M.C.I. Karlsson, G. Bouma, S.O. Burns, M.N.E. Forsell, A.J. Thrasher, S. Nylén, and L.S. Westerberg. 2016. Deletion of Wiskott–Aldrich syndrome protein triggers Rac2 activity and increased cross-presentation by dendritic cells. *Nature Communications*. 7:12175.
- Barbier, L., P.J. Sáez, R. Attia, A.M. Lennon-Duménil, I. Lavi, M. Piel, and P. Vargas. 2019. Myosin II Activity Is Selectively Needed for Migration in Highly Confined Microenvironments in Mature Dendritic Cells. *Frontiers in immunology*. 10:747.
- Bardin, S., and B. Goud. 2021. Generating Rab6 Conditional Knockout Mice. *Methods in molecular biology (Clifton, N.J.)*. 2293:257-263.
- Barlan, K., and V.I. Gelfand. 2017. Microtubule-Based Transport and the Distribution, Tethering, and Organization of Organelles. *Cold Spring Harb Perspect Biol*. 9.

- Beales, P.L., H.A. Reid, M.H. Griffiths, E.R. Maher, F.A. Flinter, and A.S. Woolf. 2000. Renal cancer and malformations in relatives of patients with Bardet-Biedl syndrome. *Nephrol Dial Transplant*. 15:1977-1985.
- Berg-Larsen, A., O.J.B. Landsverk, C. Progida, T.F. Gregers, and O. Bakke. 2013. Differential Regulation of Rab GTPase Expression in Monocyte-Derived Dendritic Cells upon Lipopolysaccharide Activation: A Correlation to Maturation-Dependent Functional Properties. *PLoS ONE*. 8:e73538.
- Bhogaraju, S., M. Taschner, M. Morawetz, C. Basquin, and E. Lorentzen. 2011. Crystal structure of the intraflagellar transport complex 25/27. *The EMBO journal*. 30:1907-1918.
- Bjørnestad, S.A., N.A. Guadagno, I. Kjos, and C. Progida. 2022. Rab33b-exocyst interaction mediates localized secretion for focal adhesion turnover and cell migration. *iScience*. 25:104250.
- Blacque, O.E., N. Scheidel, and S. Kuhns. 2018. Rab GTPases in cilium formation and function. *Small GTPases*. 9:76-94.
- Blümer, J., J. Rey, L. Dehmelt, T. Mazel, Y.-W. Wu, P. Bastiaens, R.S. Goody, and A. Itzen. 2013. RabGEFs are a major determinant for specific Rab membrane targeting. *Journal of Cell Biology*. 200:287-300.
- Bodnar, A.G., M. Ouellette, M. Frolkis, S.E. Holt, C.P. Chiu, G.B. Morin, C.B. Harley, J.W. Shay, S. Lichtsteiner, and W.E. Wright. 1998. Extension of life-span by introduction of telomerase into normal human cells. *Science (New York, N.Y.)*. 279:349-352.
- Bodor, D.L., W. Pönisch, R.G. Endres, and E.K. Paluch. 2020. Of Cell Shapes and Motion: The Physical Basis of Animal Cell Migration. *Developmental Cell*. 52:550-562.
- Bond, C., A.N. Santiago-Ruiz, Q. Tang, and M. Lakadamyali. 2022. Technological advances in super-resolution microscopy to study cellular processes. *Molecular Cell*. 82:315-332.
- Bond, J., E. Roberts, K. Springell, S. Lizarraga, S. Scott, J. Higgins, D.J. Hampshire, E.E. Morrison, G.F. Leal, E.O. Silva, S.M.R. Costa, D. Baralle, M. Raponi, G. Karbani, Y. Rashid, H. Jafri, C. Bennett, P. Corry, C.A. Walsh, and C.G. Woods. 2005. A centrosomal mechanism involving CDK5RAP2 and CENPJ controls brain size. *Nature Genetics*. 37:353-355.
- Borah, N.A., and M.M. Reddy. 2021. Aurora Kinase B Inhibition: A Potential Therapeutic Strategy for Cancer. *Molecules*. 26.
- Borchers, A.-C., L. Langemeyer, and C. Ungermann. 2021. Who's in control? Principles of Rab GTPase activation in endolysosomal membrane trafficking and beyond. *Journal of Cell Biology*. 220:e202105120.
- Borg Distefano, M., I. Kjos, O. Bakke, and C. Progida. 2015. Rab7b at the intersection of intracellular trafficking and cell migration. *Communicative & Integrative Biology*:00-00.
- Borg, M., O. Bakke, and C. Progida. 2014. A novel interaction between Rab7b and actomyosin reveals a dual role in intracellular transport and cell migration. *Journal of cell science*. 127:4927-4939.
- Breslow, D.K., and A.J. Holland. 2019. Mechanism and Regulation of Centriole and Cilium Biogenesis. *Annual review of biochemistry*. 88:691-724.
- Bretou, M., P.J. Saez, D. Sanseau, M. Maurin, D. Lankar, M. Chabaud, C. Spampanato, O. Malbec, L. Barbier, S. Muallem, P. Maiuri, A. Ballabio, J. Helft, M. Piel, P. Vargas, and A.M. Lennon-Dumenil. 2017. Lysosome signaling controls the migration of dendritic cells. *Science immunology*. 2.
- Brunner, C., J. Seiderer, A. Schlamp, M. Bidlingmaier, A. Eigler, W. Haimerl, H.A. Lehr, A.M. Krieg, G. Hartmann, and S. Endres. 2000. Enhanced dendritic cell maturation by TNF-alpha or cytidine-phosphate-guanosine DNA drives T cell activation in vitro and

- therapeutic anti-tumor immune responses in vivo. *Journal of immunology (Baltimore, Md. : 1950)*. 165:6278-6286.
- Bryant, D.M., A. Datta, A.E. Rodríguez-Fraticelli, J. Peränen, F. Martín-Belmonte, and K.E. Mostov. 2010. A molecular network for de novo generation of the apical surface and lumen. *Nature Cell Biology*. 12:1035-1045.
- Bucci, C., R.G. Parton, I.H. Mather, H. Stunnenberg, K. Simons, B. Hoflack, and M. Zerial. 1992. The small GTPase rab5 functions as a regulatory factor in the early endocytic pathway. *Cell*. 70:715-728.
- Bucci, C., P. Thomsen, P. Nicoziani, J. McCarthy, and B. van Deurs. 2000. Rab7: A Key to Lysosome Biogenesis. *Molecular Biology of the Cell*. 11:467-480.
- Cabeza-Cabrerizo, M., A. Cardoso, C.M. Minutti, M. Pereira da Costa, and C. Reis e Sousa. 2021. Dendritic Cells Revisited. *Annual Review of Immunology*. 39:131-166.
- Cabrera, M., and C. Ungermann. 2013. Guanine Nucleotide Exchange Factors (GEFs) Have a Critical but Not Exclusive Role in Organelle Localization of Rab GTPases. *Journal of Biological Chemistry*. 288:28704-28712.
- Callan-Jones, A.C., and R. Voituriez. 2016. Actin flows in cell migration: from locomotion and polarity to trajectories. *Current Opinion in Cell Biology*. 38:12-17.
- Capes-Davis, A., A. Bairoch, T. Barrett, E.C. Burnett, W.G. Dirks, E.M. Hall, L. Healy, D.A. Kniss, C. Korch, Y. Liu, R.M. Neve, R.W. Nims, B. Parodi, R.E. Schweppe, D.R. Storts, and F. Tian. 2019. Cell Lines as Biological Models: Practical Steps for More Reliable Research. *Chemical Research in Toxicology*. 32:1733-1736.
- Carmena, M., S. Ruchaud, and W.C. Earnshaw. 2009. Making the Auroras glow: regulation of Aurora A and B kinase function by interacting proteins. *Current opinion in cell biology*. 21:796-805.
- Cechim, G., and J.A.B. Chies. 2019. In vitro generation of human monocyte-derived dendritic cells methodological aspects in a comprehensive review. *An. Acad. Bras. Ciênc*. 91.
- Ceresa, B.P., and S.J. Bahr. 2006. rab7 activity affects epidermal growth factor:epidermal growth factor receptor degradation by regulating endocytic trafficking from the late endosome. *The Journal of biological chemistry*. 281:1099-1106.
- Chabaud, M., M.L. Heuze, M. Bretou, P. Vargas, P. Maiuri, P. Solanes, M. Maurin, E. Terriac, M. Le Berre, D. Lankar, T. Piolot, R.S. Adelstein, Y. Zhang, M. Sixt, J. Jacobelli, O. Benichou, R. Voituriez, M. Piel, and A.-M. Lennon-Dumenil. 2015a. Cell migration and antigen capture are antagonistic processes coupled by myosin II in dendritic cells. *Nat Commun*. 6.
- Chabaud, M., M.L. Heuzé, M. Bretou, P. Vargas, P. Maiuri, P. Solanes, M. Maurin, E. Terriac, M. Le Berre, D. Lankar, T. Piolot, R.S. Adelstein, Y. Zhang, M. Sixt, J. Jacobelli, O. Bénichou, R. Voituriez, M. Piel, and A.-M. Lennon-Duménil. 2015b. Cell migration and antigen capture are antagonistic processes coupled by myosin II in dendritic cells. *Nature communications*. 6:7526-7526.
- Chandra, B., M.L. Tung, Y. Hsu, T. Scheetz, and V.C. Sheffield. 2021. Retinal ciliopathies through the lens of Bardet-Biedl Syndrome: Past, present and future. *Progress in Retinal and Eye Research*:101035.
- Chappie, J.S., and F. Dyda. 2013. Building a fission machine--structural insights into dynamin assembly and activation. *Journal of cell science*. 126:2773-2784.
- Chavrier, P., R.G. Parton, H.P. Hauri, K. Simons, and M. Zerial. 1990. Localization of low molecular weight GTP binding proteins to exocytic and endocytic compartments. *Cell*. 62:317-329.
- Chen, R.-Y., C.-J. Yen, Y.-W. Liu, C.-G. Guo, C.-Y. Weng, C.-H. Lai, J.-M. Wang, Y.-J. Lin, and L.-Y. Hung. 2020. CPAP promotes angiogenesis and metastasis by enhancing STAT3 activity. *Cell death and differentiation*. 27:1259-1273.

- Chou, E.J., L.Y. Hung, C.J. Tang, W.B. Hsu, H.Y. Wu, P.C. Liao, and T.K. Tang. 2016. Phosphorylation of CPAP by Aurora-A Maintains Spindle Pole Integrity during Mitosis. *Cell reports*. 14:2975-2987.
- Choudhary, D., A. Mossa, M. Jadhav, and C. Cecconi. 2019. Bio-Molecular Applications of Recent Developments in Optical Tweezers. *Biomolecules*. 9.
- Cole, D.G., D.R. Diener, A.L. Himelblau, P.L. Beech, J.C. Fuster, and J.L. Rosenbaum. 1998. Chlamydomonas Kinesin-II-dependent Intraflagellar Transport (IFT): IFT Particles Contain Proteins Required for Ciliary Assembly in Caenorhabditis elegans Sensory Neurons. *Journal of Cell Biology*. 141:993-1008.
- Cotton, M., P.-L. Boulay, T. Houndolo, N. Vitale, J.A. Pitcher, and A. Claing. 2007. Endogenous ARF6 Interacts with Rac1 upon Angiotensin II Stimulation to Regulate Membrane Ruffling and Cell Migration. *Molecular Biology of the Cell*. 18:501-511.
- Croisé, P., C. Estay-Ahumada, S. Gasman, and S. Ory. 2014. Rho GTPases, phosphoinositides, and actin: a tripartite framework for efficient vesicular trafficking. *Small GTPases*. 5:e29469-e29469.
- Crosas-Molist, E., R. Samain, L. Kohlhammer, J.L. Orgaz, S.L. George, O. Maiques, J. Barcelo, and V. Sanz-Moreno. 2021. Rho GTPase signaling in cancer progression and dissemination. *Physiological reviews*. 102:455-510.
- Cross, J.A., and M.P. Dodding. 2019. Motor-cargo adaptors at the organelle-cytoskeleton interface. *Curr Opin Cell Biol*. 59:16-23.
- Cullen, B.R. 2006. Enhancing and confirming the specificity of RNAi experiments. *Nat Methods*. 3:677-681.
- Dacks, J.B., and M.S. Robinson. 2017. Outerwear through the ages: evolutionary cell biology of vesicle coats. *Current Opinion in Cell Biology*. 47:108-116.
- Dalod, M., R. Chelbi, B. Malissen, and T. Lawrence. 2014. Dendritic cell maturation: functional specialization through signaling specificity and transcriptional programming. *The EMBO journal*. 33:1104-1116.
- Dana, H., G.M. Chalbatani, H. Mahmoodzadeh, R. Karimloo, O. Rezaiean, A. Moradzadeh, N. Mehmandoost, F. Moazzen, A. Mazraeh, V. Marmari, M. Ebrahimi, M.M. Rashno, S.J. Abadi, and E. Gharagouzlo. 2017. Molecular Mechanisms and Biological Functions of siRNA. *Int J Biomed Sci*. 13:48-57.
- De Renzis, S., B. Sönnichsen, and M. Zerial. 2002. Divalent Rab effectors regulate the sub-compartmental organization and sorting of early endosomes. *Nature Cell Biology*. 4:124-133.
- Deal, J., D.J. Pleshinger, S.C. Johnson, S.J. Leavesley, and T.C. Rich. 2020. Milestones in the development and implementation of FRET-based sensors of intracellular signals: A biological perspective of the history of FRET. *Cellular Signalling*. 75:109769.
- Del Nery, E., S. Miserey-Lenkei, T. Falguières, C. Nizak, L. Johannes, F. Perez, and B. Goud. 2006. Rab6A and Rab6A' GTPases play non-overlapping roles in membrane trafficking. *Traffic (Copenhagen, Denmark)*. 7:394-407.
- Delaval, B., A. Bright, N.D. Lawson, and S. Doxsey. 2011. The cilia protein IFT88 is required for spindle orientation in mitosis. *Nature cell biology*. 13:461-468.
- Diekmann, Y., E. Seixas, M. Gouw, F. Tavares-Cadete, M.C. Seabra, and J.B. Pereira-Leal. 2011. Thousands of rab GTPases for the cell biologist. *PLoS Comput Biol*. 7:e1002217.
- Dirac-Svejstrup, A.B., T. Sumizawa, and S.R. Pfeffer. 1997. Identification of a GDI displacement factor that releases endosomal Rab GTPases from Rab-GDI. *The EMBO Journal*. 16:465-472.
- Doornbos, C., and R. Roepman. 2021. Moonlighting of mitotic regulators in cilium disassembly. *Cellular and molecular life sciences : CMLS*. 78:4955-4972.

- Doyle, A.D., S.S. Nazari, and K.M. Yamada. 2022. Cell-extracellular matrix dynamics. *Physical biology*. 19.
- Echard, A., F.J. Opdam, H.J. de Leeuw, F. Jollivet, P. Savelkoul, W. Hendriks, J. Voorberg, B. Goud, and J.A. Fransen. 2000. Alternative splicing of the human Rab6A gene generates two close but functionally different isoforms. *Mol Biol Cell*. 11:3819-3833.
- Edwards, D.C., L.C. Sanders, G.M. Bokoch, and G.N. Gill. 1999. Activation of LIM-kinase by Pak1 couples Rac/Cdc42 GTPase signalling to actin cytoskeletal dynamics. *Nat Cell Biol*. 1:253-259.
- Eguether, T., F.P. Cordelieres, and G.J. Pazour. 2018. Intraflagellar transport is deeply integrated in hedgehog signaling. *Mol Biol Cell*. 29:1178-1189.
- Eguether, T., J.T. San Agustin, B.T. Keady, J.A. Jonassen, Y. Liang, R. Francis, K. Tobita, C.A. Johnson, Z.A. Abdelhamed, C.W. Lo, and G.J. Pazour. 2014. IFT27 links the BBSome to IFT for maintenance of the ciliary signaling compartment. *Dev Cell*. 31:279-290.
- Eme, L., D. Moreira, E. Talla, and C. Brochier-Armanet. 2009. A Complex Cell Division Machinery Was Present in the Last Common Ancestor of Eukaryotes. *PLOS ONE*. 4:e5021.
- Faheem, M., M.I. Naseer, M. Rasool, A.G. Chaudhary, T.A. Kumosani, A.M. Ilyas, P. Pushparaj, F. Ahmed, H.A. Algahtani, M.H. Al-Qahtani, and H. Saleh Jamal. 2015. Molecular genetics of human primary microcephaly: an overview. *BMC Med Genomics*. 8 Suppl 1:S4.
- Faure-André, G., P. Vargas, M.I. Yuseff, M. Heuzé, J. Diaz, D. Lankar, V. Steri, J. Manry, S. Hugues, F. Vascotto, J. Boulanger, G. Raposo, M.R. Bono, M. Roseblatt, M. Piel, and A.M. Lennon-Duménil. 2008. Regulation of dendritic cell migration by CD74, the MHC class II-associated invariant chain. *Science (New York, N.Y.)*. 322:1705-1710.
- Filin, I.Y., K.V. Kitaeva, C.S. Rutland, A.A. Rizvanov, and V.V. Solovyeva. 2021. Recent Advances in Experimental Dendritic Cell Vaccines for Cancer. *Frontiers in Oncology*. 11.
- Fourriere, L., A. Kasri, N. Gareil, S. Bardin, H. Bousquet, D. Pereira, F. Perez, B. Goud, G. Boncompain, and S. Miserey-Lenkei. 2019. RAB6 and microtubules restrict protein secretion to focal adhesions. *Journal of Cell Biology*. 218:2215-2231.
- Frémont, S., and A. Echard. 2018. Membrane Traffic in the Late Steps of Cytokinesis. *Current biology : CB*. 28:R458-r470.
- Frémont, S., G. Romet-Lemonne, A. Houdusse, and A. Echard. 2017. Emerging roles of MICAL family proteins – from actin oxidation to membrane trafficking during cytokinesis. *Journal of cell science*. 130:1509-1517.
- Gallwitz, D., C. Donath, and C. Sander. 1983. A yeast gene encoding a protein homologous to the human c-has/bas proto-oncogene product. *Nature*. 306:704-707.
- Gey, G.O., W.D. Coffman, and M.T. Kubicek. 1952. Tissue culture studies of the proliferative capacity of cervical carcinoma and normal epithelium. *Cancer Res*. 12:264-265.
- Gibieža, P., and R. Prekeris. 2018. Rab GTPases and cell division. *Small GTPases*. 9:107-115.
- Gigante, E.D., and T. Caspary. 2020. Signaling in the primary cilium through the lens of the Hedgehog pathway. *WIREs Developmental Biology*. 9:e377.
- Gillingham, A.K., and S. Munro. 2019. Transport carrier tethering - how vesicles are captured by organelles. *Curr Opin Cell Biol*. 59:140-146.
- Girod, A., B. Storrie, J.C. Simpson, L. Johannes, B. Goud, L.M. Roberts, J.M. Lord, T. Nilsson, and R. Pepperkok. 1999. Evidence for a COP-I-independent transport route from the Golgi complex to the endoplasmic reticulum. *Nat Cell Biol*. 1:423-430.

- Goitre, L., E. Trapani, L. Trabalzini, and S.F. Retta. 2014. The Ras superfamily of small GTPases: the unlocked secrets. *Methods in molecular biology (Clifton, N.J.)*. 1120:1-18.
- Goodson, H.V., and E.M. Jonasson. 2018. Microtubules and Microtubule-Associated Proteins. *Cold Spring Harbor perspectives in biology*. 10:a022608.
- Gorvel, J.P., P. Chavrier, M. Zerial, and J. Gruenberg. 1991. rab5 controls early endosome fusion in vitro. *Cell*. 64:915-925.
- Goud, B., S. Liu, and B. Storrie. 2018. Rab proteins as major determinants of the Golgi complex structure. *Small GTPases*. 9:66-75.
- Goud, B., A. Salminen, N.C. Walworth, and P.J. Novick. 1988. A GTP-binding protein required for secretion rapidly associates with secretory vesicles and the plasma membrane in yeast. *Cell*. 53:753-768.
- Goud, B., A. Zahraoui, A. Tavitian, and J. Saraste. 1990. Small GTP-binding protein associated with Golgi cisternae. *Nature*. 345:553-556.
- Granucci, F., E. Ferrero, M. Foti, D. Aggujaro, K. Vettoretto, and P. Ricciardi-Castagnoli. 1999. Early events in dendritic cell maturation induced by LPS. *Microbes and Infection*. 1:1079-1084.
- Grecco, H.E., and P.J. Verveer. 2011. FRET in Cell Biology: Still Shining in the Age of Super-Resolution? *ChemPhysChem*. 12:484-490.
- Grigoriev, I., D. Splinter, N. Keijzer, P.S. Wulf, J. Demmers, T. Ohtsuka, M. Modesti, I.V. Maly, F. Grosveld, C.C. Hoogenraad, and A. Akhmanova. 2007. Rab6 Regulates Transport and Targeting of Exocytotic Carriers. *Developmental Cell*. 13:305-314.
- Grigoriev, I., Ka L. Yu, E. Martinez-Sanchez, A. Serra-Marques, I. Smal, E. Meijering, J. Demmers, J. Peränen, R.J. Pasterkamp, P. van der Sluijs, Casper C. Hoogenraad, and A. Akhmanova. 2011. Rab6, Rab8, and MICAL3 Cooperate in Controlling Docking and Fusion of Exocytotic Carriers. *Current Biology*. 21:967-974.
- Han, T.H., P. Jin, J. Ren, S. Slezak, F.M. Marincola, and D.F. Stroncek. 2009. Evaluation of 3 clinical dendritic cell maturation protocols containing lipopolysaccharide and interferon-gamma. *J Immunother*. 32:399-407.
- Hason, M., and P. Bartůněk. 2019. Zebrafish Models of Cancer-New Insights on Modeling Human Cancer in a Non-Mammalian Vertebrate. *Genes (Basel)*. 10.
- Hehnly, H., and S. Doxsey. 2014. Rab11 endosomes contribute to mitotic spindle organization and orientation. *Dev Cell*. 28:497-507.
- Heuze, M.L., P. Vargas, M. Chabaud, M. Le Berre, Y.J. Liu, O. Collin, P. Solanes, R. Voituriez, M. Piel, and A.M. Lennon-Dumenil. 2013. Migration of dendritic cells: physical principles, molecular mechanisms, and functional implications. *Immunological reviews*. 256:240-254.
- Hill, E., M. Clarke, and F.A. Barr. 2000. The Rab6-binding kinesin, Rab6-KIFL, is required for cytokinesis. *The EMBO Journal*. 19:5711-5719.
- Homem, C.C., M. Repic, and J.A. Knoblich. 2015. Proliferation control in neural stem and progenitor cells. *Nat Rev Neurosci*. 16:647-659.
- Homma, Y., S. Hiragi, and M. Fukuda. 2021. Rab family of small GTPases: an updated view on their regulation and functions. *The FEBS journal*. 288:36-55.
- Huang, H., Y. Jiang, Y. Wang, T. Chen, L. Yang, H. He, Z. Lin, T. Liu, T. Yang, D.W. Kamp, B. Wu, and G. Liu. 2015. miR-5100 promotes tumor growth in lung cancer by targeting Rab6. *Cancer Letters*. 362:15-24.
- Huang, J., T. Imamura, and J.M. Olefsky. 2001. Insulin can regulate GLUT4 internalization by signaling to Rab5 and the motor protein dynein. *Proceedings of the National Academy of Sciences*. 98:13084.

- Huet, D., T. Blisnick, S. Perrot, and P. Bastin. 2014. The GTPase IFT27 is involved in both anterograde and retrograde intraflagellar transport. *eLife*. 3:e02419.
- Hughes, P., D. Marshall, Y. Reid, H. Parkes, and C. Gelber. 2007. The costs of using unauthenticated, over-passaged cell lines: how much more data do we need? *BioTechniques*. 43:575-586.
- Hung, L.-Y., H.-L. Chen, C.-W. Chang, B.-R. Li, and T.K. Tang. 2004. Identification of a Novel Microtubule-destabilizing Motif in CPAP That Binds to Tubulin Heterodimers and Inhibits Microtubule Assembly. *Molecular Biology of the Cell*. 15:2697-2706.
- Izawa, I., H. Goto, K. Kasahara, and M. Inagaki. 2015. Current topics of functional links between primary cilia and cell cycle. *Cilia*. 4:12-12.
- Jacquemet, G., H. Hamidi, and J. Ivaska. 2015. Filopodia in cell adhesion, 3D migration and cancer cell invasion. *Current Opinion in Cell Biology*. 36:23-31.
- Jeong, B.Y., K.H. Cho, K.J. Jeong, Y.Y. Park, J.M. Kim, S.Y. Rha, C.G. Park, G.B. Mills, J.H. Cheong, and H.Y. Lee. 2018. Rab25 augments cancer cell invasiveness through a β 1 integrin/EGFR/VEGF-A/Snail signaling axis and expression of fascin. *Exp Mol Med*. 50:e435.
- Jiang, X.R., G. Jimenez, E. Chang, M. Frolkis, B. Kusler, M. Sage, M. Beeche, A.G. Bodnar, G.M. Wahl, T.D. Tlsty, and C.P. Chiu. 1999. Telomerase expression in human somatic cells does not induce changes associated with a transformed phenotype. *Nat Genet*. 21:111-114.
- Johnson, J.L., J. Monfregola, G. Napolitano, W.B. Kiosses, and S.D. Catz. 2012. Vesicular trafficking through cortical actin during exocytosis is regulated by the Rab27a effector JFC1/Slp1 and the RhoA-GTPase-activating protein Gem-interacting protein. *Molecular Biology of the Cell*. 23:1902-1916.
- Jonuleit, H., U. Kühn, G. Müller, K. Steinbrink, L. Paragnik, E. Schmitt, J. Knop, and A.H. Enk. 1997. Pro-inflammatory cytokines and prostaglandins induce maturation of potent immunostimulatory dendritic cells under fetal calf serum-free conditions. *European journal of immunology*. 27:3135-3142.
- Jordan, M.A., and G. Pigino. 2021. The structural basis of intraflagellar transport at a glance. *Journal of cell science*. 134:jcs247163.
- Kauanova, S., A. Urazbayev, and I. Vorobjev. 2021. The Frequent Sampling of Wound Scratch Assay Reveals the “Opportunity” Window for Quantitative Evaluation of Cell Motility-Impeding Drugs. *Frontiers in cell and developmental biology*. 9.
- Kaur, G., and J.M. Dufour. 2012. Cell lines: Valuable tools or useless artifacts. *Spermatogenesis*. 2:1-5.
- Kessler, D., G.C. Gruen, D. Heider, J. Morgner, H. Reis, K.W. Schmid, and V. Jendrossek. 2012. The action of small GTPases Rab11 and Rab25 in vesicle trafficking during cell migration. *Cellular physiology and biochemistry : international journal of experimental cellular physiology, biochemistry, and pharmacology*. 29:647-656.
- Kjos, I., K. Vestre, N.A. Guadagno, M. Borg Distefano, and C. Progidia. 2018. Rab and Arf proteins at the crossroad between membrane transport and cytoskeleton dynamics. *Biochimica et Biophysica Acta (BBA) - Molecular Cell Research*. 1865:1397-1409.
- Klaver, E.J., T.C.T.M. van der Pouw Kraan, L.C. Laan, H. Kringel, R.D. Cummings, G. Bouma, G. Kraal, and I. van Die. 2015. Trichuris suis soluble products induce Rab7b expression and limit TLR4 responses in human dendritic cells. *Genes & Immunity*. 16:378-387.
- Kouranti, I., M. Sachse, N. Arouche, B. Goud, and A. Echard. 2006. Rab35 regulates an endocytic recycling pathway essential for the terminal steps of cytokinesis. *Current biology : CB*. 16:1719-1725.

- Kozminski, K.G., K.A. Johnson, P. Forscher, and J.L. Rosenbaum. 1993. A motility in the eukaryotic flagellum unrelated to flagellar beating. *Proceedings of the National Academy of Sciences*. 90:5519.
- Kucera, A., M. Borg Distefano, A. Berg-Larsen, F. Skjeldal, U. Repnik, O. Bakke, and C. Progidia. 2015. Spatiotemporal Resolution of Rab9 and CI-MPR Dynamics in the Endocytic Pathway. *Traffic (Copenhagen, Denmark)*. 17:211-229.
- Kumar, D., and J. Reiter. 2021. How the centriole builds its cilium: of mothers, daughters, and the acquisition of appendages. *Curr Opin Struct Biol*. 66:41-48.
- Lamber, E.P., A.C. Siedenburg, and F.A. Barr. 2019. Rab regulation by GEFs and GAPs during membrane traffic. *Curr Opin Cell Biol*. 59:34-39.
- Langemeyer, L., A.-C. Borchers, E. Herrmann, N. Füllbrunn, Y. Han, A. Perz, K. Auffarth, D. Kümmel, and C. Ungermann. 2020. A conserved and regulated mechanism drives endosomal Rab transition. *eLife*. 9:e56090.
- Lanzetti, L. 2012. A novel function of Rab5 in mitosis. *Small GTPases*. 3:168-172.
- Lehtreck, K.F., J.C. Van De Weghe, J.A. Harris, and P. Liu. 2017. Protein transport in growing and steady-state cilia. *Traffic (Copenhagen, Denmark)*. 18:277-286.
- Lee, P.L., M.B. Ohlson, and S.R. Pfeffer. 2015. The Rab6-regulated KIF1C kinesin motor domain contributes to Golgi organization. *eLife*. 4:e06029.
- Lehtimäki, J., M. Hakala, and P. Lappalainen. 2017. Actin Filament Structures in Migrating Cells. *Handb Exp Pharmacol*. 235:123-152.
- Lens, S.M.A., and R.H. Medema. 2019. Cytokinesis defects and cancer. *Nature Reviews Cancer*. 19:32-45.
- Leung, K.F., R. Baron, and M.C. Seabra. 2006. Thematic review series: lipid posttranslational modifications. geranylgeranylation of Rab GTPases. *J Lipid Res*. 47:467-475.
- Liew, Gerald M., F. Ye, Andrew R. Nager, J.P. Murphy, Jaelyn S. Lee, M. Aguiar, David K. Breslow, Steven P. Gygi, and Maxence V. Nachury. 2014. The Intraflagellar Transport Protein IFT27 Promotes BBSome Exit from Cilia through the GTPase ARL6/BBS3. *Developmental Cell*. 31:265-278.
- Lindsay, A.J., F. Jollivet, C.P. Horgan, A.R. Khan, G. Raposo, M.W. McCaffrey, and B. Goud. 2013. Identification and characterization of multiple novel Rab–myosin Va interactions. *Molecular Biology of the Cell*. 24:3420-3434.
- Liu, S., L. Hunt, and B. Storrie. 2013. Rab41 is a novel regulator of Golgi apparatus organization that is needed for ER-to-Golgi trafficking and cell growth. *PLoS One*. 8:e71886.
- Liu, Y.J., M. Le Berre, F. Lautenschlaeger, P. Maiuri, A. Callan-Jones, M. Heuzé, T. Takaki, R. Voituriez, and M. Piel. 2015. Confinement and low adhesion induce fast amoeboid migration of slow mesenchymal cells. *Cell*. 160:659-672.
- Lu, R., and J.M. Wilson. 2016. Rab14 specifies the apical membrane through Arf6-mediated regulation of lipid domains and Cdc42. *Scientific reports*. 6:38249.
- Lucker, B.F., R.H. Behal, H. Qin, L.C. Siron, W.D. Taggart, J.L. Rosenbaum, and D.G. Cole. 2005. Characterization of the intraflagellar transport complex B core: direct interaction of the IFT81 and IFT74/72 subunits. *The Journal of biological chemistry*. 280:27688-27696.
- Lürick, A., J. Gao, A. Kuhlee, E. Yavavli, L. Langemeyer, A. Perz, S. Raunser, and C. Ungermann. 2016. Multivalent Rab interactions determine tether-mediated membrane fusion. *Molecular Biology of the Cell*. 28:322-332.
- Lämmermann, T., B.L. Bader, S.J. Monkley, T. Worbs, R. Wedlich-Söldner, K. Hirsch, M. Keller, R. Förster, D.R. Critchley, R. Fässler, and M. Sixt. 2008. Rapid leukocyte migration by integrin-independent flowing and squeezing. *Nature*. 453:51-55.

- Magnaghi-Jaulin, L., G. Eot-Houllier, E. Gallaud, and R. Giet. 2019. Aurora A Protein Kinase: To the Centrosome and Beyond. *Biomolecules*. 9:28.
- Maldonado, M.D.M., J.I. Medina, L. Velazquez, and S. Dharmawardhane. 2020. Targeting Rac and Cdc42 GEFs in Metastatic Cancer. *Frontiers in cell and developmental biology*. 8:201-201.
- Malicki, J.J., and C.A. Johnson. 2017. The Cilium: Cellular Antenna and Central Processing Unit. *Trends in Cell Biology*. 27:126-140.
- Mallard, F., B.L. Tang, T. Galli, D. Tenza, A. Saint-Pol, X. Yue, C. Antony, W. Hong, B. Goud, and L. Johannes. 2002. Early/recycling endosomes-to-TGN transport involves two SNARE complexes and a Rab6 isoform. *The Journal of cell biology*. 156:653-664.
- Manser, E., T. Leung, H. Salihuddin, Z.S. Zhao, and L. Lim. 1994. A brain serine/threonine protein kinase activated by Cdc42 and Rac1. *Nature*. 367:40-46.
- Margiotta, A., and C. Bucci. 2016. Role of Intermediate Filaments in Vesicular Traffic. *Cells*. 5.
- Margiotta, A., C. Progida, O. Bakke, and C. Bucci. 2017. Rab7a regulates cell migration through Rac1 and vimentin. *Biochimica et Biophysica Acta (BBA) - Molecular Cell Research*. 1864:367-381.
- Martinez, O., C. Antony, G. Pehau-Arnaudet, E.G. Berger, J. Salamero, and B. Goud. 1997. GTP-bound forms of rab6 induce the redistribution of Golgi proteins into the endoplasmic reticulum. *Proceedings of the National Academy of Sciences of the United States of America*. 94:1828-1833.
- Matanis, T., A. Akhmanova, P. Wulf, E. Del Nery, T. Weide, T. Stepanova, N. Galjart, F. Grosveld, B. Goud, C.I. De Zeeuw, A. Barnekow, and C.C. Hoogenraad. 2002. Bicaudal-D regulates COPI-independent Golgi-ER transport by recruiting the dynein-dynactin motor complex. *Nat Cell Biol*. 4:986-992.
- McNeely, K.C., and N.D. Dwyer. 2020. Cytokinesis and postabscission midbody remnants are regulated during mammalian brain development. *Proceedings of the National Academy of Sciences*. 117:9584-9593.
- Michelsen, K.S., A. Aicher, M. Mohaupt, T. Hartung, S. Dimmeler, C.J. Kirschning, and R.R. Schumann. 2001. The role of toll-like receptors (TLRs) in bacteria-induced maturation of murine dendritic cells (DCS). Peptidoglycan and lipoteichoic acid are inducers of DC maturation and require TLR2. *The Journal of biological chemistry*. 276:25680-25686.
- Miserey-Lenkei, S., H. Bousquet, O. Pylypenko, S. Bardin, A. Dimitrov, G. Bressanelli, R. Bonifay, V. Fraissier, C. Guillou, C. Bougeret, A. Houdusse, A. Echard, and B. Goud. 2017. Coupling fission and exit of RAB6 vesicles at Golgi hotspots through kinesin-myosin interactions. *Nat Commun*. 8:1254.
- Miserey-Lenkei, S., G. Chalancon, S. Bardin, E. Formstecher, B. Goud, and A. Echard. 2010. Rab and actomyosin-dependent fission of transport vesicles at the Golgi complex. *Nat Cell Biol*. 12:645-654.
- Miserey-Lenkei, S., and M.I. Colombo. 2016. Small RAB GTPases Regulate Multiple Steps of Mitosis. *Frontiers in cell and developmental biology*. 4.
- Miserey-Lenkei, S., F. Waharte, A. Boulet, M.H. Cuif, D. Tenza, A. El Marjou, G. Raposo, J. Salamero, L. Hélot, B. Goud, and S. Monier. 2007. Rab6-interacting protein 1 links Rab6 and Rab11 function. *Traffic (Copenhagen, Denmark)*. 8:1385-1403.
- Mishra, A.K., J.P. Campanale, J.A. Mondo, and D.J. Montell. 2019. Cell interactions in collective cell migration. *Development (Cambridge, England)*. 146:dev172056.
- Mosaddeghzadeh, N., and M.R. Ahmadian. 2021. The RHO Family GTPases: Mechanisms of Regulation and Signaling. *Cells*. 10.

- Moshal, K.S., K.F. Ferri-Lagneau, J. Haider, P. Pardhanani, and T. Leung. 2011. Discriminating different cancer cells using a zebrafish in vivo assay. *Cancers (Basel)*. 3:4102-4113.
- Murphy, N.P., A.M. binti Ahmad Mokhtar, H.R. Mott, and D. Owen. 2021. Molecular subversion of Cdc42 signalling in cancer. *Biochemical Society Transactions*. 49:1425-1442.
- Müller, M.P., and R.S. Goody. 2018. Molecular control of Rab activity by GEFs, GAPs and GDI. *Small GTPases*. 9:5-21.
- Nakayama, K., and Y. Katoh. 2020. Architecture of the IFT ciliary trafficking machinery and interplay between its components. *Crit Rev Biochem Mol Biol*. 55:179-196.
- Nassari, S., T. Del Olmo, and S. Jean. 2020. Rabs in Signaling and Embryonic Development. *International Journal of Molecular Sciences*. 21.
- Neumeier, J., and G. Meister. 2021. siRNA Specificity: RNAi Mechanisms and Strategies to Reduce Off-Target Effects. *Frontiers in Plant Science*. 11.
- Numrich, J., and C. Ungermann. 2014. Endocytic Rabs in membrane trafficking and signaling. *Biological chemistry*. 395:327-333.
- Oke, A., D. Pearce, R.W. Wilkinson, C. Crafter, R. Odedra, J. Cavenagh, J. Fitzgibbon, A.T. Lister, S. Joel, and D. Bonnet. 2009. AZD1152 Rapidly and Negatively Affects the Growth and Survival of Human Acute Myeloid Leukemia Cells In vitro and In vivo. *Cancer Research*. 69:4150-4158.
- Oliveira, M.M.S., S.-Y. Kung, H.D. Moreau, M. Maurin, J. Record, D. Sanséau, S. Nylén, A.-M. Lennon-Duménil, and L.S. Westerberg. 2022. The WASp L272P gain-of-function mutation alters dendritic cell coordination of actin dynamics for migration and adhesion. *Journal of Leukocyte Biology*. 111:793-803.
- Opdam, F.J., A. Echard, H.J. Croes, J.A. van den Hurk, R.A. van de Vorstenbosch, L.A. Ginsel, B. Goud, and J.A. Fransen. 2000. The small GTPase Rab6B, a novel Rab6 subfamily member, is cell-type specifically expressed and localised to the Golgi apparatus. *Journal of cell science*. 113 (Pt 15):2725-2735.
- Palamidessi, A., E. Frittoli, M. Garre, M. Faretta, M. Mione, I. Testa, A. Diaspro, L. Lanzetti, G. Scita, and P.P. Di Fiore. 2008. Endocytic trafficking of Rac is required for the spatial restriction of signaling in cell migration. *Cell*. 134:135-147.
- Park, B.S., and J.-O. Lee. 2013. Recognition of lipopolysaccharide pattern by TLR4 complexes. *Experimental & Molecular Medicine*. 45:e66-e66.
- Patwardhan, A., S. Bardin, S. Miserey-Lenkei, L. Larue, B. Goud, G. Raposo, and C. Delevoye. 2017. Routing of the RAB6 secretory pathway towards the lysosome related organelle of melanocytes. *Nature Communications*. 8:15835.
- Paul, N.R., J.L. Allen, A. Chapman, M. Morlan-Mairal, E. Zindy, G. Jacquemet, L. Fernandez del Ama, N. Ferizovic, D.M. Green, J.D. Howe, E. Ehler, A. Hurlstone, and P.T. Caswell. 2015. $\alpha 5\beta 1$ integrin recycling promotes Arp2/3-independent cancer cell invasion via the formin FHOD3. *The Journal of cell biology*. 210:1013-1031.
- Pazour, G.J., C.G. Wilkerson, and G.B. Witman. 1998. A dynein light chain is essential for the retrograde particle movement of intraflagellar transport (IFT). *The Journal of cell biology*. 141:979-992.
- Pellinen, T., A. Arjonen, K. Vuoriluoto, K. Kallio, J.A.M. Fransen, and J. Ivaska. 2006. Small GTPase Rab21 regulates cell adhesion and controls endosomal traffic of $\beta 1$ -integrins. *Journal of Cell Biology*. 173:767-780.
- Pereira-Leal, J.B., and M.C. Seabra. 2000. The mammalian Rab family of small GTPases: definition of family and subfamily sequence motifs suggests a mechanism for functional specificity in the Ras superfamily. Edited by M. Yaniv. *Journal of Molecular Biology*. 301:1077-1087.

- Pereira-Leal, J.B., and M.C. Seabra. 2001. Evolution of the Rab family of small GTP-binding proteins. *J Mol Biol.* 313:889-901.
- Perez, C.R., and M. De Palma. 2019. Engineering dendritic cell vaccines to improve cancer immunotherapy. *Nature Communications.* 10:5408.
- Petsalaki, E., and G. Zachos. 2021. The Abscission Checkpoint: A Guardian of Chromosomal Stability. *Cells.* 10:3350.
- Pfeffer, S.R. 2013. Rab GTPase regulation of membrane identity. *Current Opinion in Cell Biology.* 25:414-419.
- Pfeffer, S.R. 2017. Rab GTPases: master regulators that establish the secretory and endocytic pathways. *Molecular Biology of the Cell.* 28:712-715.
- Pollard, T.D. 2016. Actin and Actin-Binding Proteins. *Cold Spring Harb Perspect Biol.* 8.
- Poltorak, A., X. He, I. Smirnova, M.-Y. Liu, V. Huffel Christophe, X. Du, D. Birdwell, E. Alejos, M. Silva, C. Galanos, M. Freudenberg, P. Ricciardi-Castagnoli, B. Layton, and B. Beutler. 1998. Defective LPS Signaling in C3H/HeJ and C57BL/10ScCr Mice: Mutations in Tlr4 Gene. *Science (New York, N.Y.).* 282:2085-2088.
- Pontén, J., and E. Saksela. 1967. Two established in vitro cell lines from human mesenchymal tumours. *Int J Cancer.* 2:434-447.
- Porter, A.P., A. Papaioannou, and A. Malliri. 2016. Deregulation of Rho GTPases in cancer. *Small GTPases.* 7:123-138.
- Poulter, N.S., W.T. Pitkeathly, P.J. Smith, and J.Z. Rappoport. 2015. The physical basis of total internal reflection fluorescence (TIRF) microscopy and its cellular applications. *Methods in molecular biology (Clifton, N.J.).* 1251:1-23.
- Progida, C. 2019. Multiple Roles of Rab GTPases at the Golgi. In *The Golgi Apparatus and Centriole: Functions, Interactions and Role in Disease.* M. Kloc, editor. Springer International Publishing, Cham. 95-123.
- Progida, C., L. Cogli, F. Piro, A. De Luca, O. Bakke, and C. Bucci. 2010. Rab7b controls trafficking from endosomes to the TGN. *Journal of cell science.* 123:1480-1491.
- Progida, C., M.S. Nielsen, G. Koster, C. Bucci, and O. Bakke. 2012. Dynamics of Rab7b-dependent transport of sorting receptors. *Traffic (Copenhagen, Denmark).* 13:1273-1285.
- Pylypenko, O., H. Hammich, I.M. Yu, and A. Houdusse. 2018. Rab GTPases and their interacting protein partners: Structural insights into Rab functional diversity. *Small GTPases.* 9:22-48.
- Qin, H., Z. Wang, D. Diener, and J. Rosenbaum. 2007. Intraflagellar transport protein 27 is a small G protein involved in cell-cycle control. *Current biology : CB.* 17:193-202.
- Radhakrishna, H., O. Al-Awar, Z. Khachikian, and J.G. Donaldson. 1999. ARF6 requirement for Rac ruffling suggests a role for membrane trafficking in cortical actin rearrangements. *Journal of cell science.* 112:855-866.
- Rahajeng, J., S.S. Panapakkam Giridharan, B. Cai, N. Naslavsky, and S. Caplan. 2012. MICAL-L1 is a Tubular Endosomal Membrane Hub that Connects Rab35 and Arf6 With Rab8a. *Traffic (Copenhagen, Denmark).* 13:82-93.
- Reis e Sousa, C. 2006. Dendritic cells in a mature age. *Nature reviews. Immunology.* 6:476-483.
- Reiter, J.F., and M.R. Leroux. 2017. Genes and molecular pathways underpinning ciliopathies. *Nat. Rev. Mol. Cell Biol.* 18:533-547.
- Renkawitz, J., K. Schumann, M. Weber, T. Lämmermann, H. Pflücke, M. Piel, J. Polleux, J.P. Spatz, and M. Sixt. 2009. Adaptive force transmission in amoeboid cell migration. *Nature Cell Biology.* 11:1438-1443.
- Ridley, A.J. 2015a. Rho GTPase signalling in cell migration. *Current Opinion in Cell Biology.* 36:103-112.

- Ridley, A.J. 2015b. Rho GTPase signalling in cell migration. *Curr Opin Cell Biol.* 36:103-112.
- Ridley, A.J., M.A. Schwartz, K. Burridge, R.A. Firtel, M.H. Ginsberg, G. Borisy, J.T. Parsons, and A.R. Horwitz. 2003. Cell migration: integrating signals from front to back. *Science (New York, N.Y.)*. 302:1704-1709.
- Rosing, M., E. Ossendorf, A. Rak, and A. Barnekow. 2007. Giantin interacts with both the small GTPase Rab6 and Rab1. *Experimental cell research.* 313:2318-2325.
- Russo, A.J., A.J. Mathiowetz, S. Hong, M.D. Welch, and K.G. Campellone. 2016. Rab1 recruits WHAMM during membrane remodeling but limits actin nucleation. *Molecular Biology of the Cell.* 27:967-978.
- Römer, W., L.-L. Pontani, B. Sorre, C. Rentero, L. Berland, V. Chambon, C. Lamaze, P. Bassereau, C. Sykes, K. Gaus, and L. Johannes. 2010. Actin Dynamics Drive Membrane Reorganization and Scission in Clathrin-Independent Endocytosis. *Cell.* 140:540-553.
- Salminen, A., and P.J. Novick. 1987. A ras-like protein is required for a post-Golgi event in yeast secretion. *Cell.* 49:527-538.
- Santy, L.C., and J.E. Casanova. 2001. Activation of ARF6 by ARNO stimulates epithelial cell migration through downstream activation of both Rac1 and phospholipase D. *The Journal of cell biology.* 154:599-610.
- Schaefer, E., C. Delvallée, L. Mary, C. Stoetzel, V. Geoffroy, C. Marks-Delesalle, M. Holder-Espinasse, J. Ghomid, H. Dollfus, and J. Muller. 2019. Identification and Characterization of Known Biallelic Mutations in the IFT27 (BBS19) Gene in a Novel Family With Bardet-Biedl Syndrome. *Front Genet.* 10:21.
- Schafer, J.C., M.E. Winkelbauer, C.L. Williams, C.J. Haycraft, R.A. Desmond, and B.K. Yoder. 2006. IFTA-2 is a conserved cilia protein involved in pathways regulating longevity and dauer formation in *Caenorhabditis elegans*. *Journal of cell science.* 119:4088-4100.
- Schlienger, S., S. Campbell, and A. Claing. 2014. ARF1 regulates the Rho/MLC pathway to control EGF-dependent breast cancer cell invasion. *Mol Biol Cell.* 25:17-29.
- Schmitt, H.D., P. Wagner, E. Pfaff, and D. Gallwitz. 1986. The ras-related YPT1 gene product in yeast: A GTP-binding protein that might be involved in microtubule organization. *Cell.* 47:401-412.
- Schoebel, S., L.K. Oesterlin, W. Blankenfeldt, R.S. Goody, and A. Itzen. 2009. RabGDI Displacement by DrrA from *Legionella* Is a Consequence of Its Guanine Nucleotide Exchange Activity. *Molecular Cell.* 36:1060-1072.
- Seabra, M.C., J.L. Goldstein, T.C. Südhof, and M.S. Brown. 1992. Rab geranylgeranyl transferase. A multisubunit enzyme that prenylates GTP-binding proteins terminating in Cys-X-Cys or Cys-Cys. *The Journal of biological chemistry.* 267:14497-14503.
- Segev, N., J. Mulholland, and D. Botstein. 1988. The yeast GTP-binding YPT1 protein and a mammalian counterpart are associated with the secretion machinery. *Cell.* 52:915-924.
- Sengupta, P., P. Satpute-Krishnan, A.Y. Seo, D.T. Burnette, G.H. Patterson, and J. Lippincott-Schwartz. 2015. ER trapping reveals Golgi enzymes continually revisit the ER through a recycling pathway that controls Golgi organization. *Proceedings of the National Academy of Sciences of the United States of America.* 112:E6752-6761.
- Seok, H., H. Lee, E.S. Jang, and S.W. Chi. 2018. Evaluation and control of miRNA-like off-target repression for RNA interference. *Cellular and molecular life sciences : CMLS.* 75:797-814.
- Serra-Marques, A., M. Martin, E.A. Katrukha, I. Grigoriev, C.A.E. Peeters, Q. Liu, P.J. Hooikaas, Y. Yao, V. Solianova, I. Smal, L.B. Pedersen, E. Meijering, L.C. Kapitein, and A. Akhmanova. 2020. Concerted action of kinesins KIF5B and KIF13B promotes efficient secretory vesicle transport to microtubule plus ends. *eLife.* 9:e61302.

- Shafaq-Zadah, M., C.S. Gomes-Santos, S. Bardin, P. Maiuri, M. Maurin, J. Iranzo, A. Gautreau, C. Lamaze, P. Caswell, B. Goud, and L. Johannes. 2016. Persistent cell migration and adhesion rely on retrograde transport of [beta]1 integrin. *Nat Cell Biol.* 18:54-64.
- Shamsipour, F., S. Hosseinzadeh, S.S. Arab, S. Vafaei, S. Farid, M. Jeddi-Tehrani, and S. Balalaie. 2014. Synthesis and investigation of new Hesperadin analogues antitumor effects on HeLa cells. *Journal of Chemical Biology.* 7:85-91.
- Shomron, O., K. Hirschberg, A. Burakov, R. Kamentseva, E. Kornilova, E. Nadezhdina, and I. Brodsky. 2021. Positioning of endoplasmic reticulum exit sites around the Golgi depends on BicaudalD2 and Rab6 activity. *Traffic (Copenhagen, Denmark).* 22:64-77.
- Short, B., C. Preisinger, J. Schaletzky, R. Kopajtich, and F.A. Barr. 2002. The Rab6 GTPase regulates recruitment of the dynactin complex to Golgi membranes. *Current biology : CB.* 12:1792-1795.
- Sigal Yaron, M., R. Zhou, and X. Zhuang. 2018. Visualizing and discovering cellular structures with super-resolution microscopy. *Science (New York, N.Y.).* 361:880-887.
- Silva, D.A., X. Huang, R.H. Behal, D.G. Cole, and H. Qin. 2012. The RABL5 homolog IFT22 regulates the cellular pool size and the amount of IFT particles partitioned to the flagellar compartment in *Chlamydomonas reinhardtii*. *Cytoskeleton.* 69:33-48.
- Sivars, U., D. Aivazian, and S.R. Pfeffer. 2003. Yip3 catalyses the dissociation of endosomal Rab-GDI complexes. *Nature.* 425:856-859.
- Skjeldal, F.M., L.H. Haugen, D. Mateus, D.M. Frei, A.V. Rødseth, X. Hu, and O. Bakke. 2021. De novo formation of early endosomes during Rab5-to-Rab7a transition. *Journal of cell science.* 134.
- Smith, H.L., H. Southgate, D.A. Tweddle, and N.J. Curtin. 2020. DNA damage checkpoint kinases in cancer. *Expert Rev Mol Med.* 22:e2.
- Starr, T., Y. Sun, N. Wilkins, and B. Storrie. 2010. Rab33b and Rab6 are functionally overlapping regulators of Golgi homeostasis and trafficking. *Traffic (Copenhagen, Denmark).* 11:626-636.
- Steger, M., F. Tonelli, G. Ito, P. Davies, M. Trost, M. Vetter, S. Wachter, E. Lorentzen, G. Duddy, and S. Wilson. 2016. Phosphoproteomics reveals that Parkinson's disease kinase LRRK2 regulates a subset of Rab GTPases. *elife.* 5:e12813.
- Steigemann, P., C. Wurzenberger, M.H. Schmitz, M. Held, J. Guizetti, S. Maar, and D.W. Gerlich. 2009. Aurora B-mediated abscission checkpoint protects against tetraploidization. *Cell.* 136:473-484.
- Stein, M., M. Pilli, S. Bernauer, B.H. Habermann, M. Zerial, and R.C. Wade. 2012. The interaction properties of the human Rab GTPase family--comparative analysis reveals determinants of molecular binding selectivity. *PLoS One.* 7:e34870.
- Stengel, K., and Y. Zheng. 2011. Cdc42 in oncogenic transformation, invasion, and tumorigenesis. *Cellular signalling.* 23:1415-1423.
- Styers, M.L., A.P. Kowalczyk, and V. Faundez. 2005. Intermediate Filaments and Vesicular Membrane Traffic: The Odd Couple's First Dance? *Traffic (Copenhagen, Denmark).* 6:359-365.
- Sun, Y., K.G. Buki, O. Ettala, J.P. Vaaraniemi, and H.K. Vaananen. 2005a. Possible role of direct Rac1-Rab7 interaction in ruffled border formation of osteoclasts. *The Journal of biological chemistry.* 280:32356-32361.
- Sun, Y., K.G. Buki, O. Ettala, J.P. Vaaraniemi, and H.K. Vaananen. 2005b. Possible Role of Direct Rac1-Rab7 Interaction in Ruffled Border Formation of Osteoclasts *. *Journal of Biological Chemistry.* 280:32356-32361.
- Sung, K.E., G. Su, C. Pehlke, S.M. Trier, K.W. Eliceiri, P.J. Keely, A. Friedl, and D.J. Beebe. 2009. Control of 3-dimensional collagen matrix polymerization for reproducible human mammary fibroblast cell culture in microfluidic devices. *Biomaterials.* 30:4833-4841.


- Sönnichsen, B., S. De Renzis, E. Nielsen, J. Rietdorf, and M. Zerial. 2000. Distinct Membrane Domains on Endosomes in the Recycling Pathway Visualized by Multicolor Imaging of Rab4, Rab5, and Rab11. *Journal of Cell Biology*. 149:901-914.
- Taulet, N., B. Vitre, C. Anguille, A. Douanier, M. Rocancourt, M. Taschner, E. Lorentzen, A. Echard, and B. Delaval. 2017. IFT proteins spatially control the geometry of cleavage furrow ingression and lumen positioning. *Nature Communications*. 8:1928.
- Teng, Y., X. Xie, S. Walker, D.T. White, J.S. Mumm, and J.K. Cowell. 2013. Evaluating human cancer cell metastasis in zebrafish. *BMC Cancer*. 13:453.
- Terai, T., N. Nishimura, I. Kanda, N. Yasui, and T. Sasaki. 2006. JRAB/MICAL-L2 Is a Junctional Rab13-binding Protein Mediating the Endocytic Recycling of Occludin. *Molecular Biology of the Cell*. 17:2465-2475.
- Thiam, H.-R., P. Vargas, N. Carpi, C.L. Crespo, M. Raab, E. Terriac, M.C. King, J. Jacobelli, A.S. Alberts, T. Stradal, A.-M. Lennon-Dumenil, and M. Piel. 2016. Perinuclear Arp2/3-driven actin polymerization enables nuclear deformation to facilitate cell migration through complex environments. *Nature Communications*. 7:10997.
- Tsukuba, T., Y. Yamaguchi, and T. Kadowaki. 2021. Large Rab GTPases: Novel Membrane Trafficking Regulators with a Calcium Sensor and Functional Domains. *Int J Mol Sci*. 22.
- Ueno, H., X. Huang, Y. Tanaka, and N. Hirokawa. 2011. KIF16B/Rab14 Molecular Motor Complex Is Critical for Early Embryonic Development by Transporting FGF Receptor. *Developmental Cell*. 20:60-71.
- Ullrich, O., H. Stenmark, K. Alexandrov, L.A. Huber, K. Kaibuchi, T. Sasaki, Y. Takai, and M. Zerial. 1993. Rab GDP dissociation inhibitor as a general regulator for the membrane association of rab proteins. *The Journal of biological chemistry*. 268:18143-18150.
- Ungermann, C., and D. Kümmel. 2019. Structure of membrane tethers and their role in fusion. *Traffic (Copenhagen, Denmark)*. 20:479-490.
- Utskarpen, A., H.H. Slagsvold, T.G. Iversen, S. Wälchli, and K. Sandvig. 2006. Transport of ricin from endosomes to the Golgi apparatus is regulated by Rab6A and Rab6A'. *Traffic (Copenhagen, Denmark)*. 7:663-672.
- Valente, C., R. Polishchuk, and M.A. De Matteis. 2010. Rab6 and myosin II at the cutting edge of membrane fission. *Nat Cell Biol*. 12:635-638.
- van der Sluijs, P., M. Hull, P. Webster, P. Måle, B. Goud, and I. Mellman. 1992. The small GTP-binding protein rab4 controls an early sorting event on the endocytic pathway. *Cell*. 70:729-740.
- Vargas, P., L. Barbier, P.J. Sáez, and M. Piel. 2017. Mechanisms for fast cell migration in complex environments. *Current Opinion in Cell Biology*. 48:72-78.
- Vargas, P., M. Chabaud, H.R. Thiam, D. Lankar, M. Piel, and A.-M. Lennon-Duménil. 2016a. Study of dendritic cell migration using micro-fabrication. *Journal of immunological methods*. 432:30-34.
- Vargas, P., P. Maiuri, M. Bretou, P.J. Saez, P. Pierobon, M. Maurin, M. Chabaud, D. Lankar, D. Obino, E. Terriac, M. Raab, H.-R. Thiam, T. Brocker, S.M. Kitchen-Goosen, A.S. Alberts, P. Sunareni, S. Xia, R. Li, R. Voituriez, M. Piel, and A.-M. Lennon-Dumenil. 2016b. Innate control of actin nucleation determines two distinct migration behaviours in dendritic cells. *Nat Cell Biol*. 18:43-53.
- Vargas, P., E. Terriac, A.M. Lennon-Duménil, and M. Piel. 2014. Study of cell migration in microfabricated channels. *J Vis Exp*:e51099.
- Vaughan, L., C.-T. Tan, A. Chapman, D. Nonaka, N.A. Mack, D. Smith, R. Booton, Adam F.L. Hurlstone, and A. Malliri. 2015. HUWE1 Ubiquitylates and Degrades the RAC Activator TIAM1 Promoting Cell-Cell Adhesion Disassembly, Migration, and Invasion. *Cell reports*. 10:88-102.

- Verdijk, P., E.H.J.G. Aarntzen, W.J. Lesterhuis, A.C.I. Boullart, E. Kok, M.M. van Rossum, S. Strijk, F. Eijckeler, J.J. Bonenkamp, J.F.M. Jacobs, W. Blokx, J.H.J.M. vanKrieken, I. Joosten, O.C. Boerman, W.J.G. Oyen, G. Adema, C.J.A. Punt, C.G. Figdor, and I.J.M. de Vries. 2009. Limited Amounts of Dendritic Cells Migrate into the T-Cell Area of Lymph Nodes but Have High Immune Activating Potential in Melanoma Patients. *Clinical Cancer Research*. 15:2531-2540.
- Vertii, A., A. Bright, B. Delaval, H. Hehny, and S. Doxsey. 2015. New frontiers: discovering cilia-independent functions of cilia proteins. *EMBO Rep*. 16:1275-1287.
- Vetter, I.R., and A. Wittinghofer. 2001. The guanine nucleotide-binding switch in three dimensions. *Science (New York, N.Y.)*. 294:1299-1304.
- Vicente-Manzanares, M., X. Ma, R.S. Adelstein, and A.R. Horwitz. 2009. Non-muscle myosin II takes centre stage in cell adhesion and migration. *Nature reviews. Molecular cell biology*. 10:778-790.
- Villarroel-Campos, D., F.C. Bronfman, and C. Gonzalez-Billault. 2016. Rab GTPase signaling in neurite outgrowth and axon specification. *Cytoskeleton*. 73:498-507.
- Vitre, B., A. Guesdon, and B. Delaval. 2020. Non-ciliary Roles of IFT Proteins in Cell Division and Polycystic Kidney Diseases. *Frontiers in cell and developmental biology*. 8.
- Wachter, S., J. Jung, S. Shafiq, J. Basquin, C. Fort, P. Bastin, and E. Lorentzen. 2019. Binding of IFT22 to the intraflagellar transport complex is essential for flagellum assembly. *The EMBO Journal*. 38:e101251.
- Wang, M., Q. Dong, and Y. Wang. 2016. Rab23 is overexpressed in human astrocytoma and promotes cell migration and invasion through regulation of Rac1. *Tumor Biology*. 37:11049-11055.
- Wang, W., T. Wu, and M.W. Kirschner. 2014. The master cell cycle regulator APC-Cdc20 regulates ciliary length and disassembly of the primary cilium. *eLife*. 3:e03083.
- Wang, Y., T. Chen, C. Han, D. He, H. Liu, H. An, Z. Cai, and X. Cao. 2007. Lysosome-associated small Rab GTPase Rab7b negatively regulates TLR4 signaling in macrophages by promoting lysosomal degradation of TLR4. *Blood*. 110:962-971.
- Wang, Z., Z.-C. Fan, S.M. Williamson, and H. Qin. 2009. Intraflagellar Transport (IFT) Protein IFT25 Is a Phosphoprotein Component of IFT Complex B and Physically Interacts with IFT27 in Chlamydomonas. *PLOS ONE*. 4:e5384.
- Watson, H. 2015. Biological membranes. *Essays in Biochemistry*. 59:43-69.
- White, J., L. Johannes, F. Mallard, A. Girod, S. Grill, S. Reinsch, P. Keller, B. Tzschaschel, A. Echard, B. Goud, and E.H. Stelzer. 1999. Rab6 coordinates a novel Golgi to ER retrograde transport pathway in live cells. *The Journal of cell biology*. 147:743-760.
- Wood, C.R., Z. Wang, D. Diener, J.M. Zones, J. Rosenbaum, and J.G. Umen. 2012. IFT Proteins Accumulate during Cell Division and Localize to the Cleavage Furrow in Chlamydomonas. *PLOS ONE*. 7:e30729.
- Worbs, T., S.I. Hammerschmidt, and R. Förster. 2017. Dendritic cell migration in health and disease. *Nature Reviews Immunology*. 17:30-48.
- Xu, L., Y. Nagai, Y. Kajihara, G. Ito, and T. Tomita. 2021. The Regulation of Rab GTPases by Phosphorylation. *Biomolecules*. 11:1340.
- Yamada, K.M., and M. Sixt. 2019. Mechanisms of 3D cell migration. *Nat. Rev. Mol. Cell Biol*. 20:738-752.
- Yan, X., and Y. Shen. 2021. Rab-like small GTPases in the regulation of ciliary Bardet-Biedl syndrome (BBS) complex transport. *The FEBS journal*. n/a.
- Yang, M., T. Chen, C. Han, N. Li, T. Wan, and X. Cao. 2004. Rab7b, a novel lysosome-associated small GTPase, is involved in monocytic differentiation of human acute promyelocytic leukemia cells. *Biochemical and biophysical research communications*. 318:792-799.

- Yao, M., X. Liu, D. Li, T. Chen, Z. Cai, and X. Cao. 2009. Late endosome/lysosome-localized Rab7b suppresses TLR9-initiated proinflammatory cytokine and type I IFN production in macrophages. *Journal of immunology (Baltimore, Md. : 1950)*. 183:1751-1758.
- Yarwood, R., J. Hellicar, P.G. Woodman, and M. Lowe. 2020. Membrane trafficking in health and disease. *Dis Model Mech*. 13.
- Yeung, S.C., C. Gully, and M.H. Lee. 2008. Aurora-B kinase inhibitors for cancer chemotherapy. *Mini Rev Med Chem*. 8:1514-1525.
- Young, J., J. Ménétrey, and B. Goud. 2010. RAB6C is a retrogene that encodes a centrosomal protein involved in cell cycle progression. *J Mol Biol*. 397:69-88.
- Young, J., T. Stauber, E. del Nery, I. Vernos, R. Pepperkok, and T. Nilsson. 2005. Regulation of microtubule-dependent recycling at the trans-Golgi network by Rab6A and Rab6A'. *Mol Biol Cell*. 16:162-177.
- Yu, J., H. Sun, W. Cao, Y. Song, and Z. Jiang. 2022. Research progress on dendritic cell vaccines in cancer immunotherapy. *Experimental Hematology & Oncology*. 11:3.
- Zampedri, C., W.A. Martínez-Flores, and J. Melendez-Zajgla. 2021. The Use of Zebrafish Xenotransplant Assays to Analyze the Role of lncRNAs in Breast Cancer. *Frontiers in Oncology*. 11.
- Zhang, B., C. Xuan, Y. Ji, W. Zhang, and D. Wang. 2015. Zebrafish xenotransplantation as a tool for in vivo cancer study. *Fam Cancer*. 14:487-493.
- Zhang, Q., J. Calafat, H. Janssen, and S. Greenberg. 1999. ARF6 is required for growth factor- and rac-mediated membrane ruffling in macrophages at a stage distal to rac membrane targeting. *Mol Cell Biol*. 19:8158-8168.
- Zhang, Y., and F.M. Hughson. 2021. Chaperoning SNARE Folding and Assembly. *Annual Review of Biochemistry*. 90:581-603.
- Zhang, Y., H. Liu, W. Li, Z. Zhang, X. Shang, D. Zhang, Y. Li, S. Zhang, J. Liu, R.A. Hess, G.J. Pazour, and Z. Zhang. 2017. Intraflagellar transporter protein (IFT27), an IFT25 binding partner, is essential for male fertility and spermiogenesis in mice. *Developmental biology*. 432:125-139.
- Zhen, Y., and H. Stenmark. 2015. Cellular functions of Rab GTPases at a glance. *Journal of cell science*. 128:3171-3176.
- Zobywalski, A., M. Javorovic, B. Frankenberger, H. Pohla, E. Kremmer, I. Bigalke, and D.J. Schendel. 2007. Generation of clinical grade dendritic cells with capacity to produce biologically active IL-12p70. *J Transl Med*. 5:18.



Rab6 regulates cell migration and invasion by recruiting Cdc42 and modulating its activity

Katharina Vestre^{1,2} · Ingrid Kjos^{1,2} · Noemi Antonella Guadagno^{1,2} · Marita Borg Distefano^{1,2} · Felix Kohler³ · Federico Fenaroli¹ · Oddmund Bakke^{1,2} · Cinzia Progida^{1,2} 

Received: 20 March 2018 / Revised: 8 February 2019 / Accepted: 26 February 2019 / Published online: 4 March 2019
© Springer Nature Switzerland AG 2019

Abstract

Rab proteins are master regulators of intracellular membrane trafficking, but they also contribute to cell division, signaling, polarization, and migration. The majority of the works describing the mechanisms used by Rab proteins to regulate cell motility involve intracellular transport of key molecules important for migration. Interestingly, a few studies indicate that Rabs can modulate the activity of Rho GTPases, important regulators for the cytoskeleton rearrangements, but the mechanisms behind this crosstalk are still poorly understood. In this work, we identify Rab6 as a negative regulator of cell migration *in vitro* and *in vivo*. We show that the loss of Rab6 promotes formation of actin protrusions and influences actomyosin dynamics by upregulating Cdc42 activity and downregulating myosin II phosphorylation. We further provide the molecular mechanism behind this regulation demonstrating that Rab6 interacts with both Cdc42 and Trio, a GEF for Cdc42. In sum, our results uncover a mechanism used by Rab proteins to ensure spatial regulation of Rho GTPase activity for coordination of cytoskeleton rearrangements required in migrating cells.

Keywords Rab proteins · Rab6 · small GTPases · cell migration

Introduction

Rab proteins constitute the largest family of the Ras superfamily of small GTPases, with more than 60 members in humans. The role of Rab proteins in vesicle transport was identified for the first time in yeast already in the 1980s, and since then, more and more studies have established them as the master regulators of intracellular membrane traffic [1–4].

To perform their tasks each Rab protein cycles between membrane and cytosol, switching between a GTP-bound and a GDP-bound conformation. Upon membrane recruitment, Rab proteins in their GTP-bound state can bind a variety of different effector molecules, including sorting adaptors, tethering factors, fusion regulators, kinases, phosphatases, and motor proteins [4, 5].

Lately, it has been demonstrated that in addition to regulating intracellular traffic, Rab proteins take part in several other cellular processes. Indeed, these small GTPases are also important for regulation of mitotic spindle positioning and abscission during cell division, apical lumen formation and polarization of epithelial cells, and nutrient sensing and signaling [6–9].

Interestingly, an increasing amount of evidence demonstrates that Rab proteins also have a role in cell migration [10–12]. So far, regulation of cytoskeleton dynamics involved in cell shape and motility has been mainly attributed to another family of small GTPases, namely, the Rho proteins, and thus, the contribution by the Rab family to this process remains much less characterized [13, 14]. We recently demonstrated that Rab7b can affect cell migration through regulation of the actin cytoskeleton [10]. By directly

Katharina Vestre and Ingrid Kjos contributed equally to this work.

Electronic supplementary material The online version of this article (<https://doi.org/10.1007/s00018-019-03057-w>) contains supplementary material, which is available to authorized users.

✉ Cinzia Progida
c.a.m.progida@ibv.uio.no

- ¹ Department of Biosciences, University of Oslo, Oslo, Norway
- ² Centre for Immune Regulation, University of Oslo, Oslo, Norway
- ³ Department of Physics, The NJORD Centre, University of Oslo, Oslo, Norway

interacting with the actin motor myosin II, Rab7b is able to modulate the activity of RhoA and thereby the phosphorylation of myosin light chain (MLC). In this way, Rab7b influences actin cytoskeleton dynamics, including the formation of stress fibers, cell adhesions, and thus cell migration [10].

Intriguingly, also Rab6 is known to interact directly with myosin II in a GTP-dependent manner [15]. Rab6 is an evolutionary conserved and ubiquitously expressed Rab protein [16, 17]. It localizes to the Golgi apparatus and Golgi-derived vesicles and regulates many trafficking routes, both anterograde and retrograde, between the Golgi apparatus, endoplasmic reticulum (ER), plasma membrane (PM), and endosomes [17–21]. In addition, Rab6 is involved in cell division and phagosome maturation [22–24].

To execute all these functions, Rab6 interacts with many different effector molecules, including motor proteins and their interactors such as KIF1C, KIF5B, KIF20A (also known as Rabkinesin-6), the dynein–dynactin complex through Bicaudal D, myosin II, and myosin VA [15, 18, 25–29].

In this study, we investigated whether Rab6, similar to Rab7b, can regulate cell migration through its interaction with myosin II. Our results show that Rab6 knockdown indeed affects cell migration by increasing cell speed and, therefore, wound closure. We also demonstrate that Rab6 depletion influences the actomyosin system by upregulation of Cdc42 activity and downregulation of MLC phosphorylation. Intriguingly, we discover that Rab6 interacts with both the Rho GTPase Cdc42 and Trio, a GEF for Cdc42 [30]. By modulating Cdc42 activity, Rab6 regulates the formation and dynamics of actin-dependent protrusions such as filopodia. We finally confirm that Rab6 is a negative regulator of cell migration using xenotransplantation of human cancer cells into zebrafish embryos. In sum, our results support a novel emerging mechanism for Rab proteins in the regulation of actin cytoskeleton dynamics and cell migration by crosstalk with Rho GTPases.

Materials and methods

Cell culture

U2OS, HeLa, and H1299 cells were grown in Dulbecco's modified Eagle's medium (DMEM; Lonza, BioWhittaker). RPE-1 cells were grown DMEM F-12 (Lonza, BioWhittaker). Both DMEM and DMEM F-12 were supplemented with 10% fetal calf serum (FCS), 2 mM L-glutamine, 100 U/ml penicillin, and 100 µg/ml streptomycin.

Constructs and antibodies

pEGFP-C1 was purchased from BD Biosciences, Clontech. pEGFP-C1 Rab6A wt, pEGFP-C1 Rab6A Q72L, and pEGFP-C1 Rab6A T27 N were a gift from Marci Scidmore (Addgene plasmid #49,469, #49,483, and #49,484, respectively) [31]. pcDNA3-EGFP-Cdc42-Q61L and pcDNA3-EGFP-Cdc42-T17 N were a gift from Gary Bokoch (Addgene plasmid #12,986 and #12,976, respectively) [32]. pTriEx- mCherry-cdc42 Q61L and the biosensor constructs, pTriEX Cdc42 wt and pTriEX Cdc42 G12 V, were a gift from Luis Hodgson (Albert Einstein College of Medicine, NY, USA). mCherry-Cdc42-C-10 was a gift from Michael Davidson (Addgene plasmid #55,014). p^{CMV}-LifeAct-RFP was purchased from Ibidi. pEGFP-C3 Cdc42 wt was a gift from Keith Burridge, University of North Carolina, Chapel Hill, USA. pcDNA 3.1-HA Rab6A, pcDNA 3.1-HA Rab6A Q72L, and pcDNA 3.1-HA Rab6A T27 N were purchased from Genscript. pEGFP-C1-Trio was a kind gift from Jaap D. Van Buul (University of Amsterdam, The Netherlands) [33].

Primary antibodies used in this study were: anti-giantin (Abcam, ab24586, 1:1000), anti-tubulin (Life Technologies, # 13-8000, 1:12,000), anti-phospho-myosin light chain 2 (Ser19) (Cell Signaling Technology, # 3671, 1:300), anti-myosin light chain (Sigma-Aldrich, # M4401, 1:50), anti-GFP (Abcam, ab6556, 1:3000), anti-HA (Abcam, ab9110, 1:1000), anti-RhoA (Cytoskeleton Inc., ARH04, 1:500), anti-Rac1 (Cytoskeleton Inc., ARC03, 1:500), anti-Cdc42 (Cytoskeleton Inc., ACD03, 1:250), anti-Cdc42 (Abcam, ab155940, 1:200), anti-Trio (Abnova, H00007204-A01), anti-Rab6A (Abcam, ab95954, 1:200), anti-actin (Cytoskeleton Inc., AAN01, 1:500), anti-N-WASP (Cell Signaling Technology, # 30D10, 1:300), anti-IQGAP1 (BD Laboratories, #610,611, 1:300), anti-DOCK10 (Abcam, ab75258, 1:1000), and mouse IgG1 (×0931, Dako, 1:50). Rhodamine-conjugated phalloidin was purchased from Invitrogen (R415). The SiR-actin kit was purchased from Cytoskeleton, Inc. and used according to manufacturer's protocol (Cytoskeleton, Inc./Spirochrome #CY-SC001). For immunofluorescence experiments, Alexa Fluor secondary antibodies (Invitrogen) were used at dilution 1:200. Secondary antibodies conjugated to horseradish peroxidase for immunoblotting studies (GE Healthcare) were diluted 1:5000. Hoechst (Life Technologies, H3569) was used at 0.2 µg/ml and DAPI (Sigma-Aldrich, D9542) was used at 0.1 µg/ml.

Transfection and RNA interference

U2OS cells were transiently transfected using Lipofectamine 2000 (Life Technologies), while HeLa cells

were transfected using FuGENE 6 (ProMega), following the producer's protocol. Cells were transfected at approximately 50–70% confluency for 24 h prior to further execution of experiments. U2OS, RPE-1, and H1299 cells were transfected with siRNA using Lipofectamine RNAiMAX Transfection Reagent (Life Technologies) according to the manufacturer's instructions. The cells were transfected either the day after plating or the same day by reverse transfection, and analyzed after 72 h. siRNA transfections in HeLa cells were performed using Oligofectamine (Invitrogen) as described previously [34]. In short, cells were plated in 6-cm dishes 1 day prior to transfection ($\sim 4 \times 10^5$ cells/dish), and replated 72 h after transfection. Experiments were performed after 48 h.

Nontargeting control siRNA (sense sequence 5'-ACUUCGAGCGUGCAUGGCUTT-3' and antisense 5'-AGCAUGCACGCUCGAAGUTT-3') was purchased from MWG-Biotech (Ebersberg, Germany).

siRNAs against Rab6 (siRab6 #1, J-008975-08; siRab6 #2, J-008975-09; siRab6 #3, J-008975-07; siRab6 #4, J-008975-10). Trio (siTrio, J-005047-05) and DOCK10 (siDOCK10, J-023079-05) were purchased from Dharmacon™.

For rescue experiments, cells were first transfected with siRNA using RNAiMax (for U2OS cells) or Oligofectamine (for HeLa cells). After 48 h, the cells were transfected with pEGFP-Rab6 using Lipofectamine 2000 (for U2OS cells) or FuGENE 6 (for HeLa cells) according to the manufacturers' instructions. The experiments were performed 72 h after siRNA transfection.

Cell migration assays

Cells were grown to form confluent monolayers in IncuCyte ImageLock 96-well plates (Essen Bioscience) and scratched with IncuCyte® WoundMaker (Essen Bioscience). Cell migration was monitored by time-lapse imaging using an IncuCyte® ZOOM (10× objective, Essen Bioscience). Relative wound density (percent) was calculated using the IncuCyte® ZOOM software analysis program. Cell tracking and quantification of velocity and directionality was done using Fiji/ImageJ manual tracking plugin and Ibidi Chemotaxis software.

Particle image velocimetry (PIV) analysis was done using OpenPIV and OpenPIV spatial analysis toolbox in MATLAB R2015b. The interrogation windows were set to 32×32 -pixels with 50% overlap.

Cell proliferation and cell death assays

Cell proliferation and cell death assays were performed on cells subjected to wound healing assays as described above. For the cell proliferation assays, the Click-iT™ Plus Edu

Alexa Fluor™ 488 Imaging Kit (Molecular Probes) was used according to the manufacturer's instructions. Briefly, medium containing 10 μ M Edu was added to the cells before imaging, and after 24 h, the cells were fixed using 3% paraformaldehyde and permeabilized with 0.5% Triton® X-100. Incorporated Edu was detected by adding the Click-iT® Plus reaction cocktail as described by the manufacturer, and DNA was stained with 5 μ g/ml Hoechst® 33342 (Molecular Probes). Cells were imaged using an Andor Dragonfly microscope with a 10× objective and quantification of the percentage of Edu-positive cells was done using the Fiji/ImageJ analysis software.

For the cell death assays, medium containing 250 nM IncuCyte® Cytotox Reagent (Essen Bioscience) was added to label dying cells green. The number of green objects per image was calculated using the IncuCyte® ZOOM software analysis program. Cell death was quantified by dividing the number of green objects at each timepoint with the number of green objects at time 0.

Golgi reorientation measurements

Cells were grown to form a confluent monolayer on glass slides, scratched with a pipette tip, and incubated for 2 h at 37 °C and 5% CO₂. Subsequently, the cells were fixed and stained with anti-giantin, rhodamine-conjugated phalloidin and Hoechst to visualize the Golgi complex, actin cytoskeleton, and nuclei, respectively. Golgi reorientation was measured by dividing the cells on the wound edge into three equal sectors and calculating the percentage of cells having their Golgi apparatus in the front sector (facing in the direction of migration) as previously described [10].

Cell-spreading assay

Cells were seeded onto fibronectin-coated coverslips (10 μ g/ml) and incubated for 1 h at 37 °C and 5% CO₂ before fixation and staining with rhodamine-conjugated phalloidin and DAPI. Quantification of the cell area was done using the Fiji/ImageJ analysis software.

Micropatterns

96-well CYTOO plates (CYTOO, 20-900-00) containing L-shaped micropattern (1100 μ m²) were coated with 20 μ g/ml sterile fibronectin (Sigma F2006) in PBS for 2 h at room temperature. 3×10^3 cells were then added to each well and kept at room temperature for 30 min and subsequently at 37 °C for 3 h. Cells were then fixed and stained with rhodamine-conjugated phalloidin and Hoechst.

Analysis of actin distribution in cells seeded on the L-shaped micropatterns was performed in ImageJ, using the CYTOOL-IP Reference Cell macro (RefCell) that provides

a statistical representation of the spatial distribution of intracellular compartments, in our case the actin fibers. Using the Reference Cell macro, a normalized mean cell was obtained by alignment and overlay of 40 cells per experiment and averaging the signals for each condition. A Reference Cell was constructed by making a projection of the filtered and aligned images from a stack [35]. The rigidity/collapse of the actin fibers along the hypotenuse was quantified using the Hypotenuse Macro [35]. Briefly, thresholded images of the empty *L*-micropatterns were used to define the theoretical hypotenuse of the triangle shape. Next, thresholding of the actin stained images was performed to define the actual cell shape. The hypotenuse macro was modified by shifting the theoretical hypotenuse of 2.4 μm to be able to recognize smaller difference in the collapse of the actin fibers. The difference in the areas between the theoretical hypotenuse and the actual cell border was then measured and represented as percentage of collapsed cells (curved when the area difference resulted in a positive value) and non-collapsed cells (straight when no differences in the areas between the theoretical hypotenuse and the actual cell border were detected).

Immunofluorescence and live-cell microscopy

Cells were grown on coverslips, fixed with 3% paraformaldehyde, and quenched using 50 mM NH_4Cl . Afterwards, 0.25% saponin in PBS 1 \times was used for permeabilization and 5% FCS in PBS 1 \times for blocking. The cells were incubated with primary antibodies at room temperature for 20 min, washed in PBS/saponin, incubated with secondary antibodies in darkness at room temperature for 20 min, washed again in PBS/saponin, and finally mounted with Mowiol.

Fixed cells were imaged with an Olympus FluoView 1000 IX81 confocal laser scanning microscope (inverted) using a 60 \times PlanApo NA 1.35 objective, or with an Olympus FluoView 1000 BX61WI confocal laser scanning microscope (upright) using a 60 \times PlanApo 1.4 objective and FV1000 software.

For live-cell imaging, cells were seeded on MatTek glass-bottom dishes. Before imaging, the culture medium was replaced to phenol red-free DMEM. For live-cell image acquisition the cells were kept in an incubation chamber (Solent Scientific) at 37 $^\circ\text{C}$ and 5% CO_2 and imaged using a Yokagawa CSU22 spinning-disk confocal unit with an Andor Ixon EMCCD camera and a 60 \times NA 1.42 objective provided with the Andor iQ1.8 software.

Total internal reflection fluorescence (TIRF) microscopy acquisition was done on an Andor Dragonfly microscope using a 100 \times objective with NA 1.45 and the Fusion software.

To measure Cdc42 activity in live cells, a biosensor for Cdc42 based on Förster resonance energy transfer (FRET) was used [49]. This single-chain biosensor incorporates

the donor/acceptor FRET pair of the monomeric Cerulean (mCer) and monomeric Venus (mVen) fluorescent proteins. When Cdc42 is in an inactive GDP-bound state, the mCer and mVen are at a distance from each other, only given off a weak FRET signal when excited. However, when Cdc42 upon binding to GTP changes its conformation, the mCer and mVen fluorescent proteins are brought into closer proximity and therefore the FRET signal increases. For excitation of the biosensor (excitation of mCer), the 405 nm laser was used to reduce the amount of mVen cross excitation to a minimum. The emission was measured using the Zeiss LSM880 microscope equipped with a 32 array spectral GaAsP detector using a 63 \times oil C Plan Apo objective with NA 1.4 or a 40 \times oil Plan Apo objective with NA 1.3 and the ZEN Black software. To measure the activity of Cdc42, the emission values were recorded at 477 nm, which corresponds to the maximum emission peak of mCer, and at 530 nm, which corresponds to the maximum emission peak for mVen. Since the 405 nm laser was used for excitation, which does not excite mVen, the observed emission at 530 nm of mVen corresponds to the FRET in the sample. To make our measurements comparable between cells, we divided the intensities at 530 nm by the intensities at 477 nm to obtain the FRET/mCer ratio. Image acquisition was performed on a focal plane close to the cell surface/dish.

Optical tweezers

HeLa cells were seeded on MatTek glass-bottom dishes at low confluency to assure a good access for the optical tweezers. Before mounting the dishes on the optical tweezers setup, the medium was replaced by phenol red-free DMEM containing 1 μm carboxylated latex beads (Bangs Laboratories). The experiments were performed on an optical tweezers setup (NanoTracker2, JPK, Germany) equipped with a confocal unit (C2, Nikon, Japan) and a temperature-controlled stage at 37 $^\circ\text{C}$. Before every experiment, the optical trap and the QPD detection system were calibrated using the implemented calibration function based on thermal fluctuations [36]. To investigate the filopodial properties, a trapped bead was moved close to the filopodial tip. After binding of the bead to the filopodium, the filopodium usually starts to retract [37, 38]. The bead's position was tracked during the entire retraction process of each filopodium. Hereby, a force clamp was used, where the set point has been changed every 10 s to test the reaction on different forces. The trajectory segments were analyzed by a linear fit of the projection on the main retraction velocity, which reveals a velocity for the respective counteracting force during acquisition of the segment. Velocities below a threshold of 0.5 nm/s were considered as a stall event.

Immunoblotting

Cell lysates were subjected to SDS-PAGE and blotted onto polyvinylidene fluoride (PVDF) membranes (Millipore). The membranes were incubated with primary antibodies diluted in 2% blotting grade non-fat dry milk (BioRad), followed by secondary antibodies conjugated to horseradish peroxidase (HRP) (GE Healthcare). Either the ECL Prime Western Blotting Detection (GE Healthcare) or the Super-Signal West Femto Maximum Sensitivity Substrate (Thermo Scientific) were used to detect the chemiluminescent signals. Quantification of band intensity was done by densitometry analysis with the ImageQuant TL software (GE Healthcare) or with the Carestream software.

RhoA, Rac1, and Cdc42 activation assay

RhoA, Rac1, and Cdc42 activation was assessed using the Activation Assay Biochem Kit (Cytoskeleton, Inc.) according to manufacturer's protocol. Briefly, GTP-bound RhoA was immunoprecipitated from cell lysates with beads coupled to the Rho-binding domain (RBD) of the Rho effector protein rhotekin, while Rac1 and Cdc42 were immunoprecipitated using beads coupled to the Interactive Binding (CRIB/PDB) region of the Cdc42/Rac1 effector protein p21 activated kinase I (PAK1). Immunoprecipitated samples and total lysates were analyzed by immunoblotting.

F- and G-actin quantification

F- and G-actin extractions were performed with the G-Actin/F-actin In Vivo Assay Biochem Kit (Cytoskeleton, Inc.) according to the manufacturer's instructions. Briefly, U2OS cells were lysed in a buffer that stabilized and maintained the globular and filamentous forms of actin, incubated for 10 min at 37 °C, and subjected to ultracentrifugation for 2 h at 100,000×g at room temperature. The supernatants, containing the G-actin fractions, and the re-suspended pellets, containing F-actin, were subjected to Western Blot analysis. The amounts of F-actin and G-actin relative to the total actin were quantified by detecting the intensity of the bands using the program ImageQuant (Amersham Biosciences). To control that the F-actin was efficiently pelleted during centrifugation, 100× phalloidin (AE01, Cytoskeleton inc.) was added at 1× final concentration to an additional control sample directly after lysis.

Co-immunoprecipitation

Co-immunoprecipitation experiments were done using the GFP-Trap[®]_MA (Chromotek) according to the producer's protocol. In short, lysates from cells transfected with GFP-fusion proteins were incubated for 1 h at 4 °C with magnetic

beads coupled to anti-GFP antibodies for co-immunoprecipitation. Immunoprecipitated samples and total lysates were subsequently loaded on SDS-PAGE gels and subjected to western blotting analysis.

Dynabead protein G (Life Technologies) was used according to the manufacturer's protocol for IP of HA-Rab6. Briefly, Dynabeads (0.6 µg) were washed in RIPA buffer and incubated with either IgG isotype control or with the antibody against HA, for 60 min with end-over-end-rotation at room temperature. Pre-cleared cell lysates were thereafter incubated with the antibody-coupled beads for 90 min with end-over-end-rotation at room temperature. Immunoprecipitated samples were loaded on SDS-PAGE and analyzed by western blotting.

Zebrafish xenotransplants

Wild-type zebrafish embryos were kept at 28.5 °C in standard embryo medium [39] containing 0.003% phenylthiourea (Aldrich). The experiments were conducted in agreement with the provisions enforced by the Norwegian national animal research authority (NARA).

Embryos were decorionated 24 h post-fertilization (hpf). At day 2 post-fertilization, H1299 were injected in the otic vesicle. For this, larvae were first sedated in a 230 µg/ml tricaine bath before being placed on a dish containing 2% of hardened agarose gel in water.

Before the injection, 10⁵ H1299 cells were transfected for 16–20 h with either a control siRNA or a siRNA against Rab6. For rescue experiments, cells were electroporated with GFP-Rab6 (Amara nucleofector, Lonza) the day after silencing. 6–7 h after electroporation the cells were injected in the otic vesicle of zebrafish embryos. Before the injection, cells were stained with Q-tracker 655 cell-labelling kit (Life Technologies) for 45 min at 37 °C following the manufacturer's instructions. After staining, cells were trypsinized, re-suspended in culture medium, and centrifuged for 8 min at 400×g. The supernatant was discarded and 1 ml PBS $-/-$ Ca²⁺/Mg²⁺ was added to each cell pellet. Cells were re-suspended and centrifuged again for 8 min, at 400×g. The PBS was removed until the pellet was only partially covered and re-suspended in the small remaining volume of PBS. The cell suspension was then loaded onto a glass capillary connected to a pump (Eppendorf Femtojet Express) and controlled using a micromanipulator (MN153, Narishige). Prior to injection, the number of cells was regulated by varying the applied pressure of the pump. 2–3 nl of cell suspension was injected in the otic vesicle of each animal that were subsequently placed at 35 °C to facilitate cell growth. No adverse effects on embryo development were observed. Images were acquired directly after the injection (time zero) and at 24 and 48 h post-injection using a Leica DFC365FX stereomicroscope with a 1.0× PlanApo lens. For

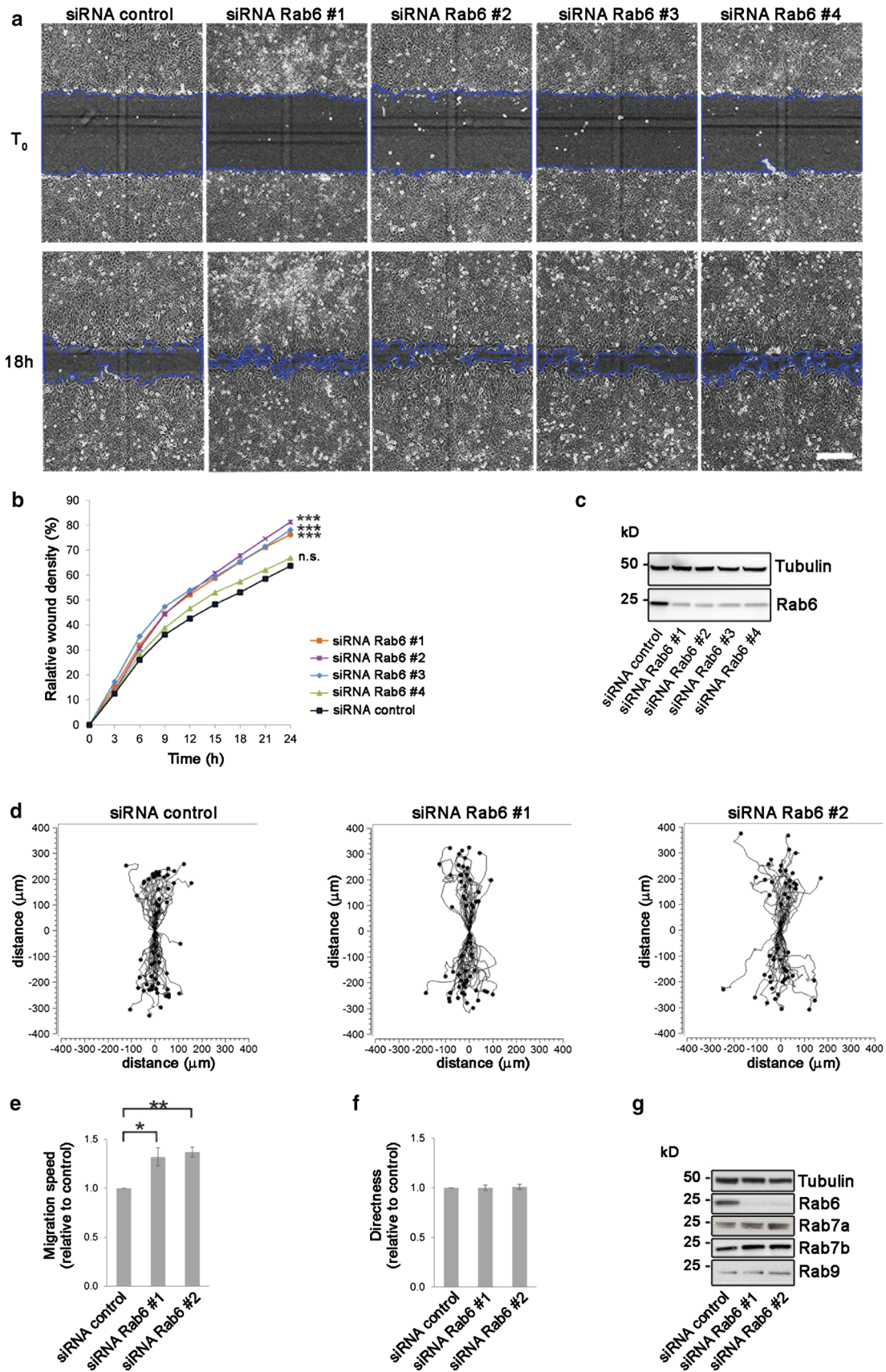


Fig. 1 Rab6 silencing promotes cell migration. **a** U2OS cells transfected with control siRNA or 4 different siRNAs against Rab6 (#1, #2, #3, #4) were scratch-wounded and imaged every 3rd hour for 24 h. Representative images of (T_0) and 18 h after scratching are shown. Scale bar: 300 μm . **b** Quantification of the relative wound density (%) as function of time for control cells and Rab6-depleted cells. Data represents the mean of three independent experiments. $***P < 0.001$ compared to control (two-way repeated measures ANOVA followed by Tukey's post test for $t = 24$ h). **c** Cell lysates from each sample were subjected to Western blot analysis with antibodies against Rab6 and tubulin (as a loading control). **d** Representative track plots of the single-cell distances of migration for cells transfected with siRNA control, siRNA Rab6#1 or siRNA Rab6#2. Individual tracks are shown so that each starts at the origin (distance 0). Quantification of the mean \pm SEM of speed (**e**) and directness (**f**) relative to the control. $n > 150$ cells from at least five independent experiments. $*P < 0.05$; $**P < 0.01$ (paired Student's t test). **g** Lysates from cells transfected with either siRNA control or siRNA against Rab6 (#1 and #2) were subjected to Western blot analysis with the indicated antibodies

the quantification of cell migration, the distance of the cells from the injection site was measured as the area obtained by drawing a line along the cells outside of the injection site at 24 and 48 h after the injection. The quantification was performed using the software ImageJ.

Image processing and analysis

Image analysis and processing was performed using ImageJ (National Institutes of Health) and Adobe Photoshop (Adobe Systems). Analysis of the total filopodia number per cell was done using FiloQuant plugin for ImageJ, kindly provided by Guillaume Jacquemet, University of Turku, Finland.

For the analysis of filopodia at the leading edge of migrating cells, the FiloQuant plugin was used to measure the cell border, and the filopodia were manually counted to include only protrusions extending from the membrane facing the wound.

For the quantification of Cdc42-positive vesicles in the cell front of migrating cells, the total number of Cdc42-positive vesicles was calculated using ImageJ. A line parallel to the migration front was drawn over the perinuclear region, half-way between the nucleus and the cell border and the number of vesicles above the line in the cell front was counted and expressed as percentage compared to the total number of vesicles per cell.

Statistical analysis

Assessment of statistical differences was done by two-tailed paired Student's t test using the Excel software, or ANOVA followed by post hoc tests in the GraphPad Prism 8 software as indicated in the figure legends. In the figures, statistical significance is indicated as follows: $*P < 0.05$, $**P < 0.01$, $***P < 0.001$. The statistical analysis of the filopodial

retraction force and velocity was done in Matlab using a two-sample Student's t test and a two-sample Kolmogorov–Smirnov test.

Results

Rab6 depletion increases cell migration

Rab proteins are master regulators of intracellular membrane transport. However, increasing evidence shows that Rabs are also involved in the process of cell migration [10–12]. Rab7b interferes with cell migration by modulating actomyosin dynamics through direct interaction with the actin motor myosin II [10]. Since also Rab6 interacts directly with myosin II [15], we investigated whether Rab6, similar to Rab7b, is important for the process of cell migration.

To test our hypothesis, we performed a wound healing assay using U2OS cells transfected with an siRNA control or with four different siRNAs against Rab6 (siRNA Rab6 #1, siRNA Rab6 #2, siRNA Rab6 #3, and siRNA Rab6 #4). The quantification of the relative wound density showed that Rab6 knockdown does indeed affect cell migration by increasing the rate of wound closure (Fig. 1a–c). Importantly, all the four different siRNAs used to knockdown Rab6 gave similar results, with an increase in wound density of approximately 20% 24 h after wounding (except siRNA Rab6 #4 that resulted in only 5% increase), indicating that Rab6 specifically influences cell migration and that the result obtained was unlikely caused by off-target effects.

We further analyzed in more detail the effect of Rab6 depletion on migrating cells. For this purpose, we chose the two siRNAs that gave the strongest effect in the wound healing assay (siRNA Rab6 #1 and siRNA Rab6 #2) and measured single-cell speed and directionality in both U2OS (cancer cell line) and RPE-1 cells (epithelial cell line). The single-cell analysis revealed that the depletion of Rab6 increased cell speed by about 30% compared to control cells in both U2OS and RPE-1 cells, while directionality was only modestly affected (Fig. 1d–g; Suppl. Fig. 1a–f). The movement of continuous sheets of epithelial RPE-1 cells was also visualized by velocity fields, showing that the increased migration speed upon Rab6 depletion can be observed throughout the cell monolayer (Suppl. Fig. 1g).

The re-expression of Rab6 in U2OS cells depleted for this small GTPase, using either oligos, rescued the migration at levels similar to the control (Suppl. Fig. 2a, b), thus excluding that this effect was a consequence of increased proliferation or reduced cell death (Suppl. Fig. 2c, d). This further validates the specificity of the Rab6 siRNAs and of the migration phenotype upon Rab6 knockdown.

In addition to U2OS and RPE-1 cells, we also measured the effect on cell migration upon Rab6 silencing on

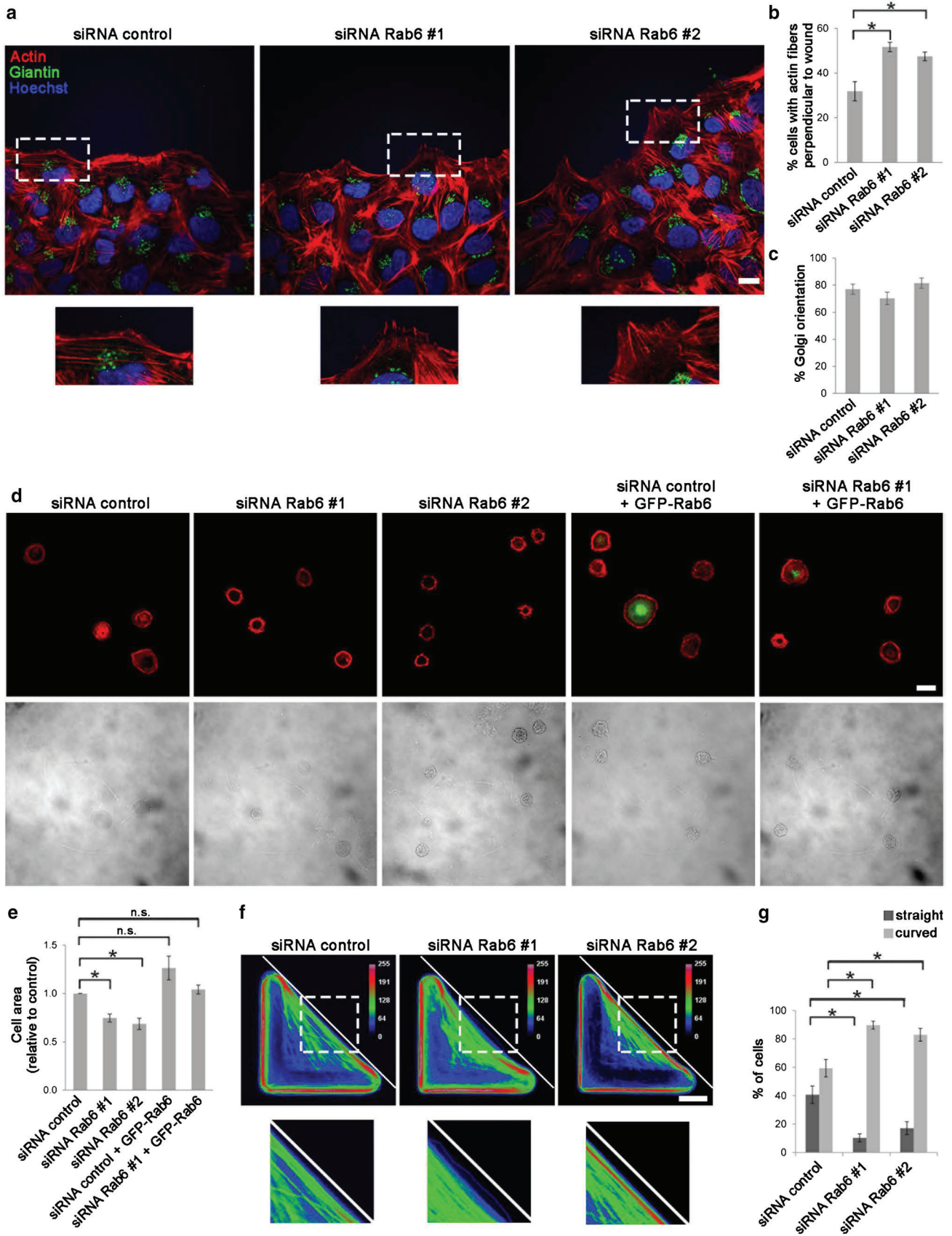


Fig. 2 Rab6 influences actin dynamics and cell spreading. **a** U2OS cells treated with siRNA control, siRNA Rab6 #1 or siRNA Rab6 #2 were scratched with a pipet tip and fixed after 2 h. Cells were immunostained with an antibody against giantin. Actin was labeled with rhodamine-conjugated phalloidin and nuclei with Hoechst. The lower insets show magnifications of the boxed areas. Scale bar: 20 μm . **b** Quantification of the percentage of cells with actin fibers perpendicular to the wound is represented as mean \pm SEM; $n > 150$ cells from four independent experiments. $*P < 0.05$ (paired Student's t test). **c** Quantification of the percentage of cells having Golgi located between the nucleus and the leading edge. The graph shows the mean \pm SEM; $n > 120$ cells from four independent experiments. **d** U2OS cells transfected with siRNA control, siRNA Rab6 #1, siRNA Rab6 #2, or silenced with siRNA control or siRNA Rab6 #1 and subsequently transfected with GFP-Rab6 were plated on fibronectin-coated coverslips and left to adhere for 1 h before fixation and staining with Hoechst and rhodamine-conjugated phalloidin. Lower panel shows transmission images for comparison. Scale bar: 20 μm . **e** Quantification of the average area. The graph represents the mean \pm SEM normalized to the control; $n > 90$ cells from at least three independent experiments. $*P < 0.05$ (one-way ANOVA followed by Tukey's post test). **f** U2OS cells treated with siRNA control, siRNA Rab6 #1 or siRNA Rab6 #2 were plated onto dishes with fibronectin-coated L-shaped micropattern and left to adhere for 3.5 h before fixation and staining with rhodamine-conjugated phalloidin. Color-coded frequency map of averaged Z-projected images from one representative experiment are shown. Scale bar: 10 μm . **g** The graph shows the quantification for each condition of the percentage of cells with straight or curved hypotenuse (mean \pm SEM) normalized to the control. $n > 60$ cells from three independent experiments. $*P < 0.05$; $**P < 0.01$ (paired Student's t test)

HeLa cells. Similar to the previously tested cell lines, also migration in HeLa cells was increased in cells silenced with either oligos (Suppl. Fig. 2e, g).

Having discovered that depletion of Rab6 increases cell migration, and knowing that Rab6 directly interacts with myosin II [15], we next investigated whether the effect of Rab6 on cell migration is a consequence of an effect on the actomyosin cytoskeleton. U2OS cells transfected with siRNA control or siRNAs against Rab6 were subjected to wound healing assays and the arrangement of the actin cytoskeleton was analyzed by confocal microscopy. The results showed a clear difference in the formation of actin protrusions at the leading edge of the migrating cells. In about 50% of the cells silenced for Rab6 the actin fibers were oriented perpendicular to the wound in contrast to only 30% for control cells (Fig. 2a, b). This result suggests that Rab6 influences actin dynamics.

We also checked whether Rab6 influences cell polarization in migrating cells. It is known that the Golgi apparatus reorients in migrating cells from a random perinuclear position to the area between the nucleus and the leading edge [40, 41]. However, Golgi reorientation was unaffected after Rab6 depletion (Fig. 2a–c).

All together, these data indicate that Rab6 depletion promote cell migration and actin fiber reorientation.

Rab6 is required for cell spreading

Having observed that Rab6 affects cell motility, we further investigated whether Rab6 is required for cell spreading. U2OS cells transfected with siRNA control, siRNA Rab6 #1 or siRNA Rab6 #2 were trypsinized and plated on fibronectin-coated cover slips, fixed and finally stained with rhodamine–phalloidin. Quantification of the cell area clearly shows that knockdown of Rab6 decreases cell spreading in U2OS cells by circa 30% for both the tested oligos (Fig. 2d, e).

In line with this, overexpression of Rab6 leads to an increased cell area by almost 30% (Fig. 2d, e), indicating that Rab6 is a modulator of cell spreading. Moreover, in samples knocked down using siRNA Rab6 #1, transfection of GFP-Rab6 rescued the spreading defect by restoring the normal cellular area (Fig. 2d, e).

To shed more light on how Rab6 influences cell migration and cell spreading, we took advantage of L-shaped adhesive micropatterns. Cells plated on regular culture dishes can take on a variety of different shapes and are constantly changing as their cytoskeleton reorganizes. Having all cells confined to specific and identical shapes makes it easier to compare them and identify possible effects on cytoskeleton architecture after Rab6 knockdown. On L-shaped fibronectin-coated micropatterns, cells are forced to assume a right-angled triangular shape with the adhesive micropattern on two sides and a long non-adhesive stretch along the hypotenuse (Fig. 2f).

U2OS cells were seeded on fibronectin-coated L-shaped micropatterns for 3.5 h before fixation and staining with rhodamine–phalloidin to visualize the actin network. Interestingly, more than 80% of the cells silenced for Rab6 displayed an actin network architecture that appeared less straight and more collapsed along the non-adhesive side resulting in a hypotenuse with higher curvature, compared to 60% of the control cells (Fig. 2f, g). To overcome the absence of the underlying adhesive substrate, cells are dependent on actomyosin contraction. Indeed, upon myosin inhibition, the non-adhesive stretch takes on a relaxed (curved) instead of straight cell border [42]. Therefore, our results suggest that the increased curvature after depletion of Rab6 could be a consequence of reduced actomyosin contractility.

To test this hypothesis, we next checked if Rab6 knockdown alter the phosphorylation status of MLC, as phosphorylation of MLC is known to regulate myosin II assembly and contraction [43]. As Ser19 is the primary phosphorylation site of MLC [44–46], we investigated whether MLC phosphorylation on Ser19 was affected upon Rab6 silencing. In line with our hypothesis, MLC phosphorylation was strongly downregulated after knockdown of Rab6 (Fig. 3a, b).

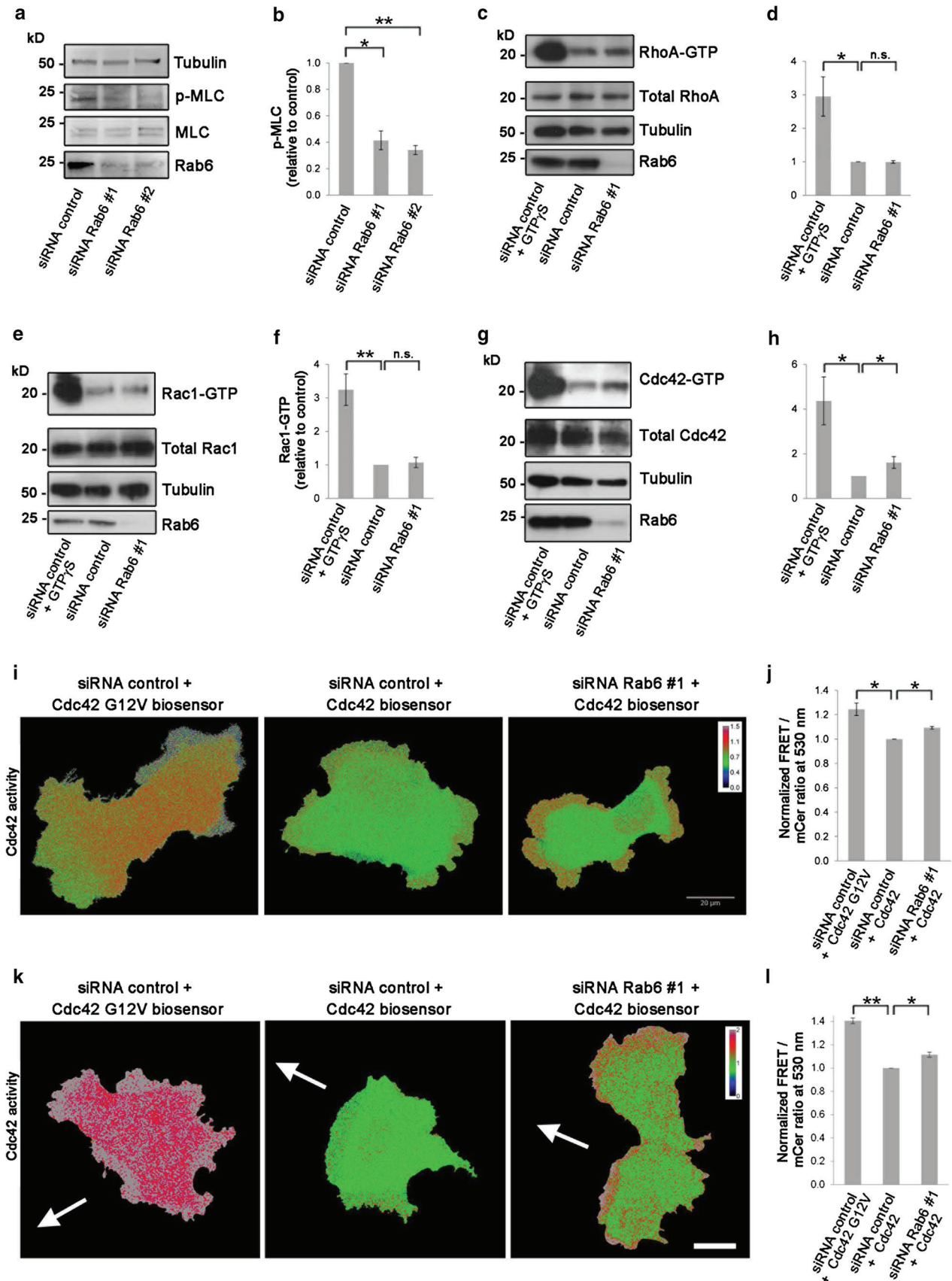


Fig. 3 Rab6 regulates MLC phosphorylation and Cdc42 activity. **a** Lysates from U2OS cells transfected with control siRNA, siRNA Rab6 #1 or siRNA Rab6 #2 were subjected to western blot analysis using antibodies against phosphorylated myosin light chain (p-MLC), total MLC and tubulin (as a loading control). **b** Quantification of the amount of p-MLC normalized to the total amount of MLC for each of the indicated sample. The data represent the mean \pm SEM relative to the siRNA control sample of three independent experiments. **c–h** Lysates from U2OS cells treated with control siRNA or siRNA Rab6 #1 were mixed with beads coupled to either GST–Rhotekin–RBD to pull down the active form (GTP-bound) of RhoA (**c**), or to GST–PAK–PBD to pull down the active forms of Rac1 (**e**) or Cdc42 (**g**) and analyzed by western blot. As a positive control, cells were loaded with GTP γ S. The levels of active RhoA (**d**), Rac1 (**f**), and Cdc42 (**h**) were normalized to the amount of tubulin and plotted relative to the intensities of GTP-bound Rho proteins in the control sample. The graphs represent the mean \pm SEM normalized to the control of at least three independent experiments. **i** U2OS cells treated with siRNA control or siRNA Rab6 #1 and transfected with either Cdc42 G12 V biosensor or Cdc42 wt biosensor as indicated, were imaged live with spectral imaging. Scale bar: 20 μ m. **j** Graph shows the mean \pm SEM of the normalized FRET/mCerulean ratios for the indicated samples; $n > 70$ cells from three independent experiments. **k** U2OS cells treated with siRNA control or siRNA Rab6 #1 and transfected with either Cdc42 G12 V biosensor or Cdc42 wt biosensor as indicated, were scratched and let migrate for 4 h before live spectral imaging. The white arrows indicate the direction of migration. Scale bar: 20 μ m. **l** Graph shows the mean \pm SEM of the normalized FRET/mCerulean ratios for the indicated samples; $n > 12$ cells from four independent experiments. * $P < 0.05$; ** $P < 0.01$ (paired Student's *t* test)

Taken together, these results suggest that Rab6 is important for regulation of actin dynamics and actomyosin contractility by regulating the activity of myosin II.

Cdc42 activity is regulated by Rab6

The phosphorylation status of MLC is tightly regulated by a myosin specific phosphatase and several different kinases working at distinct places in the cell to locally control myosin activity [45, 47–52]. The upstream control of these kinases is orchestrated by members of the Rho GTPase family that are master regulators of cytoskeleton rearrangements [47, 53, 54]. We, therefore, hypothesized that Rab6 influences myosin phosphorylation through the regulation of Rho GTPase family members. To test this, we investigated if Rab6 knockdown affected the activity of the most extensively characterized Rho GTPases, namely, RhoA, Rac1, or Cdc42 [53, 54], by pull-down assays.

GST-tagged Rho-binding domain (RBD) of the RhoA effector Rhotekin was used to pull down the active form of RhoA, while GST-tagged p21 Binding Domain (PBD) of the Cdc42 and Rac1 effector protein p21 activated kinase I (PAK) was used to pull down the active forms of Rac1 and Cdc42 in U2OS cell lysates treated with siRNA control or siRNA Rab6 #1. As shown in Fig. 3c–f, Rab6 depletion did not affect RhoA or Rac1 activity. However, Cdc42 activity

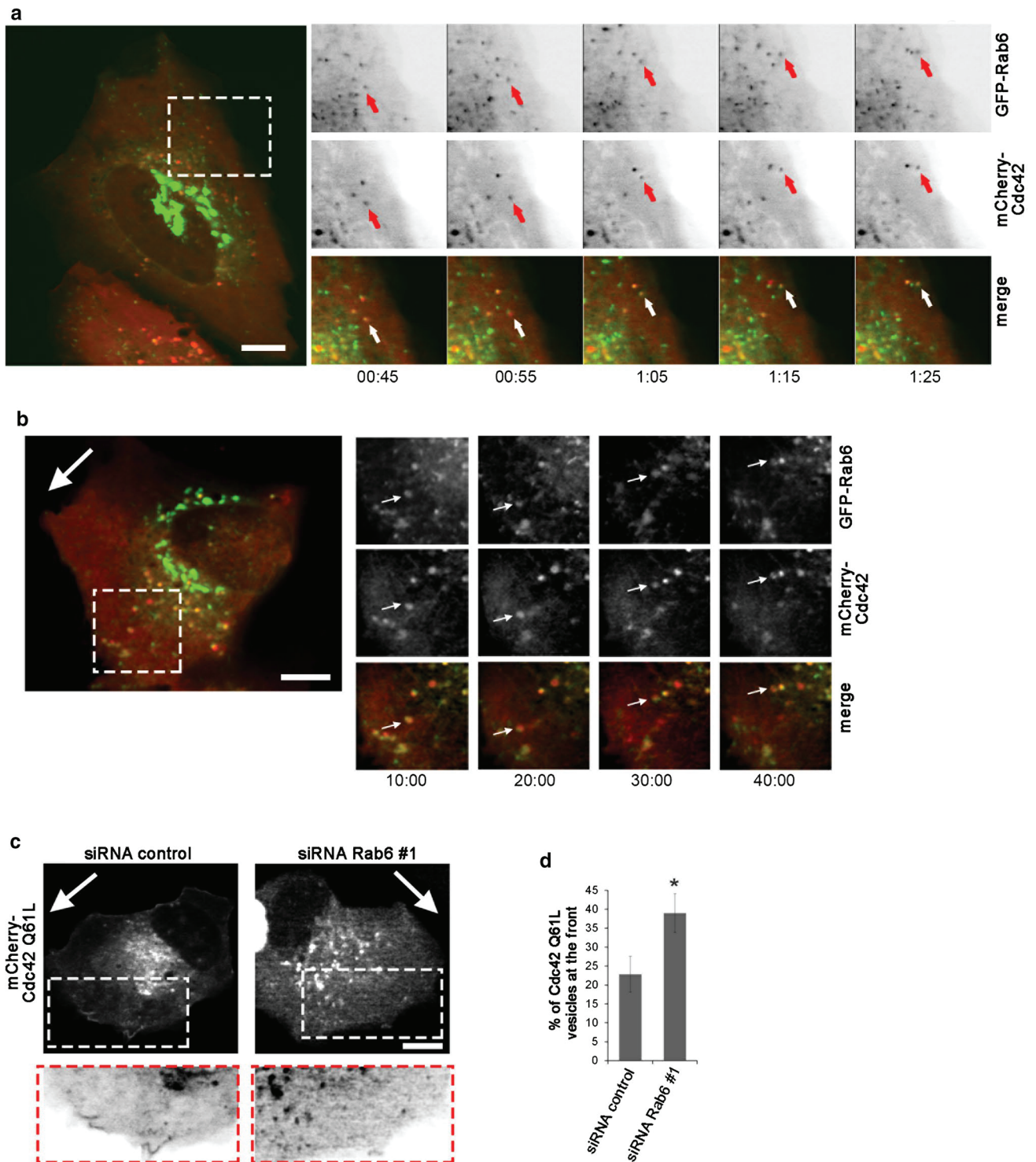
was increased more than 1.6-fold compared to control cells, indicating that Rab6 regulates actin dynamics through the modulation of Cdc42 activity (Fig. 3g, h).

To further detect the localized Cdc42 activation in live cells, we next took advantage of a fluorescence resonance energy transfer (FRET)-based biosensor for Cdc42 [55]. U2OS cells treated with siRNA control or siRNA Rab6 #1 were transfected with either wild-type Cdc42 biosensor or Cdc42 G12 V constitutively active mutant biosensor as control, and imaged for FRET analysis. We measured Cdc42 activity in regions at the cell periphery as we had previously detected differences in actin arrangement in cell protrusions after Rab6 depletion (Fig. 2a, b). Spectral imaging and measurement of the FRET/Cerulean ratio at 530 nm confirmed a significant increase in Cdc42 activity in cells depleted for Rab6 compared to the control, thus verifying the results from the pull-down assay and further demonstrating a localized activation of Cdc42 at the cell periphery (Fig. 3i, j). A similar increase in Cdc42 activity in cells depleted for Rab6 was measured also in migrating U2OS cells (Fig. 3k, l). All together, these results support a model in which Rab6 knockdown induces the activation of Cdc42 at the cell periphery.

Cdc42 and its GEF Trio interact with Rab6

To understand how Rab6 affects Cdc42 activity, we next looked at the intracellular localization and dynamics of these molecules by live-cell confocal microscopy. U2OS cells were co-transfected with GFP-Rab6 and mCherry-Cdc42 before time-lapse image acquisition. As shown in Fig. 4a, GFP-Rab6 was present in the perinuclear/Golgi region from where Rab6-positive vesicles emerged and moved towards the cell periphery as previously reported [18, 56]. Some of these vesicles were also positive for mCherry-Cdc42, although the percentage of mCherry-Cdc42-positive vesicles that co-localized with GFP-Rab6 varied considerably between cells. Interestingly, time-lapse imaging revealed that these vesicles moved from the perinuclear region towards the cell periphery (Fig. 4a, Movie 1). Similar dynamics were also observed in migrating cells, where vesicles positive for both Rab6 and Cdc42 were observed to move towards the cell periphery at the leading edge, but also often return back towards the cell centre (Fig. 4b).

As Rab6 depletion promotes the activation of Cdc42, we then studied whether it also influences the localization of GTP-bound Cdc42. For this, we transfected control cells and cells silenced for Rab6 with the constitutively active mutant of Cdc42. We left the cells to migrate for 3 h after a scratch was made with a pipette tip in the confluent cell monolayer, and then, we imaged the cells using time-lapse video microscopy. Interestingly, the percentage of Cdc42-positive vesicles present in the front of the migrating cells



was higher in cells silenced for Rab6, suggesting that Rab6 might have a role in balancing the transport of active Cdc42 to the cell periphery (Fig. 4c, d).

Having observed that Cdc42 is present on Rab6-positive vesicles, we next investigated if these two small GTPases also interact. To test this, we performed co-immunoprecipitation (co-IP) experiments in U2OS cells transiently

transfected with either GFP, GFP-Cdc42 wt, GFP-Cdc42 Q61L (constitutively active mutant), or GFP-Cdc42 T17 N (dominant negative mutant). The results in Fig. 5a show that Rab6 interacts with all forms of Cdc42, and indicate that this interaction does not depend on the nucleotide binding state of Cdc42. As controls, both N-WASP and IQGAP1, known interactors of Cdc42, were immunoprecipitated by

Fig. 4 Cdc42 is transported towards the cell periphery in Rab6-positive vesicles. **a** U2OS cells co-transfected with GFP-Rab6 and mCherry-Cdc42 were imaged using a spinning-disk confocal microscope for the indicated time points. The arrows indicate a vesicle positive for both Rab6 and Cdc42 moving towards the cell periphery. Scale bar: 10 μm . **b** U2OS cells co-transfected with GFP-Rab6 and mCherry-Cdc42 were scratch-wounded with a pipet tip and imaged 3 h later by using a spinning-disk confocal microscope for the indicated time points. The image represents maximum-intensity projections of z-stacks. The big white arrow indicates the direction of migration. Magnifications of the boxed area are shown in the insets. The arrows in the insets indicate a vesicle positive for both Rab6 and Cdc42 moving both towards the cell periphery and back. Scale bar: 10 μm . **c** U2OS cells treated with siRNA control or siRNA Rab6 #1 and transfected with pTriEx-mCherry-Cdc42 Q61L were scratched with a pipet tip and imaged 3 h later. The images represent maximum-intensity projections of z-stacks. The white arrows indicate the direction of migration. Magnifications of the boxed areas are shown in the insets. Scale bar: 10 μm . **d** Quantification of the percentage of Cdc42 Q61L-positive vesicle in the cell front compared to the total number of Cdc42 Q61L-positive vesicles within the cell. The graph shows the mean \pm SEM from two independent experiments ($n=8$). * $P<0.05$ (paired Student's t test)

Cdc42 wt and its constitutively active mutant, but not by the dominant negative mutant (Fig. 5a), in agreement with the previous reports [57–59]. This further supports the specificity of the interaction of Rab6 with all forms of Cdc42. We additionally performed a reverse co-IP, where U2OS cells were transiently transfected with HA-Rab6. HA-Rab6 was able to immunoprecipitate endogenous Cdc42, again confirming the interaction between Rab6 and Cdc42 (Fig. 5b).

Cdc42 is a small GTPase, whose activity is regulated by guanine nucleotide exchange factors (GEFs) and GTPase-activating proteins (GAPs) that activate and inactivate it, respectively. Intriguingly, in a study from 2014, a GEF for the Rho family GTPases, Trio, was identified as a putative Rab6-binding protein [5]. Importantly, while Trio has been considered a GEF for RhoG and Rac1, a recent work has challenged this view by demonstrating that Trio, although with a lower exchange rate than RhoG and Rac1, potently activates both RhoA and Cdc42 [30].

We, therefore, investigated whether Rab6 modulates Cdc42 activity by regulating the recruitment of a Cdc42 GEF, and verified the putative interaction between Rab6 and Trio by co-IP in HeLa cells as U2OS cells express lower levels of endogenous Trio. Cells were transiently transfected with GFP, GFP-Rab6 wt, GFP-Rab6 Q72L (constitutively active mutant), or GFP-Rab6 T27 N (dominant negative mutant) and the immunoprecipitation was performed using GFP-Trap magnetic agarose beads. Immunoblotting using an antibody against Trio indeed demonstrated that GTP-bound Rab6 and endogenous Trio interact (Fig. 5c). We also performed a reverse co-IP in U2OS cells by transiently transfecting cells with either GFP or GFP-Trio, as well as HA-tagged Rab6 wt, HA-Rab6 Q72L, or HA-Rab6 T27 N, and verified the interaction between Rab6 and Trio (Fig. 5d).

Taken together, these findings indicate that Rab6 is able to recruit both Cdc42 and the GEF Trio and thus suggest a possible mechanism for Rab6 to modulate Cdc42 activity.

To further investigate whether the enhanced activation of Cdc42 upon Rab6 knockdown depends on Trio, we silenced both Rab6 and Trio and measured Cdc42 activity. As shown in Suppl. Fig. 3a, b, Trio depletion alone inhibits Cdc42 activation down to levels comparable to another well-known GEF for Cdc42, DOCK10. The activity of Cdc42 in Rab6 and Trio double-knockdown cells was also significantly reduced, indicating that the effect on Cdc42 activation upon Rab6 knockdown depends, at least to a certain extent, on Trio.

We next studied the contribution of Trio on cell migration. In line with previous work [60], silencing of Trio considerably inhibited cell migration in a wound healing assay (Suppl. Fig. 3c). Overexpression of Rab6 wt did not further influence the effect of Trio depletion, while double-knockdown of Trio and Rab6 reduced the Rab6-dependent increase in cell migration to the level of control cells. Taken together, these results suggest that the increased migration upon Rab6 depletion may be at least in part dependent on Trio-mediated activation of Cdc42.

Rab6 depletion influences F/G-actin ratio and filopodia formation and dynamics

Cdc42 is a regulator of actin cytoskeleton dynamics that promotes formation of filopodia [61]. Since our results indicate that Rab6 influences Cdc42 activity at the cell periphery, we next checked whether actin polymerization and filopodia formation were altered after Rab6 knockdown.

To determine if Rab6 influences actin polymerization, we quantified the relative amounts of cellular G-actin and F-actin in control cells and cells depleted for Rab6. Cell lysates were subjected to high-speed centrifugation to separate the G- and F-actin pools, followed by quantitative Western blot analysis to assess the ratio of F-to-G-actin. As expected, pretreatment with phalloidin, which stabilizes F-actin, increased the F/G-actin ratio with almost 2.5-fold compared to control cells (Fig. 6a, b). Importantly, Rab6 knockdown also increased the ratio between F/G-actin of 0.6-fold compared to control cells (Fig. 6a, b).

As this result is in line with increased actin polymerization, we next investigated whether the augmented pool of F-actin in cells knocked down for Rab6 could correlate with an increase in filopodia formation. We silenced HeLa cells for Rab6 as filopodia are easier to detect in this cell line than in U2Os cells, before fixation and staining of actin filaments with rhodamine-phalloidin. Consistent with the augmented Cdc42 activity after Rab6 knockdown, quantification revealed an increase in filopodia number by 17% in cells depleted for Rab6b compared to control cells (Suppl.

Fig. 5 Cdc42 and its GEF Trio interact with Rab6. **a** Lysates from U2OS cells transiently transfected with either GFP, GFP-Cdc42 wt, GFP-Cdc42-Q61L or GFP-Cdc42-T17N were subjected to immunoprecipitation with GFP-Trap or control-Trap magnetic agarose beads. Whole-cell lysates (WCL) and immunoprecipitates (IP) were subjected to western blot analysis with the indicated antibodies. **b** Lysates from U2OS cells transiently transfected with HA-Rab6 wt, were subjected to immunoprecipitation with an antibody against HA or an isotype control (IgG1). WCL and IP were subjected to western blot analysis using antibodies against HA or Cdc42. **c** HeLa cells were transiently transfected with GFP, GFP-Rab6 wt, GFP-Rab6 Q72L, or GFP-Rab6 T27N, lysed and subjected to immunoprecipitation with GFP-Trap or control-Trap magnetic agarose beads. WCL and immunoprecipitates IP were subjected to western blot analysis using the indicated antibodies. **d** U2OS cells transiently transfected with either GFP or GFP-TRIO, together with HA-Rab6 wt, HA-Rab6 Q72L or HA-Rab6 T27N, were subjected to immunoprecipitation with GFP-Trap magnetic agarose beads. WCL and immunoprecipitates IP were subjected to western blot analysis with the indicated antibodies

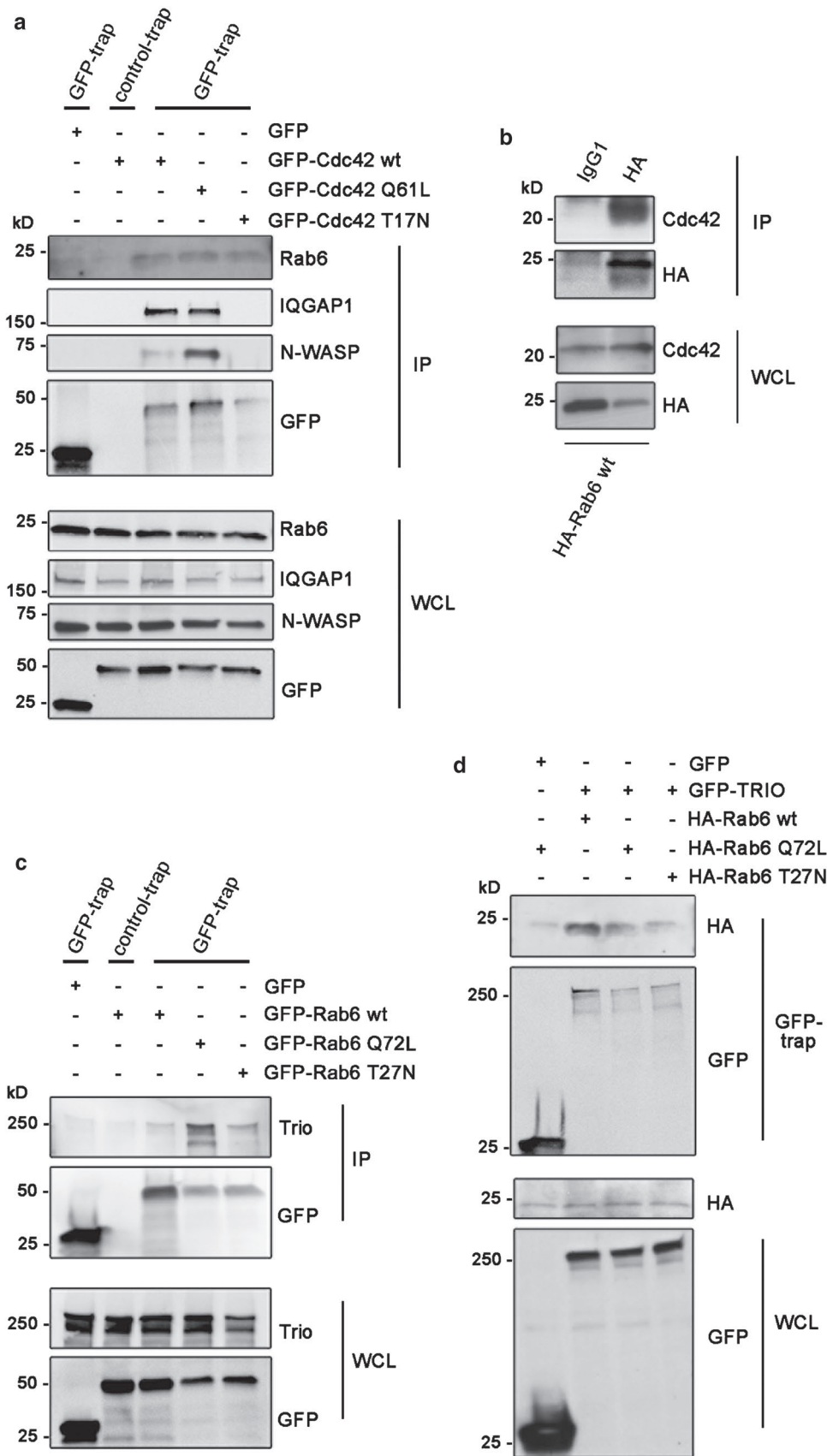


Fig. 4a, b). Interestingly, the number of filopodia at the leading edge of migrating cells was even higher (27% more than in control cells) upon Rab6 depletion and the re-expression of GFP-Rab6 in these cells was able to reduce the filopodia number (Fig. 6c, d). Since Rab6 is able to affect filopodia formation, it is reasonable to expect that Rab6 is localized to filopodia. To confirm this, U2OS cells were transiently transfected with GFP-Rab6 and imaged using TIRF microscopy (TIRFM). TIRFM showed that Rab6-positive vesicles were transported towards the cell surface and often localized to filopodia (Suppl. Fig. 4c, Movie 2).

Filopodia are dynamic structures consisting of F-actin bundles. Their growth and retraction is dependent on actin polymerization rate at the tip of the filopodia and on the actin retrograde flow [38]. To further investigate whether Rab6 in addition to filopodia formation also influences filopodia dynamics, we measured the retraction velocity and the force exerted by filopodia on optically trapped beads in control cells and in cells silenced for Rab6 (Fig. 6e). As shown in Fig. 6g, the velocity of filopodia retraction increased in cells knocked down for Rab6 as the mean retraction velocity of filopodia resulted in 41.2 ± 23.9 nm/s compared to 28.5 ± 12.7 nm/s in control cells. In addition, the mean stall force of the filopodia was quantified. The stall force is evaluated by the considering both the highest counteracting force at which still a retraction could be determined and the lowest counteracting force which led to a stall of the retraction process. The mean stall force of the filopodia in cells depleted for Rab6 (15.7 ± 11 pN) was slightly higher than the one of the control cells (13.5 ± 5.9 pN) (Fig. 6f). In sum, our results show that the enhanced activation of Cdc42 induced by Rab6 silencing results in an increase in filopodia formation and influences filopodia dynamics.

Rab6 knockdown promotes spread of cancer cells in vivo

In this study, we have shown using in vitro systems that Rab6 depletion leads to increased cell migration by inhibiting myosin II phosphorylation and promoting Cdc42 activation. This results in increased actin polymerization that in turn leads to an enhanced formation of cell protrusions. We next investigated whether Rab6 depletion also promotes cell migration in vivo. To test this, we examined if Rab6 silencing influences the dissemination of human cancer cells with known invasion/metastasis potential, such as H1299 [62, 63] in zebrafish embryos. 20 h after silencing, control cells, or cells silenced for Rab6 were labeled with fluorescent quantum dots (QDs) and injected into the otic vesicle of zebrafish larvae at 48 h post-fertilization. Analysis was performed at 24 and 48 h post-injection by acquiring images using a stereomicroscope, as the spread of cancer cells could be seen in the body of the fish. The invasion potential of

these cells was assessed by calculating the ability of the cells to migrate out from the otic vesicle. The results show that, compared to the control, cells silenced for Rab6 were able to migrate from the otic vesicle already at 24 h post-injection and even more at 48 h post injections (Fig. 7). Moreover, transfection of GFP-Rab6 in cells knocked down using siRNA Rab6 #1 rescued the increased invasive ability induced by Rab6 depletion (Fig. 7a, c). The effect of Rab6 depletion on in vivo cell migration was additionally confirmed by using a second siRNA targeting Rab6. Similar to the results obtained with siRNA #1, cells silenced with Rab6 #2 were able to migrate in zebrafish embryos from the otic vesicle at 24 h post-injection and at 48 h post injections more than control cells (suppl. Fig. 5). In conclusion, using a zebrafish xenograft model, we demonstrated that silencing of Rab6 potentiates invasion of H1299 cells in vivo, further confirming the role of Rab6 in cell migration.

Discussion

Rab6 is known to regulate the transport between the endoplasmic reticulum, Golgi apparatus, plasma membrane, and endosomes [17–21]. In this study, we reveal a novel function of this GTPase as a negative regulator of cell migration by interacting with both a Rho family member and its GEF and influencing actin cytoskeleton organization.

Rab proteins are known to interact with different motor proteins to facilitate distinct processes in intracellular trafficking [64–67]. Between them, only Rab6 and Rab7b have so far been shown to directly interact with the non-processive motor protein myosin II [10, 15]. Interestingly, while Rab6 is reported to mediate the fission of vesicles from the Golgi apparatus by recruiting myosin II [15], the interaction between Rab7b and myosin II has proven to be important not only for vesicular transport but also for proper cytoskeleton dynamics required in cell migration [10].

In the present study, we reveal a new function for Rab6 in the regulation of cytoskeleton organization and cell migration by showing that Rab6 modulates myosin II activity. Indeed, depletion of Rab6 decreases myosin II phosphorylation on Ser 19 (Fig. 3a, b). These results are further supported by the decreased ability of cells knocked down for Rab6 to generate enough actomyosin contractility to support full extension of their free edge when grown on L-shaped micropatterns (Fig. 2f, g).

Myosin II knockdown or inhibition by drugs has been generally shown to increase the speed of migrating cells in many different cell types [68–71]. These studies support our finding that increased cell migration after Rab6 knockdown is a consequence of a decrease in myosin II phosphorylation. Even though there is no general consensus on the role of myosin II in cell spreading and on the effects of its inhibition

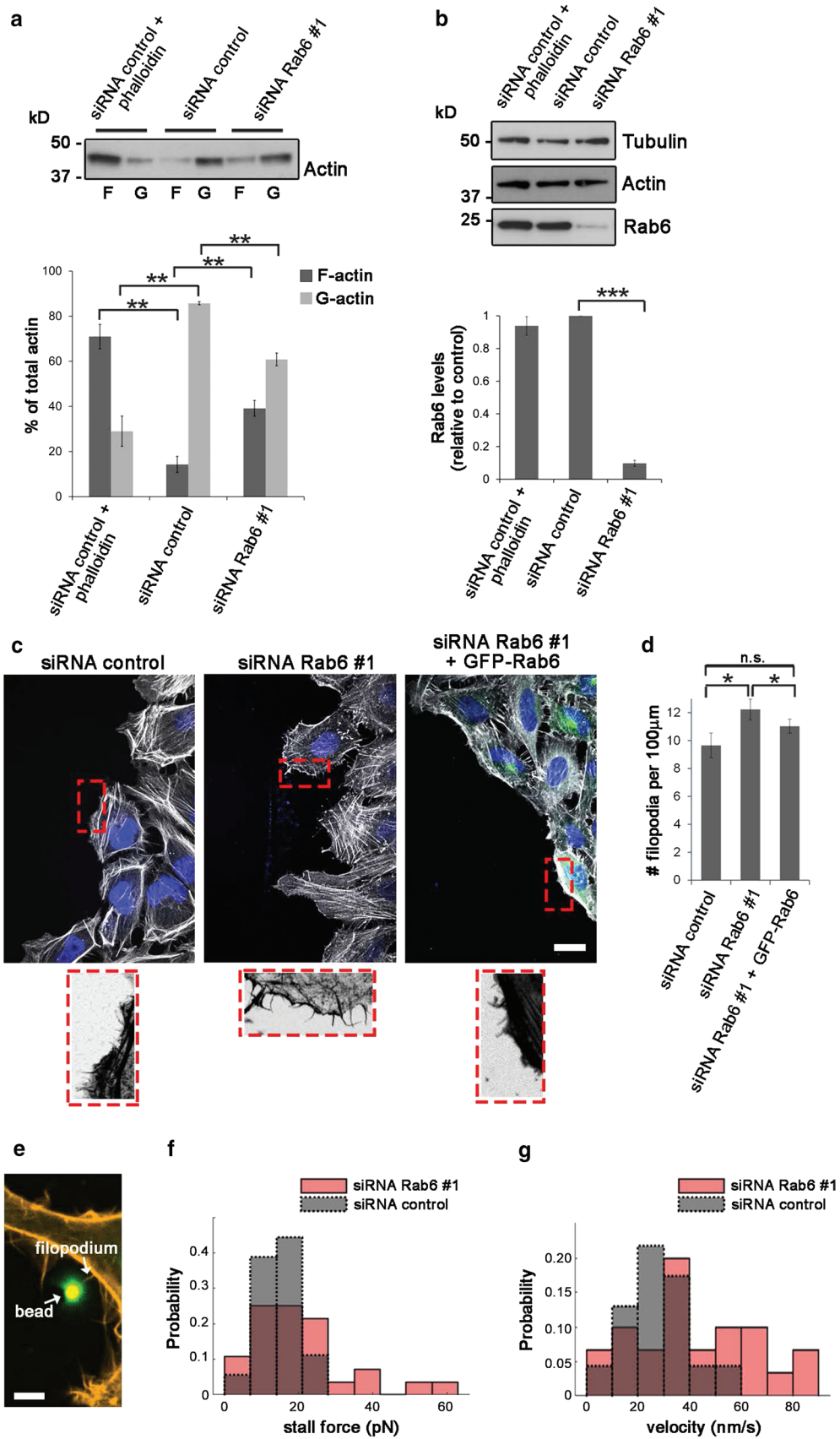


Fig. 6 Filopodia formation and dynamics are affected by Rab6 depletion. **a** F-actin (F) and G-actin (G) pools were separated from lysates of U2OS cells transfected with siRNA control or siRNA Rab6 #1 by ultracentrifugation. Phalloidin was added to a control sample to verify that the F- and G-actin pools were successfully separated. Samples were loaded on SDS-PAGE and subjected to Western blot analysis using an antibody against actin. The graph shows the percentage of F-actin and G-actin relative to the total amount of actin. Data represents the average of four independent experiments. $**P < 0.01$ (paired Student's *t* test). **b** Cell lysates from each of the indicated sample were subjected to Western blot analysis with antibodies against Rab6 and tubulin (as a loading control). The intensities of the bands were quantified using densitometry, normalized against the amount of tubulin, and plotted relative to the intensities obtained in cells transfected with siRNA control. The values represent the mean \pm SEM for four independent experiments. $***P < 0.001$ (paired Student's *t* test). **c** HeLa cells treated with siRNA control or siRNA Rab6 #1, or silenced for Rab6 and subsequently transfected with GFP-Rab6, were scratched and let migrate for 3 h before fixation and staining with DAPI and rhodamine-conjugated phalloidin. The lower insets show magnifications of the boxed areas. Scale bar: 20 μ m. **d** Quantification of the number of filopodia per 100 μ m of cell membrane facing the wound. The graph represents the mean \pm SEM; $n > 50$ cells from three independent experiments. $P < 0.05$ (one-way ANOVA followed by Fisher's LSD test). **e** Confocal image of HeLa cells transfected with LifeAct-RFP showing an optically trapped bead attached to a filopodium. Scale bar: 2 μ m. **f** Distribution of the mean filopodial retraction velocity from 8 independent experiments ($n = 30$ for siRNA Rab6 #1 and $n = 23$ for siRNA control). Average values: 41.2 nm/s for siRNA Rab6 #1 and 28.5 nm/s for siRNA control. The measured velocities reject the null hypothesis that they originate from the same sample using a two-sample Kolmogorov–Smirnov test and a two-sample *t* test at a 5% significance level. **g** Distribution of measured stall forces from 8 independent experiments ($n = 27$ for siRNA Rab6 #1 and $n = 15$ for siRNA control). Mean stall force for siRNA Rab6 #1 = 12.6 pN and for siRNA control = 10.6 pN. Neither a two-sample Kolmogorov–Smirnov test nor a two-sample *t* test of the data does allow to reject the null hypothesis that they originate from the same sample

[72–77], Nisenholz et al. recently found that the balance of the forces exerted by myosin II between the periphery and the center of the cell is important for the regulation of cell spreading [78]. They demonstrated that the forces exerted by myosin II in the periphery facilitated cell spreading, while those exerted more centrally opposed spreading. Based on this model, the decrease in cell spreading we measured after Rab6 knockdown could be a consequence of less myosin-dependent forces exerted towards the cell periphery due to the decreased myosin II phosphorylation.

Intriguingly, our results also show that depletion of Rab6 increases Cdc42 activity (Fig. 3g, h). In addition, using a Cdc42 FRET biosensor construct, we demonstrate that the Cdc42 activity is increased at the cell periphery in both migrating and non-migrating cells (Fig. 3i, l). It is well established that the activation of the small GTPase Cdc42 promotes Arp2/3-dependent actin nucleation and polymerization important for initiation and dynamics of filopodia [53, 79–82]. In agreement with this, we found an increase not only in the amount of F-actin after depletion of Rab6, but

also in cell protrusions and filopodia formation (Figs. 2a, b, 6a–d, Suppl. Fig. 4a, b).

It is tempting to hypothesize that the increased activation of Cdc42 after Rab6 knockdown could be the cause for the reduced phosphorylation of myosin II. Indeed, phosphorylation of myosin II on Ser 19 is tightly controlled by myosin specific phosphatase and kinases, some of which are regulated by Cdc42 [44–46, 83, 84]. In line with this hypothesis, studies on force generation of cortical actin and cell protrusions have shown that less myosin II contractility in the cortical actin can lead to more protrusions [85, 86]. This is again consistent with the increased formation of protrusions and filopodia observed in cells silenced for Rab6. In the light of this, our results are compatible with a model, where Rab6 modulates Cdc42 activity at the cell periphery, thereby regulating actin cytoskeleton dynamics and myosin II activity, which results in decreased spreading and increased filopodia formation and protruding potential. Indeed, we demonstrate that Cdc42 is present on Rab6-positive vesicles directed towards the cell periphery that afterwards can also move back towards the center of the cell (Fig. 4a, b). Most interestingly, depletion of Rab6 redistributes active Cdc42 towards the leading edge of migrating cells (Fig. 4c, d). This suggests that Rab6 may modulate either how much Cdc42 should be transported to the cell periphery or its time of residence at the periphery of the cells, and that upon Rab6 depletion this control is lost.

How then, does Rab6 regulate Cdc42 activity? Evidence of crosstalk between the Rab and Rho family of small GTPases in the regulation of cytoskeleton dynamics is starting to emerge as some Rab proteins have been shown to regulate the activity of Rho family members [10, 12, 67, 87–90]. However, a general mechanism behind this regulation is not well characterized. Our results show that Rab6 and Cdc42 are not only present on the same transport vesicle, but can also interact. This interaction is independent on the nucleotide binding state of Cdc42 (Fig. 5a, b), suggesting that Rab6 may recruit another factor for the direct modulation of Cdc42 activity. As we found that GTP-bound Rab6 binds to the Rho family GEF Trio (Fig. 5c, d), it is tempting to speculate that the recruitment of Trio by active Rab6 may prevent the activation of Cdc42.

Trio is a member of the Dbl family of GEFs whose activity is inhibited by direct interaction with phosphorylated myosin II [91]. A reduction in myosin II phosphorylation decreases the Dbl GEF–myosin II interaction, resulting in increased GEF activity [91]. In light of this, the reduced amount of phosphorylated myosin II we measured after knockdown of Rab6 could trigger the increase in Trio GEF activity and thereby promote Cdc42 activation. As both Trio and Rab6 are known to bind to myosin II [15, 91], an intriguing scenario is, therefore, that Rab6, Trio and myosin II may form a complex for the specific

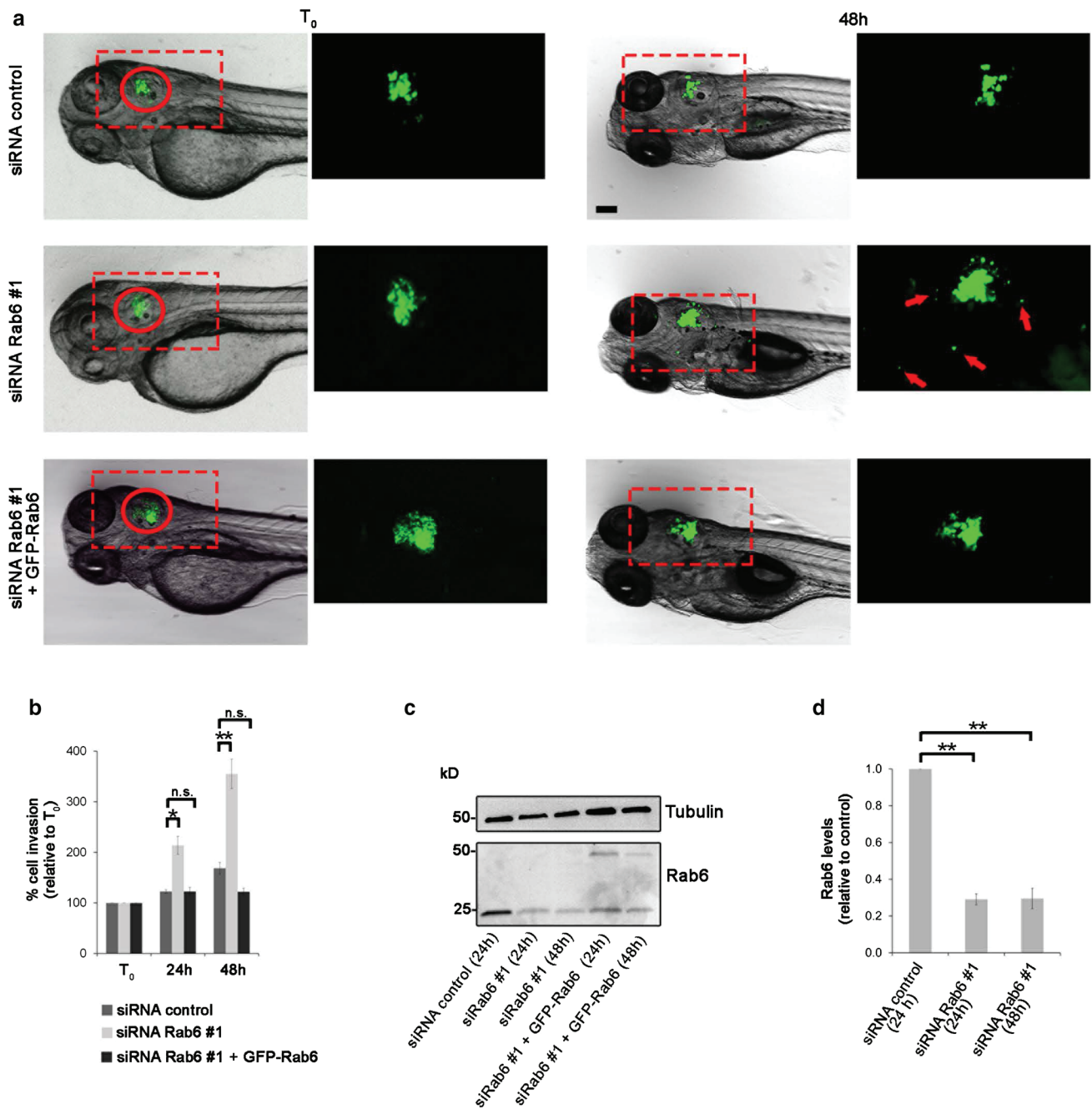


Fig. 7 Rab6 knockdown promotes spread of cancer cells in zebrafish embryos following xenotransplantation. **a** H1299 cells transfected with control siRNA, siRNA Rab6 #1, or silenced with siRNA Rab6 #1 and subsequently transfected with GFP-Rab6, were stained with QDs Q-Tracker 655 and injected into the otic vesicle (red circle) of 2-dpf zebrafish wild-type embryos. Representative images of (T₀) and 48 h after injection are shown. In contrast to the control cells (top panels), and to cells silenced with siRNA Rab6 #1 and transfected with GFP-Rab6 (lower panels), that remained confined to the injection area, cell silenced for Rab6 (middle panels) showed higher ability to migrate outside from the otic vesicle at 48 h (arrows). Magnification of the boxed areas are shown in the inset on the right of each panel. Scale bar: 100 μ m. **b** Quantification of cell migration was performed by measuring the area occupied by the cells at 24 h and

48 h after injection and was normalized to the area occupied by the cells in the otic vesicle at T₀. The graph represents the mean \pm SEM from $n > 10$ embryos. **c** H1299 cells transfected with control siRNA or siRNA Rab6 #1 for 24 or 48 h, or silenced with siRNA Rab6 #1 and subsequently transfected with GFP-Rab6 for 24 or 48 h, were subjected to western blot analysis using antibodies against Rab6 and tubulin (as a loading control). $*P < 0.05$; $**P < 0.01$ (one-way ANOVA followed by Fisher's LSD test). **d** Quantification of Rab6 levels normalized to the amount of tubulin, and plotted relative to the intensities obtained in cells transfected with siRNA control for each of the indicated sample. The data represent the mean \pm SEM relative to the siRNA control sample of three independent experiments. $**P < 0.01$ (paired Student's *t* test)

regulation of Cdc42 activity. The formation of such complex could explain how Rab6 recruits Trio and prevents Cdc42 activation: active Rab6 binds to both myosin II and Trio, sequestering this GEF as the binding of myosin II to Trio inhibits its GEF activity [91].

In line with the involvement of Trio in the Rab6-dependent modulation of Cdc42 activity, double knock-down of Rab6 and Trio-reduced Cdc42 activation and to some extent also the Rab6-dependent increase in cell migration (Suppl. Fig. 3). However, as both the activation of Cdc42 and the migration in the double-knockdown cells were not decreased to the same levels as Trio silencing alone, this suggests that the increased migration caused by Rab6 depletion is only in part dependent on Trio-mediated activation of Cdc42. Therefore, additional mechanisms contribute to Cdc42 activation or to the increased migration, and based on our results, one of these is likely to involve myosin II phosphorylation.

In conclusion, in this study, we have revealed a new role for Rab6 in cell migration. We have also elucidated the underlying molecular mechanisms involved by showing that Rab6 can influence filopodia formation through the modulation of Cdc42 activity. Intriguingly, we further demonstrated that Rab6 knockdown promotes cancer cell spreading after xenotransplantation in zebrafish embryos (Fig. 7, Suppl. Fig. 5), in line with the evidence that an increased protrusion potential and filopodia formation contribute to cancer cell invasion [92, 93], thus establishing Rab6 as a negative regulator of cell migration.

Acknowledgements We acknowledge the NorMIC Oslo imaging platform (Department of Biosciences, University of Oslo), Catherine Anne Heyward, and Frode Skjeldal for technical assistance, Hesso Farhan and Salim Ghannoum (Institute of Basic Medical Sciences, University of Oslo) for assistance and access to the InCuCyte ZOOM instrument. We thank Luis Hodgson (Albert Einstein College of Medicine, USA), Keith Burrige (University of North Carolina, USA), and Jaap D. Van Buul (University of Amsterdam, The Netherlands), for the kind gift of the pTriEX Cdc42 constructs, pEGFP-C3 Cdc42 plasmids, and pEGFPC1-Trio respectively. We thank Guillaume Jacquemet (University of Turku, Finland) for providing the FiloQuant plugin for Fiji/ImageJ, Giorgio Scita (IFOM, Milan, Italy) and Fabio Giavazzi (University of Milan, Italy) for advice on PIV analysis. We are grateful to Bruno Goud (Institut Curie, Paris, France) for critically reading the manuscript. The financial support of the Norwegian Cancer Society [Grants 5760850 to C.P. and 4604944 to O.B.], the Research Council of Norway [grants 239903 to C.P., 230779 to O.B., and through its Centre of Excellence funding scheme, Project Number 179573], and a Mayent-Rothschild- Institut Curie Award to OB is gratefully acknowledged.

Author contributions KV, IK, NAG, MBD, FK, and CP performed the experiments and analyzed data. FF helped with setting up the Zebrafish xenotransplantation model. CP conceived and supervised the project. IK and CP wrote the manuscript with input from all the authors. CP and OB procured funding.

Compliance with ethical standards

Conflict of interest The authors declare that they have no conflict of interest.

References

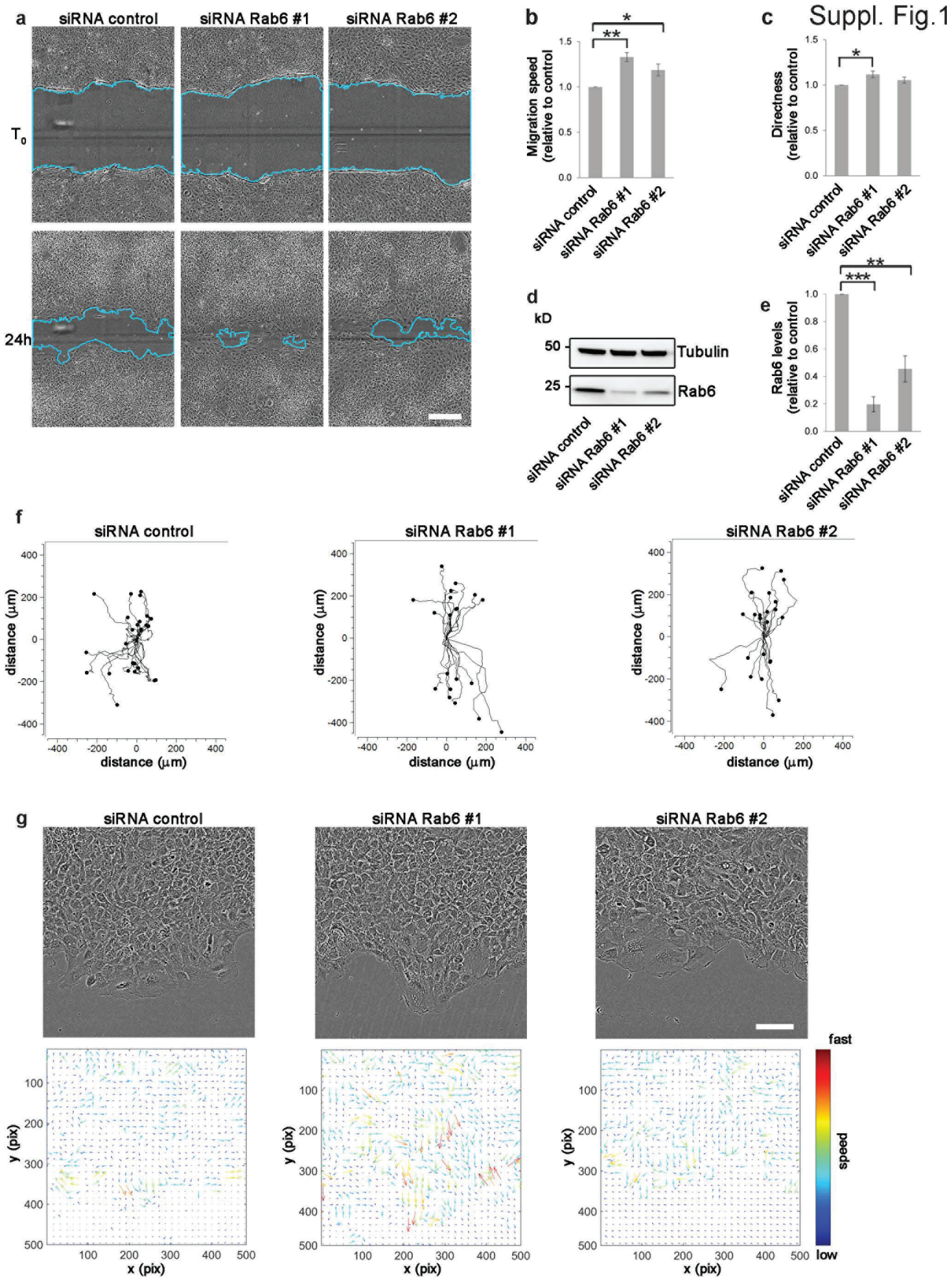
- Novick P, Field C, Schekman R (1980) Identification of 23 complementation groups required for post-translational events in the yeast secretory pathway. *Cell* 21(1):205–215
- Salminen A, Novick PJ (1987) A ras-like protein is required for a post-Golgi event in yeast secretion. *Cell* 49(4):527–538
- Chavrier P, Parton RG, Hauri HP, Simons K, Zerial M (1990) Localization of low molecular weight GTP binding proteins to exocytic and endocytic compartments. *Cell* 62(2):317–329
- Zhen Y, Stenmark H (2015) Cellular functions of Rab GTPases at a glance. *J Cell Sci* 128(17):3171–3176. <https://doi.org/10.1242/jcs.166074>
- Gillingham AK, Sinka R, Torres IL, Lilley KS, Munro S (2014) Toward a comprehensive map of the effectors of rab GTPases. *Dev Cell* 31(3):358–373. <https://doi.org/10.1016/j.devcel.2014.10.007>
- Bryant DM, Datta A, Rodriguez-Fraticelli AE, Peranen J, Martin-Belmonte F, Mostov KE (2010) A molecular network for de novo generation of the apical surface and lumen. *Nat Cell Biol* 12(11):1035–1045. <https://doi.org/10.1038/ncb2106>
- Gibieza P, Prekeris R (2017) Rab GTPases and cell division. *Small GTPases*. <https://doi.org/10.1080/21541248.2017.1313182>
- Kouranti I, Sachse M, Arouche N, Goud B, Echard A (2006) Rab35 regulates an endocytic recycling pathway essential for the terminal steps of cytokinesis. *Curr Biol* 16(17):1719–1725. <https://doi.org/10.1016/j.cub.2006.07.020>
- Thomas JD, Zhang YJ, Wei YH, Cho JH, Morris LE, Wang HY, Zheng XF (2014) Rab1A is an mTORC1 activator and a colorectal oncogene. *Cancer Cell* 26(5):754–769. <https://doi.org/10.1016/j.ccr.2014.09.008>
- Borg M, Bakke O, Progidia C (2014) A novel interaction between Rab7b and actomyosin reveals a dual role in intracellular transport and cell migration. *J Cell Sci* 127(22):4927–4939. <https://doi.org/10.1242/jcs.155861>
- Linford A, Yoshimura S, Nunes Bastos R, Langemeyer L, Geronopoulos A, Rigden DJ, Barr FA (2012) Rab14 and its exchange factor FAM116 link endocytic recycling and adherens junction stability in migrating cells. *Dev Cell* 22(5):952–966. <https://doi.org/10.1016/j.devcel.2012.04.010>
- Palamidessi A, Frittoli E, Garre M, Faretta M, Mione M, Testa I, Diaspro A, Lanzetti L, Scita G, Di Fiore PP (2008) Endocytic trafficking of Rac is required for the spatial restriction of signaling in cell migration. *Cell* 134(1):135–147. <https://doi.org/10.1016/j.cell.2008.05.034>
- Etienne-Manneville S, Hall A (2002) Rho GTPases in cell biology. *Nature* 420(6916):629–635. <https://doi.org/10.1038/nature01148>
- Hodge RG, Ridley AJ (2016) Regulating Rho GTPases and their regulators. *Nat Rev Mol Cell Biol* 17(8):496–510. <https://doi.org/10.1038/nrm.2016.67>
- Miserey-Lenkei S, Chalancon G, Bardin S, Formstecher E, Goud B, Echard A (2010) Rab and actomyosin-dependent fission of transport vesicles at the Golgi complex. *Nat Cell Biol* 12(7):645–654. <https://doi.org/10.1038/ncb2067>
- Goud B, Zahraoui A, Tavitian A, Saraste J (1990) Small GTP-binding protein associated with Golgi cisternae. *Nature* 345(6275):553–556. <https://doi.org/10.1038/345553a0>
- Antony C, Cibert C, Geraud G, Santa Maria A, Maro B, Mayau V, Goud B (1992) The small GTP-binding protein rab6p is

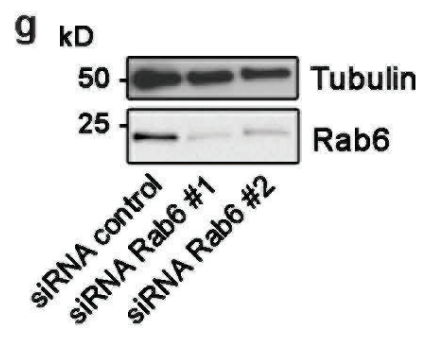
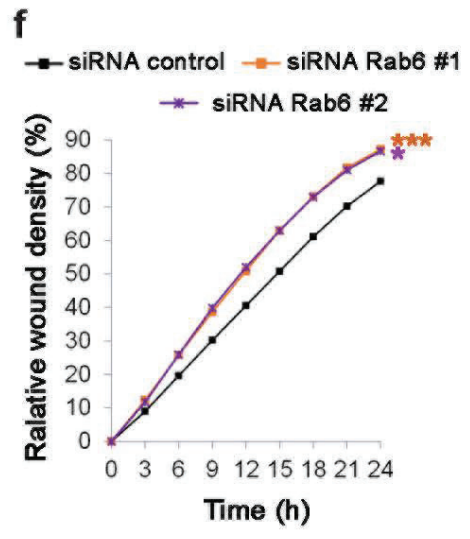
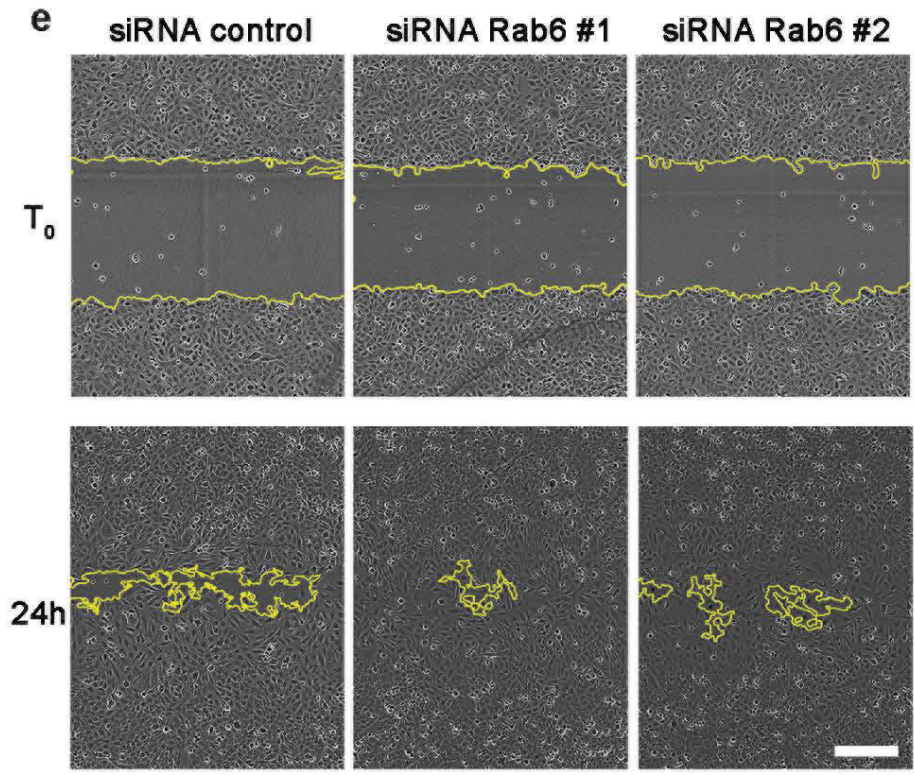
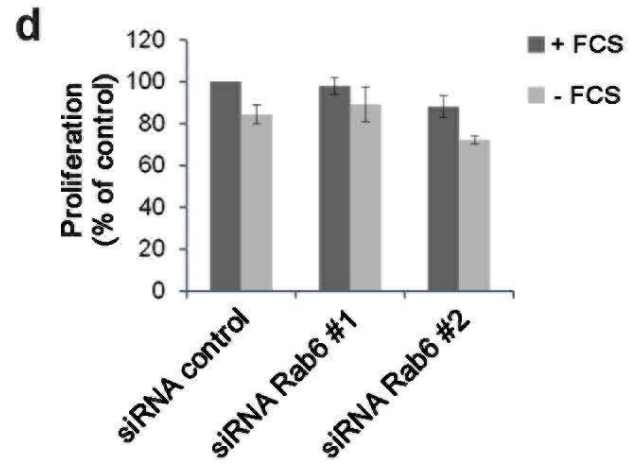
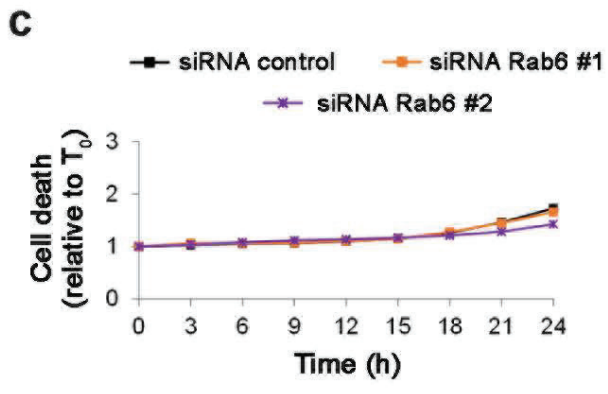
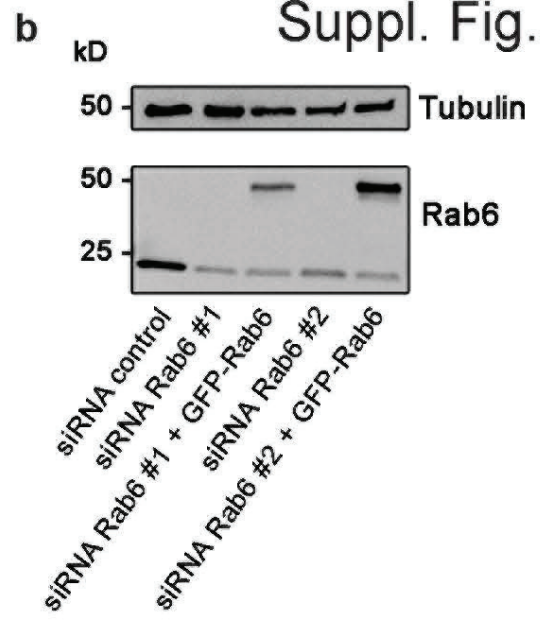
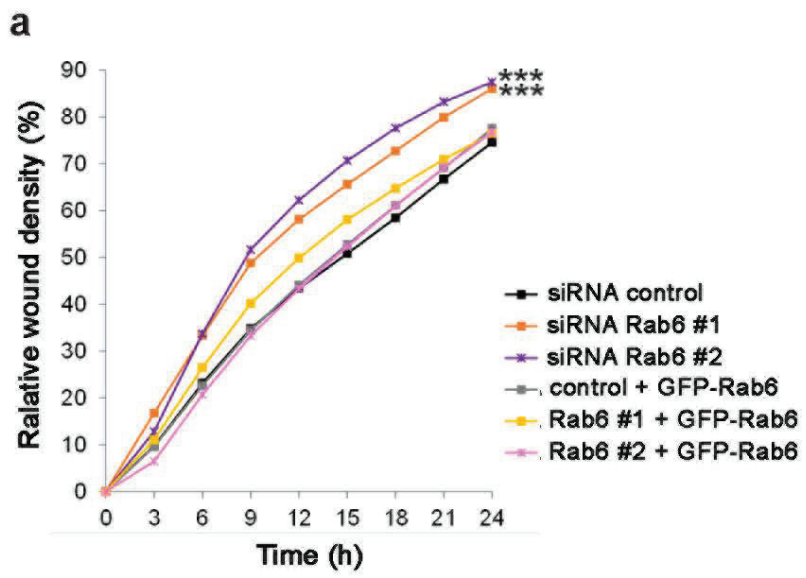
- distributed from medial Golgi to the trans-Golgi network as determined by a confocal microscopic approach. *J Cell Sci* 103(Pt 3):785–796
18. Grigoriev I, Splinter D, Keijzer N, Wulf PS, Demmers J, Ohtsuka T, Modesti M, Maly IV, Grosveld F, Hoogenraad CC, Akhmanova A (2007) Rab6 regulates transport and targeting of exocytotic carriers. *Dev Cell* 13(2):305–314. <https://doi.org/10.1016/j.devce.1.2007.06.010>
 19. White J, Johannes L, Mallard F, Girod A, Grill S, Reinsch S, Keller P, Tzschaschel B, Echard A, Goud B, Stelzer EH (1999) Rab6 coordinates a novel Golgi to ER retrograde transport pathway in live cells. *J Cell Biol* 147(4):743–760
 20. Monier S, Jollivet F, Janoueix-Lerosey I, Johannes L, Goud B (2002) Characterization of novel Rab6-interacting proteins involved in endosome-to-TGN transport. *Traffic* 3(4):289–297
 21. Patwardhan A, Bardin S, Miserey-Lenkei S, Larue L, Goud B, Raposo G, Delevoye C (2017) Routing of the RAB6 secretory pathway towards the lysosome related organelle of melanocytes. *Nat Commun* 8:15835. <https://doi.org/10.1038/ncomms15835>
 22. Hill E, Clarke M, Barr FA (2000) The Rab6-binding kinesin, Rab6-KIFL, is required for cytokinesis. *EMBO J* 19(21):5711–5719. <https://doi.org/10.1093/emboj/19.21.5711>
 23. Miserey-Lenkei S, Waharte F, Boulet A, Cuif MH, Tenza D, El Marjou A, Raposo G, Salamero J, Heliot L, Goud B, Monier S (2007) Rab6-interacting protein 1 links Rab6 and Rab11 function. *Traffic* 8(10):1385–1403. <https://doi.org/10.1111/j.1600-0854.2007.00612.x>
 24. Chen Y, Jiang C, Jin M, Gong Y, Zhang X (2015) The role of Rab6 GTPase in the maturation of phagosome against *Staphylococcus aureus*. *Int J Biochem Cell Biol* 61:35–44. <https://doi.org/10.1016/j.biocel.2015.01.016>
 25. Echard A, Jollivet F, Martinez O, Lacapere JJ, Rousselet A, Janoueix-Lerosey I, Goud B (1998) Interaction of a Golgi-associated kinesin-like protein with Rab6. *Science* 279(5350):580–585
 26. Short B, Preisinger C, Schaletzky J, Kopajtich R, Barr FA (2002) The Rab6 GTPase regulates recruitment of the dynactin complex to Golgi membranes. *Curr Biol* 12(20):1792–1795
 27. Lee PL, Ohlson MB, Pfeffer SR (2015) Rab6 regulation of the kinesin family KIF1C motor domain contributes to Golgi tethering. *Elife*. <https://doi.org/10.7554/elife.06029>
 28. Miserey-Lenkei S, Bousquet H, Pylypenko O, Bardin S, Dimitrov A, Bressanelli G, Bonifay R, Fraissier V, Guillou C, Bougeret C, Houdusse A, Echard A, Goud B (2017) Coupling fission and exit of RAB6 vesicles at Golgi hotspots through kinesin-myosin interactions. *Nat Commun* 8(1):1254. <https://doi.org/10.1038/s41467-017-01266-0>
 29. Lindsay AJ, Jollivet F, Horgan CP, Khan AR, Raposo G, McCaffrey MW, Goud B (2013) Identification and characterization of multiple novel Rab-myosin Va interactions. *Mol Biol Cell* 24(21):3420–3434. <https://doi.org/10.1091/mbc.E13-05-0236>
 30. Peurois F, Veyron S, Ferrandez Y, Ladid I, Benabdi S, Zeghouf M, Peyroche G, Cherfils J (2017) Characterization of the activation of small GTPases by their GEFs on membranes using artificial membrane tethering. *Biochem J* 474(7):1259–1272. <https://doi.org/10.1042/BCJ20170015>
 31. Moorhead AR, Rzomp KA, Scidmore MA (2007) The Rab6 effector Bicaudal D1 associates with *Chlamydia trachomatis* inclusions in a biovar-specific manner. *Infect Immun* 75(2):781–791. <https://doi.org/10.1128/IAI.01447-06>
 32. Subauste MC, Von Herrath M, Benard V, Chamberlain CE, Chuang TH, Chu K, Bokoch GM, Hahn KM (2000) Rho family proteins modulate rapid apoptosis induced by cytotoxic T lymphocytes and Fas. *J Biol Chem* 275(13):9725–9733
 33. van Rijssel J, Hoogenboezem M, Wester L, Hordijk PL, Van Buul JD (2012) The N-terminal DH-PH domain of Trio induces cell spreading and migration by regulating lamellipodia dynamics in a Rac1-dependent fashion. *PLoS One* 7(1):e29912. <https://doi.org/10.1371/journal.pone.0029912>
 34. Progidia C, Malerod L, Stuffers S, Brech A, Bucci C, Stenmark H (2007) RILP is required for the proper morphology and function of late endosomes. *J Cell Sci* 120(Pt 21):3729–3737. <https://doi.org/10.1242/jcs.017301>
 35. Degot S, Auzan M, Chapuis V, Beghin A, Chadeyras A, Nelep C, Calvo-Munoz ML, Young J, Chatelain F, Fuchs A (2010) Improved visualization and quantitative analysis of drug effects using micropatterned cells. *J Vis Exp*. <https://doi.org/10.3791/2514>
 36. Gittes F, Schmidt CF (1998) Signals and noise in micromechanical measurements. *Methods Cell Biol* 55:129–156
 37. Kress H, Stelzer EH, Holzer D, Buss F, Griffiths G, Rohrbach A (2007) Filopodia act as phagocytic tentacles and pull with discrete steps and a load-dependent velocity. *Proc Natl Acad Sci USA* 104(28):11633–11638. <https://doi.org/10.1073/pnas.0702449104>
 38. Bornschloegl T, Romero S, Vestergaard CL, Joanny JF, Van Nieuw GT, Bassereau P (2013) Filopodial retraction force is generated by cortical actin dynamics and controlled by reversible tethering at the tip. *Proc Natl Acad Sci USA* 110(47):18928–18933. <https://doi.org/10.1073/pnas.1316572110>
 39. Westerfield M (2000) The zebrafish book A guide for the laboratory use of zebrafish (*Danio rerio*), 4th edn. Univ. of Oregon Press, Eugene
 40. Kupfer A, Louvard D, Singer SJ (1982) Polarization of the Golgi apparatus and the microtubule-organizing center in cultured fibroblasts at the edge of an experimental wound. *Proc Natl Acad Sci USA* 79(8):2603–2607
 41. Bisel B, Wang Y, Wei JH, Xiang Y, Tang D, Miron-Mendoza M, Yoshimura S, Nakamura N, Seemann J (2008) ERK regulates Golgi and centrosome orientation towards the leading edge through GRASP65. *J Cell Biol* 182(5):837–843. <https://doi.org/10.1083/jcb.200805045>
 42. Thery M, Pepin A, Dressaire E, Chen Y, Bornens M (2006) Cell distribution of stress fibres in response to the geometry of the adhesive environment. *Cell Motil Cytoskeleton* 63(6):341–355. <https://doi.org/10.1002/cm.20126>
 43. Watanabe T, Hosoya H, Yonemura S (2007) Regulation of myosin II dynamics by phosphorylation and dephosphorylation of its light chain in epithelial cells. *Mol Biol Cell* 18(2):605–616. <https://doi.org/10.1091/mbc.E06-07-0590>
 44. Betapudi V (2014) Life without double-headed non-muscle myosin II motor proteins. *Front Chem* 2:45. <https://doi.org/10.3389/fchem.2014.00045>
 45. Vicente-Manzanares M, Ma X, Adelstein RS, Horwitz AR (2009) Non-muscle myosin II takes centre stage in cell adhesion and migration. *Nat Rev Mol Cell Biol* 10(11):778–790. <https://doi.org/10.1038/nrm2786>
 46. Ikebe M, Hartshorne DJ (1985) Phosphorylation of smooth muscle myosin at two distinct sites by myosin light chain kinase. *J Biol Chem* 260(18):10027–10031
 47. Amano M, Ito M, Kimura K, Fukata Y, Chihara K, Nakano T, Matsuura Y, Kaibuchi K (1996) Phosphorylation and activation of myosin by Rho-associated kinase (Rho-kinase). *J Biol Chem* 271(34):20246–20249
 48. Katoh K, Kano Y, Amano M, Onishi H, Kaibuchi K, Fujiwara K (2001) Rho-kinase-mediated contraction of isolated stress fibers. *J Cell Biol* 153(3):569–584
 49. Ito M, Nakano T, Erdodi F, Hartshorne DJ (2004) Myosin phosphatase: structure, regulation and function. *Mol Cell Biochem* 259(1–2):197–209
 50. Vilarino-Guell C, Wider C, Ross OA, Dachselt JC, Kachergus JM, Lincoln SJ, Soto-Ortolaza AI, Cobb SA, Wilhoite GJ, Bacon JA, Behrouz B, Melrose HL, Hentati E, Puschmann A, Evans DM, Conibear E, Wasserman WW, Aasly JO, Burkhard PR, Djaldetti

- R, Ghika J, Hentati F, Krygowska-Wajs A, Lynch T, Melamed E, Rajput A, Rajput AH, Solida A, Wu RM, Uitti RJ, Wszolek ZK, Vingerhoets F, Farrer MJ (2011) VPS35 mutations in Parkinson disease. *Am J Hum Genet* 89(1):162–167. <https://doi.org/10.1016/j.ajhg.2011.06.001>
51. Daniel JL, Adelstein RS (1976) Isolation and properties of platelet myosin light chain kinase. *Biochemistry* 15(11):2370–2377
 52. Singh TJ, Akatsuka A, Huang KP (1983) Phosphorylation of smooth muscle myosin light chain by five different kinases. *FEBS Lett* 159(1–2):217–220
 53. Ridley AJ (2015) Rho GTPase signalling in cell migration. *Curr Opin Cell Biol* 36:103–112. <https://doi.org/10.1016/j.ceb.2015.08.005>
 54. Ridley AJ (2001) Rho family proteins: coordinating cell responses. *Trends Cell Biol* 11(12):471–477
 55. Hanna S, Miskolci V, Cox D, Hodgson L (2014) A new genetically encoded single-chain biosensor for Cdc42 based on FRET, useful for live-cell imaging. *PLoS One* 9(5):e96469. <https://doi.org/10.1371/journal.pone.0096469>
 56. Grigoriev I, Yu KL, Martinez-Sanchez E, Serra-Marques A, Smal I, Meijering E, Demmers J, Peranen J, Pasterkamp RJ, van Sluijs P, Hooogenraad CC, Akhmanova A (2011) Rab6, Rab8, and MICAL3 cooperate in controlling docking and fusion of exocytotic carriers. *Curr Biol* 21(11):967–974. <https://doi.org/10.1016/j.cub.2011.04.030>
 57. Miki H, Sasaki T, Takai Y, Takenawa T (1998) Induction of filopodium formation by a WASP-related actin-depolymerizing protein N-WASP. *Nature* 391(6662):93–96. <https://doi.org/10.1038/34208>
 58. Hart MJ, Callow MG, Souza B, Polakis P (1996) IQGAP1, a calmodulin-binding protein with a rasGAP-related domain, is a potential effector for cdc42Hs. *EMBO J* 15(12):2997–3005
 59. Schwarz J, Proff J, Havemeier A, Ladwein M, Rottner K, Barlag B, Pich A, Tatge H, Just I, Gerhard R (2012) Serine-71 phosphorylation of Rac1 modulates downstream signaling. *PLoS One* 7(9):e44358. <https://doi.org/10.1371/journal.pone.0044358>
 60. Hou C, Zhuang Z, Deng X, Xu Y, Zhang P, Zhu L (2018) Knock-down of Trio by CRISPR/Cas9 suppresses migration and invasion of cervical cancer cells. *Oncol Rep* 39(2):795–801. <https://doi.org/10.3892/or.2017.6117>
 61. Kozma R, Ahmed S, Best A, Lim L (1995) The Ras-related protein Cdc42Hs and bradykinin promote formation of peripheral actin microspikes and filopodia in Swiss 3T3 fibroblasts. *Mol Cell Biol* 15(4):1942–1952
 62. Yang L, Yang J, Li J, Shen X, Le Y, Zhou C, Wang S, Zhang S, Xu D, Gong Z (2015) MicroRNA-33a inhibits epithelial-to-mesenchymal transition and metastasis and could be a prognostic marker in non-small cell lung cancer. *Sci Rep* 5:13677. <https://doi.org/10.1038/srep13677>
 63. Moshal KS, Ferri-Lagneau KF, Haider J, Pardhanani P, Leung T (2011) Discriminating different cancer cells using a zebrafish in vivo assay. *Cancers (Basel)* 3(4):4102–4113. <https://doi.org/10.3390/cancers3044102>
 64. Seabra MC, Coudrier E (2004) Rab GTPases and myosin motors in organelle motility. *Traffic* 5(6):393–399. <https://doi.org/10.1111/j.1398-9219.2004.00190.x>
 65. Goud B, Gleeson PA (2010) TGN golgins, Rabs and cytoskeleton: regulating the Golgi trafficking highways. *Trends Cell Biol* 20(6):329–336. <https://doi.org/10.1016/j.tcb.2010.02.006>
 66. Horgan CP, McCaffrey MW (2011) Rab GTPases and microtubule motors. *Biochem Soc Trans* 39(5):1202–1206. <https://doi.org/10.1042/BST0391202>
 67. Kjos I, Vestre K, Guadagno NA, Borg Distefano M (1865) Progidia C (2018) Rab and Arf proteins at the crossroad between membrane transport and cytoskeleton dynamics. *Biochim Biophys Acta* 10:1397–1409. <https://doi.org/10.1016/j.bbamcr.2018.07.009>
 68. Doyle AD, Kutys ML, Conti MA, Matsumoto K, Adelstein RS, Yamada KM (2012) Micro-environmental control of cell migration—myosin IIA is required for efficient migration in fibrillar environments through control of cell adhesion dynamics. *J Cell Sci* 125(Pt 9):2244–2256. <https://doi.org/10.1242/jcs.098806>
 69. Even-Ram S, Doyle AD, Conti MA, Matsumoto K, Adelstein RS, Yamada KM (2007) Myosin IIA regulates cell motility and actomyosin-microtubule crosstalk. *Nat Cell Biol* 9(3):299–309. <https://doi.org/10.1038/ncb1540>
 70. Sandquist JC, Swenson KI, Demali KA, Burridge K, Means AR (2006) Rho kinase differentially regulates phosphorylation of nonmuscle myosin II isoforms A and B during cell rounding and migration. *J Biol Chem* 281(47):35873–35883. <https://doi.org/10.1074/jbc.M605343200>
 71. Jorisch MH, Shih W, Yamada S (2013) Myosin IIA deficient cells migrate efficiently despite reduced traction forces at cell periphery. *Biol Open* 2(4):368–372. <https://doi.org/10.1242/bio.20133707>
 72. Giannone G, Dubin-Thaler BJ, Dobereiner HG, Kieffer N, Bresnick AR, Sheetz MP (2004) Periodic lamellipodial contractions correlate with rearward actin waves. *Cell* 116(3):431–443
 73. Qiu Y, Brown AC, Myers DR, Sakurai Y, Mannino RG, Tran R, Ahn B, Hardy ET, Kee MF, Kumar S, Bao G, Barker TH, Lam WA (2014) Platelet mechanosensing of substrate stiffness during clot formation mediates adhesion, spreading, and activation. *Proc Natl Acad Sci USA* 111(40):14430–14435. <https://doi.org/10.1073/pnas.1322917111>
 74. Cai Y, Rossier O, Gauthier NC, Biais N, Fardin MA, Zhang X, Müller LW, Ladoux B, Cornish VW, Sheetz MP (2010) Cytoskeletal coherence requires myosin-IIA contractility. *J Cell Sci* 123(Pt 3):413–423. <https://doi.org/10.1242/jcs.058297>
 75. Wakatsuki T, Wysolmerski RB, Elson EL (2003) Mechanics of cell spreading: role of myosin II. *J Cell Sci* 116(Pt 8):1617–1625
 76. Mih JD, Marinkovic A, Liu F, Sharif AS, Tschumperlin DJ (2012) Matrix stiffness reverses the effect of actomyosin tension on cell proliferation. *J Cell Sci* 125(Pt 24):5974–5983. <https://doi.org/10.1242/jcs.108886>
 77. Betapudi V, Licate LS, Egelhoff TT (2006) Distinct roles of nonmuscle myosin II isoforms in the regulation of MDA-MB-231 breast cancer cell spreading and migration. *Cancer Res* 66(9):4725–4733. <https://doi.org/10.1158/0008-5472.CAN-05-4236>
 78. Nisenholz N, Paknikar A, Koster S, Zemel A (2016) Contribution of myosin II activity to cell spreading dynamics. *Soft Matter* 12(2):500–507. <https://doi.org/10.1039/c5sm01733e>
 79. Nobes CD, Hall A (1995) Rho, rac, and cdc42 GTPases regulate the assembly of multimolecular focal complexes associated with actin stress fibers, lamellipodia, and filopodia. *Cell* 81(1):53–62
 80. Rohatgi R, Ma L, Miki H, Lopez M, Kirchhausen T, Takenawa T, Kirschner MW (1999) The interaction between N-WASP and the Arp2/3 complex links Cdc42-dependent signals to actin assembly. *Cell* 97(2):221–231
 81. Carlier MF, Ducruix A, Pantaloni D (1999) Signalling to actin: the Cdc42-N-WASP-Arp2/3 connection. *Chem Biol* 6(9):R235–R240
 82. Svitkina TM, Bulanova EA, Chaga OY, Vignjevic DM, Kojima S, Vasiliev JM, Borisy GG (2003) Mechanism of filopodia initiation by reorganization of a dendritic network. *J Cell Biol* 160(3):409–421. <https://doi.org/10.1083/jcb.200210174>
 83. Manser E, Leung T, Salihuddin H, Zhao ZS, Lim L (1994) A brain serine/threonine protein kinase activated by Cdc42 and Rac1. *Nature* 367(6458):40–46. <https://doi.org/10.1038/367040a0>
 84. Edwards DC, Sanders LC, Bokoch GM, Gill GN (1999) Activation of LIM-kinase by Pak1 couples Rac/Cdc42 GTPase signalling to actin cytoskeletal dynamics. *Nat Cell Biol* 1(5):253–259. <https://doi.org/10.1038/12963>

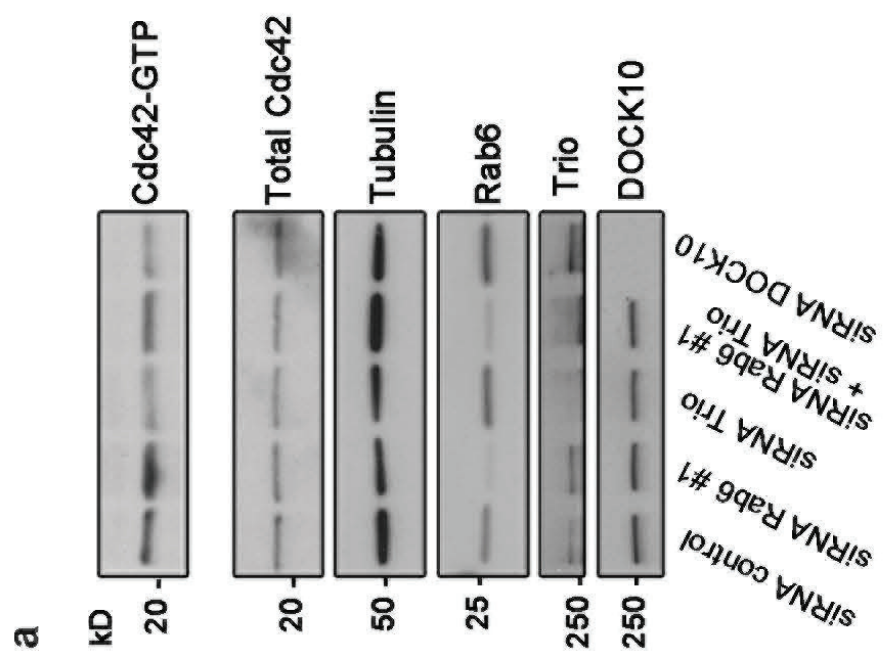
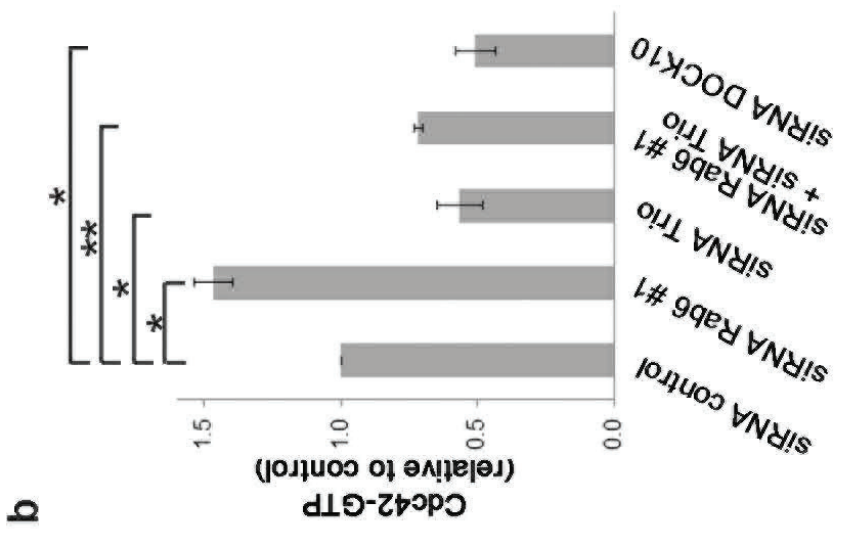
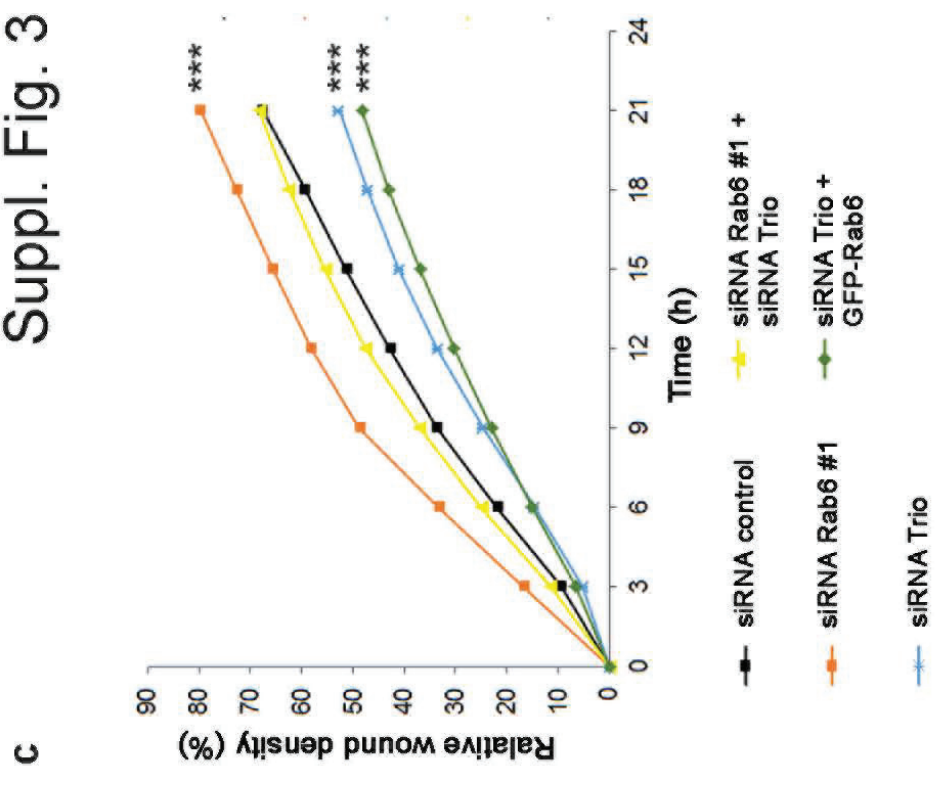
85. van Leeuwen FN, van Delft S, Kain HE, van der Kammen RA, Collard JG (1999) Rac regulates phosphorylation of the myosin-II heavy chain, actinomyosin disassembly and cell spreading. *Nat Cell Biol* 1(4):242–248. <https://doi.org/10.1038/12068>
86. Ridley AJ (2001) Rho GTPases and cell migration. *J Cell Sci* 114(Pt 15):2713–2722
87. Jian Q, Miao Y, Tang L, Huang M, Yang Y, Ba W, Liu Y, Chi S, Li C (2016) Rab23 promotes squamous cell carcinoma cell migration and invasion via integrin beta1/Rac1 pathway. *Oncotarget* 7(5):5342–5352. <https://doi.org/10.18632/oncotarget.6701>
88. Margiotta A, Progida C, Bakke O (1864) Bucci C (2017) Rab7a regulates cell migration through Rac1 and vimentin. *Biochim Biophys Acta* 2:367–381. <https://doi.org/10.1016/j.bbamcr.2016.11.020>
89. Chevallier J, Koop C, Srivastava A, Petrie RJ, Lamarche-Vane N, Presley JF (2009) Rab35 regulates neurite outgrowth and cell shape. *FEBS Lett* 583(7):1096–1101. <https://doi.org/10.1016/j.febslet.2009.03.012>
90. Bravo-Cordero JJ, Cordani M, Soriano SF, Diez B, Munoz-Agudo C, Casanova-Acebes M, Boullosa C, Guadamillas MC, Ezkurdia I, Gonzalez-Pisano D, Del Pozo MA, Montoya MC (2016) A novel high-content analysis tool reveals Rab8-driven cytoskeletal reorganization through Rho GTPases, calpain and MT1-MMP. *J Cell Sci* 129(8):1734–1749. <https://doi.org/10.1242/jcs.174920>
91. Lee CS, Choi CK, Shin EY, Schwartz MA, Kim EG (2010) Myosin II directly binds and inhibits Dbl family guanine nucleotide exchange factors: a possible link to Rho family GTPases. *J Cell Biol* 190(4):663–674. <https://doi.org/10.1083/jcb.201003057>
92. Jacquemet G, Hamidi H, Ivaska J (2015) Filopodia in cell adhesion, 3D migration and cancer cell invasion. *Curr Opin Cell Biol* 36:23–31. <https://doi.org/10.1016/j.ceb.2015.06.007>
93. Jacquemet G, Paatero I, Carisey AF, Padzik A, Orange JS, Hamidi H, Ivaska J (2017) FiloQuant reveals increased filopodia density during breast cancer progression. *J Cell Biol* 216(10):3387–3403. <https://doi.org/10.1083/jcb.201704045>

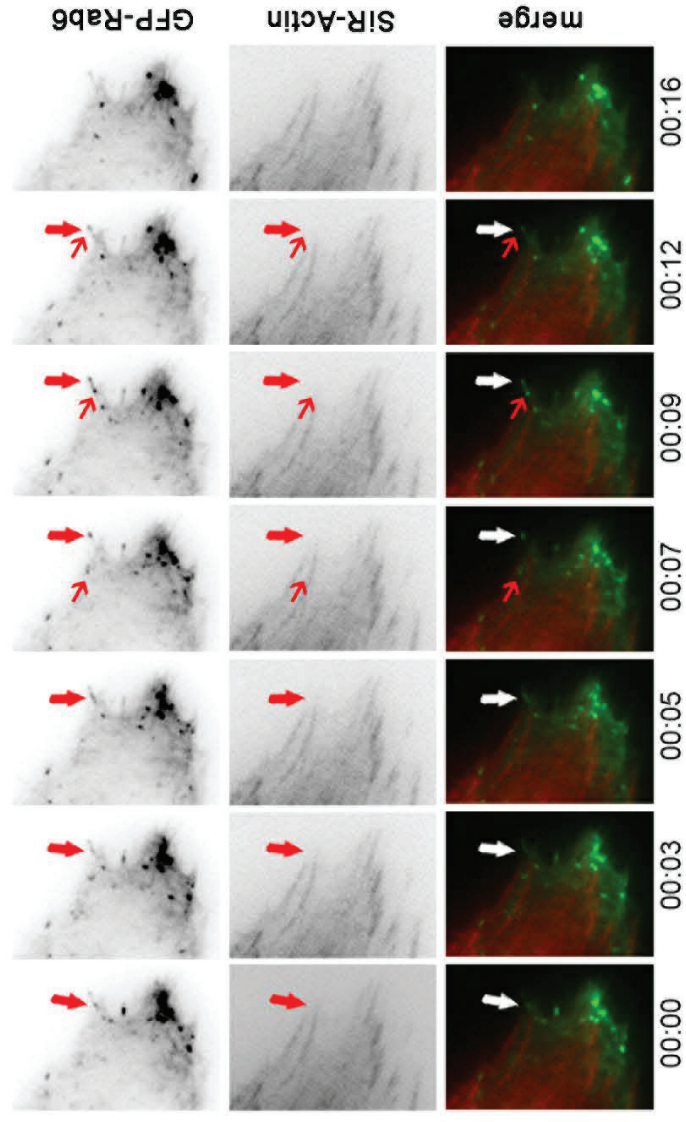
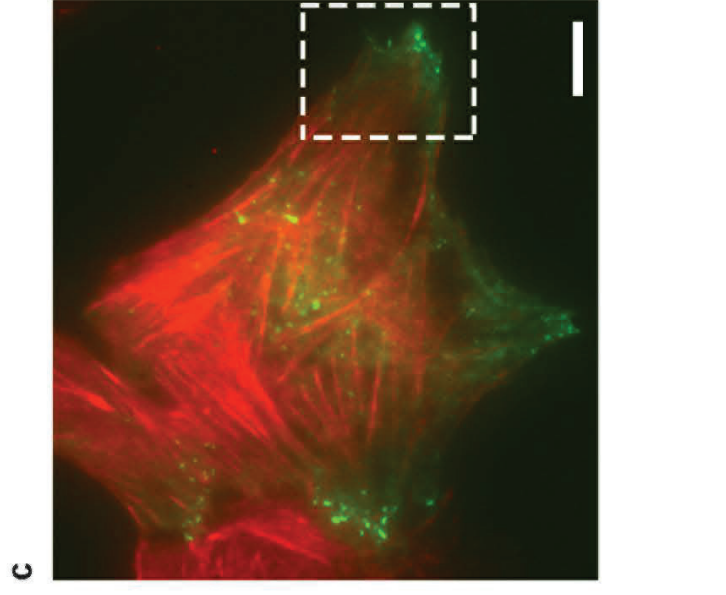
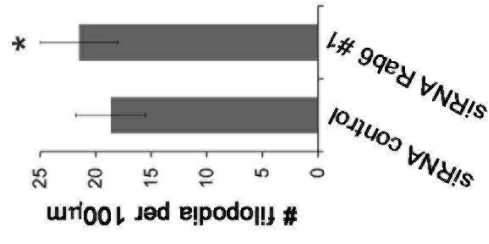
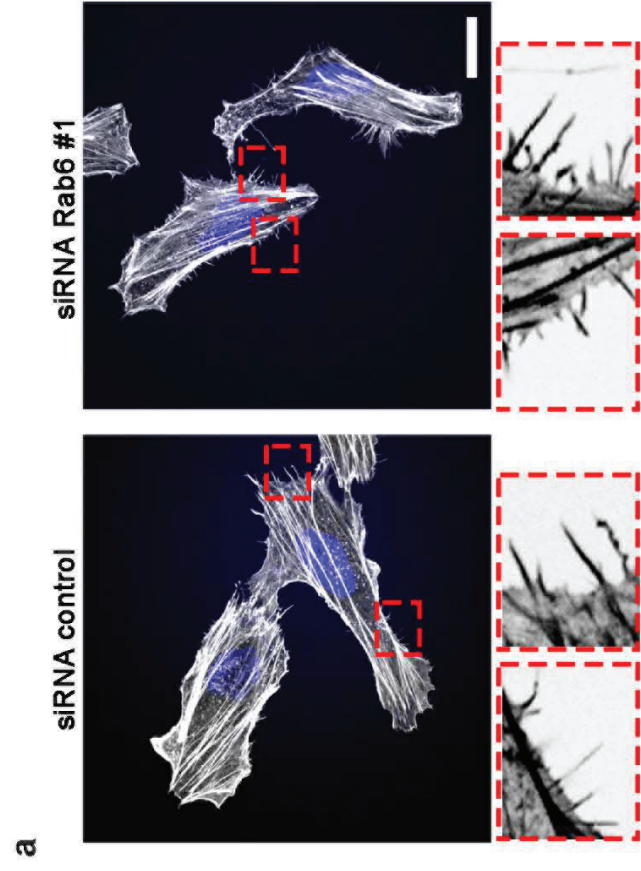
Publisher's Note Springer Nature remains neutral with regard to jurisdictional claims in published maps and institutional affiliations.



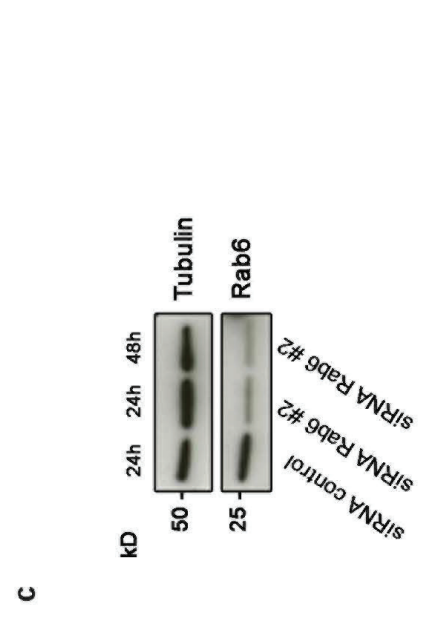
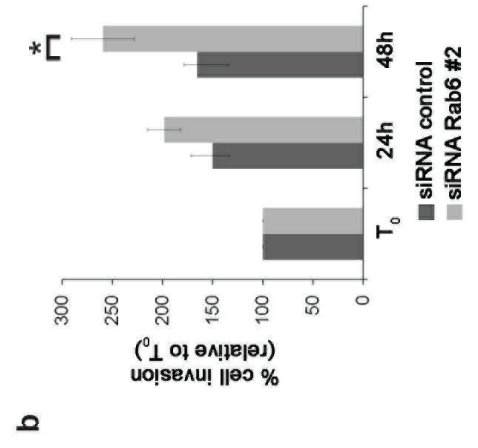
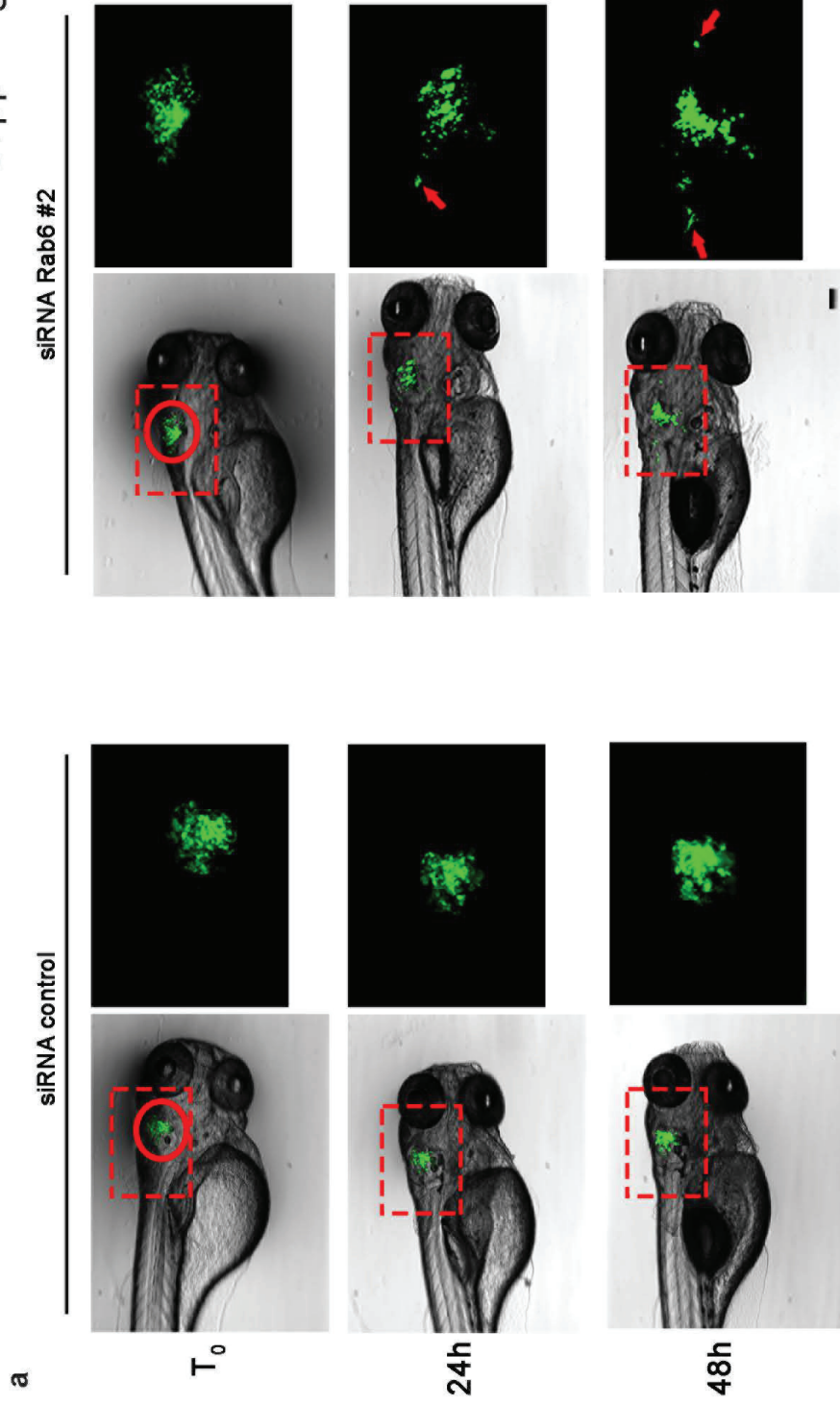


Suppl. Fig. 3





Suppl. Fig. 5



RESEARCH ARTICLE

Rab7b regulates dendritic cell migration by linking lysosomes to the actomyosin cytoskeleton

Katharina Vestre¹, Irene Persiconi^{1,*}, Marita Borg Distefano^{1,*}, Nadia Mensali², Noemi Antonella Guadagno¹, Marine Bretou^{3,4}, Sébastien Wälchli², Catharina Arnold-Schrauf⁵, Oddmund Bakke¹, Marc Dalod⁵, Ana-Maria Lennon-Dumenil³ and Cinzia Progida^{1,‡}

ABSTRACT

Lysosomal signaling facilitates the migration of immune cells by releasing Ca²⁺ to activate the actin-based motor myosin II at the cell rear. However, how the actomyosin cytoskeleton physically associates to lysosomes is unknown. We have previously identified myosin II as a direct interactor of Rab7b, a small GTPase that mediates the transport from late endosomes/lysosomes to the *trans*-Golgi network (TGN). Here, we show that Rab7b regulates the migration of dendritic cells (DCs) in one- and three-dimensional environments. DCs are immune sentinels that transport antigens from peripheral tissues to lymph nodes to activate T lymphocytes and initiate adaptive immune responses. We found that the lack of Rab7b reduces myosin II light chain phosphorylation and the activation of the transcription factor EB (TFEB), which controls lysosomal signaling and is required for fast DC migration. Furthermore, we demonstrate that Rab7b interacts with the lysosomal Ca²⁺ channel TRPML1 (also known as MCOLN1), enabling the local activation of myosin II at the cell rear. Taken together, our findings identify Rab7b as the missing physical link between lysosomes and the actomyosin cytoskeleton, allowing control of immune cell migration through lysosomal signaling.

This article has an associated First Person interview with the first author of the paper.

KEY WORDS: Rab7b, Rab protein, Actomyosin, Cell migration, Dendritic cells

INTRODUCTION

Dendritic cells (DCs) are professional antigen-presenting cells that engulf extracellular material in peripheral tissues and transport it to lymph nodes for presentation to T cells. When encountering danger-associated antigens, for example, microbial products, DCs start a maturation program, where they undergo massive phenotypical and

functional changes (Banchereau et al., 2000; Reis e Sousa, 2006). In particular, while immature DCs are characterized by a high antigen uptake capacity and a slow intermittent migration mode (Chabaud et al., 2015), mature DCs are less capable of antigen uptake but are highly motile (Vargas et al., 2016). This increase in their migration capacity, together with the upregulation of the CCR7 chemokine receptor at their surface, promotes their migration to lymph nodes for the initiation of adaptive immune responses (Mellman and Steinman, 2001). Therefore, DCs strongly rely on their ability to migrate to exert their immunosurveillance function (Alvarez et al., 2008).

The fast and directional migration that characterizes mature DCs is regulated by lysosomal signaling (Bretou et al., 2017). Lipopolysaccharide (LPS) stimulation in DCs promotes the nuclear translocation of the transcription factor EB (TFEB), the master regulator of lysosome biogenesis and function (Bretou et al., 2017; Sardiello et al., 2009). This results in the expression of a plethora of genes involved in lysosome activity and biogenesis, including the lysosomal Ca²⁺ channel TRPML1 (also known as MCOLN1). Ca²⁺ release through TRPML1 promotes the activity of the actin-based motor myosin II at the cell rear, which regulates fast and directional migration (Bretou et al., 2017). However, it is not known how the actomyosin cytoskeleton physically associates to the lysosomal compartment.

We previously reported that the small GTPase Rab7b, which regulates the transport from late endosomes towards the *trans*-Golgi network (TGN) (Borg Distefano et al., 2018; Progida et al., 2010, 2012), interacts directly with the actin motor protein myosin II (Borg et al., 2014; Distefano et al., 2015). Interestingly, Rab7b was originally identified in DCs (Yang et al., 2004) and later shown to be also expressed upon monocytic and megakaryocytic differentiation (He et al., 2011; Yang et al., 2004). In DCs, Rab7b is strongly upregulated upon LPS-induced maturation, before a gradual downregulation as the cells fully mature (Berg-Larsen et al., 2013), suggesting a possible involvement in some of the initial changes that occur upon maturation.

Here, we investigated the role of Rab7b in DCs. We show that the lack of Rab7b compromises the switch from slow to fast migration that occurs upon DC maturation, with antigen uptake remaining unaffected. We further highlight that lysosomal signaling and myosin II activity are reduced in Rab7b-knockout (KO) DCs. Finally, we demonstrate that Rab7b interacts with the lysosomal Ca²⁺ channel TRPML1, bridging it to myosin II for the local activation at the cell rear. These results strongly suggest that Rab7b acts as the missing physical link between lysosomes and the actomyosin cytoskeleton, thereby promoting fast DC migration.

RESULTS

Rab7b is needed for actomyosin polarization in mature DCs

Rab7b is highly expressed in DCs, and strongly upregulated upon LPS-induced maturation (Berg-Larsen et al., 2013; Progida et al.,

¹Department of Biosciences, Centre for Immune Regulation, University of Oslo, 0316 Oslo, Norway. ²Department of Cellular Therapy, the Radium Hospital, Oslo University Hospital, 0379 Oslo, Norway. ³Institut Curie, Inserm U932, F-75005 Paris, France. ⁴VIB-KU Leuven Center for Brain and Disease Research, 3000 Leuven, Belgium. ⁵Aix Marseille Univ, CNRS, INSERM, Centre d'Immunologie de Marseille-Luminy, 13288 Marseille, France.

*These authors contributed equally to this work

‡Author for correspondence (c.a.m.progida@ibv.uio.no)

© S.W., 0000-0001-5869-1746; C.A.-S., 0000-0002-2477-337X; O.B., 0000-0003-4843-7626; M.D., 0000-0002-6436-7966; C.P., 0000-0002-9254-0690

This is an Open Access article distributed under the terms of the Creative Commons Attribution License (<https://creativecommons.org/licenses/by/4.0>), which permits unrestricted use, distribution and reproduction in any medium provided that the original work is properly attributed.

Handling Editor: Daniel Billadeau

Received 2 August 2021; Accepted 16 August 2021

2010). However, it is currently unknown what the role of this small GTPase in maturing DCs is. To assess the function of Rab7b in DCs, we first analyzed the intracellular localization of the endogenous protein in monocyte-derived human DCs (MDDCs). As shown in Fig. 1A and Fig. S1A, Rab7b localizes to lysosomes but not to early endosomes nor the TGN in MDDCs. We also found Rab7b to colocalize with its interactor myosin II. We therefore next investigated how the actomyosin organization was affected in cells depleted of Rab7b. MDDCs were transfected with siRNA targeting Rab7b, stimulated with LPS, seeded on poly-L-lysine (PLL)-coated coverslips, were fixed and stained with the actin marker phalloidin and an antibody against myosin II. Intriguingly, while control cells were clearly organized in a polarized and directional manner, with actin-rich structures called podosomes only at the leading edge, DCs depleted of Rab7b lacked polarization, and podosome orientation was altered (Fig. 1A,B). Interestingly, the altered orientation and distribution of podosomes observed upon Rab7b knockdown resembled the ones observed in immature DCs (Fig. S1B). As we did not detect any significant differences in the size or number of podosomes per cell in cells depleted of Rab7b compared to control cells (Fig. 1C,D), we conclude that Rab7b does not affect podosome formation, but rather their distribution and the polarization of mature human DCs.

Depletion of Rab7b does not prevent DC maturation or antigen presentation ability

To investigate whether the altered DC polarization upon Rab7b depletion was a consequence of defective maturation rather than a specific effect on the actomyosin cytoskeleton, we measured the expression of maturation markers on the DC surface by flow cytometry (Banchereau et al., 2000). Both immature and mature LPS-treated DCs were efficiently depleted of Rab7b (Fig. 2A,B). We found no significant difference in surface expression of maturational markers between Rab7b siRNA-treated and control siRNA-treated DCs (Fig. 2C). Indeed, the levels of the co-stimulatory molecules CD80 and CD86, as well as human leukocyte antigen (HLA)-class I and HLA-DR, remained unchanged upon Rab7b knockdown. Likewise, the surface levels of the immunoregulatory molecule CD83, the chemokine receptor CCR7 and the DC marker CD11c (also known as ITGAX) were unaffected (Fig. 2C). We excluded that the electroporation or the depletion of Rab7b by itself initiated the DC maturation process, as immature DCs depleted of Rab7b, similar to immature control cells, displayed lower levels of the surface markers of mature DCs, like CD80, CD86 and CD83 (Fig. 2C). Thus, Rab7b does not affect the maturation of DCs as Rab7b-depleted DCs show a normal maturation pattern upon LPS treatment.

Phenotypic markers are commonly used to assess DCs maturation (Banchereau et al., 2000; Manh et al., 2013). However, this assessment is not sufficient to determine whether DCs have acquired the ability to present antigens. Therefore, we also investigated whether depletion of Rab7b affects the ability of DCs to present antigens to T cells *in vitro* by performing a CD107a (also known as LAMP1) mobilization assay. DCs isolated from healthy donors were successfully depleted for Rab7b (Fig. S2A,B), loaded with a specific cancer peptide (a TGFBR2 frameshift mutation-derived epitope), and further incubated with autologous T cells transfected with the validated cognate T cell receptor (TCR), Radium-1 (Inderberg et al., 2017). The amount of specifically stimulated CD8+ T cells, monitored by measuring the levels of the degranulation marker CD107a, was measured by flow cytometry. As shown in Fig. 2D, depletion of Rab7b did not affect the antigen presentation abilities of mature DCs, as both the control siRNA- and the Rab7b

siRNA-treated DCs stimulated T cell activation to the same extent. Taken together, our results indicate that although Rab7b regulates actin polarization in DCs, it does not play any role in their maturation and ability to present antigens to T lymphocytes.

Rab7b depletion prevents fast and persistent DC migration

As cell polarization is important for cell migration, we next evaluated whether Rab7b knockdown also affects DC motility. DC migration is strongly dependent on external geometry, and DCs migrate faster in confined environments (Heuze et al., 2013; Lammermann et al., 2008). To study the effect of Rab7b depletion on DC migration under confinement, we used micro-fabricated channels (Fig. 3A). These experiments were performed with bone marrow-derived murine DCs (BMDCs), as previously described (Bretou et al., 2017; Chabaud et al., 2015; Vargas et al., 2016, 2014). Similar to human MDDCs, BMDCs were successfully depleted for Rab7b, and the depletion did not affect their maturation (Fig. S2C,D). BMDCs transfected with control siRNA or siRNA targeting Rab7b were loaded into microchannels and imaged overnight. Our results showed that for cells transfected with the control siRNA, immature DCs were slower (mean speed 4.8 $\mu\text{m}/\text{min}$) than the mature LPS-stimulated DCs (LPS-DCs; mean speed 8.4 $\mu\text{m}/\text{min}$) (Fig. 3B,C), as expected. However, cells depleted of Rab7b failed to speed up after addition of LPS (Fig. 3B,C).

While immature DCs are known to change direction frequently, undergoing important speed fluctuations during motion, mature DCs are more persistent (Chabaud et al., 2015; Vargas et al., 2016). Interestingly, upon depletion of Rab7b, LPS-DCs still behave like immature DCs, as they have low speed and significantly higher local speed variations compared to control cells, indicating that DCs depleted of Rab7b change direction more frequently while migrating in microchannels (Fig. 3D). These results point to a role for Rab7b in DC polarization and migration, suggesting that the lack of this small GTPase prevents the switch to the faster and more persistent locomotion typical of mature DCs.

To further explore the role of Rab7b in DC migration, we generated a CD11c conditional knockout (KO) mouse model for this small GTPase. We then investigated whether the Rab7b-dependent migration defects observed in LPS-DCs affected their chemotactic migration. When exposed to the chemokine CCL21 *in vivo*, DCs increase their persistency and are guided towards lymphatic vessels (Weber et al., 2013). To model this process, mature LPS-DCs from conditional KO mice were embedded in collagen gels and left to migrate in the presence of a CCL21 gradient. Consistent with our previous results, we found that Rab7b KO DC migration speed was significantly decreased. Indeed, Rab7b KO DCs were over 20% slower than wild-type (WT) cells (Fig. 3E,F; Movie 1). Similarly, Rab7b KO LPS-DCs were also significantly less persistent in comparison to the WT cells (Fig. 3G). Taken together, these results demonstrate that Rab7b is needed for mature DCs to switch to a fast and directional migration mode.

Rab7b affects actomyosin distribution and macropinocytosis in LPS-DCs

The migration of DCs in confined environments depends on contractile forces driven by myosin II (Chabaud et al., 2015; Lammermann et al., 2008). To promote fast migration, mature DCs increase the amount of actin and myosin at the cell rear, while immature DCs have more actin and myosin at the cell front to perform macropinocytosis (Chabaud et al., 2015; Vargas et al., 2016). Since our data indicate that Rab7b is important for polarization of DCs, we speculated that the decreased migratory ability of DCs lacking Rab7b

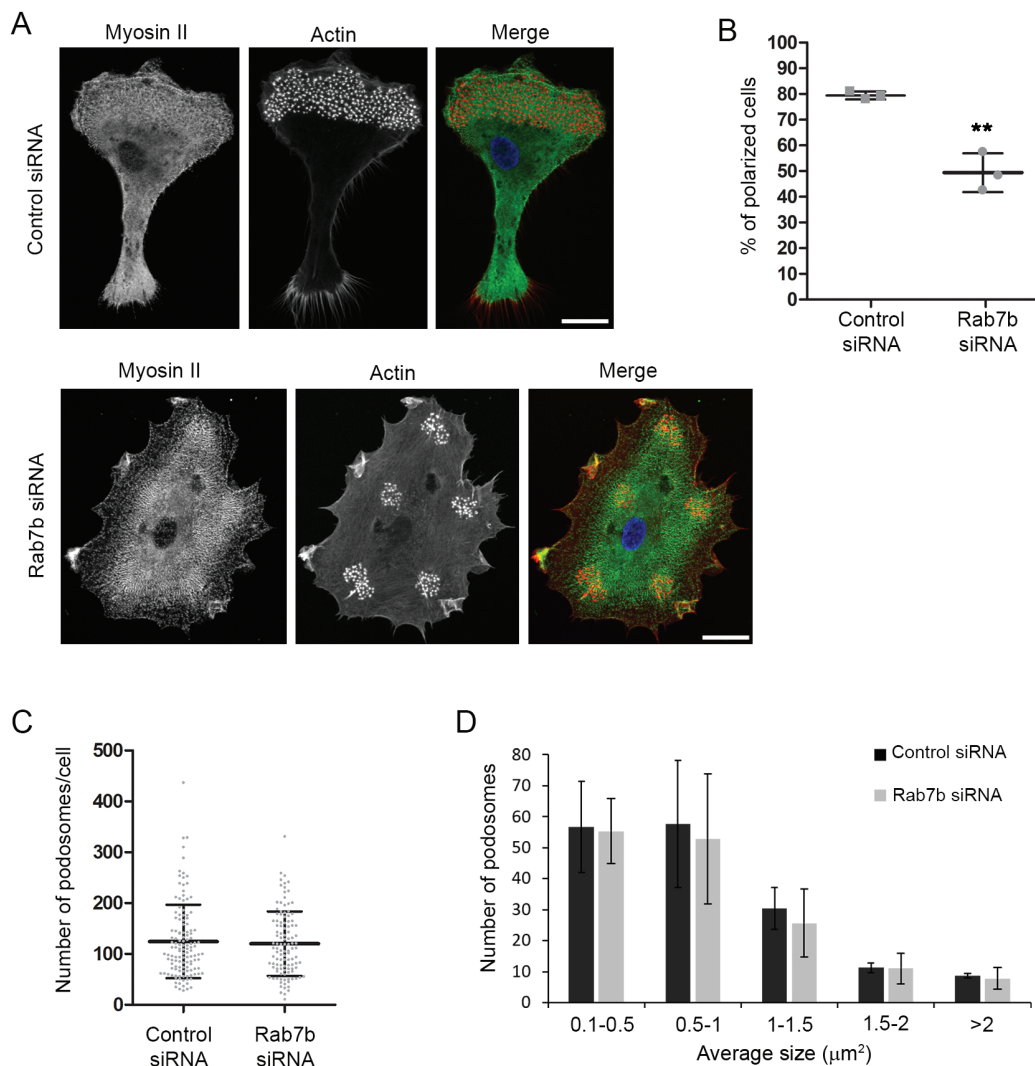


Fig. 1. Rab7b is required for DC polarization. (A) MDDCs were transfected by electroporation with either control siRNA or Rab7b siRNA, and stimulated with LPS for 48 h. Thereafter, DCs were plated on PLL-coated coverslips and left to adhere for additional 24 h, before fixation and immunostaining with anti-myosin II (green). Actin was labeled with Rhodamine-conjugated phalloidin (red) and nuclei with Hoechst 33258 (blue). Images represent maximum intensity projections of Z stacks. Scale bars: 10 μm. (B) Quantification of the percentage of polarized cells. Polarized cells have a clear podosome-rich leading edge and a trailing edge devoid of podosomes. Cells with podosomes equally distributed and with no distinction between leading and trailing edges are accounted as not polarized. Data represent the mean ± s.d. of three independent experiments ($n > 145$). ** $P < 0.005$ (two-tailed unpaired Student's *t*-test). (C,D) Quantification of the number (C) and size (D) of podosomes per cell. The graphs show the mean ± s.d. from three independent experiments ($n > 120$).

might be a consequence of the altered actomyosin distribution. We therefore compared myosin II distribution in immature and mature WT and Rab7b KO DCs migrating in micro-fabricated channels. The analysis of density maps of the mean myosin II distribution showed that Rab7b KO cells, in contrast to WT cells, failed to increase the amount of myosin II at the cell rear after addition of LPS (Fig. 4A–C). While the front-to-back ratio for myosin II was not significantly different between WT and KO immature cells, the front-to-back ratio in Rab7b KO LPS-DCs was 32% higher than in the WT LPS-DCs (Fig. 4C).

Having observed that the myosin II distribution is altered in LPS-treated Rab7b KO DCs, we next looked at whether the actin distribution was affected in a similar way in these cells. In line with our results for myosin II, density maps of the mean actin distribution showed that the fraction of actin located at the cell front in LPS-DCs was almost 30% higher in the Rab7b KO cells than in the WT cells (Fig. 4D,E). Intriguingly, this distribution is similar to

the distribution in immature DCs during phases of slow locomotion (Chabaud et al., 2015; Vargas et al., 2016).

Immature DCs are characterized by a high antigen uptake capacity, and they sample their environment by engulfing large amounts of extracellular material using macropinocytosis. The enrichment of actin and myosin at the cell front is typical for DCs performing macropinocytosis, and, in line with this, the actin at the cell front in Rab7b KO DCs was mainly localized in ruffles and around macropinosomes (Fig. 4F). We therefore verified whether the increased actin concentration at the front of Rab7b-KO DCs was the result of increased macropinocytic activity. For this, LPS-DCs were imaged in microchannels filled with fluorescently labeled dextran to visualize macropinosomes. Similar to what was found in previous studies (Chabaud et al., 2015), we observed large dextran-containing macropinosomes that formed at the front of the DCs (Fig. 5A; Movie 2). As expected for LPS-DCs, the majority of WT cells displayed few or no macropinosomes. However, in the Rab7b-

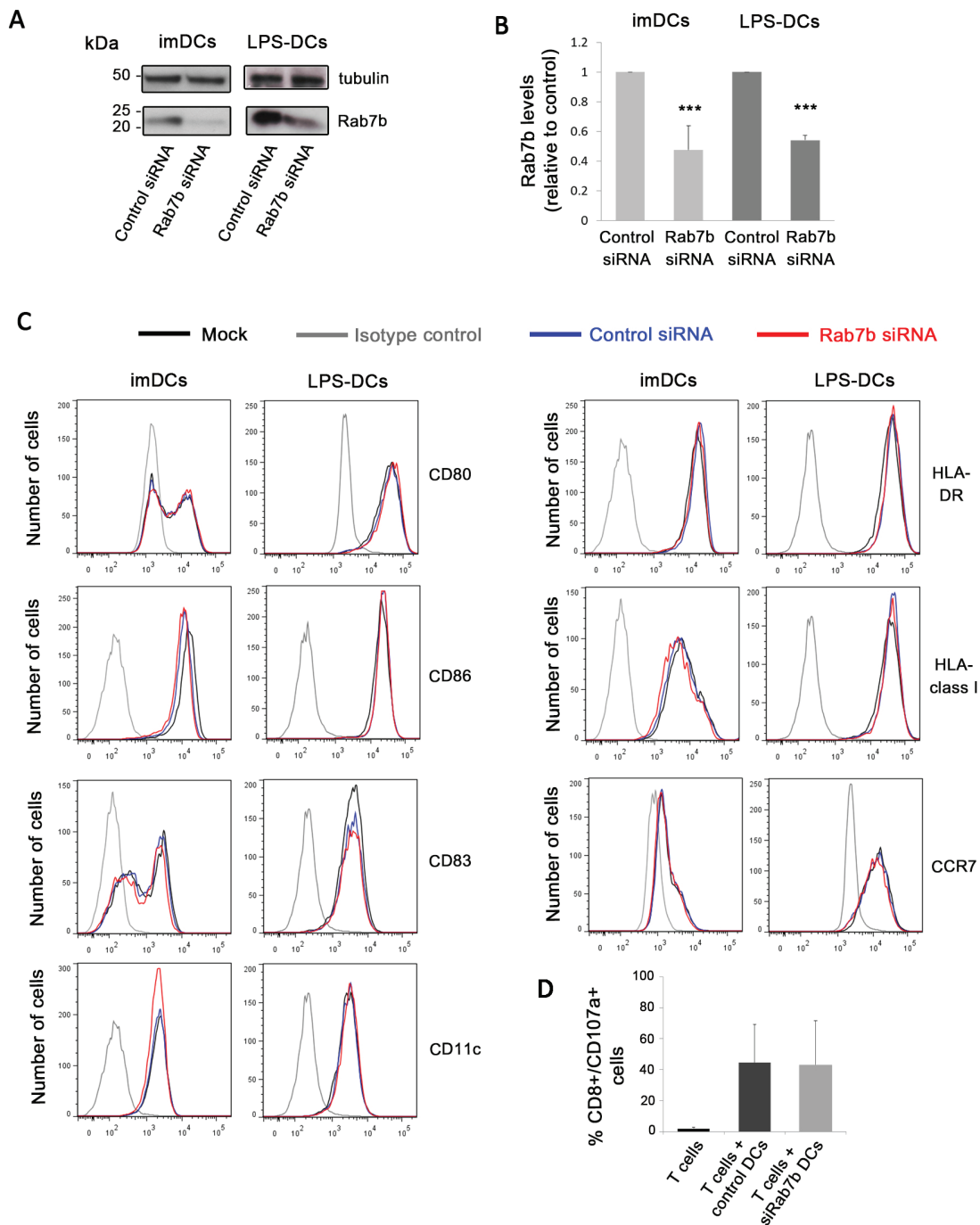


Fig. 2. Rab7b depletion does not affect DC maturation and antigen presentation ability. (A) MDDCs were transfected by electroporation with either control siRNA or Rab7b siRNA. 18 h (for immature DCs; imDCs) or 48 h (for LPS-DCs) after transfection the DCs were harvested, lysed and subjected to western blot analysis with antibodies against Rab7b and tubulin as a loading control. (B) Quantification of Rab7b levels in MDDCs silenced with control siRNA or Rab7b siRNA. The intensity of the bands from western blots was quantified using ImageQuant, and the level of Rab7b was normalized to the amount of tubulin. Data represent the mean \pm s.d. of three independent experiments. *** P <0.0001 (two-tailed unpaired Student's t -test). (C) FACS analysis of the surface expression markers CD80, CD86, CD83 and CD11c (left panels), and HLA-DR, HLA class I and CCR7 (right panels). A representative histogram overlay is shown for each marker. The black line represents mock electroporated (without siRNA) MDDCs, the blue line the control siRNA and the red line the Rab7b siRNA electroporated MDDCs. The gray line corresponds to isotype antibodies. The x-axis represents the mean fluorescence intensity of the conjugated markers indicated for each histogram. The histograms are representative examples from one out of three independent experiments. All experiments were repeated three independent times. (D) Radium-1 TCR-expressing T cells were stimulated for 5 h with either control siRNA- or Rab7b siRNA-treated DCs loaded with a specific 19-mer peptide encoded by the *TGFB2* frameshift mutation. An anti-CD107a antibody was used to assess the amount of degranulation by CD8 $^{+}$ cytotoxic T cells specifically activated by DCs. Data represents the mean \pm s.d. of three independent experiments.

KO LPS-DCs, both the number of macropinosomes and the area of internalized dextran were significantly increased (Fig. 5A–C). Furthermore, while the macropinosomes in the WT cells

disappeared quickly after they were formed, the macropinosomes in the Rab7b KO DCs persisted for a longer time. Indeed, the average lifetime of single macropinosomes in Rab7b KO LPS-DCs

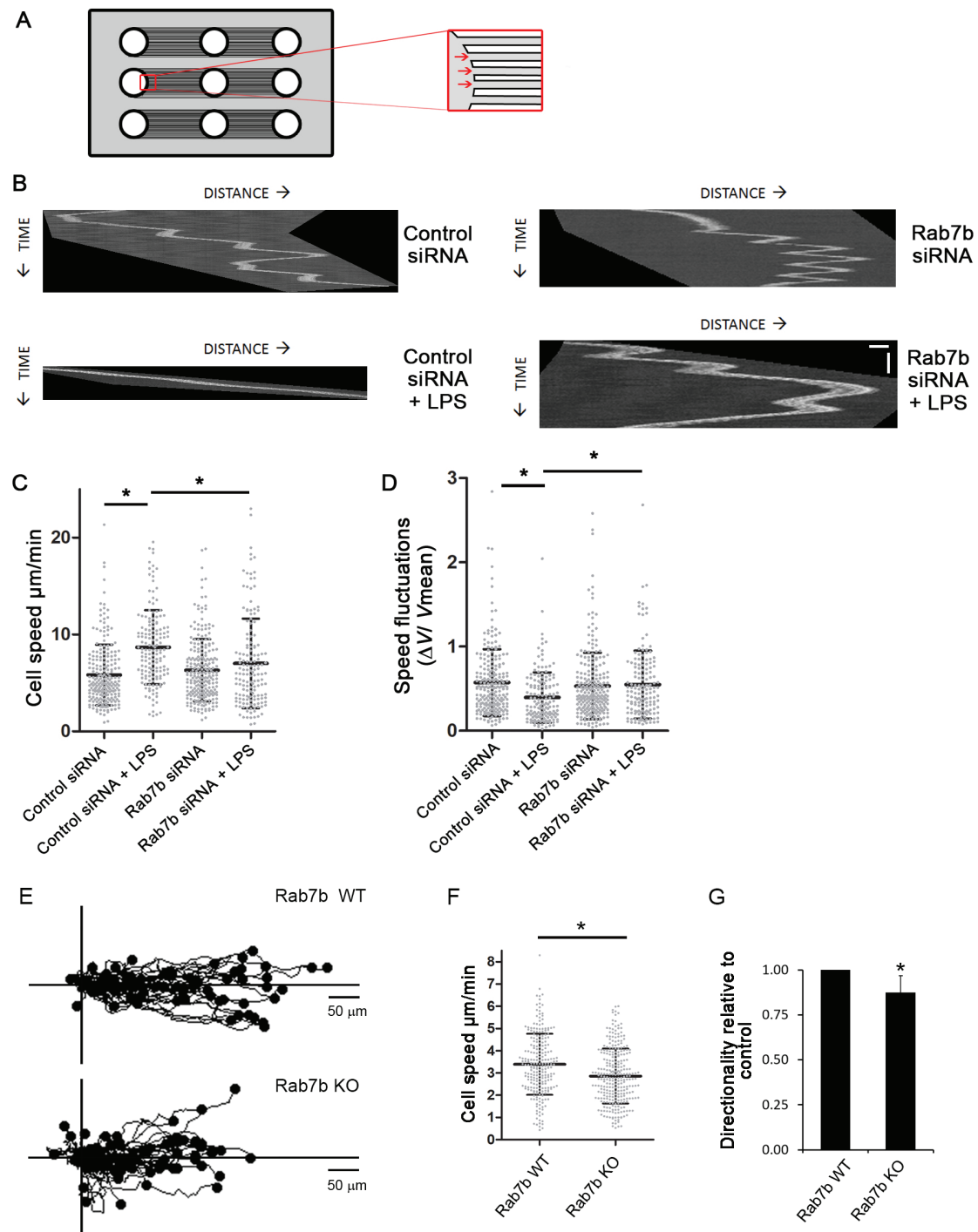


Fig. 3. See next page for legend.

was 28% longer than in WT LPS-DCs (Fig. 5D; Movie 2). Altogether, these results indicate that the decreased motility of Rab7b KO LPS-DCs is associated with their sustained macropinocytic activity.

Lysosome signaling is inhibited in Rab7b KO DCs

Antigens taken up by macropinocytosis are delivered to lysosomes, which become more active during maturation (Trombetta et al., 2003). Previous studies have shown that the

inhibition of macropinocytosis after DC maturation activates lysosomal signaling, which in turn is important for controlling the changes in DC migration by facilitating the formation and/or maintenance of actomyosin at the cell rear (Bretou et al., 2017). Since Rab7b is involved in lysosomal transport (Progida et al., 2010) and also affects DC migration and macropinocytic activity, we next analyzed lysosome distribution in Rab7b KO DCs. LPS-DCs were incubated with fluorescent wheat germ agglutinin (WGA) to label lysosomes, as previously described (Bretou et al.,

Fig. 3. Rab7b is required for fast and persistent migration of LPS-DCs.

(A) Scheme of a micro-fabricated device used to study DC motility under confinement. Cells are loaded in the loading chambers, and spontaneously enter into the microchannels (inset with arrows indicating entry points). (B) BMDCs were either mock treated or LPS-treated for 20 min, before transfection with either control siRNA or Rab7b siRNA. DCs were loaded in 5×5 μm micro-fabricated channels and imaged for 20 h in an epifluorescence Nikon TiE microscope equipped with a cooled CCD camera, using a 10× objective and acquiring one transmission phase image every 2 min. Representative kymographs are shown for DCs treated with either control siRNA, with or without LPS (left panels), or Rab7b siRNA, with or without LPS (right panels). Scale bars: horizontal (distance), 20 μm; vertical (time), 30 min. (C) Quantification of the mean±s.d cell speed (μm/min). *n*>150, three independent experiments. **P*<0.05 (two-tailed unpaired Student's *t*-test). (D) Quantification of mean±s.d. speed fluctuations [calculated as s.d./mean instantaneous speed (Chaubaud et al., 2015; Faure-Andre et al., 2008)]. *n*>150, three independent experiments. **P*<0.05 (two-tailed unpaired Student's *t*-test). (E) Chemotactic response of LPS-DCs embedded in a collagen gel containing a CCL21 gradient. The plot represents movement in the *x*- and *y*-direction of single cells, each track starting at distance 0, from one representative experiment. (F) Quantification of the mean cell speed of WT and Rab7b KO LPS-DCs. Data represents the mean±s.d. of four independent experiments (*n*=238 and 284 cells for WT and Rab7b-KO, respectively). **P*<0.05 (two-tailed paired Student's *t*-test). (G) Quantification of the cell persistency of WT and Rab7b KO LPS-DCs. Cell persistency was calculated by dividing the Euclidian distance with the accumulated distance of each cell trajectory, and is presented relative to WT. Data represents the mean±s.d. of four independent experiments (*n*=238 and 284 cells for WT and Rab7b-KO, respectively). **P*<0.05 (two-tailed unpaired Student's *t*-test).

2017), before loading the cells into dextran-filled microchannels. Consistent with what has been seen in previous studies (Bretou et al., 2017), we observed a large cluster of lysosomes located at the rear in WT LPS-DCs. A similar distribution was also observed in Rab7b KO cells (Fig. 5E), and no differences in either size or distribution of lysosomes or orientation of the microtubule-organizing center (MTOC) was detected between WT and Rab7b KO DCs (Fig. S4A–E). However, while WT cells also had several small and highly dynamic lysosomes that mainly moved between the main cluster and the cell front making contact with the macropinosomes, Rab7b KO cells were devoid of this lysosomal population (Fig. 5E; Movie 3). Indeed, the number of small lysosomes (with an area <0.5 μm²) per cell in WT LPS-DCs was over three times higher than in Rab7b KO cells (Fig. 5E,F).

This result suggests that Rab7b influences lysosome dynamics in DCs. We thus investigated whether it also affects the nuclear translocation of the transcription factor TFEB, the master regulator of lysosome biogenesis and function (Bretou et al., 2017; Sardiello et al., 2009). LPS stimulation in DCs promotes the nuclear translocation of TFEB, which is required for triggering the fast and directional migration that characterizes mature DCs (Bretou et al., 2017). Interestingly, the lack of Rab7b reduces by ~60% the fraction of TFEB in the nucleus in LPS-DCs (Fig. 5G,H). Altogether, our results indicate that Rab7b modulates lysosomal signaling through TFEB, which is in turn required for the re-organization of the actin cytoskeleton and fast migration of mature DCs.

Lack of Rab7b reduces myosin II phosphorylation

The lysosomal signaling pathway activated by TFEB also leads to increased phosphorylation of myosin II, a direct interaction partner of Rab7b. Indeed, TFEB triggers the activation of myosin light-chain kinase, which is responsible for phosphorylation of the light chain of myosin II (MLC; herein referring to MYL9) (Bretou et al., 2017). The phosphorylation of MLC is important for the regulation of actin cytoskeletal dynamics, therefore, we investigated whether

Rab7b influences MLC phosphorylation in DCs. Our data confirmed that the proportion of phosphorylated MLC is reduced by ~50% in Rab7b KO cells compared to WT cells (Fig. 6A,B). Immunofluorescence analysis further revealed that phosphorylated MLC (pMLC) is enriched at the cell rear edge of WT but not Rab7b KO DCs migrating in microchannels (Fig. 6C,D). This suggests that Rab7b is involved in the activation of myosin II at the cell rear that is responsible for triggering fast motility.

The phosphorylation of MLC triggered by TFEB is dependent on the local release of Ca²⁺ from the lysosomes via the transient receptor potential cation channel, mucolipin subfamily, member 1 (TRPML1) (Bretou et al., 2017). To investigate whether the reduced MLC phosphorylation in Rab7b KO LPS-DCs was caused by the inactivation of TRPML1 or by the impaired Rab7b-mediated recruitment of myosin II to the lysosomes, we treated the cells with ML-SA1, an agonist of the TRPML1 channel (Shen et al., 2012). As shown in Fig. 6E,F, stimulation of lysosomal Ca²⁺ release by ML-SA1 in Rab7b KO DCs was not sufficient to restore MLC phosphorylation. As Rab7b interacts directly with myosin II (Borg et al., 2014; Distefano et al., 2015), this result supports a model where, in the absence of Rab7b, the localized Ca²⁺ release from the lysosomes cannot activate myosin II as the recruitment of this motor protein to the lysosomes is prevented. As a result, actin localization at the rear of LPS-DCs is hampered, thereby preventing fast and persistent DC migration. Intriguingly, and in line with this model, we demonstrated that His-tagged Rab7b pulled down TRPML1 from total cell extracts (Fig. 6G), and the two proteins colocalize at the cell rear in migrating DCs (Fig. 6H).

Altogether, these data point to a role of Rab7b in the regulation of DC migration by physically linking actomyosin to lysosomes.

DISCUSSION

After antigen uptake, DCs modify their migratory behavior, triggering a fast and directed migration mode. Lysosomal signaling is involved in this process, by stimulating local Ca²⁺ release and the activity of myosin II. How the actomyosin cytoskeleton physically associates to lysosomes has nonetheless remained elusive. Here, we show that Rab7b is the missing link between lysosomes and the actomyosin cytoskeleton, controlling the fast migration of DCs through lysosomal signaling.

Rab7b is a small GTPase that regulates the transport from late endosomes/lysosomes to the TGN (Progida et al., 2010, 2012). It is highly expressed in DCs, with a burst of expression upon LPS-induced maturation (Berg-Larsen et al., 2013; Yang et al., 2004). Why maturing DCs upregulate the expression of this small GTPase is, however, unknown. Here, we found that DCs depleted of Rab7b are significantly less polarized (Fig. 1), demonstrating that this small GTPase is important for the polarization of the mature DCs. In line with this, Rab7b KO LPS-DCs migrating in microchannels have more actin and myosin in the front compared to WT cells (Fig. 4), indicating that, in the absence of Rab7b, mature DCs fail to re-orient their actin and myosin properly.

This actomyosin reorganization is essential for the ability of mature DCs to migrate fast and efficiently towards lymph nodes. The pool of actin and myosin at the cell front is indeed associated with slow motility, which is mainly observed in immature DCs and is responsible for membrane ruffling and macropinosome formation. On the contrary, the presence of an actomyosin pool at the cell rear characterizes mature DCs and their ability to migrate faster and more persistently (Vargas et al., 2016). In agreement with this, the retained actin distribution at the front of DCs lacking Rab7b is consistent with their increased macropinosome activity

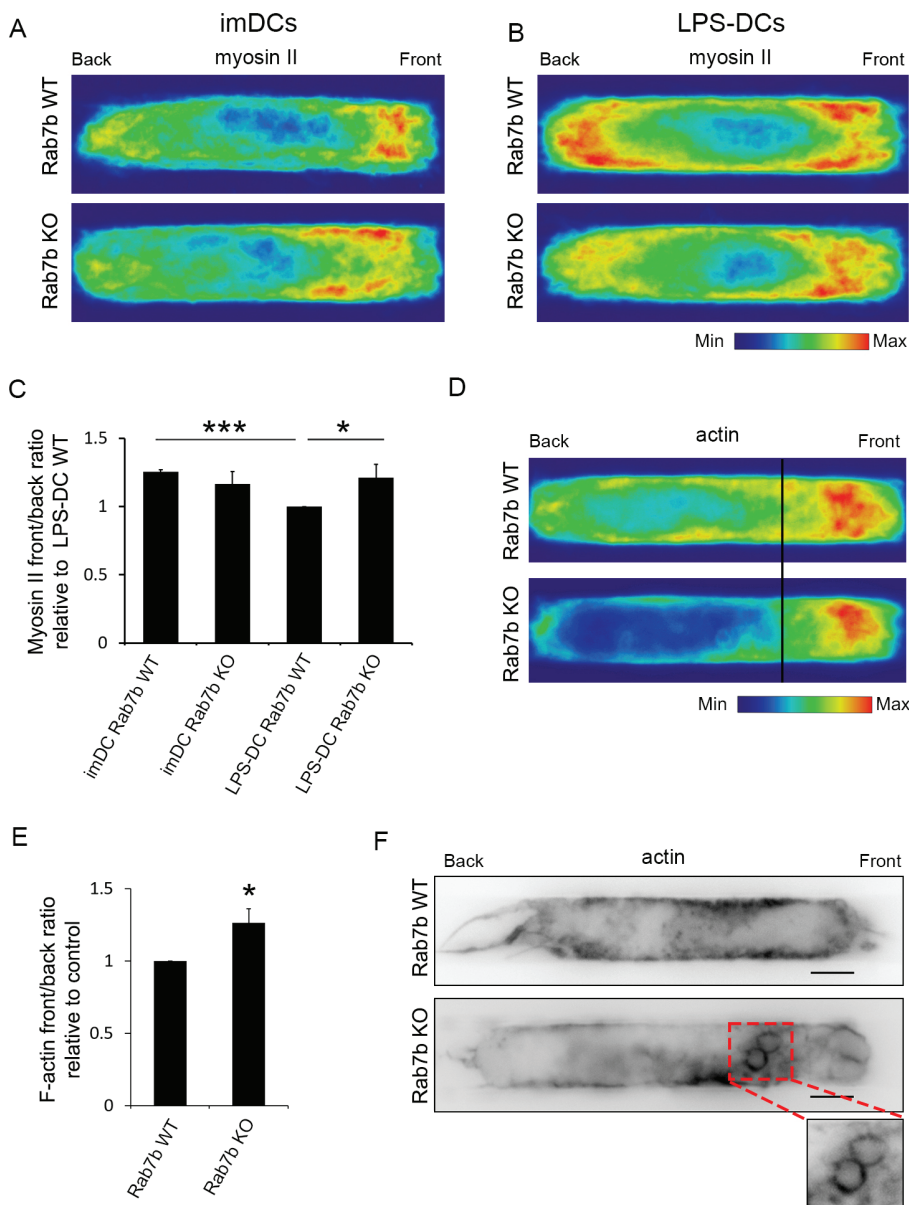


Fig. 4. Rab7b affects actomyosin distribution.

(A,B) LPS-DCs were loaded in $5 \times 8 \mu\text{m}$ micro-fabricated channels, fixed after 16 h and stained with an antibody against myosin II. The intensity of each cell for each condition was averaged into a single density map. One representative experiment out of three is shown. imDCs, immature DCs. (C) Quantification of the myosin front-to-back ratio. Data represents the mean \pm s.d. of three independent experiments ($n > 48$ cells for each condition). * $P < 0.05$; *** $P < 0.001$ (two-tailed unpaired Student's *t*-test). (D) LPS-DCs were loaded in $5 \times 8 \mu\text{m}$ micro-fabricated channels, fixed after 16 h and labeled with Rhodamine-conjugated phalloidin to visualize actin. The intensity of each cell for each condition was averaged into a single density map. One representative experiment out of three is shown. (E) Quantification of the F-actin front-to-back ratio relative to WT. Data represents the mean \pm s.d. of three independent experiments ($n = 51$ and 57 cells for WT and Rab7b KO, respectively). * $P < 0.05$ (two-tailed unpaired Student's *t*-test). (F) LPS-DCs were loaded in $5 \times 8 \mu\text{m}$ micro-fabricated channels, fixed after 16 h and labeled with Rhodamine-conjugated phalloidin to visualize actin. Representative images from one out of three independent experiments are shown. Images are inverted to improve visualization. Scale bars: $5 \mu\text{m}$.

compared to WT cells (Fig. 5A–D), as well as with their slow and less persistent motility (Fig. 3). As depletion of Rab7b causes a significant decrease in the speed and directionality of DCs, our findings demonstrate that this small GTPase, by regulating actomyosin distribution, is important for the reduction of macropinocytic activity and the acquisition of the fast migratory ability of mature DCs. This is supported by the defective polarization of DCs when Rab7b is silenced; if the cells cannot polarize properly, migration and directionality is also impaired (Danuser et al., 2013).

Lysosomal signaling plays a crucial role in triggering the reorganization of the actomyosin cytoskeleton at the cell rear that is necessary for the fast chemotactic DC migration upon LPS sensing. These signaling events involve translocation of the transcription factor TFEB, a master regulator of lysosome biogenesis and function (Sardiello et al., 2009), to the nucleus (Bretou et al., 2017). As Rab7b is required for proper lysosome function (Progida et al., 2010), it is not surprising that it is involved in the nuclear

translocation of TFEB. Indeed, the lack of Rab7b alters lysosome dynamics and reduces TFEB translocation to the nucleus in the LPS-DCs (Fig. 5E–H). This suggests that the failure in Rab7b KO cells in triggering fast migration is a result of impaired lysosomal signaling through TFEB.

How does Rab7b regulate TFEB translocation? DCs take up foreign material using macropinocytosis, and the ingested antigens are delivered to lysosomes (Norbury, 2006). Previous studies have shown that myosin II is important for the trafficking of macropinosomes towards the cell rear, and that it promotes the delivery of antigens to endolysosomal compartments (Chabaud et al., 2015). Since Rab7b interacts directly with myosin II (Borg et al., 2014) and has a role in the trafficking of endolysosomal compartments (Progida et al., 2010), it is likely that Rab7b, by recruiting myosin II from macropinosomes to late endocytic compartments, mediates the transport of internalized material to lysosomes. According to this model, in absence of Rab7b, myosin II is retained on macropinosomes at the front of the cells, promoting

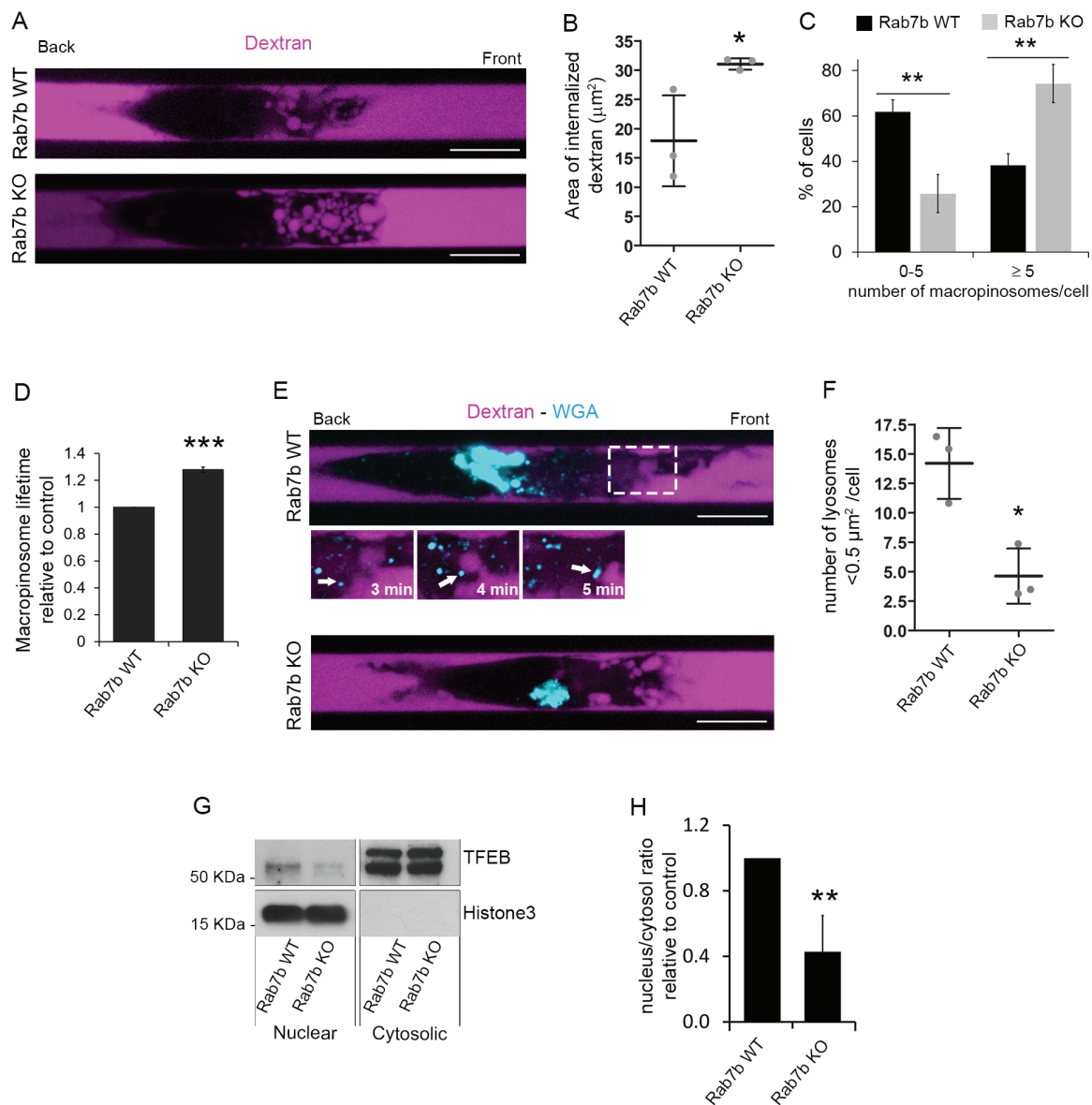


Fig. 5. Rab7b affects macropinocytosis and lysosome signaling. (A) LPS-DCs were loaded in $5 \times 8 \mu\text{m}$ micro-fabricated channels. After 16 h, the channels were filled with 10 kDa Alexa Fluor 647-conjugated dextran (magenta) and the cells were imaged 30 min later. Representative images of live WT and Rab7b KO cells are shown. Scale bars: $10 \mu\text{m}$. (B) Quantification of the area of internalized dextran in WT and Rab7b KO cells. The graph represents the mean \pm s.d. of three independent experiments ($n=39$ and 32 cells for WT and Rab7b-KO, respectively). $*P < 0.05$ (two-tailed unpaired Student's *t*-test). (C) Distribution of macropinosome numbers for WT and Rab7b KO cells from three independent experiments. Data represents the mean \pm s.d. ($n=39$ and 32 cells for WT and Rab7b KO, respectively). $**P < 0.01$ (two-tailed unpaired Student's *t*-test). (D) Quantification of the lifetime of macropinosomes in WT and Rab7b KO cells. Data represents the mean \pm s.d. of three independent experiments (>100 tracked macropinosomes per condition, $n=23$ and 28 cells for WT and Rab7b KO, respectively). $***P < 0.001$ (two-tailed unpaired Student's *t*-test). (E) Spinning disk images of live WT and Rab7b KO LPS-DCs stained with Alexa Fluor 594-conjugated WGA to label lysosomes (cyan) and loaded in $5 \times 8 \mu\text{m}$ micro-fabricated channels filled with 10 kDa Alexa Fluor 647-conjugated dextran (magenta). Representative images from one out of three independent experiments are shown. Scale bar: $10 \mu\text{m}$. The magnified area shows a lysosome (arrow) moving towards a macropinosome in a control cell. Image contrast has been increased to improve visualization. (F) Quantification of the number of lysosomes with area $< 0.5 \mu\text{m}^2$ per cell. Data represents the mean \pm s.d. of three independent experiments ($n=29$ cells for WT and Rab7b-KO). $*P < 0.05$ (two-tailed unpaired Student's *t*-test). (G) BMDCs from WT and Rab7b KO mice were pulsed with 100 ng/ml LPS for 30 min and lysed after 6 h. Cytosolic and nuclear fractions were subjected to immunoblotting analysis with the indicated antibodies. Histone 3 was used as control of the cytosolic and nuclear fraction separation. (H) The graph shows the quantification of the nucleus-to-cytoplasm ratio for TFEB in Rab7b-KO DCs relative to WT. Data represents the mean \pm s.d. of four independent experiments. $**P < 0.01$ (two-tailed unpaired Student's *t*-test).

formation of large macropinosomes and slowing down migration (Fig. 7). The sustained macropinocytosis activity inhibits TFEB nuclear translocation as this transcription factor is activated by the downregulation of macropinocytosis (Bretou et al., 2017). In line with this, stimulation of lysosomal Ca^{2+} release, which is

known to promote myosin phosphorylation, thereby triggering localized actomyosin contractility at the rear of mature DCs, is not able to rescue MLC phosphorylation defects in Rab7b KO DCs (Fig. 6A–F). Since we reveal that Rab7b interacts with the lysosomal Ca^{2+} channel TRPML1, this indicates that Rab7b

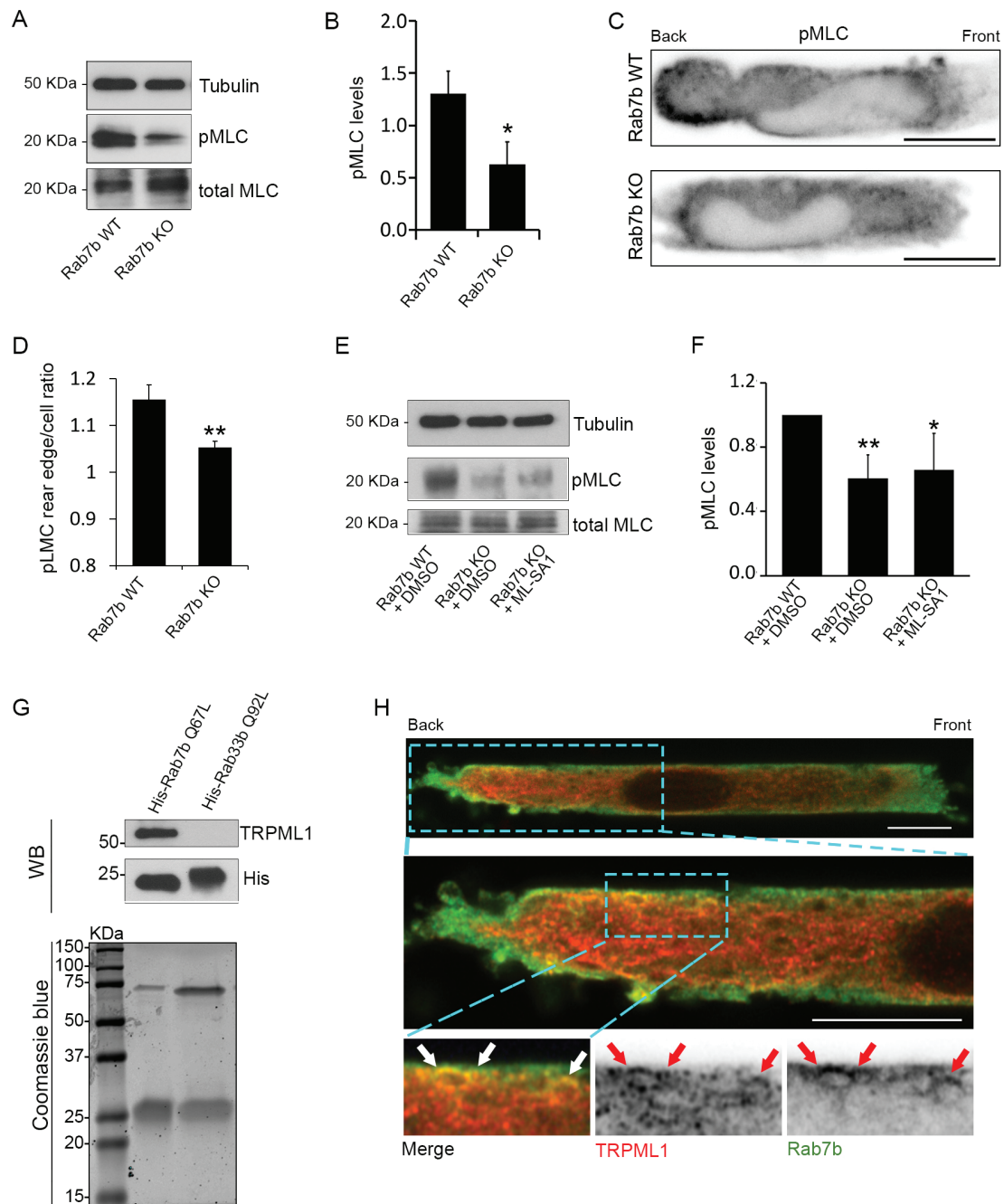


Fig. 6. Rab7b regulates myosin II activation and interacts with the lysosomal Ca^{2+} channel TRPML1. (A) Lysates from BMDCs from WT and Rab7b KO mice pulsed with 100 ng/ml LPS for 30 min were subjected to immunoblotting analysis with the indicated antibodies. Tubulin was used as loading control. (B) The graph shows the quantification of phosphorylated myosin light chain (pMLC) levels in WT and Rab7b KO DCs normalized to the tubulin levels. Data represents the mean \pm s.d. of four independent experiments. $*P < 0.05$ (two-tailed unpaired Student's *t*-test). (C) LPS-DCs were loaded in $5 \times 8 \mu\text{m}$ micro-fabricated channels, fixed after 16 h and stained with and antibody against phosphorylated myosin light chain (pMLC). Representative images from one out of three independent experiments are shown. Images are inverted to improve visualization. Scale bars: $10 \mu\text{m}$. (D) Quantification of the pMLC rear edge-to-cell ratio. Data represents the mean \pm s.d. of three independent experiments ($n = 72$ and 84 cells for WT and Rab7b-KO, respectively). $**P < 0.01$ (two-tailed unpaired Student's *t*-test). (E) BMDCs from WT and Rab7b KO mice pulsed with 100 ng/ml LPS for 30 min were treated with either DMSO or ML-SA1 $20 \mu\text{M}$ overnight and then lysed. Lysates were subjected to immunoblotting analysis with the indicated antibodies. Tubulin was used as loading control. (F) The graph shows the quantification of pMLC levels in WT and Rab7b KO DCs normalized to the tubulin levels. Data represents the mean \pm s.d. of five independent experiments. $*P < 0.05$; $**P < 0.01$ (two-tailed unpaired Student's *t*-test). (G) Lower panel, Coomassie Blue staining of bacterially expressed His-Rab7b Q67L (constitutively active mutant) and His-Rab33b Q92L (constitutively active mutant) purified using Ni-NTA agarose matrix. Upper panel: bacterially expressed and purified His-Rab7b Q67L and His-Rab33b Q92L were incubated with lysates from LPS-treated MDDCs. Proteins were pulled down using cobalt-coated magnetic beads and subjected to western blot (WB) analysis using antibodies against His and TRPML1. (H) LPS-MDDCs were loaded in $5 \times 8 \mu\text{m}$ micro-fabricated channels, fixed after 16 h and stained with antibodies against TRPML1 (red) and Rab7b (green). The red and white arrows indicate colocalization between TRPML1 and Rab7b. Scale bars: $10 \mu\text{m}$. The magnified images were acquired using super-resolution mode.

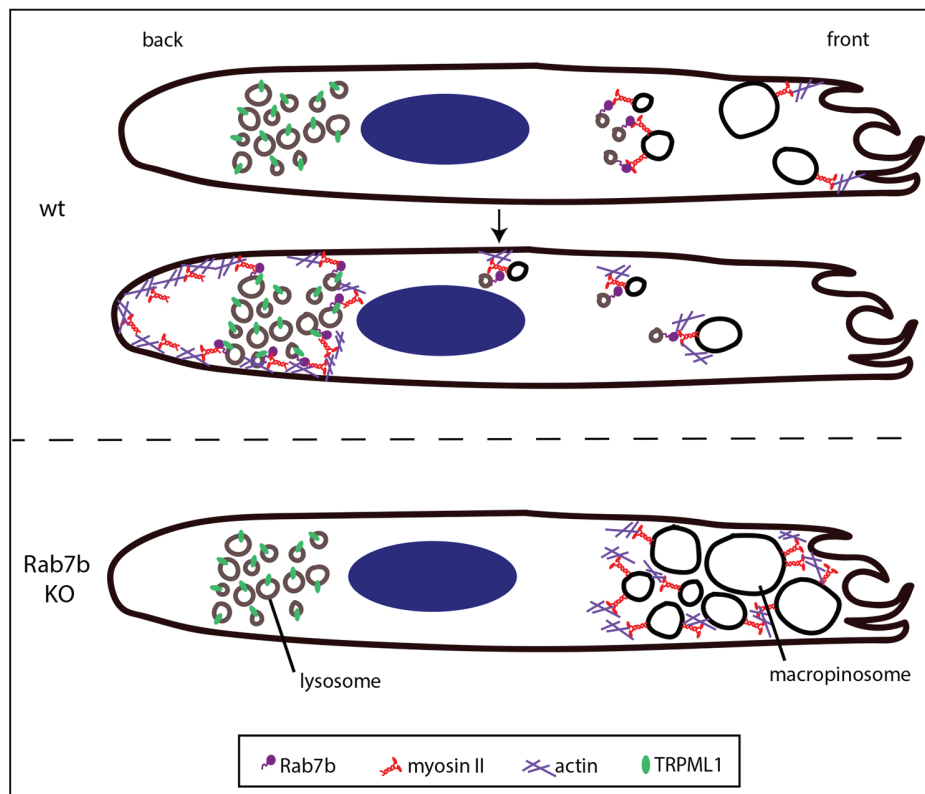


Fig. 7. Model to illustrate the role of Rab7b in DCs. Upon microbial sensing, DCs increase their migration ability and decrease their capacity of antigen uptake by macropinocytosis. Upregulation of Rab7b promotes this switch by recruiting myosin II from macropinosomes to late endocytic compartments, bringing the motor in close proximity to TRPML1, which activates myosin II at the cell rear and promotes fast DC motility. In the absence of Rab7b, myosin II is retained on macropinosomes at the front of the cells, promoting formation of large macropinosomes and slowing down migration.

brings its effector myosin II in close proximity to TRPML1 to be activated by the localized Ca^{2+} release from this channel.

In conclusion, we have identified Rab7b as a physical link between lysosomes and the actomyosin cytoskeleton in DCs, and found that this small GTPase is critical for proper polarization and the fast migratory ability of these immune cells by coordinating lysosomal signaling and actomyosin cytoskeleton reorganization.

MATERIALS AND METHODS

Mice and cells

C57BL/6 mice bearing a *Rab7b*-KO (*Rab7b^{tm2Ciphe}*) allele specifically in CD11c^+ cells, including in BMDCs, corresponding to the deletion of exon 5 of the *Rab7b* gene, have been generated by crossing *Rab7b*-floxed/reporter (*Rab7b^{tm1Ciphe}*) C57BL/6 mice with CD11c-Cre mice [B6.Cg-Tg(*Itgax-cre*)-1-Reiz/J] (Fig. S3). Monocyte-derived DCs (MDDCs) from human blood and bone-marrow derived DCs (BMDCs) from 8–16-week-old male or female C57BL/6 mice (Zhang et al., 2012) were used in this study. MDDCs were generated as previously described (Borg et al., 2014), and cultured for 5 days in RPMI medium (BioWhittaker) supplemented with 10% fetal calf serum (FCS), 2 mM L-glutamine, 100 U/ml penicillin and 100 $\mu\text{g}/\text{ml}$ streptomycin (Sigma-Aldrich). 100 ng/ml granulocyte-macrophage colony stimulating factor (GM-CSF; Immunotools) and 20 ng/ml IL-4 (Invitrogen, Life Technologies) were replenished every 2–3 days. BMDCs were cultured in medium supplemented with fetal calf serum and 50 ng/ml GM-CSF obtained from the supernatants of transfected J558 cells, as previously described (Faure-Andre et al., 2008). For the TFEB experiments, commercial GM-CSF (Sigma-Aldrich) was used. To induce DC maturation, the 2×10^6 cells/ml were pulsed with 100 ng/ml LPS (Santa Cruz Biotechnology) for 30 min.

DCs and T cells from a healthy leukapheresis donor were used for the antigen presentation assay. Leukapheresis of a healthy donor was performed at the Department of Cellular Therapy, Radium Hospitalet, Oslo, Norway to harvest monocytes and lymphocytes. T cells from leukapheresis were thawed and expanded using Dynabeads CD3/CD28. In brief, T cells were cultured

with Dynabeads (Dynabeads[®] *ClinExVivo*[™] CD3/CD28, Thermo Fisher Scientific) at a 3:1 ratio in complete CellGro DC Medium (CellGenix) with 100 U/ml recombinant human IL-2 (Novartis) for 10 days. The T cells were frozen and aliquots were thawed and rested in complete medium [CellGro DC medium (CellGenix GmbH, Germany) supplemented with 5% heat-inactivated human pooled serum (TCS Biosciences Ltd, UK), 10 mM N-acetylcysteine (Mucomyst, 200 mg/ml; AstraZeneca AS, UK), 0.01 M HEPES (Life Technologies, Norway) and 0.05 mg/ml gentamycin (Garamycin; Schering-Plough Europe, Belgium)] before transfection and antigen presentation assay. Frozen monocytes were used to generate DCs for the antigen presentation assay. Briefly, monocytes were thawed and cultured 5 days in CellGro DC medium (CellGenix) supplemented with 100 ng/ml GM-CSF (Immunotools) and 20 ng/ml IL-4 (Invitrogen, Life Technologies) followed by 24 h maturation with LPS (100 ng/ml, Santa Cruz Biotechnology).

All experiments were performed in accordance with relevant guidelines and regulations. The animals were bred under conventional conditions, regularly screened for common pathogens and housed in compliance with guidelines set by the Experimental Animal Board under the Ministry of Agriculture of Norway. All experimental protocols involving transgenic and WT animals were approved by the National Committee for Animal Experiments (Oslo, Norway). Blood components (buffy-coats) from anonymous blood donors were obtained from the local blood bank (Section for Immunology and Blood Transfusion, Ullevål University Hospital, Oslo, Norway) according to the guidelines of the local blood bank approved by the Norwegian Regional Committee for Medical Research Ethics.

Antibodies and reagents

The following antibodies were used for immunofluorescence (IF) and western blot (WB) experiments: anti-non-muscle myosin IIA (ab24762, abcam, IF 1:300), anti-myosin II light chain (M4401, Sigma-Aldrich, WB 1:200), anti-non muscle myosin IIA (ab55456, Abcam, IF 1:50), anti-phosphorylated myosin II light chain (#3671, Cell Signaling Technology, WB 1:500; IF 1:50), anti-vinculin (V9131, Sigma-Aldrich, IF 1:100), anti-

tubulin (T9026, Sigma-Aldrich, WB 1:10,000), anti-TFEB (#4240, Cell Signalling Technology, WB 1:100), anti-Histone H3 (ab1791, Abcam, WB 1:100,000), anti-Rab7b (H00338382-M01, AbNova, WB 1:300; IF 1:20), anti-TRPML1 (Abcam, WB 1:100; IF 1:40), anti-TGN46 (AHP500, Bio-Rad, IF 1:250), anti-transferrin receptor (CBL47, Chemicon, IF 1:50), rabbit polyclonal antibody against LAMP2 (IF 1:1000; a gift from Sven Carlsson, University of Umeå, Sweden), anti- γ -tubulin (ab11316, Abcam, 1:200), and anti- α -tubulin (13-8000, Invitrogen, IF 1:200). Secondary antibodies conjugated to Alexa Fluor 488, Alexa Fluor 555 or Alexa Fluor 633 fluorophores (Life Technologies, 1:200) was used for immunofluorescence, while secondary antibodies conjugated with horseradish peroxidase (GE Healthcare, 1:500) were used for western blotting. Hoechst 33258 (H3569, Life Technologies) or DAPI (D9542, Sigma-Aldrich) was used at 0.2 μ g/ml; Rhodamine-conjugated phalloidin (Invitrogen) was used at 33 nM; 10 kDa dextran, Alexa Fluor[®] 647 conjugate (Life Technologies) was used at 120 μ g/ml, and wheat germ agglutinin, Alexa Fluor[®] 647 or 594 conjugate (WGA, Invitrogen) was used at 0.25 μ g/ml. Fibronectin (Sigma-Aldrich) was used at 10 μ g/ml for coating of coverslips. ML-SA1 (Sigma-Aldrich) was used overnight at a concentration of 20 μ M.

The following antibodies were used for the flow cytometry experiments on human cells: HLA-DR (MHLDR05, Caltag Labs; 10 μ l/test), CD80 (BD557227, BD Biosciences; 20 μ l/test), HLA-ABC (BD562006, BD Biosciences; 20 μ l/test), CCR7 (FAB197A, R&D Systems; 10 μ l/test), CD11c (BD559877, BD Biosciences; 20 μ l/test), CD83 (sc19678; 20 μ l/test) and CD86 (sc19617; 20 μ l/test) (both from Santa Cruz Technology). To check the expression of the TCR Radium-1 a V β 3-FITC antibody was used (PN IM2372, Beckman Coulter-Immuntotech; data not shown). As a degranulation marker for measuring antigen specific T cell activation upon antigen presentation from DCs, a CD107a-PE-Cy5 antibody was used (BD555802, BD Biosciences). CD8-PE-Cy7 (25-0088-42, Thermo Fisher Scientific) was used as a T cell marker to identify CD8⁺ cytotoxic T cells. Isotype controls IgG2a-FITC (sc2856), IgG1-FITC (sc2855), IgG1-PE (sc2866), IgG1-APC (sc2888) and IgG2b-APC (sc2890) (all from Santa Cruz Technology) were used. For Flow Cytometry on murine DCs, an antibody against CD86 (GL1, BD Biosciences) was used.

RNA interference

For RNA interference (RNAi) in human DCs, the following siRNA oligonucleotides were used. For Rab7b siRNA, sense sequence 5'-GUA-GCUCAAGGCUGGUGUATT-3' and antisense sequence 5'-UACAC-CAGCCUUGAGCUACTT-3'. As negative control, we used the sense sequence: 5'-ACUUCGAGCGUGCAUGGCUTT-3' and antisense control 5'-AGCCAUGCACGCUCGAAGUTT-3'. The oligonucleotides were purchased from Eurofins MWG Operon.

For RNAi in murine DCs, the following siRNA oligonucleotides were used. For Rab7b siRNA, sense sequence 5'-CAAUGGUAUCAACAUU-CUATT-3' and antisense sequence 5'-UAGAAUGUUGAUACCAUUGAG-3'. As negative control, we used the sense sequence: 5'-UUCUCC-GAACGUGUCACGUTT-3' and antisense sequence 5'-ACGUGACAC-GUUCGGAGAATT-3'. The murine oligonucleotides were purchased from Qiagen.

Transfection by electroporation

After 5 days in culture, human DCs were collected, spun down at 300 *g* at 4°C, and washed in cold RPMI with no supplements. The cells were resuspended in cold RPMI to a concentration of 10⁶ cells per 300 μ l, and electroporated with 100 nM siRNA in a 4 mm gap size cuvette (VWR). Electroporation was performed with an ECM 830 Square Wave Electroporation System (BTX Technologies Inc.) for 3 ms at 500 V. Following electroporation, the cells were plated in complete RPMI medium and kept at 37°C with 5% CO₂ for minimum 24 h before further experiments.

Expanded T cells were electroporated with mRNA encoding for Radium-1 TCR, specific for the tumor neoantigen encoded by the *TGFBR2* frameshift mutant, peptide₁₂₇₋₁₄₅ KSLVRLSSCVPALMSAMT (Inderberg et al., 2017). Briefly, T cells were washed twice and resuspended in cold RPMI medium to 20 \times 10⁶ cells/ml. The mRNA was mixed with the cell suspension at 100 μ g/ml, and electroporated in a 2 mm gap cuvette at 250 V and 2 ms

using a BTX 830 Square Wave Electroporator (BTX Technologies Inc.). Immediately after transfection, T cells were transferred to complete culture medium [CellGro DC medium (CellGenix GmbH, Germany) supplemented with 5% heat-inactivated human pooled serum (TCS Biosciences Ltd, UK), 10 mM N-acetylcysteine (Mucomyst, 200 mg/ml; AstraZeneca AS, UK), 0.01M HEPES (Life Technologies, Norway) and 0.05 mg/ml gentamycin (Garamycin; Schering-Plough Europe, Belgium)] at 37°C in 5% CO₂ overnight.

BMDCs were collected on day 6–7 of differentiation, and were transfected using the Amaza mouse Dendritic Cell Nucleofector Kit (Lonza), according to the manufacturer's specifications. Briefly, cells were resuspended to 5 \times 10⁶ cells per 100 μ l of Amaza Solution containing 1 μ M siRNA. After electroporation with an Amaza Biosystems Nucleofector II electroporator (protocol Y-001), cells were incubated at 37°C for 30 min, before washing steps and re-plating for later experiments on day 10–12. The silencing efficiency was controlled either by western blotting or by quantitative real-time RT-PCR.

Quantitative real-time RT-PCR

RNA extraction was undertaken by using a miRNeasy mini kit (Qiagen), following the manufacturer's protocol. cDNA was produced from 1 μ g of RNA by using the SuperScriptVILO cDNA synthesis kit (Thermo Fisher Scientific). Quantitative PCR was performed to amplify and quantify cDNA using real-time reverse transcriptase (RT)-PCR with the Lightcycler 480 SYBR green I master mix and the Lightcycler 480 PCR system (Roche). Primers for murine *Rab7b* (forward primer, 5'-CGAGGAATACCAGAC-CACACT-3'; reverse primer, 5'-GGCTGGCCAGAACCTCAAAGG-3', and for murine *Actb* (forward primer, 5'-AGTGTGACGTTGACATCCGT-3'; reverse primer, 5'-GCAGCTCAGTAACAGTCCGC-3') were purchased from Eurofins MWG Operon. The PCR program was as follows: 1 cycle 3 min at 94°C; 40 cycles 15 s at 95°C, 30 s at 60°C, and 30 s at 72°C; 1 cycle 6 s at 75°C. The specificity and the identity of the PCR products were checked by a melting curve test. Actin transcript levels were used for the normalization of the samples.

Western blotting

DC lysates were separated by SDS-PAGE, transferred onto a PVDF membrane (Millipore) and subjected to immunoblot analysis, with specific primary antibodies diluted in 2% non-fat dry milk (Bio-Rad) overnight at 4°C, followed by incubation with secondary HRP-conjugated antibodies for 1 h at room temperature. Bands were visualized by using the ECL system (GE Healthcare), and protein levels were quantified by densitometry using ImageQuant TL software (GE Healthcare).

Antigen presentation assay

Radium-1 TCR-expressing T cells were stimulated for 5 h with DCs electroporated with either control siRNA or Rab7b siRNA and loaded with 10 μ M of 19-mer peptide encoded by the *TGFBR2* frameshift KSLVRLSSCVPALMSAMT (amino acid sequence 127–145; provided by Norsk Hydro ASA). The T-cell to target ratio was one T cell per two DCs, and the cells were incubated in the presence of an anti-CD107a antibody, as well as BD GolgiPlug (BD555029) and BD Golgistop (BD554724, both from BD Biosciences) at a 1:1000 dilution. Cells were then washed and surface stained with anti-CD8 antibody for flow cytometric analysis.

Flow cytometry

Immature and activated DCs were harvested, washed three times with cold 1 \times PBS containing 0.05% BSA, and stained for flow cytometry on ice for 30 min with the indicated antibodies. After staining, the cells were washed three times with cold 1 \times PBS containing 0.05% BSA, before fixation in 3% PFA. The antigen presentation assay was performed on a BD FACSCanto II Flow Cytometer, while phenotype experiments were performed on a LSR II Flow Cytometer, and data was analyzed using FlowJo software (Tree Star Inc, USA).

Immunofluorescence

MDDCs grown on poly-L-lysine coated coverslips (BioCoat) were gently washed with 1× PBS, then fixed in 3% PFA for 20 min at room temperature. Fixed samples were quenched for 10 min in NH_4Cl 50 mM, and permeabilized with 0.25% saponin (Sigma-Aldrich) in PBS for 10 min, before staining with primary antibodies for 20 min, followed by 20 min incubation with Alexa-Fluor-conjugated secondary antibodies. Coverslips were mounted with Mowiol (Sigma-Aldrich), and confocal images were acquired on an Olympus FV1000 confocal scanning laser upright microscope (BX61WI) with a PlanApo 60×/1.10 NA oil objective. For DCs migrating in microchannels, the PMDS was gently removed before permeabilization and staining, and the dishes were filled with PBS before imaging. Confocal images were acquired on a Zeiss LSM880 Fast AiryScan confocal microscope with a C Plan Apo 63×/1.4A oil objective. For the staining of the MTOC, cells were fixed in 3% PFA for 5 min followed by ice-cold methanol for 5 min. The cells were permeabilized and stained using a buffer containing 20 mM HEPES pH 7.5, 50 mM NaCl, 3 mM MgCl_2 and 0.1% Triton X-100.

Preparation of microchannels and speed quantification

Microchannels were prepared as previously described (Faure-Andre et al., 2008). Briefly, polydimethylsiloxane (PDMS) was added to prefabricated molds, before activation in a plasma cleaner for 30 s and attachment of the PDMS piece to a glass-bottomed dish. These were further incubated with 20 $\mu\text{g}/\text{ml}$ fibronectin (Sigma-Aldrich) for 1 h, and rinsed with 1× PBS. For quantification of mean velocity and persistency, cells were loaded into microchannels and imaged for 20 h at 37°C with 5% CO_2 , on an epifluorescence Nikon TiE video-microscope equipped with a cooled CCD camera, using a 10× objective and acquiring one transmission phase image every 2 min. Extraction of kymographs and instantaneous velocity analysis were performed using an in-house MATLAB program as described previously (Faure-Andre et al., 2008). Graphs and statistical differences were assessed with Prism software, using a two-tailed unpaired Student's *t*-test.

Migration in collagen gel

BMDCs were collected on day 9–10, stimulated with LPS for 30 min and replated in culture dishes. The following day, 7×10^4 cells were resuspended in BMDC medium and mixed with 1.4 mg/ml collagen type I (Advanced BioMatrix) and 0.2% NaHCO_3 (Sigma-Aldrich). From this, a 33.3 μl drop was spotted in a 24-well plate with glass bottom and topped with a coverslip to form a collagen sandwich. The plate was incubated at 37°C with 5% CO_2 for 30 min to allow collagen polymerization. After this, 500 μl BMDC medium supplemented with 400 ng/ml chemokine [C-C motif ligand 21 (CCL21); BioLegend] was added to the wells as a chemoattractant. Cells were imaged every 2 min for 2 h using an Andor Dragonfly spinning disk microscope equipped with a CFI Plan Apo 10×/0.45 NA objective at 37°C with 5% CO_2 . Cells tracking was performed using the Manual Tracking plugin of ImageJ software (National Institutes of Health). Cell speed and directionality was determined using the Chemotaxis and Migration Tool software (Ibidi).

Myosin and actin density map generation and analysis

Myosin and actin distribution analysis was performed on BMDCs loaded in 5×8 μm microchannels (4D Cell). Before seeding the cells, the channels were coated with 20 $\mu\text{g}/\text{ml}$ of fibronectin as previously described. BMDCs were either plated untreated (for immature DCs) or treated with LPS to induce maturation for 30 min at 37°C, 5% CO_2 . 10×10^5 cells were loaded into the access port for each channel and allowed to migrate overnight at 37°C, 5% CO_2 . On the following day, the cells in the channels were fixed with 3% PFA for 20 min and washed with PBS. After this, the PMDS structure on top of the channels was carefully removed before permeabilization with 0.25% saponin in PBS for 10 min followed by staining. All the steps were performed at room temperature. The cells were imaged using a Zeiss LSM880 Fast AiryScan confocal microscope with a C Plan Apo 63×/1.4A oil objective.

Density maps were generated using ImageJ. Briefly, images were cropped to contain single cells and resized to the average cell size. After background subtraction, the intensities were normalized and density maps were generated by projecting the mean signal of every individual cell and applying the physics look-up table (LUT; ImageJ) to the image. Intensities were measured in rectangles covering the front 20% of the cell, and in the back 20% of the cell.

Actin distribution analysis was performed similarly to the myosin distribution analysis. Rhodamine-conjugated phalloidin was used to stain the actin cytoskeleton and imaging was performed on an Andor Dragonfly microscope equipped with a CFI Plan Apo 100×/1.45 NA oil objective. Density maps were generated using the same method as for the myosin maps. Intensities were measured in a rectangle covering the first third of the cell, defined as the front, and in the last two thirds of the cell, defined as the back.

Macropinocytosis and lysosome dynamics in migrating DCs

LPS-BMDCs were stained with WGA, Alexa Fluor[®] 594 conjugate, as previously described (Bretou et al., 2017), before loading into 5×8 μm microchannels (4D Cell). The following day, channels were filled with 120 $\mu\text{g}/\text{ml}$ 10 kDa Alexa Fluor 647-conjugated dextran (Life Technologies) for 30 min and then imaged every minute for 20 min using an Andor Dragonfly microscope equipped with a CFI Plan Apo 100×/1.45 NA oil objective. A confocal section of the middle plane was selected, and multi-position mode was used to image multiple cells simultaneously from the same starting point. The area of internalized dextran and number of macropinosomes was quantified by drawing a region of interest (ROI) around each cell and using particle analysis in ImageJ to identify dextran-positive objects. Prior particle analysis, the images were processed with a median filter, and a threshold was applied to generate a binary image. The watershed function was used to split touching objects. The lysosomes were analyzed similarly, using particle analysis to identify WGA-positive objects. Macropinosome lifetime was estimated by counting the number of frames in which the same macropinosome was present.

TFEB nuclear translocation assay

On day 7 of culture, BMDCs were treated with 100 ng/ml LPS for 30 min and lysed after 6 h with a cold lysis buffer containing 20 mM Tris-HCl pH 7.5, 150 mM NaCl (Sigma-Aldrich), 2 mM EDTA (VWR), 0.1% IGEPAL CA-630 (Sigma-Aldrich), protease and phosphatase inhibitors (Sigma-Aldrich). The samples were spun at 13,400 *g* for 1 min and the supernatant was collected as the cytosolic fraction. The pellet containing the nuclei was washed three times with cold lysis buffer. Both cytosolic and nuclear fractions were resuspended in Laemmli sample buffer containing 100 mM DTT. Cytosolic fractions were heated at 96°C for 5 min while nuclear fractions were heated at 96°C for 20 min. The denatured fractions were subjected to SDS-PAGE and analyzed by western blotting.

Expression of His-tagged proteins and pull down

His-tagged Rab7bQ67L and His-tagged Rab33bQ92L were expressed in *Escherichia coli* BL21 (DE3; Agilent Technologies) transformed with pET16b His-Rab7bQ67L (Progida et al., 2012) and pET16b His-Rab33bQ92L (GenScript), after induction with 0.5 mM IPTG for 3 h at 37°C. The bacteria were centrifuged at 3000 *g* for 25 min, resuspended in 64 mM Tris-HCl pH 8.5, 8 mM MgCl_2 , 20 mM β -mercaptoethanol and 0.3 mM PMSF, and lysed with a French press. Expressed His-tagged proteins were purified from the bacterial soluble fraction using nickel-nitrilotriacetic acid resin (Qiagen) in the presence of 50 mM Tris-HCl pH 8.0, 500 mM NaCl, 5% glycerol, 1% Triton X-100, 5 mM β -mercaptoethanol, 20 mM imidazole and 0.3 mM PMSF, according to the manufacturer's protocol. For pulldown experiments, 40 μg of His-Rab fusion proteins bound to Dynabeads[™] His-Tag were incubated with precleared lysates from LPS-treated MDDCs for 30 min at 4°C and then washed six times with buffer containing 3.25 mM sodium phosphate, pH 7.4, 70 mM NaCl and 0.01% Tween-20. Bound proteins were eluted with elution buffer (50 mM sodium phosphate, pH 8.0, 300 mM NaCl, 0.01% Tween-20, 300 mM imidazole). Samples were analyzed by using SDS-PAGE and immunoblotting.

Image analysis, processing and statistical analysis

Images were processed with ImageJ and Adobe Photoshop (Adobe Systems Inc., CA, USA). Quantifications were undertaken using Fluoview 1000 (Olympus, Hamburg, Germany) and ImageJ. Statistical differences, unless otherwise stated, were assessed by two-tailed unpaired Student's *t*-test (Excel software). In the figures, statistical significance is indicated as follows: **P*<0.05, ***P*<0.01, ****P*<0.001.

Acknowledgements

We thank the NorMIC Oslo imaging platform (Department of Biosciences, University of Oslo) and the PICT IBiSA Nikon imaging centre (CNRS UMR144, Institut Curie), for assistance with imaging. We also acknowledge the animal facilities at the Institut Curie and at the Department of Comparative Medicine, University of Oslo, and Sathiarub Sivaganesh for technical support. We are grateful for the advice and support from Niladri Bhusan Pati, Lena Roth, Rune Enger and Erik Dissen at the Faculty of Medicine, University of Oslo, and Ina Meuskens for assistance with the French press. We thank Frédéric Fiore and members of the Centre d'Immunophénomique (CIPHE) (Aix Marseille Univ, INSERM US012, CNRS UMS3367, Marseille, France) for generating the *Rab7b*-floxed/reporter mice.

Competing interests

The authors declare no competing or financial interests.

Author contributions

Conceptualization: A.-M.L.-D., C.P.; Methodology: K.V., I.P., M.B.D., N.M., N.A.G., M.B., S.W., C.P.; Validation: K.V., I.P., M.B.D., N.M., M.B.; Formal analysis: K.V., I.P., M.B.D., N.M., M.B.; Investigation: K.V., I.P., M.B.D., N.M., M.B. Resources: S.W., C.A.-S., O.B., M.D., C.P.; Writing - original draft: K.V., I.P., M.B.D., C.P.; Writing - review & editing: K.V., I.P., M.B.D., N.M., N.A.G., M.B., S.W., C.A.-S., M.D., A.-M.L.-D., C.P.; Visualization: K.V., I.P., M.B.D., M.D., C.P.; Supervision: C.P.; Project administration: C.P.; Funding acquisition: O.B., C.P.

Funding

The generation and initial characterization of the *Rab7b*-targeted mice was supported by the European Research Council under the European Community's Seventh Framework Programme (FP7/2007; 2013 grant agreement 281225, to M.D.) by the DCBIOL Labex (ANR-11-LABEX-0043, grant ANR-10-IDEX-0001-02 PSL*), and by the A*MIDEX project (ANR-11-IDEX-0001-02) funded by the French Government's "Investissements d'Avenir" program managed by the Agence Nationale de la Recherche (ANR). The financial support of the Norwegian Cancer Society (Kreftforeningen) [grants 179573 and 198094 to C.P. and 4604944 to O.B.], the Norwegian Research Council (Norges Forskningsråd) [grants 287560 to C.P. and through its Centre of Excellence funding scheme, project number 179573], the Southern and Eastern Norway Regional Health Authority (Helse Sør-Øst RHF) [grant 13/00367-88 to N.M.], the Anders Jahre Foundation (Anders Jahres Humanitære Stiftelse), the S. G. Sønnefeld Foundation, and UNIFOR-FRIMED, (UNIFOR) is gratefully acknowledged. Open access funding provided by Universitetet i Oslo. Deposited in PMC for immediate release.

Peer review history

The peer review history is available online at <https://journals.biologists.com/jcs/article-lookup/doi/10.1242/jcs.259221>

References

- Alvarez, D., Vollmann, E. H. and von Andrian, U. H. (2008). Mechanisms and consequences of dendritic cell migration. *Immunity* **29**, 325-342. doi:10.1016/j.immuni.2008.08.006
- Banchereau, J., Briere, F., Caux, C., Davoust, J., Lebecque, S., Liu, Y.-J., Pulendran, B. and Palucka, K. (2000). Immunobiology of dendritic cells. *Annu. Rev. Immunol.* **18**, 767-811. doi:10.1146/annurev.immunol.18.1.767
- Berg-Larsen, A., Landsverk, O. J. B., Progida, C., Gregers, T. F. and Bakke, O. (2013). Differential regulation of Rab GTPase expression in monocyte-derived dendritic cells upon lipopolysaccharide activation: a correlation to maturation-dependent functional properties. *PLoS ONE* **8**, e73538. doi:10.1371/journal.pone.0073538
- Borg, M., Bakke, O. and Progida, C. (2014). A novel interaction between Rab7b and actomyosin reveals a dual role in intracellular transport and cell migration. *J. Cell Sci.* **127**, 4927-4939. doi:10.1242/jcs.155861
- Borg Distefano, M., Hofstad Haugen, L., Wang, Y., Perdreau-Dahl, H., Kjos, I., Jia, D., Morth, J. P., Neeftjes, J., Bakke, O. and Progida, C. (2018). TBC1D5 controls the GTPase cycle of Rab7b. *J. Cell Sci.* **131**, jcs216630. doi:10.1242/jcs.216630
- Bretou, M., Saez, P. J., Sanseau, D., Maurin, M., Lankar, D., Chabaud, M., Spampinato, C., Malbec, O., Barbier, L., Muallem, S. et al. (2017). Lysosome signaling controls the migration of dendritic cells. *Sci. Immunol.* **2**, eaak9573. doi:10.1126/sciimmunol.aak9573
- Chabaud, M., Heuzé, M. L., Bretou, M., Vargas, P., Maiuri, P., Solanes, P., Maurin, M., Terriac, E., Le Berre, M., Lankar, D. et al. (2015). Cell migration and antigen capture are antagonistic processes coupled by myosin II in dendritic cells. *Nat. Commun.* **6**, 8122. doi:10.1038/ncomms9122
- Danuser, G., Allard, J. and Mogilner, A. (2013). Mathematical modeling of eukaryotic cell migration: insights beyond experiments. *Annu. Rev. Cell Dev. Biol.* **29**, 501-528. doi:10.1146/annurev-cellbio-101512-122308
- Distefano, M. B., Kjos, I., Bakke, O. and Progida, C. (2015). Rab7b at the intersection of intracellular trafficking and cell migration. *Commun. Integr. Biol.* **8**, e1023492. doi:10.1080/19420889.2015.1023492
- Faure-Andre, G., Vargas, P., Yuseff, M.-I., Heuze, M., Diaz, J., Lankar, D., Steri, V., Manry, J., Hugues, S., Vascotto, F. et al. (2008). Regulation of dendritic cell migration by CD74, the MHC class II-associated invariant chain. *Science* **322**, 1705-1710. doi:10.1126/science.1159894
- He, D., Chen, T., Yang, M., Zhu, X., Wang, C., Cao, X. and Cai, Z. (2011). Small Rab GTPase Rab7b promotes megakaryocytic differentiation by enhancing IL-6 production and STAT3-GATA-1 association. *J. Mol. Med.* **89**, 137-150. doi:10.1007/s00109-010-0689-z
- Heuzé, M. L., Vargas, P., Chabaud, M., Le Berre, M., Liu, Y.-J., Collin, O., Solanes, P., Voituriez, R., Piel, M. and Lennon-Dumenil, A.-M. (2013). Migration of dendritic cells: physical principles, molecular mechanisms, and functional implications. *Immunol. Rev.* **256**, 240-254. doi:10.1111/imr.12108
- Inderberg, E. M., Wächli, S., Myhre, M. R., Trachsel, S., Almásbak, H., Kvalheim, G. and Gaudernack, G. (2017). T cell therapy targeting a public neoantigen in microsatellite instable colon cancer reduces in vivo tumor growth. *Oncoimmunology* **6**, e1302631. doi:10.1080/2162402X.2017.1302631
- Lämmermann, T., Bader, B. L., Monkley, S. J., Words, T., Wedlich-Söldner, R., Hirsch, K., Keller, M., Förster, R., Critchley, D. R., Fässler, R. et al. (2008). Rapid leukocyte migration by integrin-independent flowing and squeezing. *Nature* **453**, 51-55. doi:10.1038/nature06887
- Manh, T.-P. V., Alexandre, Y., Baranek, T., Crozat, K. and Dalod, M. (2013). Plasmacytoid, conventional, and monocyte-derived dendritic cells undergo a profound and convergent genetic reprogramming during their maturation. *Eur. J. Immunol.* **43**, 1706-1715. doi:10.1002/eji.201243106
- Mellman, I. and Steinman, R. M. (2001). Dendritic cells: specialized and regulated antigen processing machines. *Cell* **106**, 255-258. doi:10.1016/S0092-8674(01)00449-6
- Norbury, C. C. (2006). Drinking a lot is good for dendritic cells. *Immunology* **117**, 443-451. doi:10.1111/j.1365-2567.2006.02335.x
- Progida, C., Cogli, L., Piro, F., De Luca, A., Bakke, O. and Bucci, C. (2010). Rab7b controls trafficking from endosomes to the TGN. *J. Cell Sci.* **123**, 1480-1491. doi:10.1242/jcs.051474
- Progida, C., Nielsen, M. S., Koster, G., Bucci, C. and Bakke, O. (2012). Dynamics of Rab7b-dependent transport of sorting receptors. *Traffic* **13**, 1273-1285. doi:10.1111/j.1600-0854.2012.01388.x
- Reis e Sousa, C. (2006). Dendritic cells in a mature age. *Nat. Rev. Immunol.* **6**, 476-483. doi:10.1038/nri1845
- Sardiello, M., Palmieri, M., di Ronza, A., Medina, D. L., Valenza, M., Gennarino, V. A., Di Malta, C., Donaudy, F., Embrione, V., Polishchuk, R. S. et al. (2009). A gene network regulating lysosomal biogenesis and function. *Science* **325**, 473-477. doi:10.1126/science.1174447
- Shen, D., Wang, X., Li, X., Zhang, X., Yao, Z., Dibble, S., Dong, X. P., Yu, T., Lieberman, A. P., Showalter, H. D. et al. (2012). Lipid storage disorders block lysosomal trafficking by inhibiting a TRP channel and lysosomal calcium release. *Nat. Commun.* **3**, 731. doi:10.1038/ncomms1735
- Trombetta, E. S., Ebersold, M., Garrett, W., Pypaert, M. and Mellman, I. (2003). Activation of lysosomal function during dendritic cell maturation. *Science* **299**, 1400-1403. doi:10.1126/science.1080106
- Vargas, P., Terriac, E., Lennon-Dumenil, A.-M. and Piel, M. (2014). Study of cell migration in microfabricated channels. *J. Vis. Exp.* **84**, e51099. doi:10.3791/51099
- Vargas, P., Maiuri, P., Bretou, M., Sáez, P. J., Pierobon, P., Maurin, M., Chabaud, M., Lankar, D., Obino, D., Terriac, E. et al. (2016). Innate control of actin nucleation determines two distinct migration behaviours in dendritic cells. *Nat. Cell Biol.* **18**, 43-53. doi:10.1038/ncb3284
- Weber, M., Hauschild, R., Schwarz, J., Mousson, C., de Vries, I., Legler, D. F., Luther, S. A., Bollenbach, T. and Sixt, M. (2013). Interstitial dendritic cell guidance by haptotactic chemokine gradients. *Science* **339**, 328-332. doi:10.1126/science.1228456
- Yang, M., Chen, T., Han, C., Li, N., Wan, T. and Cao, X. (2004). Rab7b, a novel lysosome-associated small GTPase, is involved in monocytic differentiation of human acute promyelocytic leukemia cells. *Biochem. Biophys. Res. Commun.* **318**, 792-799. doi:10.1016/j.bbrc.2004.04.115
- Zhang, Y., Conti, M. A., Malide, D., Dong, F., Wang, A., Shmist, Y. A., Liu, C., Zervas, P., Daniels, M. P., Chan, C.-C. et al. (2012). Mouse models of MYH9-related disease: mutations in nonmuscle myosin II-A. *Blood* **119**, 238-250. doi:10.1182/blood-2011-06-358853

Sup.Fig.1

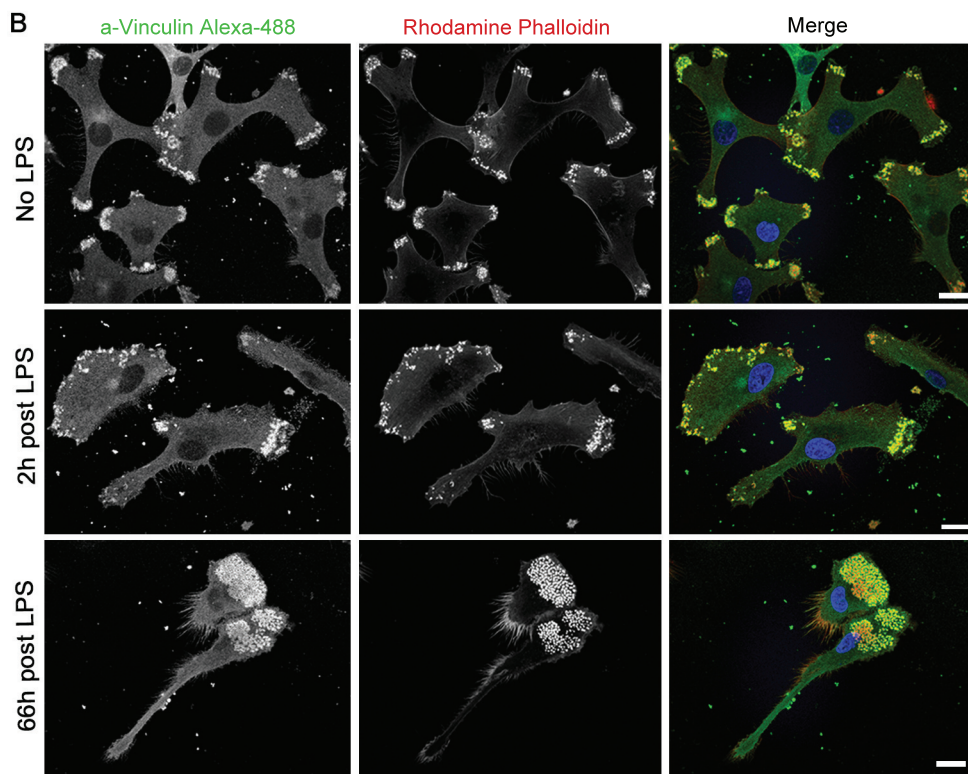
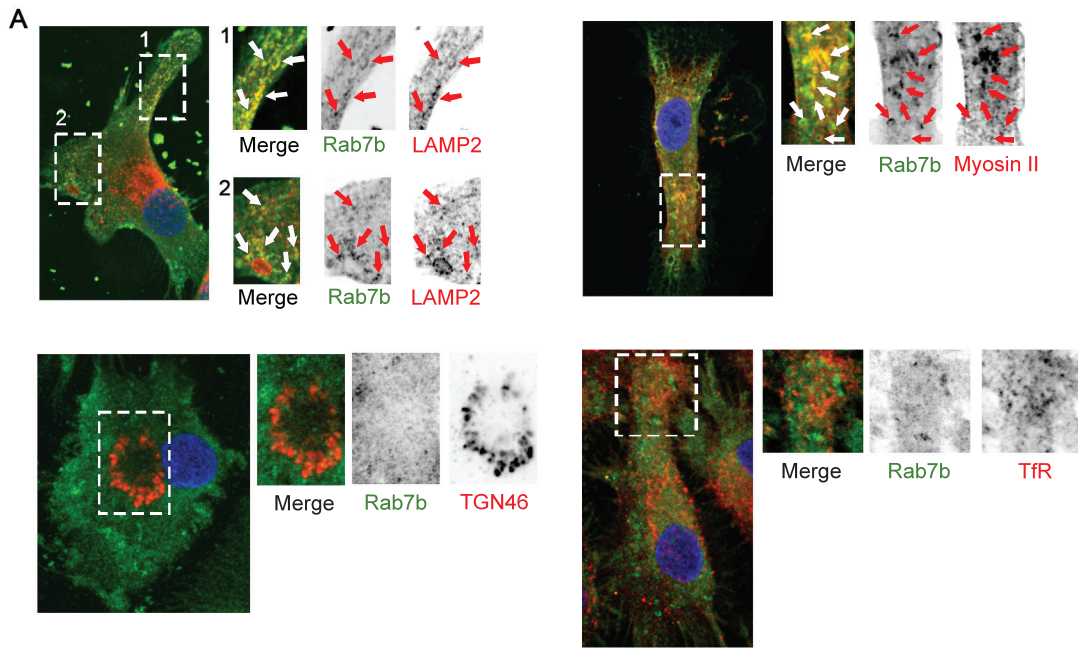


Fig. 1. Localization of endogenous Rab7b and polarization of podosomes in mature DCs

(A) MDDCs stimulated with LPS were plated on PLL-coated coverslips, fixed and immunostained with the indicated antibodies. Scale bar 10 μ m. (B) Immature MDDCs were plated on PLL-coated coverslips, and stimulated with 100 ng/ml LPS for either 2h or 66h before fixation and immunostaining with an antibody against vinculin (green). Actin was labeled with rhodamine-conjugated phalloidin (red) and nuclei with Hoechst (blue). Scale bar 10 μ m.

Sup. Fig. 2

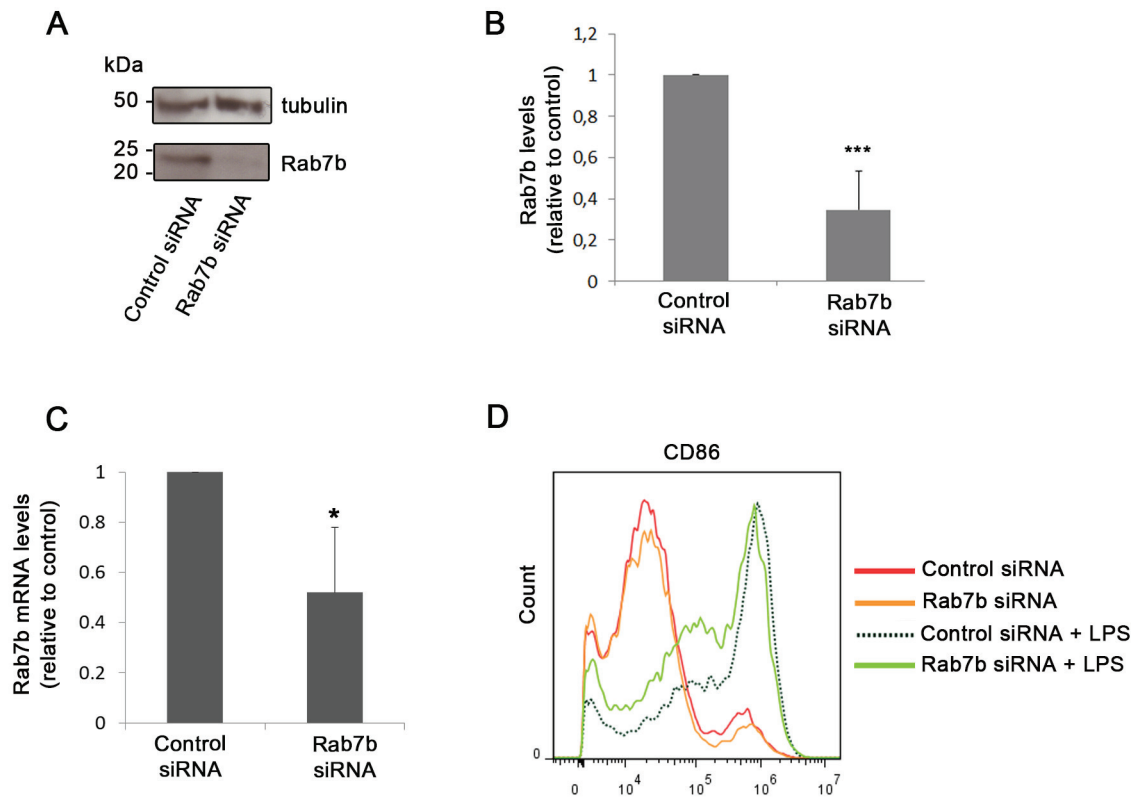


Fig. S2. Rab7b depletion in DCs

(A) DCs from a healthy donor were transfected by electroporation with either control siRNA or Rab7b siRNA, and subjected to Western blot analysis with antibodies against Rab7b and tubulin as a loading control. (B) Quantification of Rab7b levels in DCs silenced with control siRNA or Rab7b siRNA. The intensity of the bands from western blots was quantified using ImageQuant, and the level of Rab7b was normalized to the amount of tubulin. Data represents the mean \pm s.d. of three independent experiments. *** $P < 0.0001$. (C) Quantification of Rab7b mRNA levels in BMDCs. Rab7b mRNA levels were quantified by real-time RT-PCR in BMDCs transfected with either control siRNA or Rab7b siRNA. The levels of Rab7b mRNAs were normalized to the amount of actin. Data represents the average of three independent experiments \pm s.d. * $P < 0.05$. (D) FACS analysis of the surface expression marker CD86 in BMDCs. Data shows a representative histogram overlay in which the dotted and the red lines represent the control siRNA with and without LPS, while the green and the orange lines represent the Rab7b siRNA with and without LPS, respectively.

Supplementary Figure 3

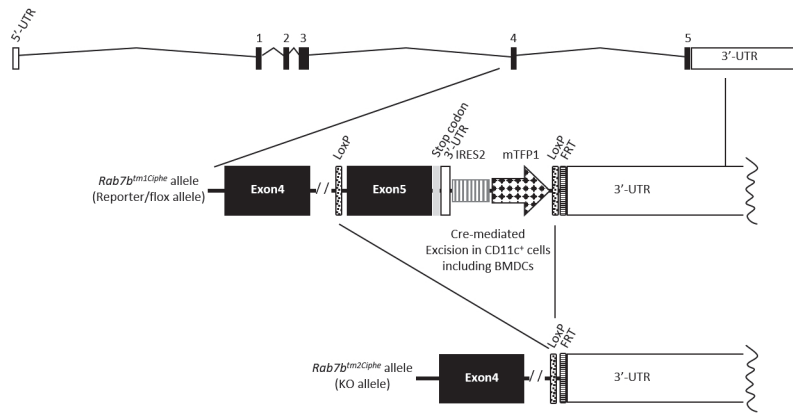


Fig. S3. Schematic representation of the genetic engineering of the *Rab7b* alleles

A LoxP site was introduced 5' of exon 5 and an IRES2-mTFP1-LoxP cassette was inserted downstream of the stop codon in the 3' -untranslated region of exon 5 of the *Rab7b* gene, by classical homologous recombination in the C57BL6/N EUCOMM JM8.F6 ES cell line, generating the *Rab7b^{tm1Ciphe}* allele preserving the expression of the *Rab7b* gene but reporting it via the expression of the mTFP1 fluorescent protein and enabling its knock-out upon deletion of exon 5 together with the reporter cassette after crossing to Cre-expressing mice. The *Rab7b^{tm2Ciphe}* conditional knock-out allele was generated specifically in CD11c⁺ cells, including BMDCs, by crossing mice bearing the *Rab7b^{tm1Ciphe}* allele with CD11c-Cre transgenic mice (B6.Cg-Tg(Itgax-cre)1-1Reiz/J).

Supplementary Figure 4

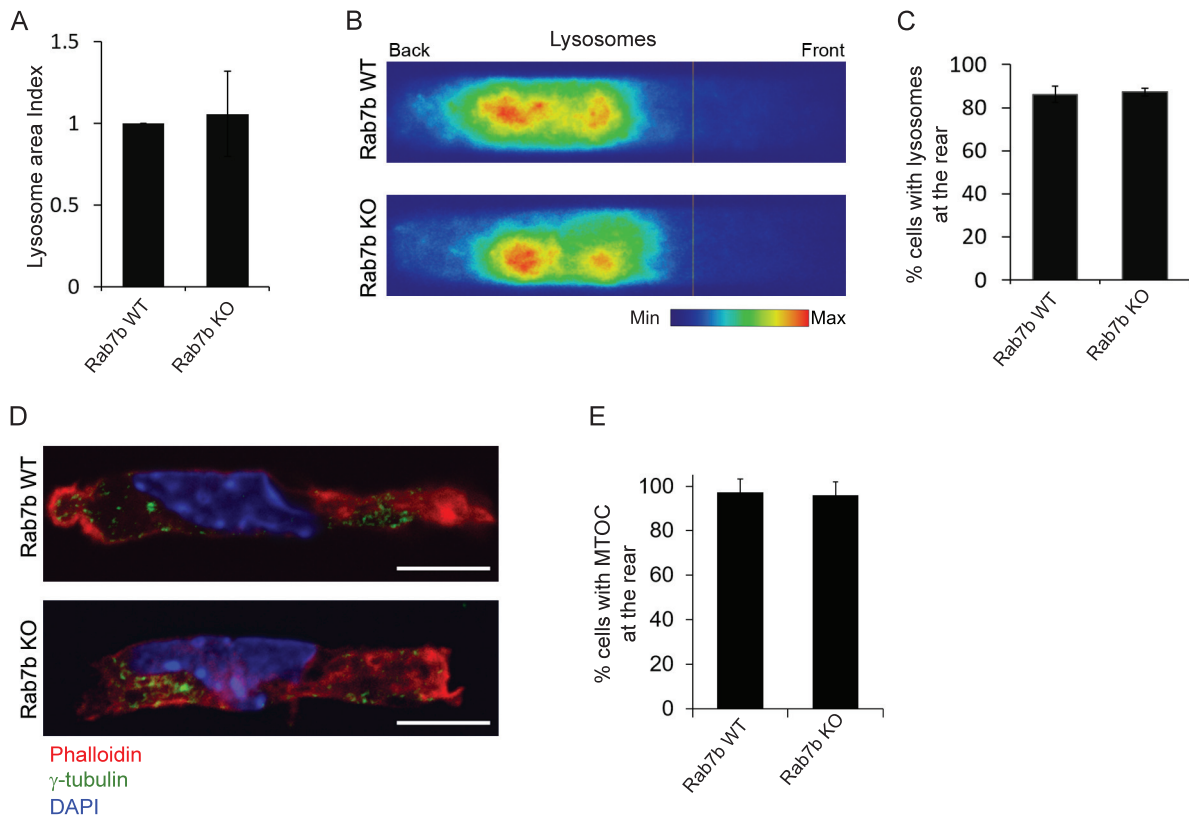
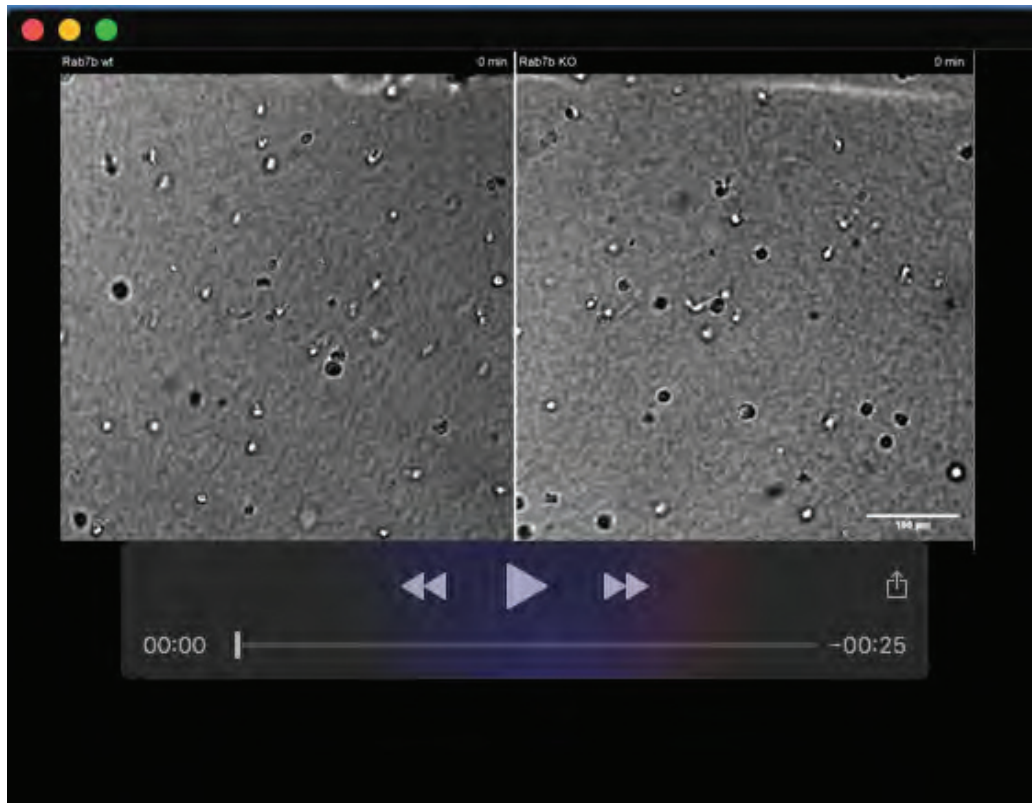


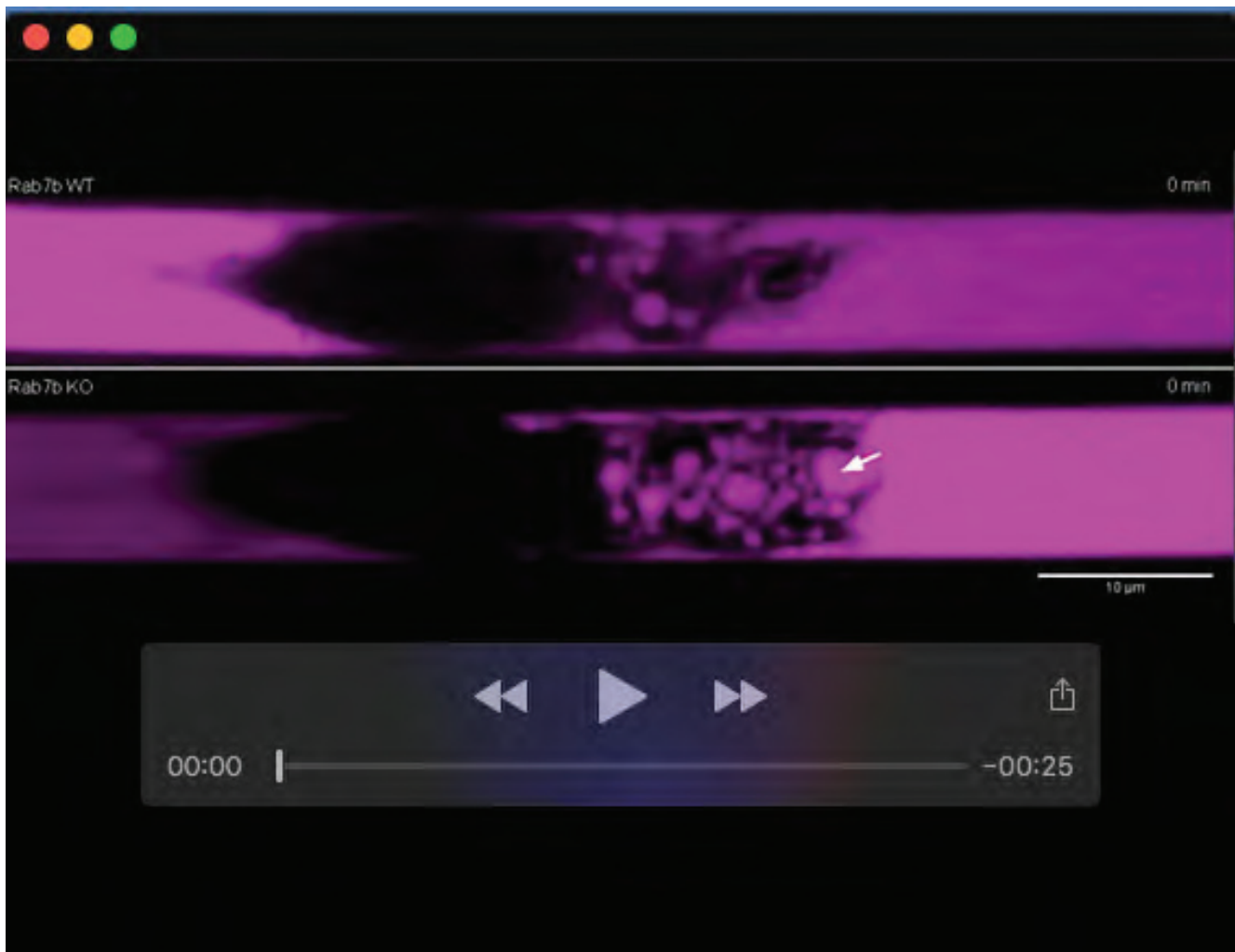
Fig. S4. Rab7b does not affect lysosome or MTOC orientation

(A-C) WT and Rab7b KO DCs were incubated with AF647-WGA to label lysosomes, treated with LPS, loaded in 5 x 8 μm micro-fabricated channels and fixed after 16 hours. (A) Quantification of the lysosome area index, defined as the area of the lysosomes relative to size and normalized to control. (B) The intensity of each cell for each condition was averaged into a single density map. One representative experiment out of three is shown. (C) Quantification of the percentage of cells with the main lysosome cluster localized at the cell rear (defined as last two thirds of the cell). Data represents the average of three independent experiments ± s.d. (n=51 and 57 cells for WT and Rab7b-KO, respectively). (D) LPSDCs were loaded in 5 x 5-8 μm wide micro-fabricated channels, fixed after 16 hours and stained with an antibody against γ-tubulin to label the MTOC. Rhodamine-conjugated phalloidin was used to visualize actin and DAPI to label the nucleus. Representative images from one out of three independent experiments are shown. Scale bar 10 μm. (E) Quantification of the percentage of cells with the MTOC positioned at the rear. Data represents the average of three independent experiments ± s.d. (n=30 and 35 cells for WT and Rab7b-KO, respectively).



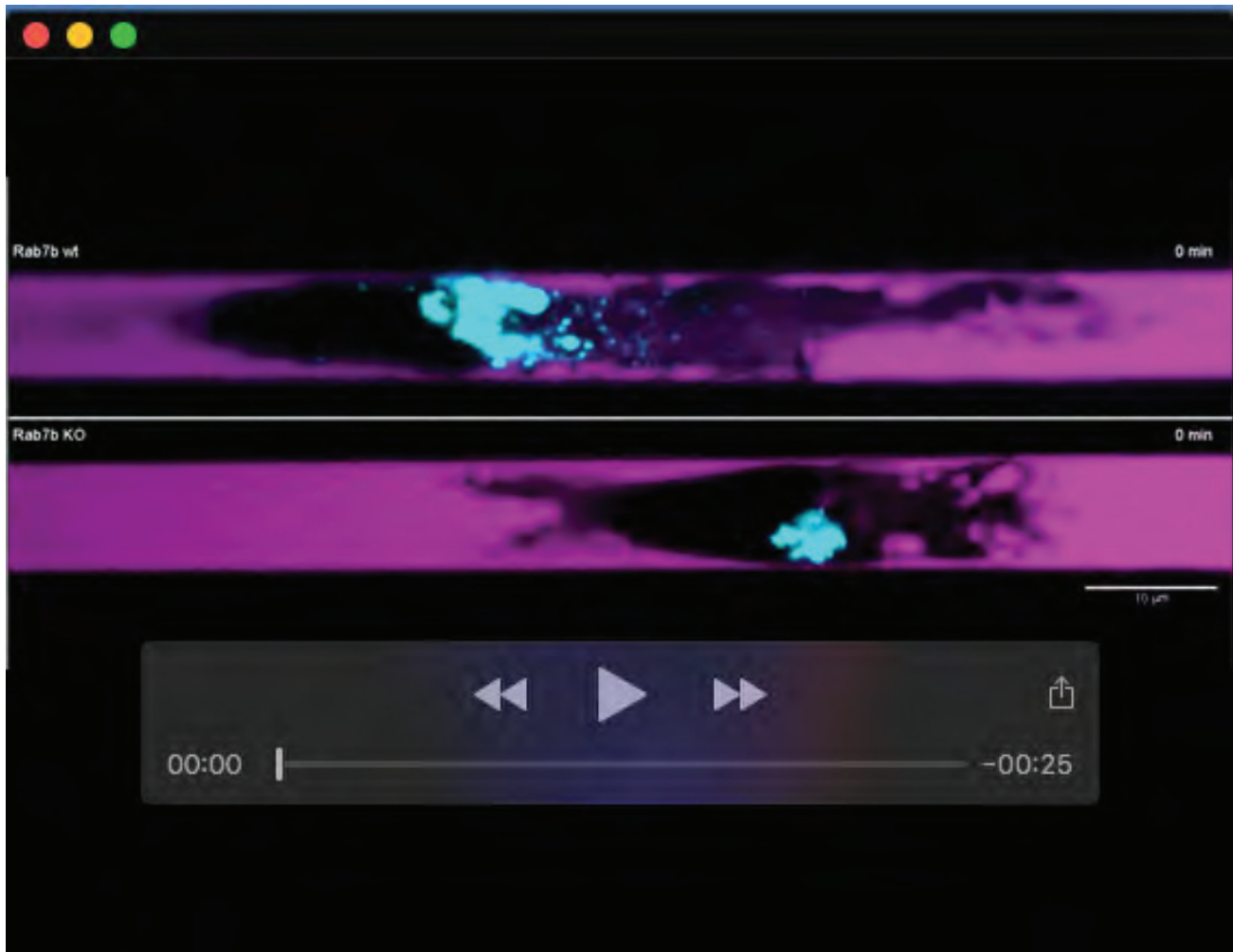
Movie 1. WT and Rab7b-KO DCs migrating in collagen gels

WT and Rab7b-KO LPS-DCs migrating in collagen gels. The source of the CCL21 chemoattractant is at the top of the movie. Cells were imaged every two minutes for two hours. Scale bar: 100 μm.



Movie 2. Macropinocytosis in WT and Rab7b-KO DCs

WT and Rab7b-KO LPS-DCs were loaded in 5 x 8 μm micro-fabricated channels. After 16 hours, the channels were filled with 10 kDa 647-Dextran (magenta), and 30 minutes later the cells were imaged at 1-minute intervals. The arrow shows an example of a macropinosome with long lifetime in the Rab7b-KO cell. Scale bar: 10 μm.



Movie 3. Lysosome dynamics during macropinocytosis in WT and Rab7b-KO DCs

WT and Rab7b-KO LPS-DCs stained with AF594-WGA to label lysosomes (cyan) were loaded in 5 x 8 μm micro-fabricated channels. After 16 hours, the channels were filled with 10 kDa 647-Dextran (magenta), and 30 minutes later the cells were imaged at 1-minute intervals. Scale bar: 10 μm.

